The Fatigue Behaviour of Toughened Epoxy Polymers

by

Takeshi Oba

A thesis submitted to the University of London
for the degree of Doctor of Philosophy and
for the diploma of Imperial College

Strength of Materials Section
Department of Mechanical Engineering
Imperial College of Science, Technology and Medicine
Exhibition Road, London SW7 2BX

1999

Abstract

Epoxy polymers are widely used as adhesives and as matrix materials in composites. Their major disadvantage, inherent brittleness, has been overcome by introducing a secondary phase into the matrix. Among the materials used for the secondary phase, rubber particles in particular have been very successful in improving their fracture toughness.

The static fracture behaviour of rubber modified epoxy polymers has been investigated by many researchers. The main toughening mechanisms are considered to be shear yielding and plastic void growth, which follows the cavitation of the particles. However, there are relatively few studies concerning the fatigue behaviour of such materials, although such behaviour is important in many applications. The main aims of the present research are, therefore, to gain a much better understanding of the toughening mechanisms in fatigue fracture, and to develop a quantitative model to describe the fatigue behaviour. Apart from rubber toughened epoxy polymers, such materials modified with thermoplastic toughners have also been studied.

Fracture mechanics tests were conducted using a range of rubber modified epoxies to study the fatigue behaviour. Fractographic studies were employed to investigate the toughening mechanisms. The experimental results show that a high static toughness does not guarantee good fatigue resistance, especially when the fatigue applied load is relatively low. This observation arises because the toughening mechanisms initiated by rubber particles can not operate effectively under such conditions. It is also revealed that the material which has relatively small rubber particles has the better fatigue resistance. Indeed, the critical value of stress intensity factor at which the toughening mechanisms become active is closely related to the particle size.

A model of the toughening mechanisms in fatigue conditions was also developed, and the energy dissipated by each mechanism was calculated. The modelling results indicate that shear yielding is the dominant toughening mechanism, and that the contribution from plastic void growth increases as the value of K_{max}, the maximum value of the stress intensity factor, in the fatigue increases. The rubber bridging mechanism plays a relatively minor role, especially for the material which possesses a relatively large ductility.

To my parents, my wife Rieko

and my children Yutaro and Marina

Acknowledgements

The present work was sponsored by Bridgestone Corporation, Japan.

I would like to thank my supervisor Professor Anthony Kinloch for his advice throughout.

I would express my gratitude to my colleagues at Imperial College, especially Ambrose Taylor, Bamber Blackman, Homayoun Hadavinia and Matthew Little. I would also like to thank Hugh MacGillivray, Pat Pathak, Peter Savage, Nick Tailor and Les Morris for their assitance with the test equipment.

I would also like to acknowledge the support and assistance of Graham Tudgey at DERA, Farnborough.

Special thanks go to my family and friends for their encouragement and support throughout.

Contents

Title Page 1

Abstract 2

Dedication 3

Acknowledgements 4

Contents 5

List of Symbols 10

Abbreviations 14

Chapter One : Introduction and Aims 15

Chapter Two : Literature Survey 17

2.1 Introduction 17

2.2 Linear elastic fracture mechanics 17

2.2.1 Energy balance approach 17

2.2.2 Stress intensity factor approach 18

2.2.3 Relationship between G_c and K_c 19

2.2.4 Crack tip plasticity 20

2.3 Deformation behaviour of polymers 22

2.3.1 Cavitation of rubbery materials 22

2.3.2 Yielding in polymers 24

2.3.2.1 Deformation of yielding 24

2.3.2.2 Viscoelastic effects on yielding 25

2.3.2.3 Yield criteria 27

2.3.3 Inhomogeneous deformation 28

2.3.3.1 Various inhomogeneous deformations 29

2.3.3.2 Shear bands in glassy polymers 30

2.3.4 Shera yielding and fracture behaviour 32
2.4 Rubber modified epoxy polymers 34
2.4.1 Chemistry and microstructure 35
2.4.2 Toughening mechanisms 36
2.4.3 Shear yielding 38
2.4.4 Cavitation, debonding and void growth 40
2.4.5 Rubber bridging 42
2.4.6 Relationship between microstructure and static fracture behaviour 43
2.4.6.1 Effect of crosslink density 43
2.4.6.2 Effect of volume fraction of rubber 47
2.4.6.3 Effect of particle size 51
2.4.6.4 Effect of interfacial particle-to-particle distance 53
2.4.6.5 Effect of adhesion between matrix and particles 55
2.5 Fatigue behaviour 56
2.5.1 Crack propagation 57
2.5.2 Effects of experimental parameters 60
2.5.2.1 Effect of frequency 60
2.5.2.2 Effect of temperature 64
2.5.2.3 Effect of mean stress and stress ratio 65
2.5.3 Effects of material properties 68
2.5.3.1 Effect of crosslink density 68
2.5.3.2 Effect of morphology 70
2.6 Concluding remarks 72

Chapter Three : Materials and Experimental Techniques 73
3.1 Introduction 73
3.2 Materials 73
3.3 Fracture toughness measurements 76
3.4 Modulus measurements 77
3.5 DSC and DMTA studies 78
3.6 Fatigue crack growth rate studies 80
3.7 Localised heating effects 82
3.8 Microscopy studies 83
3.9 Image analysis studies 85
3.10 Concluding remarks 86

Chapter Four : Basic Material Properties 87
4.1 Introduction 87
4.2 Microstructure 87
4.2.1 RME series and RME with BPA added series 87
4.2.2 TPME series 92
4.3 Glass transition temperature 94
4.3.1 Rubber modified epoxies 94
4.3.2 Thermoplastic modified epoxies 94
4.4 Molecular weight between crosslinks 96
4.5 Mechanical properties 100
4.5.1 Rubber modified epoxies 100
4.5.1.1 Effect of volume fraction of rubber 101
4.5.1.2 Effest of crosslink density 103
4.5.2 Thermoplastic modified epoxies 106
4.6 Concluding remarks 108

Chapter Five : Fatigue Crack Propagation in Rubber Modified Epoxies 109
5.1 Introduction 109
5.2 Effect of crosslink density 110
5.2.1 Introduction 110
5.2.2 Experimental results 110
5.2.3 Values of ΔK and K_{max} and M_c values 116
5.2.4 Values of K_{th} and M_c values 122
5.2.5 K_{th}/K_{Ic} plots and M_c values 123
5.3 Effect of rubber content 127
5.3.1 Introduction 127
5.3.2 The materials cured at 160°C 127
5.3.3 The materials cured at 120°C 131
5.3.4 Discussion 134
5.4 K-transition value 142
5.5 Effect of particle size 147
5.5.1 Introduction 147
5.5.2 5phrRME120 and 5phrRME120+BPA 149
5.5.3 Interpretation of the experimental results 152
5.5.4 5phrRME120 and 15phrRME120 155
5.6 Localised heating effects 158

5.7 Concluding remarks 160

Chapter Six : Fractographic Studies
and Rubber Toughening Mechanisms 162
6.1 Introduction 162
6.2 Static fracture 162
6.2.1 SEM observations 162
6.2.2 Volume fraction of void 168
6.2.3 TOM observations 169
6.2.4 TEM observations 174
6.3 Fatigue fracture 177
6.3.1 SEM observations 177
6.3.1.1 15phrRME160 177
6.3.1.2 15phrRME120 179
6.3.1.3 5phrRME120 and 5phrRME120+BPA 182
6.3.2 TOM observations 185
6.3.3 TEM observations 189
6.4 Concluding remarks 192

Chapter Seven : Modelling of Rubber Toughening Mechanisms 193
7.1 Introduction 193
7.2 Development of the theoretical model 194
7.3 The size of the plastic zone 195
7.4 The contribution of shear yielding 198
7.5 The contribution of void growth 204
7.6 The contribution of rubber bridging 206
7.7 The contribution of unmodified epoxy 208
7.8 Application of the theoretical model 210
7.8.1 15phrRME160 211
7.8.2 15phrRME120 214
7.9 Modification of the theoretical model 216
7.10 Application of the modified theoretical model 218
7.10.1 15phrRME160 218
7.10.2 15phrRME120 220
7.11 Concluding remarks 223

Chapter Eight : Fatigue Behaviour of Thermoplastic Modified Epoxies 224
8.1 Introduction 224
8.2 Effect of microstructure 225
8.2.1 Particulate microstructure 225
8.2.2 Co-continuous microstructure 228
8.2.3 Phase-inverted microstructure 231
8.2.4 Summary of the effect of microstructure 234
8.3 Thermoplactic modified epoxies and rubber modified epoxies 237
8.4 Concluding remarks 241

Chapter Nine : Conclusions 242

Chapter Ten : Recommendations for Future Work 246

Appendix A : Effect of the Addition of Bisphenol-A 248

Appendix B : Energy Density and Dissipated Energy 250

References 252

List of Symbols

English Alphabet

a	crack length
a_{eff}	effective crack length
A_E	constant
B	sample thickness
C	compliance
da/dN	fatigue crack growth rate
d_p	interfacial particle-to-particle distance
E	Young's modulus
E_r	rubbery equilibrium modulus
$f(r_y)$	scaling factor for shear band
$f_r(da/dN)$	scaling factor for the rubber bridging mechanism
$f_u(da/dN)$	scaling factor for the contribution of the unmodified epoxy
G	energy relearse rate
G_0	energy dissipation originated from the unmodified epoxy
G_c	fracture energy (critical energy release rate)
G_{Ic}	fracture energy (critical energy release rate) in mode I
G_{Icu}	G_{Ic} value of the unmodified epoxy
G_{IIc}	fracture energy (critical energy release rate) in mode II
G_{IIIc}	fracture energy (critical energy release rate) in mode III
G_{calc}	G value calculated via the theoretical model
G_r	shear modulus of rubber
G_{th}	threshold value of G
K	stress intensity factor
K_c	fracture toughenss (critical stress intensity factor)
K_{Ic}	fracture toughenss (critical stress intensity factor) in mode I
K_{Icu}	K_{Ic} value of the unmodified epoxy
K_{IIc}	fracture toughenss (critical stress intensity factor) in mode II
K_{IIIc}	fracture toughenss (critical stress intensity factor) in mode III
K_{calc}	K value calculated via the theoretical model
K_{max}	maximum stress intensity factor

K_{mean}	mean stress intensity factor
K_{min}	minimum stress intensity factor
K_Q	provisional fracture toughenss
K_r	bulk modulus of rubber
K_T	K transition value
K_{th}	threshold value of K
K_{vm}	von Mises stress concentration factor
M_c	average molecular weight between crosslinks
p	hydrostatic stress
p_c	critical value of p
P	load
P_c	critical load for crack propagation
P_{max}	maximum load
P_{min}	minimum load
r_0	defect radius
r_b	birefringent zone size
r_p	particle radius
r_y	plastic zone radius
r_{yu}	plastic zone radius for the unmodified epoxy
R	stress ratio
S(r)	intersection of shear band
T	temperature
T_g	glass transition temperature
u	displacement
U	potential energy
$U_s(r)$	energy density of the shear yielding mechanism
$U_v(r)$	energy density of the void growth mechanism
v^*	activation volume
V_f	volume fraction
V_{fr}	volume fraction of rubber
$V_{fs}(r)$	volume fraction of the shear yielded matrix
$V_{fv}(r)$	volume fraction of void
V_{fv0}	volume fraction of void at the crack surface
$V_s(r)$	volume of shear band per particle
W	sample width
$W_s(r)$	shear plastic strain energy density

Y	geometry factor
ΔE^*	activation energy
ΔG	energy dissipation arising from toughening mechanisms
ΔG_r	energy dissipation arising from rubber bridging
ΔG_s	energy dissipation arising from shear yielding
ΔG_v	energy dissipation arising from void growth
ΔK	stress intensity factor range
ΔK_T	transition value of ΔK
ΔK_{th}	threshold value of ΔK
ΔP	load range
ΔV_r	volume strain in the rubber particle

Greek Alphabet

$\alpha(r)$	scaling factor for shear band
ε	strain
$\dot{\varepsilon}$	strain rate
γ	surface energy
γ_f	shear fracture strain
γ_p	extra surface energy arising from plastic deformation
λ_t	failure extension ratio
Γ_r	surface energy of rubber
μ_m	modification factor for the von Mises criterion
ν	Poisson's ratio
θ	volumeric strain
ρ	mass density
ρ_c	crack tip radius
σ	stress
σ_0	macroscopic stress (stress remote from crack tip)
σ_i	principle stress
σ_{ij}	component of stress tensor
σ_c	critical yield stress for multiphase polymers
σ_y	yield stress
σ_{yc}	compressive yield stress
σ_{yt}	tensile yield stress
σ_{yu}	yield stress for the unmodified epoxy
σ_{vm}	von Mises stress
τ_{oct}	octahedral shear stress
τ_T	Tresca yield stress
τ_{vm}	von Mises shear stress
τ_y	yield stress in pure shear
Ω	pressure activation volume

Abbreviations

ASTM	American Society for Testing Materials
ATBN	amino-ternimated butadiene acrylonitrile
BPA	bisphenol-A
CT	compact tension
CTB	carboxyl-ternimated butadiene
CTBN	carboxyl-ternimated butadiene acrylonitrile
DDS	4,4'-diamino diphenyl sulphone
DGEBA	giglycidyl ether of bisphenol-A
DMTA	dynamic mechanical thermal analysis
DSC	differential scanning calorimetry
ETBN	epoxy-ternimated butadiene acrylonitrile
FEA	finite element analysis
HLP	hollow latex particle
HTBN	hydroxyl-ternimated butadiene acrylonitrile
LEFM	linear elastic fracture mechanics
MBS	methacrylated butadiene styrene
PC	polycarbonate
PES	polyethersulphone
PMMA	polymethylmethactylate
PS	polystyrene
PVC	polyvinylchloride
PVDF	polyvinylidenefluoride
RME	rubber modified epoxy
SEM	scanning electron microscopy
TEM	transmission electron microscopy
TGDDM	tetrablycidyl 4,4'-diamino diphenyl methane
TOM	transmission optical microscopy
TPME	thermoplastic modified epoxy
UME	unmodified epoxy
VTBN	vinyl-ternimated butadiene acrylonitrile
WLF	William-Landel-Ferry

Chapter One

Introduction and Aims

In recent years, epoxy polymers have been extensively used as adhesives and matrix materials in composites in a multitude of applications. Their use has broadened due to their excellent properties, such as high strength, high modulus, high glass transition temperature, good creep resistance, etc. They, however, do have major disadvantages for many applications. That is, they are inherently brittle and possess a poor resistance to fracture. Many workers have made efforts to improve their fracture toughness in order to overcome these disadvantages. Such improvements, without losing their other outstanding properties, have been achieved by introducing a secondary phase into the epoxy matrix. Rubber particles, hard particles such as glass spheres, thermoplastic particles, short fibres, etc. are commonly used as materials for the secondary phase. Of these materials, the introduction of rubber particles has been the most successful.

The use of rubber particles was reported first in the 1970's. Since then, many researchers have studied the fracture processes and the toughening mechanisms of the rubber modified epoxies [1-11]. The effects of the material properties on the fracture behaviour have also been investigated. However, most of the previous research has, however, concentrated on studying the fracture behaviour under monotonic loading (termed "static") conditions, and there have been relatively few studies concerning the fatigue fracture of the rubber modified epoxy polymers.

Recently, the fatigue behaviour of rubber modified epoxy polymers has been investigated by some researchers [12-16], and it has been suggested that there were some discrepancies in the fracture behaviour between the static and fatigue fracture. However, these investigations of the fatigue of rubber modified epoxy polymers focused on the fatigue crack propagation behaviour in a relatively high crack growth rate region. Furthermore, the toughening mechanisms in fatigue conditions have not been studied in any detail. Research on the toughening mechanisms in a relatively low crack growth rate region is of significant

importance, because the fatigue behaviour near any threshold value of the applied cyclic load (where below a threshold load no fatigue crack growth is observed) will have a great influence on the fatigue life of the materials.

The aims of the present study are therefore:

(1) To investigate the fatigue behaviour of rubber modified epoxy polymers over the complete range of fatigue crack propagation rates.

(2) To identify the toughening mechanisms of the rubber modified epoxies in fatigue fracture.

(3) To elucidate the effects of the microstructure of the polymer on the fatigue behaviour of rubber modified epoxies.

(4) To develop a quantitative model of the toughening mechanisms and calculate the energy dissipation caused by each toughening mechanism in fatigue fracture of rubber modified epoxies.

Chapter Two

Literature Survey

2.1 Introduction

Before proceeding with the investigations outlined in Chapter One, it is essential to have a clear understanding about the basic principles involved in the present study. The current Chapter serves this purpose by reviewing previous work on the relevant subjects.

A brief introduction to linear elastic fracture mechanics (LEFM) is presented, since it is an important tool in studying the fracture properties of materials. In the following section, the toughening mechanisms of rubber modified polymers, such as shear yielding, cavitation, rubber bridging, etc. are reviewed. The next section summarises the fatigue behaviour of polymers and rubber modified epoxies, including the effects of experimental parameters and material properties, such as frequency, stress ratio, crosslink density, etc.

2.2 Linear elastic fracture mechanics

The history of fracture mechanics can be dated back to 1920's when Griffith [17] first recognised that the strength of any real solid is governed by the distribution of flaws and that failure occurs at the largest of them. This hypothesis was the origin of the later developments of fracture mechanics.

2.2.1 Energy balance approach

Griffith concluded that the energy criterion for fracture is given by:

$$-\delta U/B\delta a > 2\gamma \qquad (2.1)$$

where U is the potential energy stored in the sample, B is the sample thickness, a

is the crack length, γ is the surface energy. The above criterion means that fracture occurs when the energy change per unit crack propagation is greater than the surface energy.

However, experimental results showed that the required energy was much larger than surface energy, due to the existence of plastic deformation. Thus, Orowan [18] and Irwin [19] suggested that the criterion should be modified as follows:

$$G > 2\gamma + \gamma_p \tag{2.2}$$

γ_p is the extra surface energy term arising from plastic deformation around the crack tip. This modification introduced the idea of G_c, which includes all the energy dissipation through plastic deformation in the vicinity of the crack tip. Generally, the criterion for crack growth can be proposed as:

$$G > G_c \tag{2.3}$$

If the material is linear elastic, G_c can be expressed as:

$$G_c = (P_c^2/2B)\delta C/\delta a \tag{2.4}$$

where P_c is the critical load for crack propagation, and C is the compliance of the specimen which can be defined as:

$$C = u/P \tag{2.5}$$

where u is the displacement in load direction, and P is the applied load.

2.2.2 Stress-intensity factor approach

Another approach is available in the case of linear elasticity. Irwin introduced the concept of the stress-intensity factor, K, to characterise the stress field in the vicinity of the crack tip. This concept indicates that the stress, $\sigma(r,\theta)$, near the crack tip is given by the following equations:

$$\sigma(r,\theta)=1/(2\pi r)^{1/2}\cdot f(\theta)\cdot K \quad (2.6)$$

$$K=Y\sigma_0 a^{1/2} \quad (2.7)$$

where r,θ are the polar co-ordinates from the crack tip and σ_0 is the remote stress, Y is the shape factor and is a function of sample geometry and crack length.

K is the stress intensity factor and a single parameter which completely specifies the stress field in the vicinity of the crack tip. The fracture criterion can be depicted as the following:

$$K>K_c \quad (2.8)$$

Thus, fracture occurs when K reaches a critical value, K_c. The value of K_c for a material is a material property and is often referred as the fracture toughness of the material or the stress intensity at the onset of crack propagation.

2.2.3 Relationship between G_c and K_c

Under the condition of linear elastic fracture mechanics, G_c and K_c are interchangeable and the relationships between G_c and K_c vary depending upon the loading mode and stress condition. There are three basic modes :

Tensile-opening mode (Mode I)
Inplane-shear mode (Mode II)
Antiplane-shear mode (Mode III)

as shown in Fig.2.1. Among them, the Mode I is technically the most important since it is the most commonly encountered and usually the one which most often results in failure. For Mode I, G_c and K_c can be connected by the following equations:

$$G_{Ic}=K_{Ic}^2/E \quad \text{(plane stress condition)} \quad (2.9)$$

$$G_{Ic}=K_{Ic}^2(1-\nu^2)/E \quad \text{(plane strain condition)} \quad (2.10)$$

where E is the modulus, ν is the Poisson ratio. The general relationship between G_c and K_c can be expressed as:

$$G_c=K_{Ic}^2/E+K_{IIc}^2/E+K_{IIIc}^2(1+\nu)/E \quad \text{(plane stress)} \tag{2.11}$$

$$G_c=K_{Ic}^2(1-\nu^2)/E+K_{IIc}^2(1-\nu^2)/E+K_{IIIc}^2(1+\nu)/E \quad \text{(plane strain)} \tag{2.12}$$

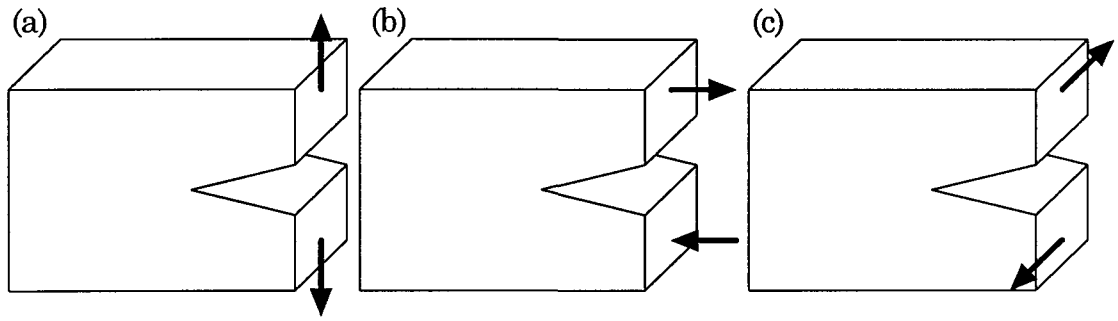


Fig.2.1 Three loading modes : (a) Tensile-opening mode (Mode I), (b) Inplane-shear mode (Mode II), (c) Antiplane-shear mode (Mode III)

2.2.4 Crack tip plasticity

Linear elastic fracture mechanics (LEFM) assumes that the bulk of the material is elastically loaded, i.e. there is negligible plastic deformation of the bulk material. However, as seen in equation 2.6, the local stress tends to infinity as the distance ahead of the crack tip tends to zero. Consequently for metallic and polymeric materials, the stress immediately ahead of the crack tip exceeds the yield stress of the material and a local region of plasticity, i.e. a plastic zone, develops.

It is often assumed that the plastic zone is circular in shape [20]. The radius of the plastic zone, r_y, is given by :

$$r_y=(K/\sigma_y)^2/2\pi \quad \text{(plane stress)} \tag{2.13}$$

$$r_y=(K/\sigma_y)^2/6\pi \quad \text{(plane strain)} \tag{2.14}$$

where σ_y is the yield stress. Therefore, if a sample is thick enough to ensure a plane strain condition, the size of plastic zone changes gradually through the thickness of the sample, as shown in Fig.2.2.

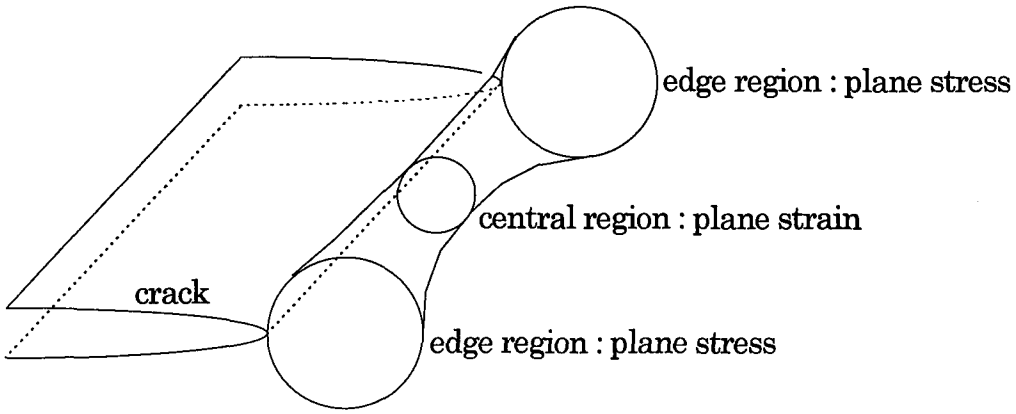


Fig.2.2 The change in plastic zone through the specimen thickness

The stress distribution inside the plastic zone is schematically depicted as Fig.2.3.

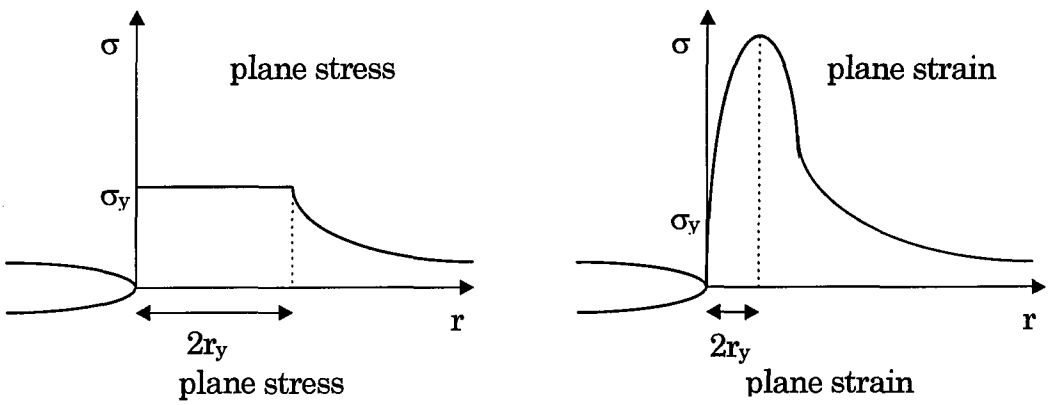


Fig.2.3 Schematic graph of the stress distribution

In the presence of crack tip plasticity, the stress field can be more accurately characterised by considering an effective crack length, a_{eff}, such that:

$$a_{eff} = a + r_y \tag{2.15}$$

$$K = Y\sigma_0(a + r_y)^{1/2} \tag{2.16}$$

This means that we can consider the stress distribution is shifted in the direction of the crack propagation by a length of r_y, due to the presence of the plastic zone.

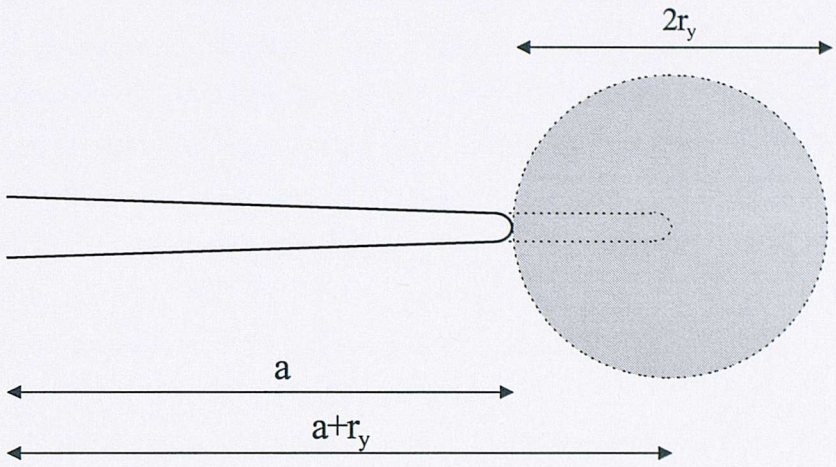


Fig.2.4 Schematic image of effective crack length

2.3 Deformation behaviour of polymers

The deformation of a material may be classified as elastic or elastic-plastic, if there is no time dependence. The simplest deformation is a linear elastic one, which is described by Hooke's law and does not dissipate any energy. For most polymers, because elastic deformation only occurs within a very small strain range, there usually exists irreversible plastic deformation. Hence, polymers normally dissipate energy during the loading cycle. In the deformation of rubber modified epoxies, cavitation of rubber particles and shear yielding of the epoxy matrix play an important role in the energy dissipation process.

2.3.1 Cavitation of rubbery materials

Under triaxial stresses, such as exist near a crack tip in plane strain conditions, microvoids initiate inside the rubbery material. If this occurs in the rubber particles of the toughened epoxies, it is observed as a cavitation of the particles. Gent and co-workers [21-23] suggested a simple model to describe the growth of a spherical microvoid in rubbery materials, and established the following relationships:

$$p/E = (5-4\lambda^{-1}-\lambda^{-4})/6 \qquad (2.17)$$

$$\lambda = r/r_0 \qquad (2.18)$$

where p is the inflating pressure, E is the Young's modulus, r_0 is the initial radius of microvoid, and r is the radius of inflated microvoid. This model indicates that the microvoid will expand infinitely at a critical pressure of 5E/6. Practically, a microvoid does not usually enlarge infinitely, but just a small, but visible, void is formed. Therefore, the critical pressure for crack initiation or void formation, p_c, is given by the following equation:

$$p_c = 5E/6 \tag{2.19}$$

Later, it was found that when the volume under the dilatational stress, $p=(\sigma_{11}+\sigma_{22}+\sigma_{33})/3$, is small, the critical pressure for crack initiation is much larger than the predicted value given by equation 2.19. This was considered due to the extra effect of surface energy, and Gent and Tompkins [24] modified the criteria as given by the following equation:

$$p_c = 5E/6 + 2\gamma/r_0 \tag{2.20}$$

where γ is the surface energy. This implies that the second term, i.e. the surface energy term, is dominant when the size of microvoid is relatively small.

It should be noted that these models were derived from the assumption of elastic instability. There exists a region where these models can not apply. For instance, if the microvoid is rather small, we have to take into account the stiffening of the rubber under high strain. If the microvoid is large, the degree of inflation, λ, is so small and the critical pressure, $p_c = 5E/6$, can not derived from equation 2.17.

The above model assumes the presence of a microvoid, and the size of the rubbery material is not mentioned. In order to evaluate the influence of the particle size on the cavitation process, Bucknall et al. [25, 26] theoretically investigated the initiation of a microvoid in dispersed rubber particles. They calculated the energy, U(r), of the rubber particle which contains a small void, including the surface energy. It is given by :

$$U(r) = \frac{2}{3}\pi r_p^3 K_r (\Delta V_r - r^3/r_p^3)^2 + 4\pi r^2 \Gamma_r + 2\pi r^3 G_r F(\lambda_f) \tag{2.21}$$

where r is radius of the hole formed at the centre of a rubber particle, r_p is radius of a rubber particle, G_r is the shear modulus of the rubber, K_r is the bulk modulus of the rubber, ΔV_r is the volume strain in the rubber particle, Γ_r is surface energy of the rubber, and the function $F(\lambda_f)$ is dependent on the failure strain of the rubber, λ_f, under biaxial stretching conditions. According to this model, a rubber particle having a relatively low shear modulus, G_r, forms a microvoid, an order of 10^{-8}m, at less volume strain. Once a microvoid forms, the particle's resistance to further dilatation is drastically reduced, and a microvoid may turn into a void. This model also predicts that the rubber particle becomes more difficult to cavitate on increased crosslinking or on cooling into the region of T_g, because of the associated increase in G_r. It also suggests that the largest particles will cavitate first.

2.3.2 Yielding in polymers

Yielding is a common phenomenon in the deformation of most materials, including polymers. Some general aspects of the yield behaviour of polymers are briefly reviewed in this section.

2.3.2.1 Definition of yielding

Yielding may be defined as the deformation which involves a permanent, irreversible, strain. When the applied stress reaches to a certain level, the material starts yielding, and after the yielding, it maintains a strain even when the stress returns to zero. This definition can be applied to both metals and polymers, but the details are rather more complicated for polymeric materials. One reason for this is the time dependency. As polymers show a relatively large time dependence in their material properties, their yielding points vary with the testing rate and test temperature. Another reason is the phenomenon that almost all the plastic deformation is recoverable in glassy polymers when the material is heated above its glass transition temperature, T_g.

A typical stress-strain curve is shown in Fig.2.5. As shown in Fig.2.5, there are two different yielding points, "intrinsic" and "extrinsic" yield points. The "intrinsic" yield point is the maximum point in the stress-strain curve. We normally use this stress value as a yield stress. It is a material property and independent of the test geometry. The "extrinsic" yield point can be defined as a

tangent to the curve through the point on the abscissa where nominal strain equals to -1. In the case of a tensile test, the deformation becomes unstable from this point, and a necking starts. It is called the "extrinsic" yield point because of its geometry dependency. After yielding, strain-softening occurs in most cases, and then strain-hardening follows. Strain-softening is an important phenomenon for the formation of shear bands, which is closely related to toughening mechanisms.

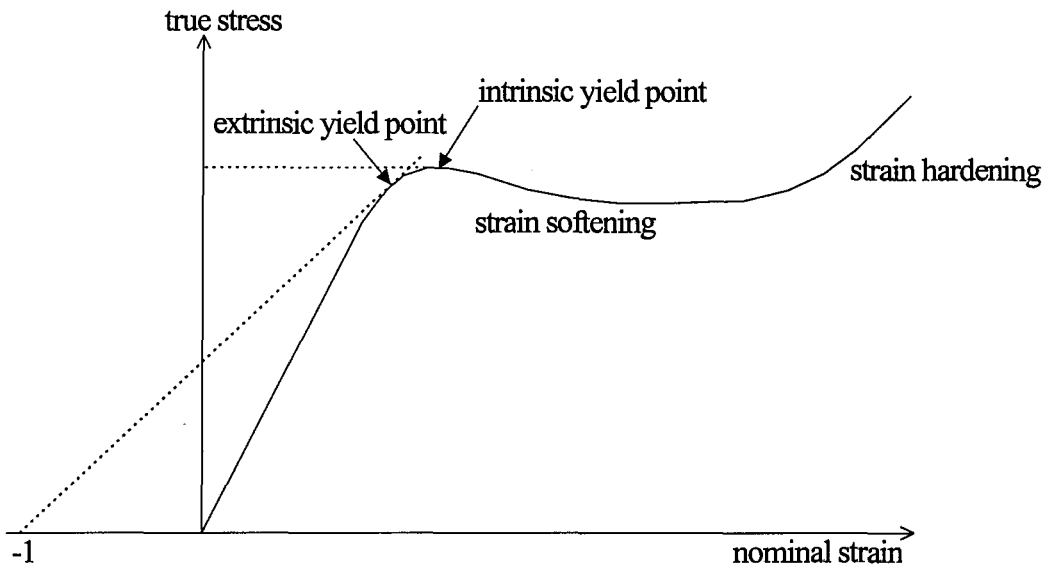


Fig.2.5 Schematic drawing of a typical stress-strain curve

Plastic deformation of the material which arises from strain-softening is basically categorised in two groups, shear yielding and crazing. Shear yielding occurs essentially at constant volume whereas crazing occurs with an increase in volume. Mathematically speaking, shear yielding is mainly related to the deviatoric component of the stress tensor, and crazing is related to the dilatational component. For epoxy polymers, crazing does not occur due to the crosslinks. The micromechanisms involved in shear yielding will be discussed later in detail.

2.3.2.2 Viscoelastic effects on yielding

The yield behaviour of polymers is strongly dependent on the temperature and the strain rate, due to their viscoelasticity. Generally, the yield stress

decreases as temperature increases, and the yield stress increases as the strain rate increases. The Eyring theory [27] gives the relationship between the yield stress and the strain rate as:

$$|\sigma_y|/T = \Delta E^*/v^*T + (R/v^*)\ln(\dot{\varepsilon}/A_E) \qquad (2.22)$$

where ΔE^* is the activation energy, v^* is the activation volume, R is the gas constant, $\dot{\varepsilon}$ is the strain rate and A_E is a constant. This suggests that a plot of σ_y/T versus log $\dot{\varepsilon}$ should give a set of parallel lines for different temperatures, as shown in Fig.2.6 [28].

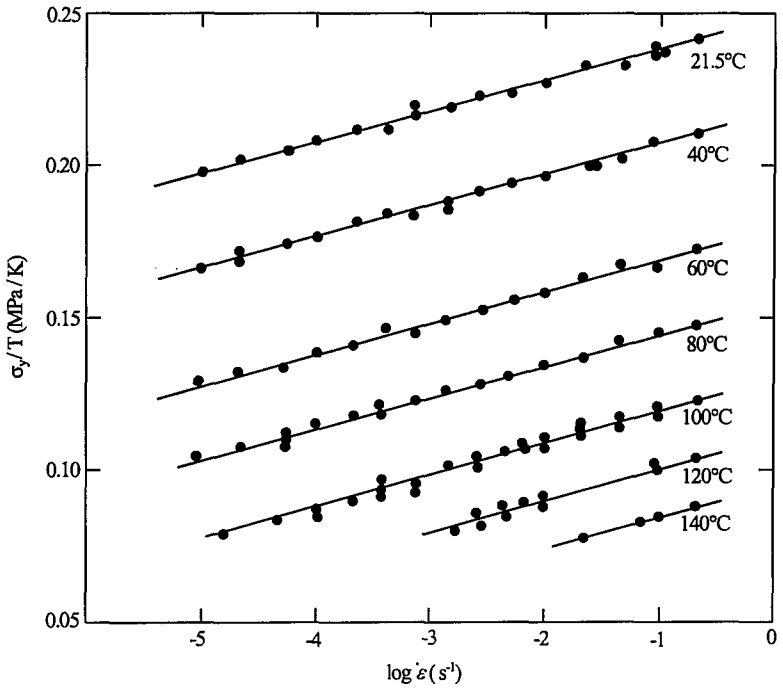


Fig.2.6 σ_y/T plotted against log($\dot{\varepsilon}$) for polycarbonate (from ref. [28])

However, it was found that equation 2.22 was inadequate to fully describe the yield behaviour. This led to a modification of the theory, and a simple modification of the Eyring model was suggested to include the effect of the hydrostatic stress. The modified equation is given by Ward and co-workers [29-31] as the following equation:

$$|\sigma_y|/T = \Delta E^*/v^*T - p\Omega/v^*T + (R/v^*)\ln(\dot{\varepsilon}/A_E) \qquad (2.23)$$

where

$$p = (\sigma_{11} + \sigma_{22} + \sigma_{33})/3 \tag{2.24}$$

and Ω is the pressure activation volume. This modification brought consistency to yield data in both tension and compression, and can model the effect of hydrostatic pressure.

2.3.2.3 Yield criteria

A yield criterion is a condition which must be satisfied by the applied stress tensor for yield to occur. The Tresca criterion is the simplest one which states that yield occurs when the maximum shear stress on any plane in the material reaches a critical value. It is given by:

$$|\sigma_1 - \sigma_3| = 2\tau_T = \sigma_y \tag{2.25}$$

where $\sigma_1 > \sigma_2 > \sigma_3$, and σ_1 , σ_2 and σ_3 are the principal stresses, and σ_y is the uniaxial yield stress. τ_T is the Tresca yield stress, which is usually taken as the yield stress of the material in pure shear, τ_y.

The von Mises criterion is expressed as:

$$(\sigma_1 - \sigma_2)^2 + (\sigma_2 - \sigma_3)^2 + (\sigma_3 - \sigma_1)^2 = 6\tau_{vm}^2 = 6\tau_y^2 = 2\sigma_{vm}^2 = 2\sigma_y^2 \tag{2.26}$$

where τ_{vm} is the von Mises shear stress. σ_{vm} is called the von Mises yield stress, and:

$$\sigma_{vm} = \{(\sigma_1 - \sigma_2)^2/2 + (\sigma_2 - \sigma_3)^2/2 + (\sigma_3 - \sigma_1)^2/2\}^{1/2} \tag{2.27}$$

Alternatively, it may be expressed in terms of the octahedral shear stress, τ_{oct}, as:

$$\tau_{oct} = \{(\sigma_1 - \sigma_2)^2 + (\sigma_2 - \sigma_3)^2 + (\sigma_3 - \sigma_1)^2\}^{1/2}/3 \tag{2.28}$$

where τ_{oct} is related to τ_{vm} and σ_{vm} by:

$$9\tau_{oct}^2 = 6\tau_{vm}^2 = 2\sigma_{vm}^2 \qquad (2.29)$$

For a Hookean material, this criterion is equivalent to stating that yield occurs when the elastic shear strain energy density reaches a critical value.

In both the Tresca and von Mises criteria the yield stress is independent of the hydrostatic component of the stress tensor. For polymers, however, the yield behaviour is strongly influenced by the hydrostatic pressure. For instance, the yield stress is higher in uniaxial compression than in tension, and the yield stress increases significantly with increasing hydrostatic pressure. To overcome this problem, Bowden [32] proposed a modified Tresca criterion which is pressure dependent. It is given by:

$$\tau_T = \tau_T^0 - \mu_T p \qquad (2.30)$$

where μ_T is a material constant, and p is hydrostatic component as shown by equation 2.24. τ_T^0 is the yield stress in pure shear, i.e. τ_y, since under this stress state the value of p is zero. The von Mises criterion may also be modified to incorporate the effect of hydrostatic pressure. Thus:

$$\tau_{vm} = \tau_{vm}^0 - \mu_{vm} p \qquad (2.31)$$

$$\tau_{oct} = \tau_{oct}^0 - (2/3)^{1/2}\mu_{vm} p \qquad (2.32)$$

As in the case of τ_T^0 in equation 2.30, τ_{vm}^0 is still the yield stress in pure shear.

2.3.3 Inhomogeneous deformation

Deformation in a material is often as homogeneous in nature, as in the above discussions. In many materials, however, plastic deformation does not always occur homogeneously, but instead, the plastic strain in some regions increases more rapidly than in the whole body. In some cases, plastic strain may occur only in certain localised regions. This inhomogeneous deformation occurs because homogeneous deformation has become unstable. This instability is caused by either geometrical effects or the material's intrinsic properties. Also, they may both act simultaneously to cause the instability.

2.3.3.1 Various inhomogeneous deformations

A common example of a geometrical instability is necking which can be observed in a specimen under a uniaxial tensile load. The instability occurs due to the stress concentration which is, for example, caused by a slight variation in the cross-sectional area. Then, yielding occurs locally at this point before the rest of sample. Once local yielding has initiated, further plastic deformation occurs preferentially at this location. Hence, the cross-sectional area will be reduced further, and a neck will develop.

A more fundamental reason for inhomogeneous deformation is strain softening. For the materials which strain soften, when the deformation reaches the yield point, further plastic deformation occurs easily. Therefore, if there is any small inhomogeneity of the local deformation, the region under the highest local strain firstly reaches the yield point and then plastically deforms further. In other words, if any small region is under a slightly higher strain than the rest of the material, this region will be softer locally and deform more easily than elsewhere. This local strain is getting higher until strain hardening starts in this region.

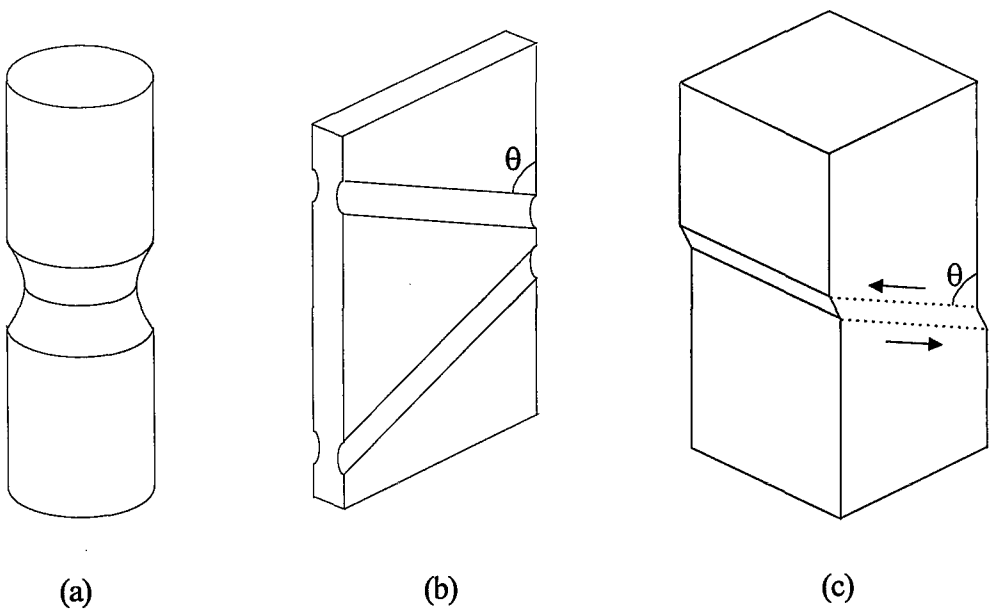


Fig.2.7 Types of inhomogeneous deformation; (a) without constraint, (b) constraint in one direction, (c) constraint in two directions [32]

The types of inhomogeneous deformation can be classified in terms of the dimensional constraint, as shown in Fig.2.7 [32]. The first case (Fig.2.7. (a)) is where there is no constraint. In this case, necking occurs under a tensile load. The main reason for this instability is the intrinsic strain softening of the material, as discussed above.

The second case (Fig.2.7 (b)) gives an example where there is constraint in one direction. It is an inclined neck which can form in a flat specimen under a uniaxial tensile load. If there is no volume change, the angle, θ, is 54.7°. However, it increases if the material dilates during plastic deformation.

The third case (Fig.2.7 (c)) is where the volume of material is constrained in two directions. This inhomogeneous deformation is quite important in the fracture process of polymers, because the material is constrained in two dimensions inside the body of a specimen, including the vicinity of crack tips. A simple shear deformation of a band, which is known as shear band, will form in a material in plain strain condition. The angle, θ, is 45° if there is no volume change. If the material dilates, volume expansion occurs normal to the plane of the band, then the angle,θ, becomes larger than 45°.

2.3.3.2 Shear bands in glassy polymers

Shear bands may form in a material which demonstrates strain softening, and all glassy polymers show this behaviour. Hence, they all possess a tendency to form shear bands. Typical shear bands are shown in Fig.2.8, which are observed under plane strain compression and viewed between cross polars.

The shear bands of polystyrene are sharply defined and have been termed microshear bands. On the contrary, the shear bands of polymethylmethacrylate, PMMA, are broad diffuse zones. Epoxy resin tends to form shear bands intermediate character between these extremes [1]. Bowden [33] suggested that this different character of shear bands comes from the difference in their propagation rate. It is controlled by the rate of strain softening and strain rate sensitivity of the yield stress. Bowden proposed a material parameter, e_{sb}, with the dimension of strain as given by :

$$e_{sb} = - \frac{[d\sigma / d(\ln \dot{\varepsilon})]_{\varepsilon}}{(d\sigma_y / d\varepsilon)_{\dot{\varepsilon}}} \qquad (2.33)$$

The parameter e_{sb} is an index of the character of the shear band. When the value of e_{sb} is small, the shear band is sharp. The shear band becomes wider and more diffuse as the value of e_{sb} increases.

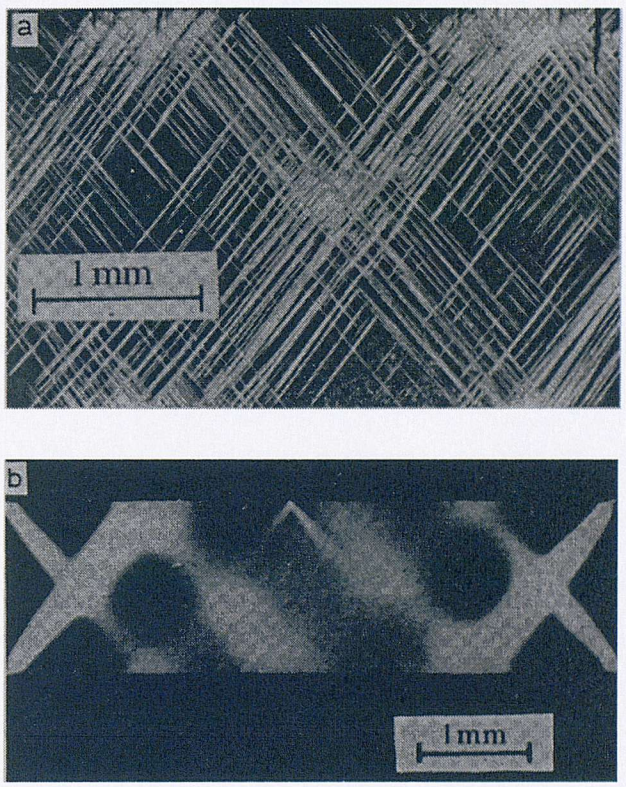


Fig.2.8 Typical examples of shear bands;(a) Polystyrene showing microshear bands; (b) PMMA showing broad diffuse zone [33]

Fig.2.9 shows the shear bands in epoxy resin under the plane strain compression. The angle which the shear bands make to the compression direction is somewhat smaller than 45°, i.e. the direction of maximum shear stress, as reported in other polymers. Bowden and Jukes [34] suggested that the deviation from the direction of maximum shear stress is due to a small volume change

during yielding, but the explanation for the deviation is still controversial.

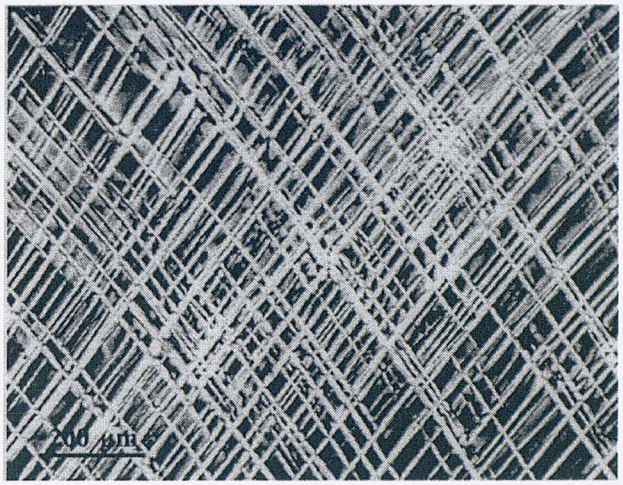


Fig.2.9 Shear bands in epoxy resin under the plane strain compression. The compression direction is vertical [35].

Wu and Li [36, 37] examined the relationships between the character of shear bands and the fracture behaviour. They suggested that when microshear bands propagated the overall plastic strain was small and the failure was brittle. On the other hand, when a diffuse shear zone was favoured, the overall plastic strain was large and the fracture behaviour was ductile.

2.3.4 Shear yielding and fracture behaviour

It is suggested that shear yielding plays an important role in the initiation of cracks in polymers. In the process of crack initiation, defects in the polymer, such as flaws, air bubbles or molecular inhomogeneities, act as stress concentrations and initiate microshear bands. Once shear bands are initiated, their intersection may cause further stress concentration. For example, if crazing is a micromechanism of failure, then an internal craze may be initiated at the maximum stress concentration, which will be a shear band intersection at the tip of the plastic zone. Finally, craze breakdown and crack initiation occur. If the failure micromechanism is shear yielding, as in crosslinked epoxies, then these

stress concentrations caused by the initial microshear bands may lead to voids which grows into intrinsic cracks or flaws.

Shear yielding mechanisms are also involved in the subsequent growth of cracks in polymers. When the shear yielding is highly localised about the crack tip, little viscoelastic and plastic energy is dissipated, and hence the fracture behaviour becomes brittle. On the other hand, when relatively homogeneous shear yielding occurs, this mechanism is associated with energy dissipation by the polymer deforming plastically prior to fracture, and hence the polymer exhibits a ductile fracture mode.

The plastic deformation that occurs around the crack effectively blunts the crack tip. The degree of crack tip blunting largely controls the mode of crack growth and the measured fracture toughness. Kinloch and Williams [38,39] have considered the elastic stress in the vicinity of crack tip, and quantified the effect of the crack tip blunting. They proposed the following relationship between the measured toughness and the crack tip radius:

$$\frac{K_{Ic}}{K_{Ics}} = \frac{(1+\rho_c/2c)^{3/2}}{1+\rho_c/c} \tag{2.34}$$

where K_{Ic} is measured stress intensity factor, K_{Ics} is stress intensity factor of a "sharp" crack, ρ_c is crack tip radius, and c is a critical distance which is a material property.

The relationship between K_{Ic}/K_{Ics} as a function of $(\rho_c/c)^{1/2}$ is shown in Fig.2.10. This figure shows that there is a slight drop in K_{Ic} for $\rho_c/c<3$, but for higher values of ρ_c/c the measured stress intensity factor increases as the crack tip radius increases. Although this model is based on linear elastic fracture mechanics, it is successful in providing a useful fracture criterion not only for brittle failure but for even quite ductile failure.

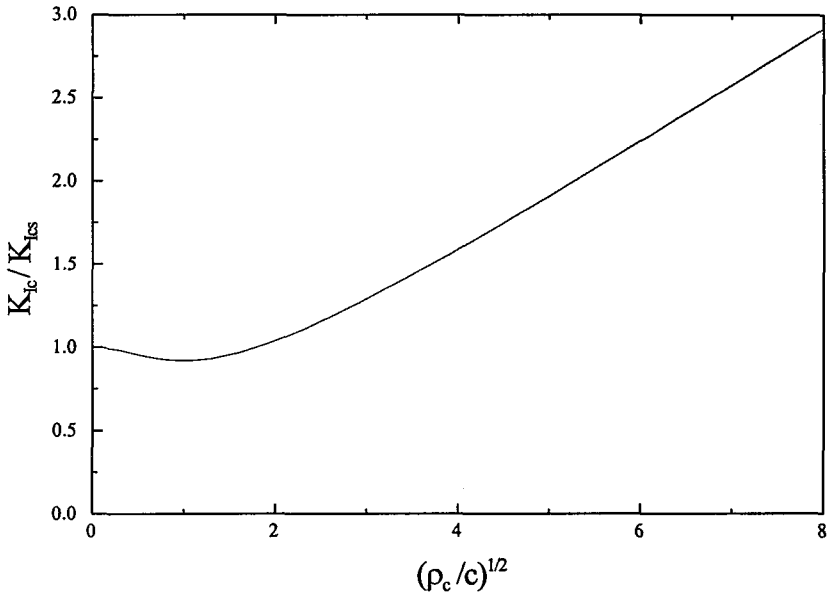


Fig.2.10 K_{Ic}/K_{Ics} as a function of the degree of crack tip blunting [1]

2.4 Rubber modified epoxy polymers

Many glassy polymers are susceptible to brittle fracture, because the energy absorbing processes such as crazing and shear yielding are highly localised in the vicinity of the crack tip. Although these processes involve large plastic strains and considerable local energy absorption, the volume where they are active is quite small compared to the size of the specimen. Thus, the total amount of absorbed plastic energy is low. In order to increase the toughness, it is necessary to increase the volume where the energy dissipating mechanisms occur. In the case of crosslinked epoxies which exhibit plastic shear yielding, it is possible to attain this goal via plasticisation of the polymer by a low molecular mass liquid. Plasticisation lowers the yield stress, and promotes ductile fracture. However, it also causes a significant reduction of the modulus, the strength and the glass transition temperature.

An alternative approach is to introduce a dispersed second phase into the matrix polymer in order to initiate localised energy absorbing processes from many sites, rather than a few isolated ones. This enables a much greater volume of the polymer to be involved in energy dissipation. Hence, the fracture toughness can be improved without a significant loss in other important material properties. One of

the most successful materials employing this approach is rubber modified epoxy .

Epoxy polymers are well known as crosslinked polymers, i.e. thermosets. They possess some outstanding material properties such as high modulus, high yield strength, high glass transition temperature, etc. All these properties can be attributed to their highly crosslinked structure. However, this structure also results in a very undesirable property, i.e. brittleness. A lot of effort has been made to overcome this disadvantage, and finally the improvement in fracture toughness was successfully achieved without any major loss in other properties by introducing a rubbery second phase. A brief review of rubber toughened epoxies will be given in the following section. Their toughening mechanisms and the typical fracture behaviour will be emphasised.

2.4.1 Chemistry and microstructure

The microstructure of rubber modified epoxies is dependent on the polymerisation chemistry of the starting reactants of epoxy resin, hardener and rubber [40]. Rubber modified epoxy polymers can be classified into three groups by the chemical properties of rubbery materials. In the first group, the rubbery material is initially miscible to epoxy resin. The preparation of such materials is started by mixing the rubber and epoxy resin. Then, the mixture is cured with hardener, the dispersed rubbery phase separates during the cure. In the second group, the rubbery material is immiscible in the epoxy resin. The rubber is dispersed by utilising a high shear/emulsification technique [41]. Thus, the rubber dispersions remains phase separated prior to and during the cure. The final group is the materials which contain relatively rigid rubbery particles, such as core-shell particles [42].

As discussed later in Chapter Three, the materials studied in the present investigation are categorised under the first group. The advantages of this group are that there is normally good bonding between the rubber particles and the matrix epoxy, and that the volume fraction and particle size of rubber can be varied easily. In the process of the preparation, the rubber is dissolved in the epoxy resin prior to the cure. If we discuss the process from the viewpoint of the free energy of mixing of the rubber/epoxy system, its free energy is initially negative. Then, during the cure, the free energy becomes positive with the increasing the

molecular weight of epoxy resin, and phase separation occurs [40].

Amongst the rubbers used, carboxyl-terminated butadiene acrylonitrile, CTBN, is most frequently used. The other rubbers used in toughened epoxies are amino-terminated butadiene acrylonitrile, ATBN [16], vinyl-terminated butadiene acrylonitrile, VTBN [16], epoxy-terminated butadiene acrylonitrile, ETBN [43], hydroxyl-terminated butadiene acrylonitrile, HTBN [44], etc. For the matrix epoxy resin, there are many kinds of materials. The choice is determined by the application.

2.4.2 Toughening mechanisms

For the rubber modified epoxy polymers, (i) cavitation (or debonding), (ii) plastic shear yielding and (iii) rubber bridging are suggested to be three main energy absorbing mechanisms. Of these, shear yielding is recognised to have the largest contribution for toughening for most glassy thermoset polymers, such as epoxies, polyesters, phenolics, etc. [1-7].

In the early days, crazing was proposed as a major toughening mechanism for rubber modified epoxy, due to the presence of the stress whitening zone with volume dilatation near the crack tip. Some researchers [45,46] considered that it was caused by crazing because shear yielding does not involve a significant volume change. However, no concrete evidence for crazing was observed. In the 1980's, Kinloch et al. [8,9] and Yee and Pearson [10,11] suggested that stress whitening was caused by the cavitation of rubber particles, and that cavitation and shear yielding were the main toughening mechanisms.

Recently, Huang et al. [7,47,48] suggested that both shear yielding and plastic void growth are the main toughening mechanisms for rubber modified epoxy. Generally, when a second phase is introduced into a matrix and there is a difference in the modulus between them, it will cause a stress concentration around the secondary phase. Thus, when a rubber modified epoxy is stressed, high stress concentrations occur around the particles dispersed in the matrix, due to the relatively low modulus of the rubber. This stress concentrations cause localised shear yielding around the rubber particles and shear bands are formed between the rubber particles as suggested by Kinloch et al. [8,9] and Yee and Pearson [10,11].

Stress concentrations also cause cavitation inside the rubber particles, or debonding between the particles and matrix when the interfacial adhesion is poor. Either cavitation or debonding creates "voids". Cavitation (or debonding) also relieves the triaxial constraints locally and "voids" can now further grow plastically in the yielded matrix to dissipate plastic energy [7]. If the triaxial constraints are not relieved, the rubber particles will be highly resistant to any volumetric deformation, due to their high bulk modulus. Thus, cavitation (or debonding) has a significant role in promoting plastic void growth, i.e. further plastic deformation of the matrix epoxy.

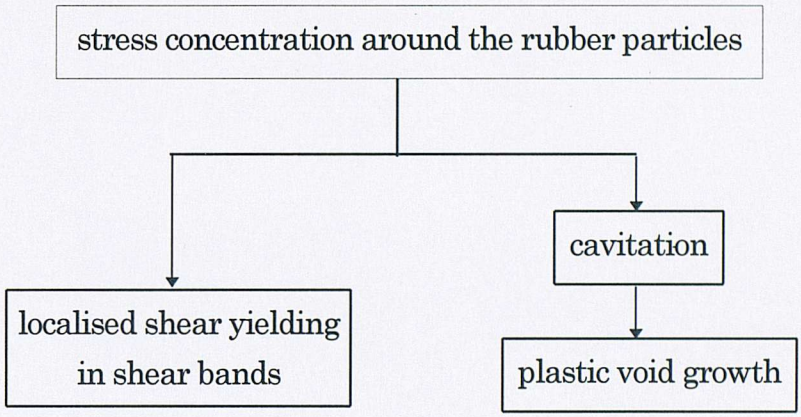


Fig.2.11 Flow chart of the toughening process

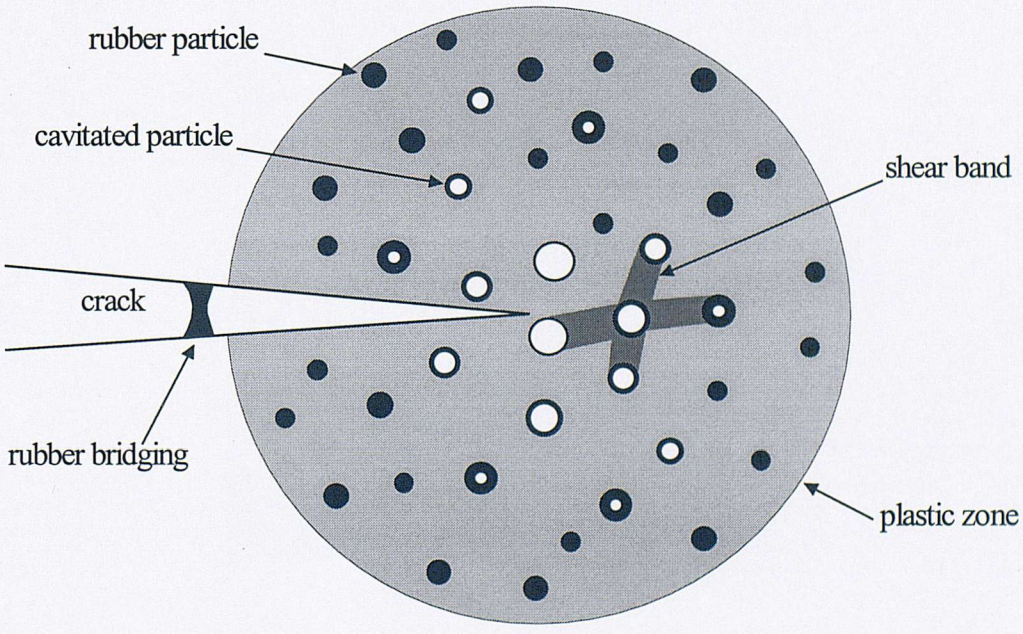


Fig.2.12 Schematic representation of toughening mechanism [7]

The above process can be summarised as shown in Fig.2.11 and Fig.2.12. The more quantitative details on these toughening mechanisms will be discussed in the following sections.

2.4.3 Shear yielding

Shear yielding is one of the main energy dissipating mechanisms of rubber modified epoxy polymers. The energy dissipated by this mechanism originates from the shear bands of matrix between the rubber particles. Huang [7] calculated the stress distribution between the rubber particles using FEA. He suggested that there is clearly a high stress region between the rubber particles, which corresponds to shear band, as shown in Fig.2.13.

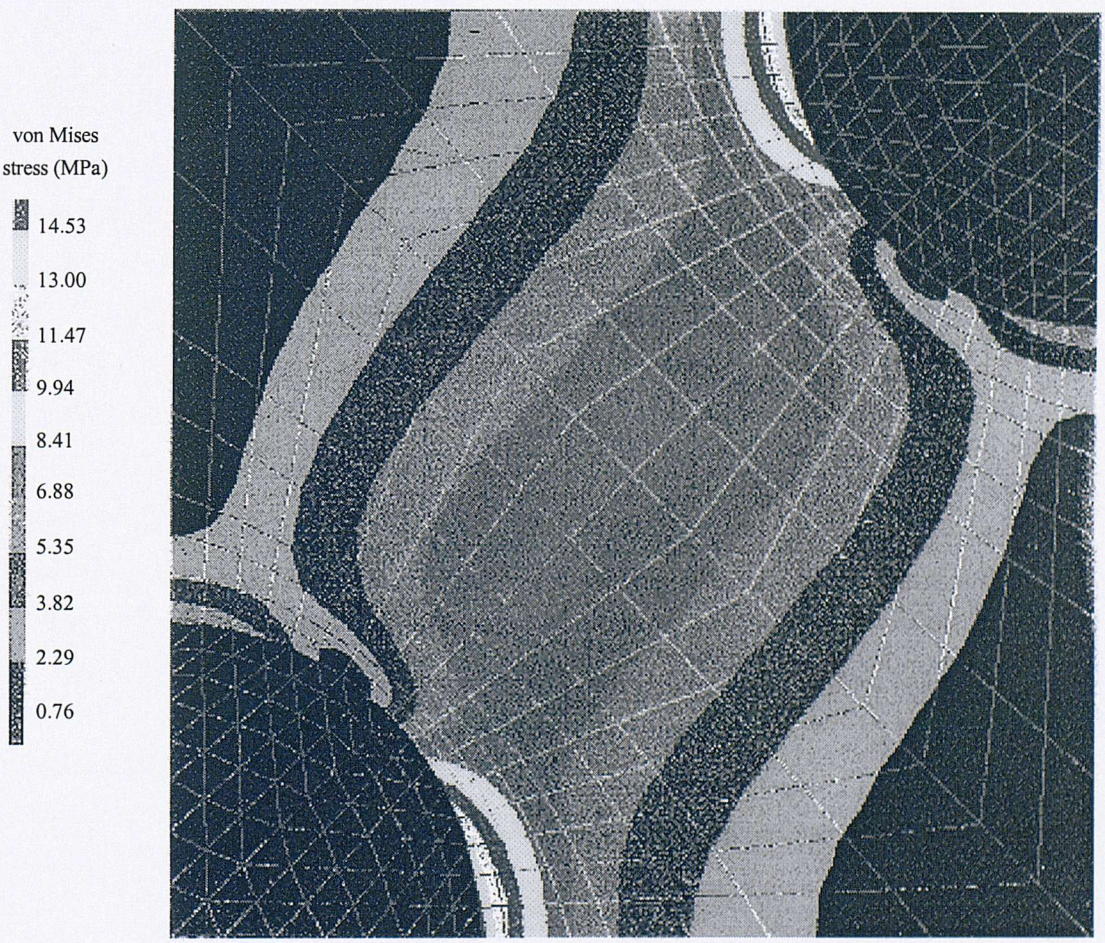


Fig.2.13 The distribution of σ_{vm} around rubber particles [7]

Some authors have estimated the contribution for fracture energy quantitatively [47-49]. Huang and Kinloch [48] calculated the fracture energy caused by shear yielding, ΔG_s. They considered that the value of ΔG_s could be calculated by integrating the energy density of the shear yielding mechanism, $U_s(r)$, over the plastic zone, as follows:

$$\Delta G_s = 2\int_0^{r_y} U_s(r)\, dr \qquad (2.35)$$

where r_y is the radius of the plastic zone, r is the distance from the crack tip. The energy density of the shear yielding mechanism, $U_s(r)$, is given by the product of the volume fraction of the shear yielded matrix material, $V_{fs}(r)$, and the shear plastic strain energy density, $W_s(r)$, as follows:

$$U_s(r) = V_{fs}(r)\, W_s(r) \qquad (2.36)$$

They assumed a simple cubic array of the rubber particles, and calculated the volume fraction of the shear yielded matrix material, $V_{fm}(r)$, as follows:

$$V_{fs}(r) = 0.5\, V_f\{3(4\pi/3V_f)^{1/3}\alpha(r) + 4[1-\alpha(r)]^{3/2} - 4\} \qquad (2.37)$$

where V_f is the volume fraction of rubber particles or voids ,and $\alpha(r)$ is the scaling factor of the shear bands. They considered that the size of the shear bands decreases with increasing the distance from the crack tip, and assumed the scaling factor, $\alpha(r)$, could be given by the following function:

$$\alpha(r) = 1 - r/r_y \qquad (2.38)$$

They also estimated the shear plastic strain energy density, $W_s(r)$, as follows:

$$W_s(r) = 0.5\sigma_{yc}\gamma_f\alpha(r) \qquad (2.39)$$

where σ_{yc} is the compressive yield stress of the matrix, and γ_f is the shear fracture strain of the matrix. By substituting equations 2.36, 2.37, 2.38 and 2.39 into 2.35, and expressing the plastic zone radius, r_y, using the plastic zone radius of the

unmodified epoxy, r_{yu}, they finally obtained the fracture energy caused by shear yielding, ΔG_s, as follows:

$$\Delta G_s=0.5(1+\mu_m/3^{1/2})^2[(4\pi/3V_f)^{1/3}-54/35]V_f\sigma_{yc}r_{yu}K_{vm}^2 \quad (2.40)$$

$$K_{vm}=\sigma_{yu}/\sigma_c \quad (2.41)$$

where r_{yu} is the plastic zone radius for the unmodified epoxy. μ_m is a material constant in the following equation:

$$\tau_{vm}=\tau_y-\mu_m p \quad (2.42)$$

where τ_{vm} is the von Mises shear stress, τ_y is the yield stress under pure shear and p is the hydrostatic stress. They reported that the contribution of shear yielding to the fracture energy depends on the temperature, and that shear yielding mechanism provides over 50% of the total toughening effect at room temperature.

2.4.4 Cavitation, debonding and void growth

As mentioned before, cavitation (or debonding) and plastic void growth make a large contribution to toughening effects. Cavitation not only creates voids inside the rubber particles but also relieves the triaxial constraints locally around the voids.

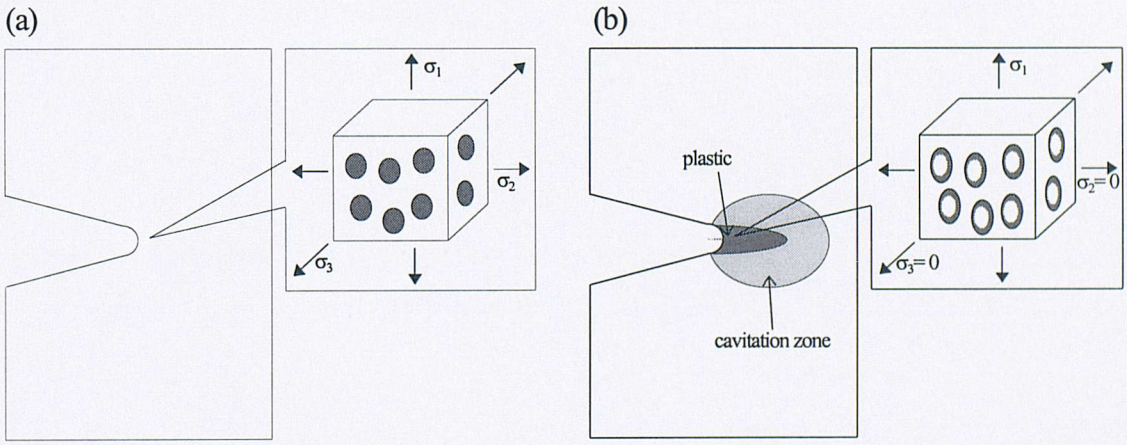


Fig.2.14 Illustration of cavitation process : (a) before rubber particle cavitation, (b) after rubber particle cavitation, the constraints in the transverse directions are relieved [50]

As the Poisson's ratio of the rubber is very close to the value of 0.5, the bulk modulus of the rubber particles is significantly high, and the volume of the rubber particles can hardly be changed. Consequently, under the dilatational stress condition, rubber particles are likely to cavitate (or debond) without any volumetric deformation, and voids are formed. As a result of the cavitation (or debonding) the triaxial constraint is relieved and the matrix epoxy surrounding the rubber particles is able to expand plastically. Thus, the cavitated rubber particles, i.e. voids, seem to grow. This process is termed plastic void growth. It has been reported [7,51] that the size of the voids on the fracture surface are larger than the initial size of the rubber particles. This gave direct evidence that plastic void growth did indeed occur.

Yee et al. [52] also investigated the importance of cavitation as a toughening mechanism, and reported that the rubber particles were unable to induce massive plastic deformation when cavitation was suppressed by hydrostatic pressure. Hence the fracture energy of rubber modified epoxy stayed at almost same level as that of the unmodified epoxy.

Huang et al. [7, 48] reported that the voids caused by cavitation grew by more than 60% in volume during the fracture of rubber modified epoxy. They also calculated the dissipated energy by plastic void growth, ΔG_v. They suggested that the value of ΔG_v can be calculated by integrating the energy density of the void growth mechanism, U_v (r), over the plastic zone, as for the shear yielding mechanism:

$$\Delta G_v = 2 \int_0^{r_y} U_v (r)\, dr \qquad (2.43)$$

When a void grows from a volume of V_0 to V_1, the energy density of the void growth mechanism, U_v(r), is given by the following equation:

$$U_v (r) = \int_{V_0}^{V_1} p\, d\theta \qquad (2.44)$$

where p is the hydrostatic stress and θ is the volumetric strain. Assuming that the ratio of V_1 and V_0 is the same as the ratio of the volume fraction of voids, V_{fv}, and

the volume fraction of rubber particles, V_{fr}, the energy density of the void growth mechanism, $U_v(r)$, is given by:

$$U_v(r) = 0.5\sigma_{yt}(V_{fv} - V_{fr}) \quad (2.45)$$

where σ_{yt} is the tensile yield stress. By substituting equation 2.45 into 2.43, and expressing the plastic zone radius, r_y, using the plastic zone radius of the unmodified epoxy, r_{yu}, the energy dissipated by plastic void growth, ΔG_v, is given by :

$$\Delta G_v = (1-\mu_m^2/3)(V_{fv} - V_{fr})\,\sigma_{yc}\, r_{yu}\, K_{vm}^2 \quad (2.46)$$

Huang et al. also reported that the contribution of ΔG_v to the total energy dissipated by the toughening mechanisms is less than 40% at room temperature, but it increases as the temperature increases.

2.4.5 Rubber bridging

Rubber bridging is the third toughening mechanism for rubber modified epoxy polymers. This mechanism originates from the possible tearing resistance of any rubber particles which might exist between the opening crack surfaces as shown in Fig.2.15.

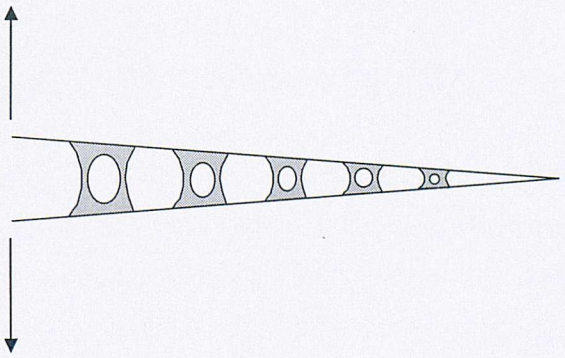


Fig.2.15 Schematic image of rubber bridging

This concept was proposed by Kunz-Douglass et al. [53]. They considered rubber bridging as a main energy dissipating mechanism, and suggested that the fracture energy due to rubber bridging mechanism, ΔG_r, can be calculated via the

following equation:

$$\Delta G_r = (1 - \frac{6}{\lambda_t^2+\lambda_t+4}) 4\Gamma_t V_{fr} \quad (2.47)$$

where λ_t is the extension at failure for rubber particles and Γ_t is the tearing energy of rubber. When λ_t is enough large, the term in brackets of the above equation converges towards unity, thus:

$$\Delta G_r = 4\Gamma_t V_{fr} \quad (2.48)$$

The value of ΔG_r is estimated at less than 0.5kJ/m^2, and this value is much lower than the observed fracture energy G_c. Indeed, Huang and Kinloch [48] reported that the contribution to the fracture energy is less than 10% at room temperature. Consequently, rubber bridging is currently thought to be a secondary toughening mechanism for rubber modified epoxy. However, the relative contribution of this mechanism increases as the temperature decreases, because other mechanisms such as shear yielding and void growth are suppressed at low temperatures.

It should be noted that rubber bridging may be neglected when the interfacial adhesion between the rubber particles and the matrix is poor, since in this case the particles may easily debond from the matrix [7].

2.4.6 Relationships between microstructure and static fracture behaviour

A number of microstructural features have been suggested to affect the static fracture behaviour. Relationships between the microstructure and static properties in rubber modified epoxy polymers have been reported by many authors [7,42,43,54-67]. The microstructural features include the crosslink density of the matrix epoxy, rubber particle size, volume fraction of rubber, interfacial adhesion, etc.

2.4.6.1 Effect of crosslink density

The crosslink density of the matrix epoxy is characterised by the value of the average molecular weight between crosslinks, M_c. A high M_c value corresponds

to a low crosslink density, and a low M_c value corresponds to a high crosslink density. The crosslink density of the matrix epoxy would be expected to affect the static fracture behaviour of rubber modified epoxy, and the crosslink density can be altered by changing curing conditions, molecular weight of monomer, curing agent, etc.

The static fracture toughness increases with an increasing value of M_c, i.e. with decreasing crosslink density. Hwang et al. [43] suggested a linear relationship between the critical stress intensity factor, K_{Ic}, and $M_c^{1/2}$ for rubber modified epoxies. However, Karger-Kocsis and Friedrich [54] reported a linear relationship between the fracture energy, G_{Ic}, and $M_c^{1/2}$ for rubber modified epoxies. However, as shown in Fig.2.16 and Fig.2.17, for the materials plotted in the graphs there is a difference, not only in the crosslink density, but also in the other material properties, such as the rubber content, particle size, etc. Therefore, the data shown in these graphs are not strong evidence for the toughness dependence on the crosslink density.

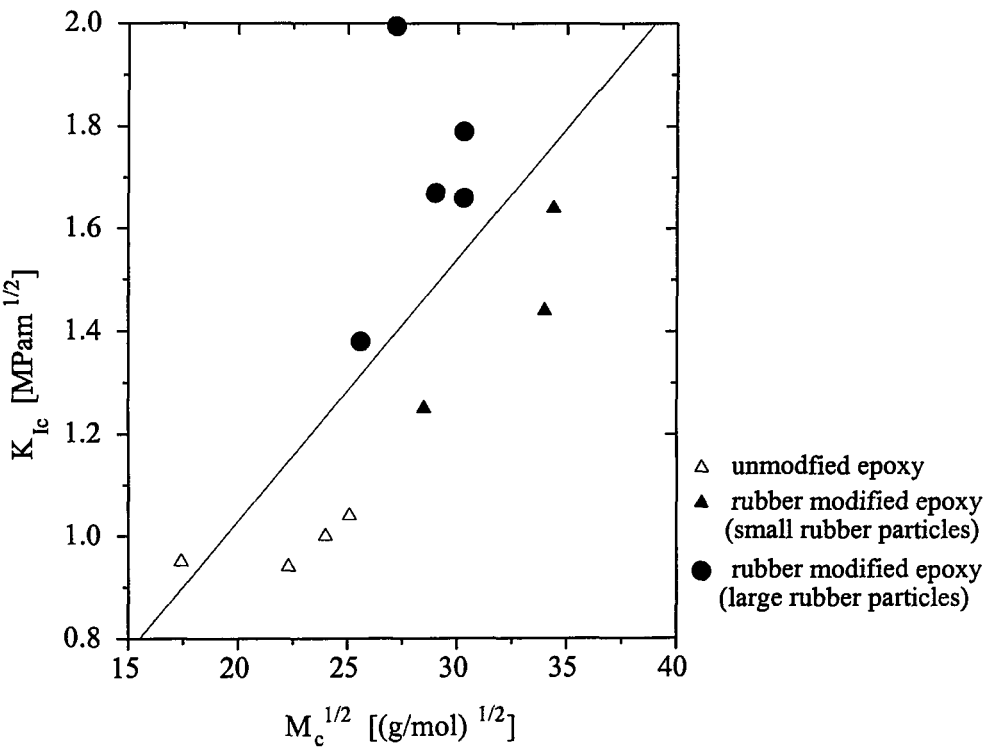


Fig.2.16 Variation of K_{Ic} as a function of M_c [43]

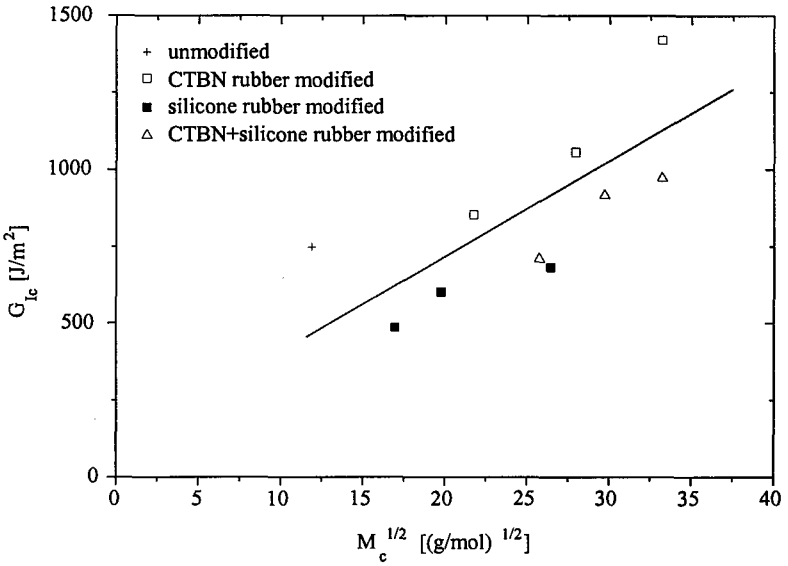


Fig.2.17 Variation of G_{Ic} as a function of M_c [54]

Pearson and Yee [55] also investigated the effect of crosslink density on the fracture toughness in both rubber modified and unmodified epoxies. As the rubber modified epoxies which they used had the same rubber content, i.e. 10vol%, their work is most useful in investigating the effect of the crosslink density. They reported that epoxies with a low crosslink density exhibit greater ductility, and consequently greater toughenability. Hence, for rubber modified epoxies, the material with a low crosslink density has much greater fracture toughness. Fig.2.18 suggests a linear relationship between the critical stress intensity factor, K_{Ic}, and $M_c^{1/2}$ for rubber modified epoxies.

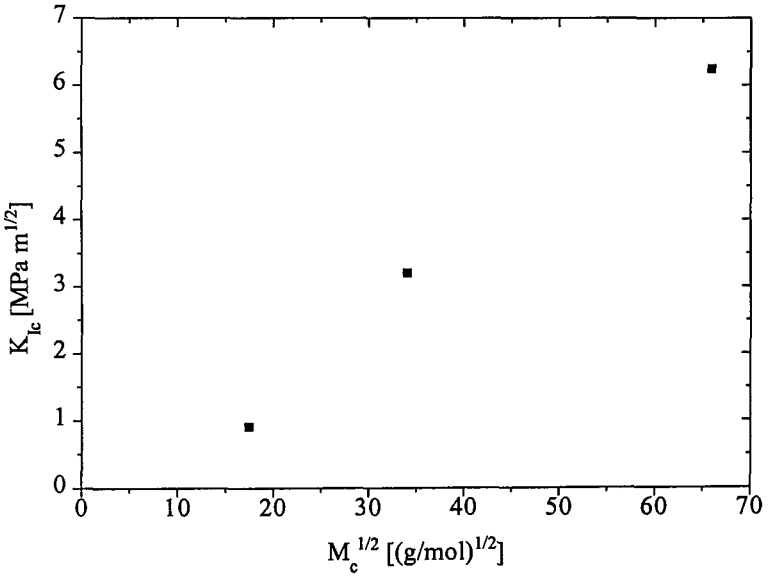


Fig.2.18 The effect of crosslink density on the K_{Ic} value for a rubber modified epoxy (data from ref. [55])

Kinloch et al. [56] also investigated the effect of crosslink density in rubber modified epoxies which have the same rubber content of 15phr, and reported that an increase in the M_c value from 610g/mol to 4640g/mol gave a large increase in the fracture energy of the rubber modified epoxy, from 2.23kJ/m^2 to 5.90kJ/m^2. As there was no significant difference in other microstructural properties such as rubber particle size, their results reflect solely the effect of crosslink density. They also reported a change of glass transition temperature of the matrix epoxy with changing the M_c value. Generally, an increase in molecular weight between crosslinks causes an increase in the mobility of the molecules. Hence, it typically causes a decrease of glass transition temperature, T_g. The results measured by Kinloch et al. [56] are shown in Table 2.1.

Table 2.1 Relationships between M_c and G_{Ic}

Curing conditions	M_c (g/mol)	G_{Ic} (kJ/m^2)	T_g (°C)
120°C x 16hours	630	2.23	101
160°C x 6hours	4370	5.90	89

According to Nielsen [68], the glass transition temperature, T_g, and the molecular weight between crosslinks, M_c, are related through the following equation:

$$T_g = T_{g0} + 3.9 \times 10^4 / M_c \qquad (2.49)$$

where T_{g0} is the reference temperature. Therefore, the higher the glass transition temperature, T_g, then the smaller is the molecular weight between crosslinks, M_c. An increase in the M_c value is consistent with a decrease in the T_g value.

Both the results of Pearson and Yee [55] and Kinloch et al. [56] are plotted in Fig.2.19 and Fig.2.20. The results of Pearson and Yee [55] show a linear relationship between K_{Ic} and $M_c^{1/2}$, whereas the results of Kinloch et al. [56] show a linear relationship between G_{Ic} and $M_c^{1/2}$. Thus, qualitatively, the smaller the M_c value, then the greater is the fracture toughness (or fracture energy) of the rubber modified epoxy. However, more research is needed to establish a more detailed and general relationship between the toughness and the crosslink density.

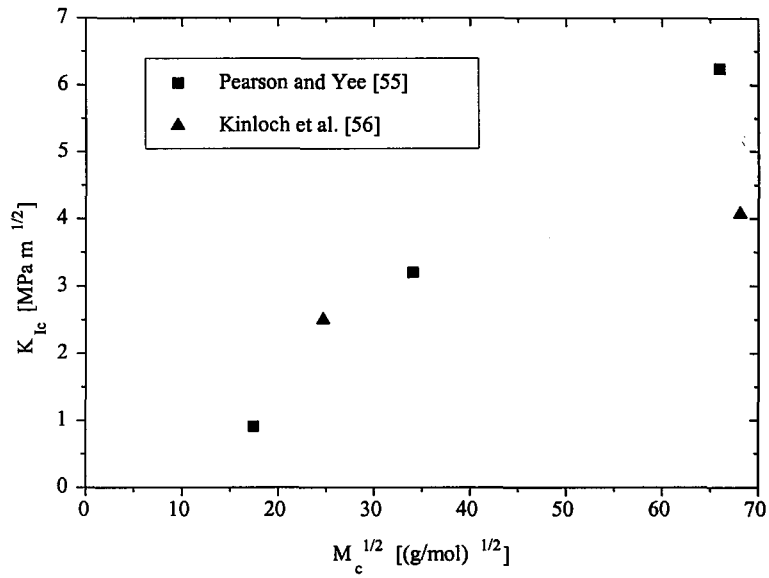


Fig.2.19 Effect of crosslink density for rubber modified epoxies: K_{Ic} plotted against $M_c^{1/2}$

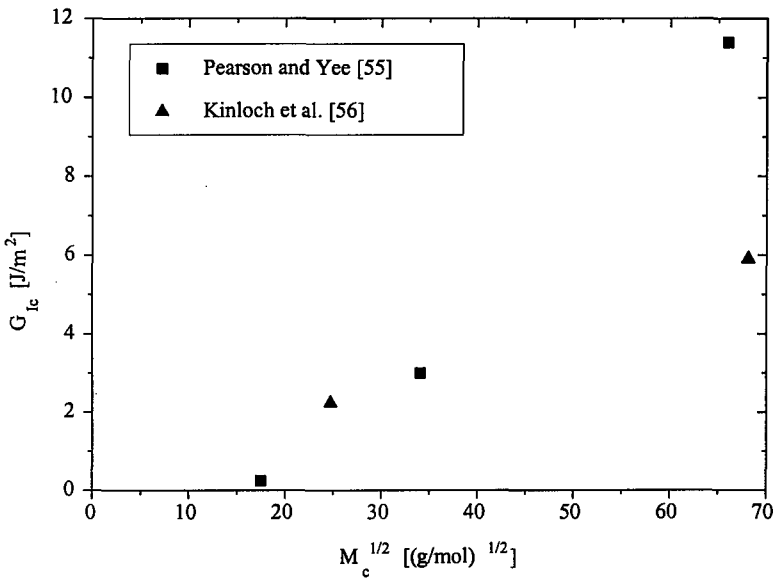


Fig.2.20 Effect of crosslink density for rubber modified epoxies: G_{Ic} plotted against $M_c^{1/2}$

2.4.6.2 Effect of volume fraction of rubber

Generally, the static toughness increases as the volume fraction of rubber increases, as reported by several researchers [7,10,54,57,58]. Bucknall and Yoshii [57] studied the toughness of several types of rubber modified epoxies containing CTBN rubber, and reported a linear relationship between the fracture energy, G_{Ic}, and the volume fraction of rubber, V_{fr}. Kinloch and Hunston [58] investigated the

effect of the volume fraction of rubber, with varying test temperature and rate, and reported the detailed relationship between the fracture energy, G_{Ic}, and the volume fraction of rubber, V_{fr}, as shown in Fig.2.21. At high temperatures and low rates of test, the fracture energy, G_{Ic}, increases steadily with an increasing volume fraction of rubber, V_{fr}, and the relationship between G_{Ic} and V_{fr} is almost linear. At low temperature or high test rates, the relationship between G_{Ic} and V_{fr} deviates somewhat from a linear relationship. For a given value of V_{fr}, the toughness is always significantly greater at high temperatures and low rates of test. This higher toughness arises from the higher ductility of the epoxy matrix under these conditions.

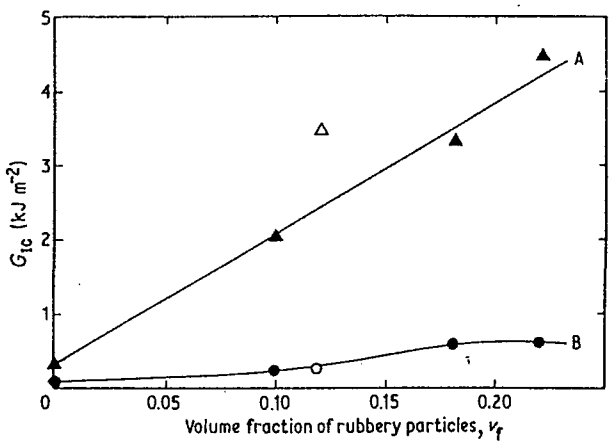


Fig.2.21 Fracture energy, G_{Ic}, against volume fraction of rubber particles, V_{fr}, A:high temperatures/low rates, B:low temperatures/high rates [57]

Karger-Kocsis and Friedrich [54] have also reported that the fracture toughness increases with increasing rubber content. They also suggested a linear relationship between the fracture toughness, K_{Ic}, and the rubber content, as shown in Fig.2.22.

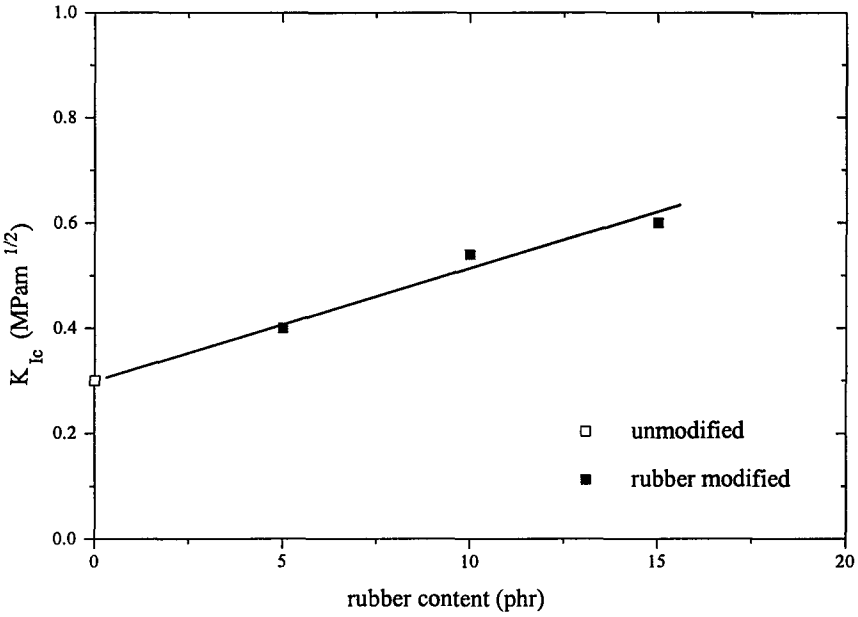


Fig.2.22 K_{Ic} values plotted against rubber content [54]

These results are generally consistent with the results of Kinloch and Hunston [58] in that toughness increases steadily with increasing rubber content. However, there is not a complete consistency between both these sets of results. Kinloch and Hunston [58] suggested a linear relationship between the fracture energy, G_{Ic}, and the volume fraction of rubber, V_{fr}. Now, G_{Ic} and K_{Ic} are related each other through the following equation:

$$G_{Ic} = (1-\nu^2)\, K_{Ic}^2 / E \qquad (2.50)$$

Thus, it would be expected that there would be a linear relationship between $(K_{Ic})^2$ and rubber content, rather than between K_{Ic} and rubber content.

On the other hand, some researchers reported a more complex relationship between the fracture toughness and rubber content. Kim and Ma [42] investigated the effect of rubber content for rubber modified epoxies. They reported that the fracture toughness increased with an increasing rubber content only when the rubber content was relatively small, as shown in Fig.2.23. In this case, there was a difference between rubber modified epoxies, not only in the rubber content, but also in the rubber particle size. The particle size at 4phr rubber content was 1-2μm, whereas the particle size at 8phr rubber content was 7-8μm. As discussed in the

next section, small particles are more efficient in producing a toughening effect than large particles. This particle size effect may affect the fracture toughness. Since it is difficult to change just the rubber content, without changing other microstructural features such as particle size etc., when materials (such as rubber modified epoxies) are made using an in-situ phase separation technique, more detailed investigations are necessary to assess quantitatively the effect of rubber content.

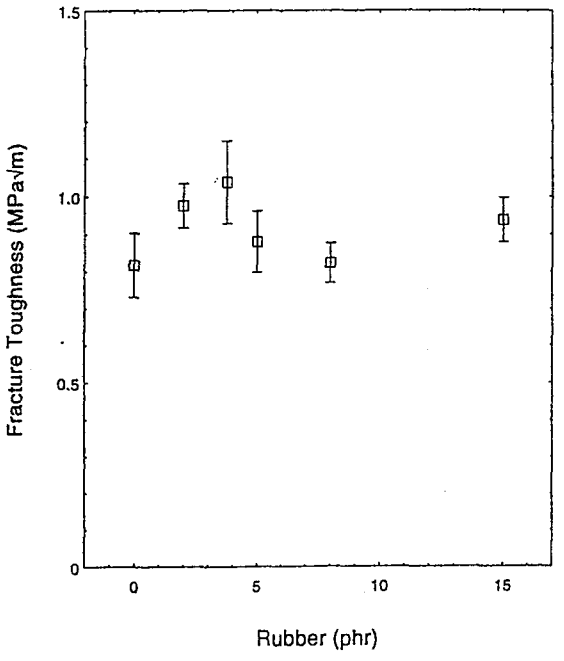


Fig.2.23 Fracture toughness, K_{Ic}, plotted against rubber content [42]

Another reason for the discrepancies in these various results shown in Figs.2.21 to 2.23 may arise from the amount of rubber precipitated out as particles is not necessarily equivalent to that initially added. It should be noted that Fig.2.21 uses the actual volume fraction of rubber particles, whilst Fig.2.22 and 2.23 are based simply upon the amount of rubber added initially to the epoxy.

It should be noted that there is normally a limit to the amount of rubber which can be dissolved, and then precipitated out as particles in an epoxy matrix. Beyond this 'limit' concentration, the added rubber can not be dispersed as particles. The morphology becomes co-continuous, or phase inversion occurs.

2.4.6.3 Effect of particle size

Pearson and Yee [59] investigated the influence of particle size in rubber modified epoxies, and reported that small rubber particles are more efficient in producing a toughening effect than large particles, as shown in Table 2.2. They suggested that this particle size dependence arose from the role played by the rubber particle in relation to the size of process zone [59]. Rubber particles larger than the size of the process zone are only able to act as bridging particles. On the other hand, small rubber particles lying in the process zone are forced to cavitate by the large hydrostatic stress component that exists in the process zone. The cavitated particles relieve the triaxial constraint, and thereby promote plastic deformation, as described earlier.

Table 2.2 Fracture toughness dependence on rubber particle size [59]

Material	rubber	Particle size (μm)	K_{Ic} (MPa $m^{1/2}$)
unmodified	----	----	0.80
rubber modified -1	CTB	~200	1.10
rubber modified -2	CTB/CTBN(1)	1-2, 100-200	1.95
rubber modified -3	CTBN(1)	1-2	2.10
rubber modified -4	CTBN(2)	1-2, 10-20	2.00
rubber modified -5	MBS	~0.2	2.90
rubber modified -6	MBS/CTBN(1)	0.2, 1-2	2.75

Note: the initially added rubber content is 10phr for all rubber modified epoxies
CTB is carboxyl terminated butadiene, "Hycar CTB2000x162"
CTBN(1) is carboxyl terminated butadiene acrylonitrile, "Hycar CTBN1300x8"
CTBN(2) is carboxyl terminated butadiene acrylonitrile, "Hycar CTBN1300x31"
MBS is methacrylated butadiene styrene, "Acryloid KM653"

As mentioned in the previous section, it is difficult to change solely the particle size without changing other microstructural features, particularly using the addition of a liquid rubber. To avoid such difficulties, some researchers have utilised core-shell particles for the investigation of the effect of rubber particle size.

However, there is little evidence from these studies that particle size has a major influence on the fracture toughness. Very recently, Kim et al. [63] reported that the effect of volume fraction of rubber is influenced by the rubber particle size, and that the fracture toughness increases as the particle size decreases, as shown in Fig.2.24.

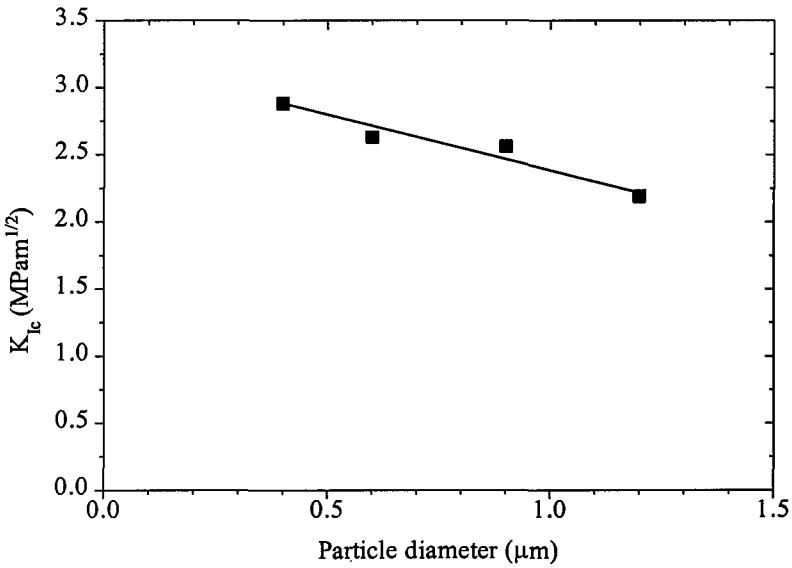


Fig.2.24 Effect of particle size on fracture toughness [60]

They also reported that very small particles, i.e. less than 0.2μm in radius, are not effective for toughening, because cavitation is difficult with rubber particles less than 0.2μm. This result agrees with the theoretical calculation by Lazzeri and Bucknall [61]. As discussed in section 2.3.1, they suggested that the energy of an internally cavitated rubber particle is given by:

$$U(r) = \frac{2}{3}\pi r_p^3 K_r (\Delta V_r - r^3/r_p^3)^2 + 4\pi r^2 \Gamma_r + 2\pi r^3 G_r F(\lambda_f) \qquad (2.51)$$

where r is radius of the hole formed at the centre of a rubber particle, r_p, is radius of a rubber particle, G_r is the shear modulus of the rubber, K_r is the bulk modulus of the rubber, ΔV_r is the volume strain in the rubber particle, Γ_r is surface energy of the rubber, and the function $F(\lambda_f)$ is dependent on the failure strain of the rubber, λ_f, under biaxial stretching conditions. As shown in Fig.2.25, when the radius of a rubber particle is greater than 0.125μm, the energy, U(r), has a minimum value at a non-zero r value. This means that the cavitated rubber particle is more stable than the non-cavitated one. In other words, rubber particles are likely to cavitate

at a given condition. On the other hand, when the radius of rubber particles is less than 0.125μm, the value of U(r) has a minimum value at r=0. This means that the condition of r=0, i.e. no internal cavity, is most stable; and that the rubber particles are unlikely to cavitate.

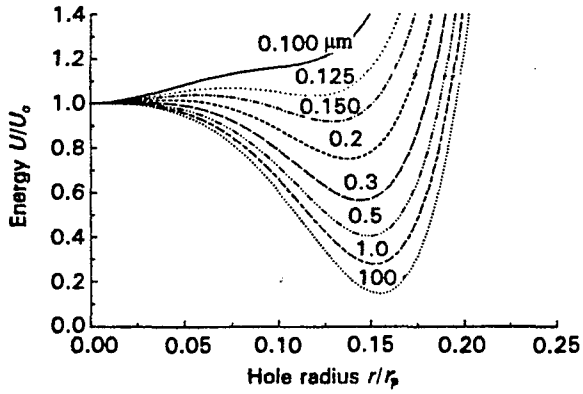


Fig.2.25 Energy of a cavitated rubber particle [61]

Summarising the above results, the following conclusions may be drawn on the effect of rubber particle size. Small rubber particles generally give a higher toughness than large rubber particles. However, very small rubber particles (approximately smaller than 0.2μm) lead to a low toughness since cavitation is difficult with such small rubber particles.

2.4.6.4 Effect of interfacial particle-to-particle distance

For a rubber toughened polyamide, it was suggested by Wu [62, 63] that there existed a critical interfacial particle-to-particle distance which was independent of the volume fraction of rubber. When the distance between particles is larger than the critical value, approximate 0.3μm, the material is quite brittle and the fracture toughness of the polymer is low. On the other hand, when the distance between particles is smaller than the critical value, the material fractures in a tough manner and its fracture toughness is relatively high. He explained that this phenomena was related to a transition in the stress state in the matrix, and that the stress state was changed from plane strain to plane stress when the distance between particles fell below the critical value. However, the dimensions

for the stress state transition to occur, which is given by $2.5(K_{Ic}/\sigma_y)^2$, is usually of the order of millimetres rather than fractions of a micrometre. Thus, the validity of Wu's model is still debatable.

For rubber modified epoxy polymers, Kim et al. [60] investigated the effect of interfacial particle-to-particle distance on the fracture toughness, using core-shell rubber particles, i.e. without changing the particle size. They reported that there is a optimum value of the interfacial particle-to-particle distance to maximise fracture toughness, as shown in Fig.2.26. Assuming a simple cubic array, the inter-particle distance, d_p, is related to the volume fraction of rubber, V_{fr}, and the rubber particle radius, r_p, via the following equation:

$$d_p = [(4\pi/3V_{fr})^{1/3} - 2]r_p \qquad (2.52)$$

Therefore, an increase in the V_{fr} value corresponds to a decrease in the d_p value. Hence, Fig.2.26 also shows that there is a optimum V_{fr} value which is necessary to maximise the fracture toughness. This result is not in agreement with the other reports by Bucknall and Yoshii [57], Kinloch and Hunston [58] and Karger-Kocsis and Friedrich [54], as discussed in the previous section. Thus, the effect of interfacial particle-to-particle distance is still controversial, and further investigation is needed to assess the effect of inter-particle distance more clearly.

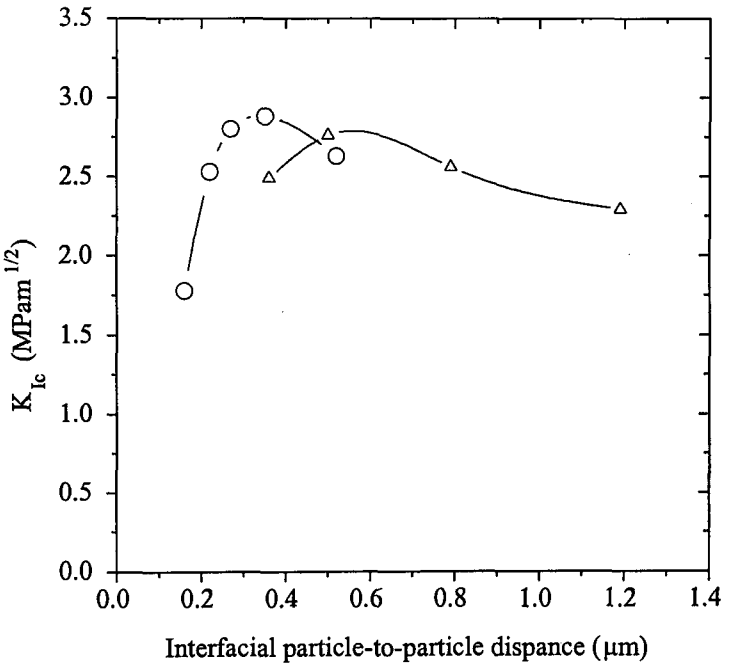


Fig.2.26 Effect of interfacial particle-to-particle distance on fracture toughness: particle radius 0.2μm (○) and 0.45μm (△) [60]

2.4.6.5 Effect of adhesion between matrix and particles

When rubber modified epoxy polymers are made using an in-situ phase separation technique, the functionality of the reactive, or unreactive, end-groups has a strong influence on the microstructural features and the adhesion between the matrix epoxy and rubber particles. It was suggested formerly [69] that poorly bonded particles did not have a load bearing capacity and therefore did not make any contribution to toughening. Recently, however, Huang et al. [7,70] investigated the effect of adhesion between the matrix and rubber particles by changing the end-groups of the rubber, and reported that the interfacial bonding has only a minor effect on the fracture toughness of the rubber modified epoxy polymers. They also reported the competition between the internal cavitation and the debonding tendencies of rubber particles during fracture depends on the strength of the adhesion between the matrix and rubber particles. When the adhesion is good, the rubber particles internally cavitate. When the adhesion is poor, the rubber particles debond from the matrix before cavitation occurs. From a mechanics viewpoint, either event relieves the triaxial constraints on the matrix, allowing further plastic deformation via a plastic void growth mechanism. The only difference is in the contribution of the rubber bridging mechanism. This mechanism can only operate when the adhesion is good, but it contributes little to the fracture toughness, except at low temperatures. Consequently, the adhesion between the matrix and rubber particles does not have a major influence on the fracture toughness. However, optimal toughening can only be achieved when the interfacial bonding is good.

Very recently, Bagheri and Pearson [64,65] investigated the difference in the toughening effect on an epoxy matrix between rubber particles and hollow latex particles. They reported that hollow particles toughened epoxies in the same manner as rubber particles, and that no significant superiority of rubber particles over voids in toughness improvement was found, as shown in Table 2.3. They concluded that there was lIttle contribution to the whole toughness improvement given by the rubber bridging mechanism.

Table 2.3 Fracture toughness dependence on the modifier [64]

Modifier	Particle size (μm)	K_{Ic} (MPa $m^{1/2}$)
None	----	0.85
CTBN	0.55	2.05
MBS	0.2	2.20
HLP-0.4	0.4	2.30
HLP-1.0	1.0	1.95

Note: CTBN is carboxyl terminated butadiene acrylonitrile (liquid rubber)
MBS is methacrylated butadiene styrene (core-shell rubber particle)
HLP-0.4 and HLP-1.0 are hollow latex particles

Kiefer et al. [66] made porous epoxies which contain spherical voids dispersed in the matrix epoxy, and reported that voids themselves, i.e. without rubber, can improve the fracture toughness. Huang and Kinloch also [67] reported that voids themselves can significantly increase the toughness of the epoxy. This is because voids also cause a stress concentration, and promote shear yielding and plastic void growth of the surrounding matrix epoxy in the same way as cavitated rubber particles. However, there has been no experimental study comparing rubber modified epoxy and "void" modified epoxy, both of which have the same material properties and microstructural features, except for the differences of rubber particle versus void.

2.5 Fatigue behaviour

In the previous section, some fracture mechanisms were reviewed. These are applicable to both static and fatigue test conditions. However, there are additional concepts which are essential in order to understand the fatigue behaviour of polymers. A brief introduction to these concepts is presented in this section. Then, the effects of test conditions such as frequency, temperature, etc., are reviewed. Furthermore, the effects of material properties, such as morphology, crosslink density, etc., are also discussed.

2.5.1 Crack propagation

The term "fatigue" usually refers to the failure process under oscillating or fluctuating loads. This process includes both crack initiation and crack propagation. In this study, however, the initiation process is not considered in detail, because in most engineering cases materials already contain pre-existing defects and the fatigue life is strongly dominated by the crack propagation process [71].

In the crack propagation process, the fatigue crack growth rate, i.e. the increment of crack length per cycle, da/dN, is the most basic parameter. Fatigue crack propagation occurs at much lower loads than the static critical load, and da/dN increases as the stress level increases. Numerous formulations have been proposed to describe the relationship between da/dN and the stress level. Amongst them, the fracture mechanics approach is the most widely adopted. Paris [72, 73] found that the key parameter was the stress-intensity factor range, ΔK, and suggested that da/dN could be described by the following equations :

$$da/dN = A\,\Delta K^m \tag{2.53}$$

$$\Delta K = K_{max} - K_{min} \tag{2.54}$$

where A and m are material constants. This relationship (equation 2.53) is known as the Paris Law.

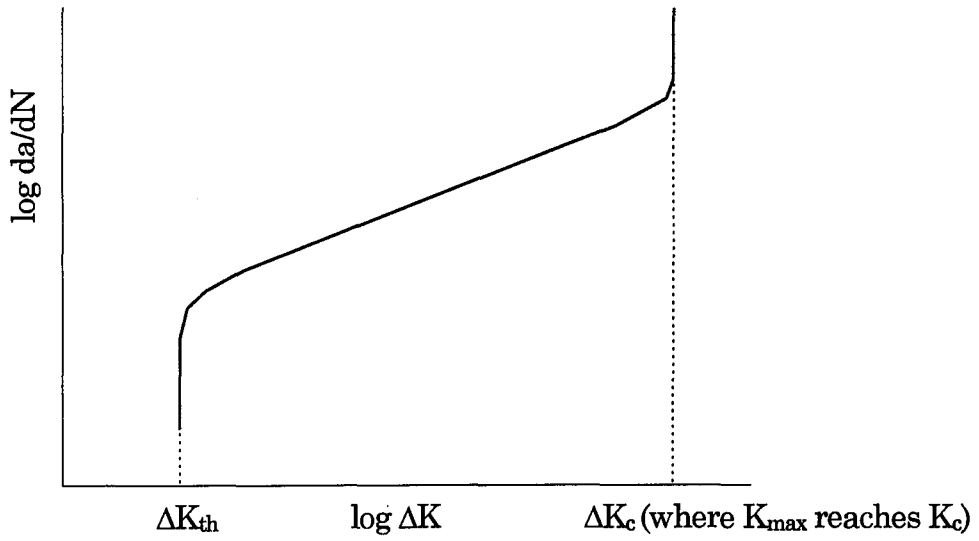


Fig.2.27 Typical graph of da/dN vs. ΔK

A typical fatigue curve is shown in Fig.2.27. The fatigue crack growth rate decreases to vanishingly small values as ΔK approaches the threshold ΔK value, ΔK_{th}, and increases to very high values as K_{max} approaches the static critical value, K_c [71]. It should be noted that the threshold K_{max} value is defined as K_{th}, when the fatigue data are plotted against K_{max}.

With regard to rubber modified epoxy materials, Azimi et al. [51,74] reported that the fatigue crack growth rate was closely related to the toughening mechanism. The concept of ΔK_T, the transition point where cavitation/shear yielding mechanisms became active, was introduced. They considered that the value of ΔK_T represented the point at which the size of the plastic zone became larger than the particle size. Below ΔK_T, the size of the plastic zone is smaller than that of the rubber particles. Hence, the rubber particles do not interact with the crack tip, and they can not promote cavitation/shear yielding mechanisms which dissipate large amounts of energy during crack propagation. Consequently, there is no difference in the fatigue crack growth rates, for a given ΔK value, between the rubber modified epoxy and the unmodified epoxy. On the other hand, above ΔK_T, as the size of the plastic zone at the crack tip is large enough so that the rubber particles can be engulfed in the plastic zone, the rubber particles interact with the crack tip stress field, and cavitation/shear yielding mechanisms become active. Consequently, for a given value of ΔK, the da/dN of rubber modified epoxy becomes lower than that of unmodified epoxy, as shown in Fig.2.28.

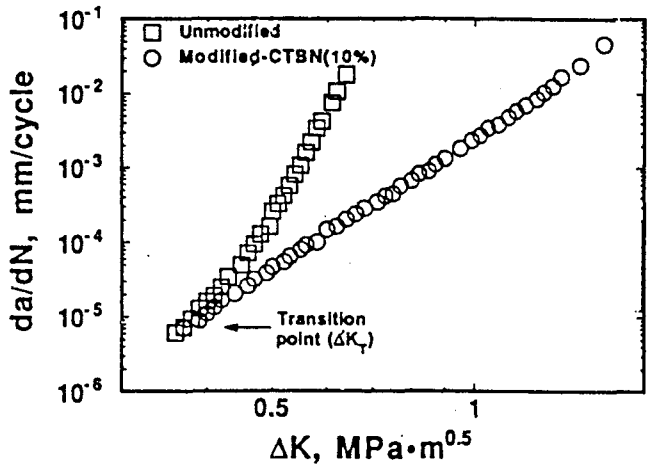


Fig.2.28 Fatigue crack growth rate of rubber modified epoxy and unmodified epoxy [51]

Recently, Jethwa and Kinloch [75] investigated the threshold G_{max} value, $G_{th}=(1-\nu^2)K_{th}/E$, of several rubber modified epoxy adhesive joints. As may be seen in Table 2.4, the threshold G_{max} value, G_{th}, is far lower than the fracture energy, G_{Ic}. We normally imagine materials having a high fracture energy to have good fatigue resistance. However, they reported some interesting results in that a high fracture toughness did not necessarily translate into a high fatigue resistance, as shown by the values of G_{th}, or G_{th}/G_{Ic}.

Table 2.4 G_{Ic}, G_{th} and G_{th}/G_{Ic} for different structural adhesives [75]

Adhesive	G_{Ic}(J/m^2)	G_{th}(J/m^2)	G_{th}/G_{Ic}
Hysol EA9309	5700	150	0.03
Ciba XD4600	3500	355	0.10
Cyanamid FM73M	2930	280	0.10
3M AF-163-2M	1720	560	0.33
Teroson Terokal4520-34	740	240	0.32

Note : All adhesives are rubber modified epoxies

As Azimi et al. suggested [51, 74], there should be a transition point, K_T (or G_T), where toughening mechanisms become active. Below this point, including the threshold region, the toughening mechanisms initiated by the rubber particles do not occur and the material properties of the matrix epoxy, i.e. the unmodified epoxy, are reflected in the fatigue behaviour. Therefore, the threshold G_{max} value, G_{th}, of the rubber modified epoxy should be not improved by the addition of rubber and will consequently the same as that of the unmodified epoxy, i.e. the matrix epoxy of the adhesive. In other words, the G_{th} values in Table 2.4 are determined by the properties of the matrix epoxy of the adhesives, regardless of the addition of rubber. This may be the reason why a high fracture toughness does not guarantee a high fatigue resistance, as judged by the threshold value, G_{th}, or G_{th}/G_{Ic}.

2.5.2 Effects of experimental parameters

Apart from the ΔK value, fatigue crack propagation is affected by experimental parameters such as the frequency, temperature, mean stress, load ratio, etc. In this section, the effects of these parameters are briefly reviewed.

2.5.2.1 Effect of frequency

The effect of frequency on the fatigue crack growth rate for the polymeric materials is rather complicated since several factors affect the frequency dependence, such as the β-transition, hysteretic heating, creep effect, strain rate effect, etc. [71].

β-transition

The β-transition is related to the movement of the side groups of the polymer. When the transition peak (β-peak) frequency of the polymer is close to the test frequency, resonance of the externally imposed test frequency with the material's internal segmental mobility occurs, and consequently the polymer has a strong frequency dependence. On the other hand, when the β-peak frequency is far away from the test frequency, the material is not sensitive to the frequency.

Skibo et al. [76,77] investigated the influence of the frequency in the range of 0.1-100Hz for several types of polymers. They reported that the fatigue crack growth rates of polyvinylchloride(PVC), polymethylmethacrylate (PMMA) and polystyrene(PS) decreased with increasing frequency; and that those of polycarbonate(PC), polyvinylidenefluoride(PVDF) and nylon-66 had little frequency dependence. The β-peak frequencies of PVC, PMMA and PS are in the range of 0.01Hz-10kHz which are close to the test frequency range of 0.1-100Hz, and The β-peak frequencies of PC, PVDF and nylon-66 are over 100kHz, which are far above the test range.

Hertzberg and coworkers [71,78-81] gave a physical interpretation of the above results and suggested that the frequency dependence arising from the β-transition is related to the hysteretic heating effect. Since the β-peak represents a region of maximum loss compliance, hysteretic heating occurs along with a

localised temperature rise. This causes a greater extent of plastic deformation and crack tip blunting, and consequently results in a lower fatigue crack growth rate. The hysteretic heating effect will be discussed in the next sub-section.

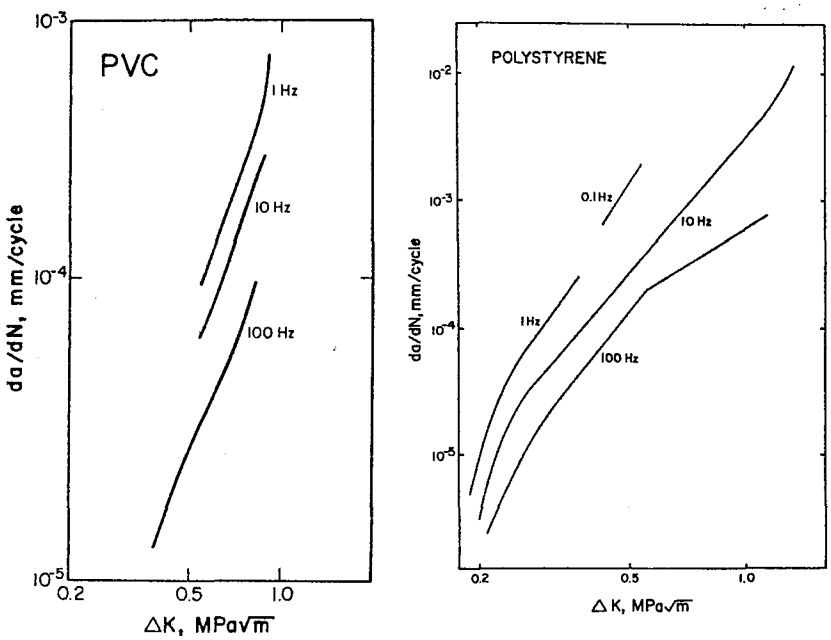


Fig.2.29 Frequency dependence of polymers (PVC from ref. [77], polystyrene from ref. [77])

Hysteretic heating

Hysteretic heating may occur under cyclic loading conditions, since polymers generally have a relatively high tanδ. The effect of hysteretic heating on the fatigue crack growth rate depends on the size of the heated region. Generally, hysteretic heating raises the temperature only in the vicinity of the crack tip (localised heating), since the heat conductivity of the polymer is rather small. In this case, the modulus and the yield stress are decreased near the crack tip. This enhances the yielding process surrounding the crack tip and leads to an increase in the crack tip radius (crack tip blunting). Consequently, hysteretic heating results in a decrease in the fatigue crack growth rate. Hence, the fatigue crack growth rate should decrease with increasing frequency [71,78].

On the other hand, if the hysteretic heating is sufficiently large and a large

scale temperature rise occurs (generalised heating), this leads to thermal failure. Therefore, it might be possible that the fatigue crack growth rate increases with increasing frequency if the polymer possesses a very high degree of internal loss [71].

Creep effect

The creep effect is not always negligible when the test frequency is relatively low. As the time period of oscillation is relatively long at a low frequency, creep crack growth may appear to be responsible for frequency dependence. Moskala [82] investigated the frequency dependence for rubber-toughened PC in the range of 0.25-25Hz, and reported that the fatigue crack growth rate decreased with decreasing frequency, especially when the test frequency was below 1Hz. He suggested that this frequency sensitivity came from the effect of creep-assisted crack growth, as given by:

$$(da/dN)_{total} = (da/dN)_{fatigue} + (da/dt)_{creep}\,(dt/dN) \qquad (2.55)$$

where (da/dt) is the time period of oscillation of the applied load. It should be noted that he, however, also reported that the localised temperature rise near the crack tip was approximately 8°C for 25Hz. Thus, the above frequency dependence might be caused by the localised hysteretic heating effect.

Strain rate effect

For a rubber modified epoxy, Hwang et al. [43] recently reported that the fatigue crack growth rate increased as frequency increased, as shown in Fig.2.30. They also investigated the influence of hysteretic heating near the crack tip using an infrared radiometric microscope which detects thermal differences as small as 0.5°C. They reported that little temperature rise near the crack tip was detected (i.e. the effect of localised hysteretic heating was insignificant), and concluded that the increase in fatigue crack growth rate with increasing frequency was caused simply by the strain rate effect.

Generally speaking, the mechanical properties such as modulus, yield stress, fracture toughness, etc. have a strain rate dependence. Normally, the

modulus and yield stress increase with increasing strain rate, and the fracture toughness decreases with increasing strain rate. Hence, it may be expected that the fatigue resistance decreases, i.e. the fatigue crack growth rate increases, with increasing strain rate.

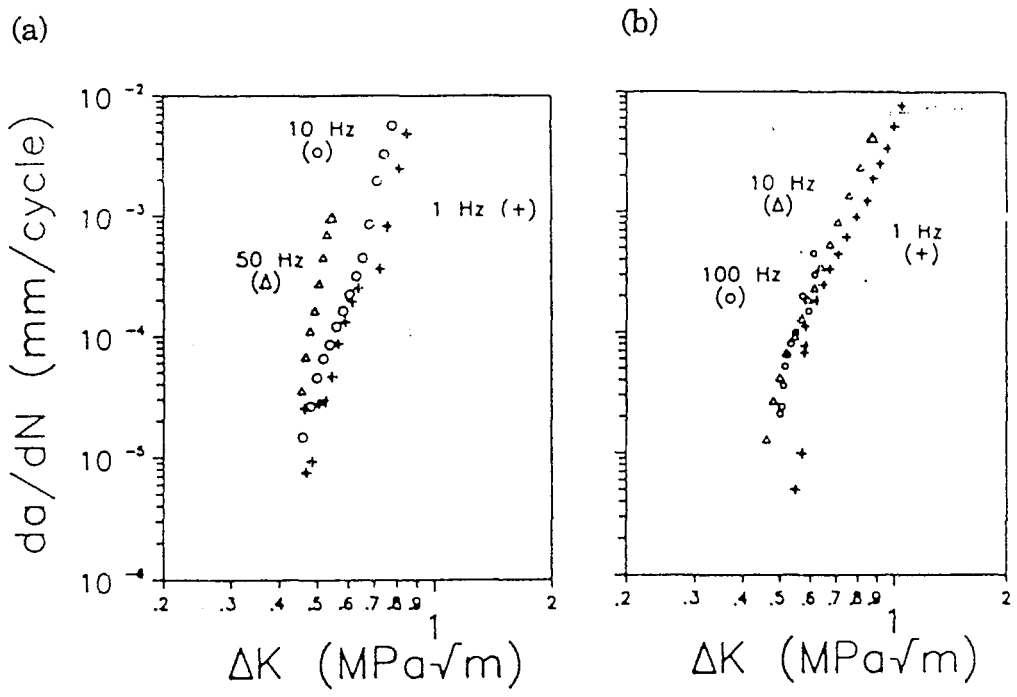


Fig.2.30 Effect of frequency on fatigue crack growth rate (a) unmodified epoxy (b) rubber modified epoxy [43]

In summary, the β-transition of the polymer affects the fatigue crack propagation associated with the localised hysteretic heating, and results in a decrease in the fatigue crack growth rate near the β-peak frequency. Localised hysteretic heating decreases the fatigue crack growth rate with increasing frequency, whereas generalised hysteretic heating causes an increase in the fatigue crack growth rate. The creep effect increases the fatigue crack growth rate with decreasing frequency, especially at relatively low frequencies (below 1Hz). The strain rate effect may therefore cause an increase in the fatigue crack growth rate with increasing frequency. Thus, the frequency dependence on the fatigue crack growth rate is determined by the balance of each of these contributions discussed above.

For rubber modified epoxies, the β-peak frequency is located in the range of over 100kHz. Therefore, the frequency dependence arising from β-transition can be considered not to be important under the testing condition (5Hz) of the present study. The creep effect is also not significant for 5Hz. Hence, the frequency dependence, if any, might arise from any hysteretic heating and strain rate effects.

2.5.2.2 Effect of temperature

The effect of temperature is briefly presented below. As is well known via the WLF equation [83], frequency and temperature are closely related to each other. Low temperature corresponds to high frequency. Conversely, high temperature corresponds to low frequency. Mai and Williams [84] reported that fatigue crack growth rate increased monotonically with increasing temperature in PS. A similar trend was observed in PMMA [76]. The temperature dependence of these polymers is consistent with their frequency dependence (i.e. the fatigue crack growth rate increases with decreasing frequency), as shown in Fig.2.31.

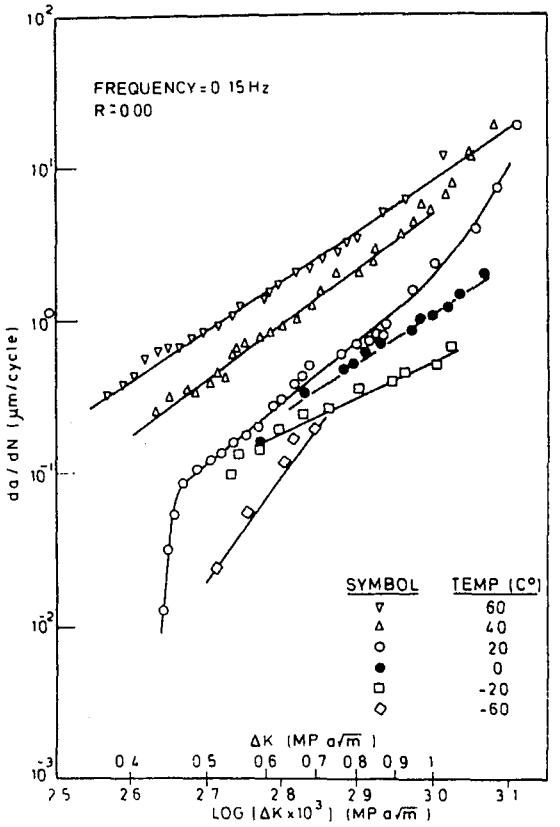


Fig.2.31 Effect of temperature on fatigue crack growth rate in PS [84]

For rubber toughened epoxy materials, however, Hwang et al. [43] reported that the fatigue crack growth rate decreased with increasing temperature as shown in Fig.2.32. This result was consistent with the frequency dependence, i.e. the fatigue crack growth rate decreased with decreasing frequency, as illustrated before in Fig.2.30. Furthermore, it is also consistent with the temperature dependence of fracture toughness reported by Kinloch et al. [85]. They reported that the fracture toughness of rubber toughened epoxy materials increased with increasing temperature.

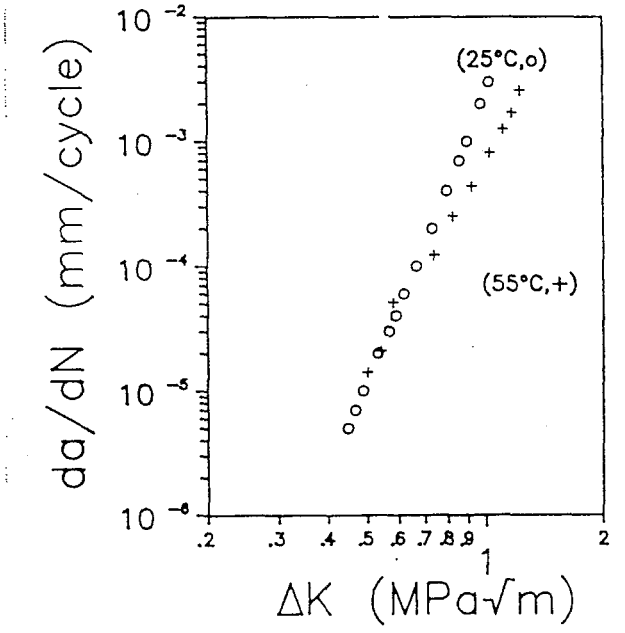


Fig.2.32 Effect of temperature on fatigue crack growth rate of a rubber modified epoxy [43]

2.5.2.3 Effect of mean stress and stress ratio

The mean stress during the fatigue crack propagation can be represented by the value of K_{mean}. When a sinusoidal cyclic load is applied, the K_{mean} value is given by:

$$K_{mean} = (K_{max} + K_{min})/2 \qquad (2.56)$$

The K_{mean} value and stress ratio, $R=K_{min}/K_{max}$, are related each other via the following equation:

$$K_{mean} = 2K_{max}\, R = 2R\Delta K/(1-R) \qquad (2.57)$$

Thus, when either K_{max} or ΔK is fixed, an increase in K_{mean} corresponds to an increase in R.

As noted earlier, the fatigue crack growth rate is generally recognised to obey the Paris Law. However, it has been observed by many researchers that the fatigue crack growth rate at a fixed ΔK value also varies with the change of mean stress, or stress ratio. Arad et al. [86] proposed the following equations to explain the fatigue crack growth rate in PMMA :

$$da/dN = k\lambda^n \qquad (2.58)$$

$$\lambda = K_{max}^2 - K_{min}^2 = 2\Delta K\, K_{mean} \qquad (2.59)$$

where k is a function of frequency, material properties and environment, and n is a constant. According to the above equations, the fatigue crack growth rate can be assumed to increase as the K_{mean} value increases. Indeed, it was reported that the fatigue crack growth rate, at a fixed ΔK, was found to increase experimentally with increasing K_{mean} (i.e. increasing stress ratio, R) in PMMA, PVDFand nylon-66 [71,86]. However, it was also observed that the fatigue crack growth rate decreases with increasing K_{mean} in PC and PVC [71,87].

Hertzberg and Manson [71] suggested that the effects of the K_{mean} value (or R value) on the fatigue crack propagation arise from conflicting mechanisms. On one hand, there may be a tendency for an increase in the fatigue crack growth rate with increasing K_{mean} (or R) because the K_{max} value approaches the critical limiting value for the material (i.e. K_{Ic}). Alternatively, there may be a tendency for a decrease in the fatigue crack growth rate with increasing K_{mean} (or R), due to the hysteretic heating effect, especially for the materials having a relatively high $\tan\delta$. As shown in Fig.2.33, the hysteretic loop normally increases as the stress level increases. Therefore, an increase in K_{mean} (or R) leads to an increase in the hysteretic heating, which causes crack tip blunting and consequently lowers the fatigue crack growth rate.

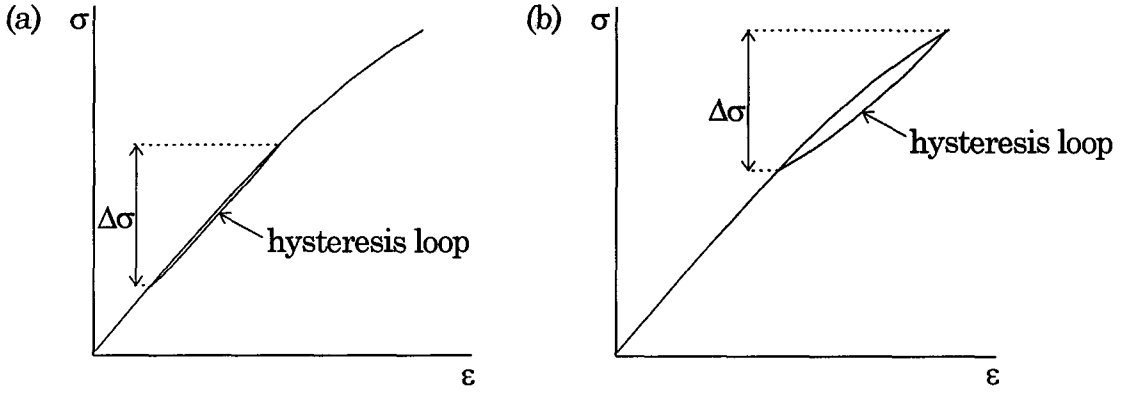


Fig.2.33 Schematic graph of hysteresis loop (a) low σ_{mean} (b) high σ_{mean}

For an epoxy polymer, Sutton [88] investigated the effect of stress ratio. He reported that the fatigue crack growth rate increases with increasing stress ratio, i.e. increasing mean stress, as shown in Fig.2.34.

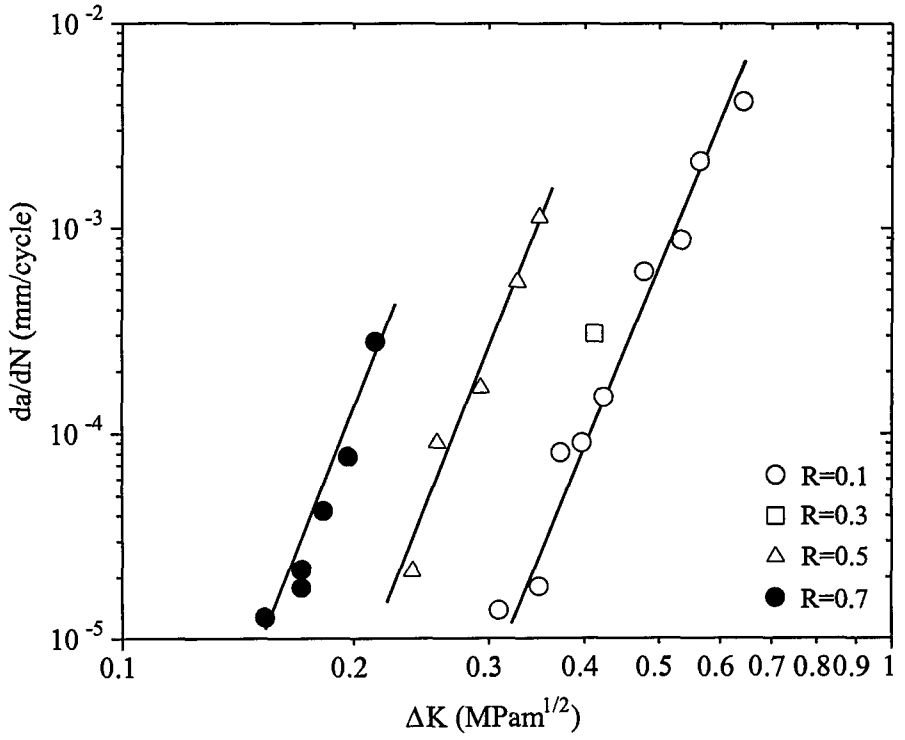


Fig.2.34 Effect of stress ratio on fatigue crack growth rate in an epoxy polymer [88]

2.5.3 Effects of material properties

Fatigue resistance is also affected by material parameters such as crosslink density (in crosslinked polymers), morphology (in multiphase polymers), etc. In this section, the effects of these parameters are briefly reviewed.

2.5.3.1 Effect of crosslink density

In crosslinked polymers, the crosslink density affects the ability for plastic deformation to occur, and therefore changes the amount of energy dissipated during deformation. Consequently, the crosslink density affects the fracture toughness and fatigue resistance. Hertzberg et al. [89] reported the effect of crosslinking agent in PMMA, and suggested that the fatigue crack growth rate increased with an increasing degree of crosslinking, corresponding to an increasing crosslink density. For an epoxy resin, Kim et al. [90] evaluated the dependence of fatigue crack growth rate in an amine-cured epoxy. They reported that the fatigue crack growth rate decreased with increasing average molecular weight between crosslinks, M_c. The higher M_c corresponds to a lower crosslink density.

Since plastic deformation is associated with fatigue crack propagation, materials which may undergo larger energy dissipation during deformation (i.e. low crosslink density) have typically superior fatigue resistance. On the other hand, materials with a high crosslink density are less likely to undergo plastic deformation. This, therefore, leads to a relatively high fatigue crack growth rate. Kishi et al. [91] reported that a relatively ductile epoxy reflecting an ability for extensive plastic deformation, had a higher fracture toughness. Hwang et al. [43] has investigated the influence of the crosslink density of epoxy matrix on the fatigue crack growth rate in both rubber modified epoxies and unmodified epoxies. They reported that the lower the crosslink density (i.e. the higher molecular weight between crosslinks, M_c) of the epoxy matrix, the greater the fatigue resistance, as shown in Fig.2.35.

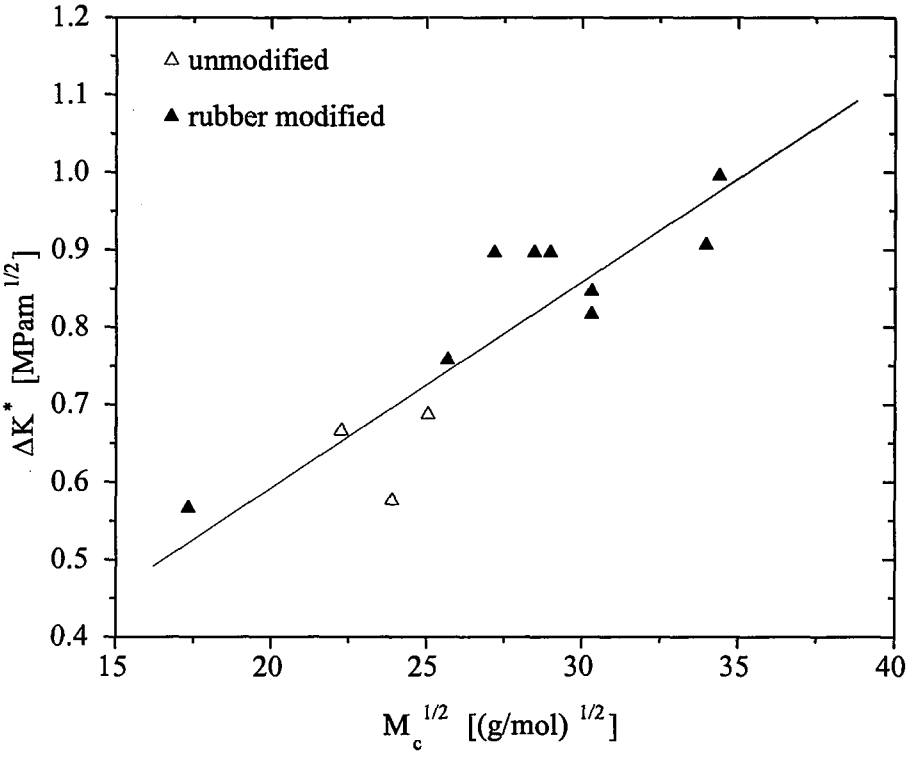


Fig.2.35 Effect of M_c on fatigue crack growth rate of rubber modified epoxies and unmodified epoxies (ΔK^* is ΔK when da/dN reaches 7.5×10^{-4}mm/cycle) [43]

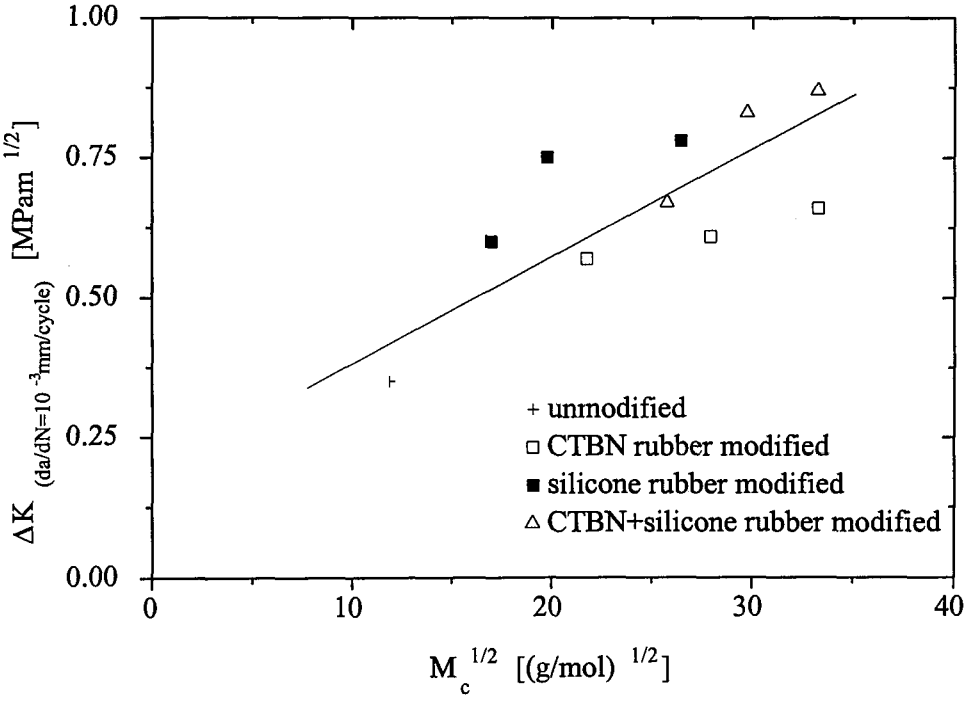


Fig.2.36 Change in ΔK at $da/dN = 10^{-3}$mm/cycle as a function of $M_c^{1/2}$ [54]

Karger-Kocsis and Friedrich [54] also reported a similar trend for rubber modified epoxies and unmodified epoxies, and suggested that the ΔK values at an fatigue crack growth rate of 10^{-3}mm/cycle have a linear relationship with respect to the square root of the mean molecular weight between crosslinks, M_c, as shown in Fig.2.36.

2.5.3.2 Effect of morphology

In multiphase polymers the morphology, e.g. the volume fraction of secondary phase, size of particular phase, etc., affects the fracture toughness. There is little information about these effects on fatigue crack propagation. However, generally, materials with a higher fracture toughness have better resistance to fatigue crack propagation.

Kinloch and Hunston [58] investigated the relationship between the volume fraction of rubber particles and G_c in rubber modified epoxy. It was reported that the fracture toughness increased monotonically as the volume fraction of rubber increased, and that the effect of volume fraction was greater in the more ductile matrix (which corresponds to a lower crosslink density), as mentioned before in section 2.4.6.2. Karger-Kocsis and Friedrich [92] studied the effect of rubber content on fatigue crack growth rate, and suggested that the ΔK values at a fixed fatigue crack growth rate increases with increasing rubber content. This suggests that the fatigue resistance increases as rubber content increases.

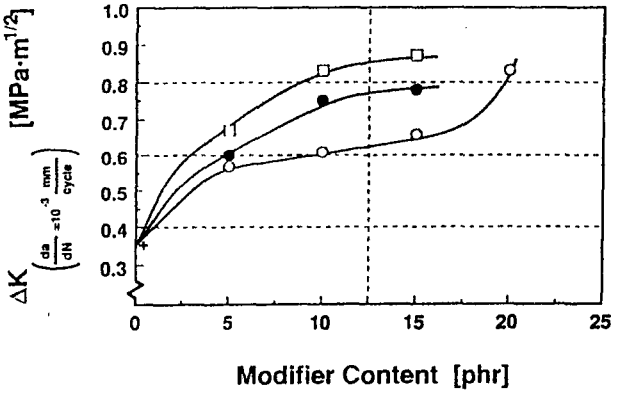


Fig.2.37 Effect of rubber content on fatigue crack propagation ; unmodified (+), CTBN rubber modified (○), silicone rubber modified (●), CTBN+silicone (□) [92]

Kim et al. [60] investigated the effect of particle size in rubber modified epoxy, without changing the volume fraction of the particles. They reported that the fracture toughness increased with decreasing particle size, for a low degree of crosslinking, but that there was little effect of particle size for highly crosslinked epoxy. They also reported that particles less than 0.2μm in diameter were ineffective for improving the toughness, because it was difficult for very small particles to cavitate, as discussed in section 2.4.6.3.

Azimi et al. [51, 93] also studied the effect of rubber content and particle size on fatigue crack growth rate in rubber modified epoxies. They reported that the fatigue resistance increases as rubber content increases, when the applied ΔK value is relatively high, and that there is little effect of rubber content on fatigue resistance at relatively low applied ΔK values. The critical value at which the rubber content starts to affect the fatigue crack growth rate is considered to be determined by the relative size of the plastic zone and the particle size.

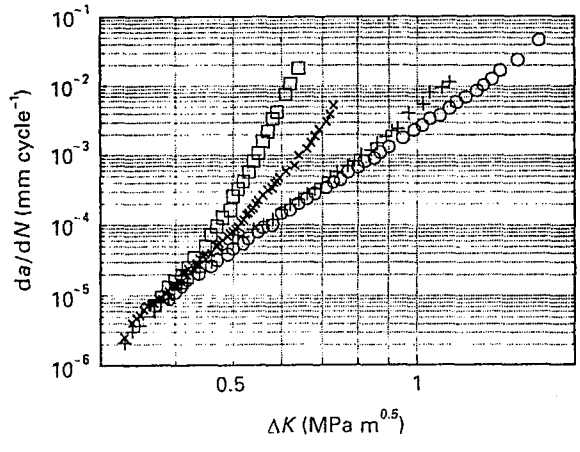


Fig.2.38 Effect of rubber volume fraction on fatigue crack growth rate in rubber modified epoxies: 0%(□), 1%(×), 5%(+), 10%(○) [93]

Azimi et al. [51,93] also reported that the materials with smaller rubber particles have a better fatigue resistance. They concluded that the volume fraction of rubber affects the slope of the fatigue crack growth rate curve, and that the near-threshold fatigue behaviour is strongly affected by the rubber particle size, but not by the rubber content.

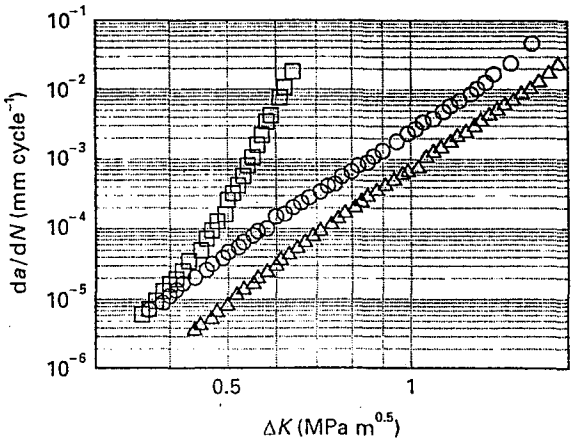


Fig.2.39 Effect of rubber particle size on fatigue crack growth rate in rubber modified epoxies: unmodified epoxy(□), 1.5mm(○), 0.2mm(△) [93]

2.6 Concluding remarks

This Chapter has reviewed the basic principles of fracture mechanics, the deformation behaviour of polymers, the toughening mechanisms of rubber modified epoxies and the factors which affect the static fracture toughness and fatigue behaviour. From an understanding of these principles it is possible to investigate in detail the fracture behaviour of toughened epoxy polymers under fatigue conditions. The materials and the experimental techniques which have been used in the present study will be described in the next Chapter.

Chapter Three

Materials and Experimental Techniques

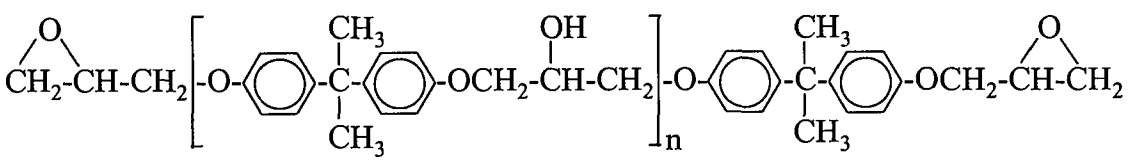
3.1 Introduction

A brief description of the materials which are used in this study is presented in this Chapter. The procedure to make the cast sheets of materials is also reviewed. The following sections then show the experimental techniques to investigate the material properties, which include the modulus, fracture toughness, glass transition temperature, fatigue crack growth rate, etc. A description of the techniques for the fractographic studies follows. Finally, the method of image analysis, which is used to quantify the microstructural parameters, is reviewed.

3.2 Materials

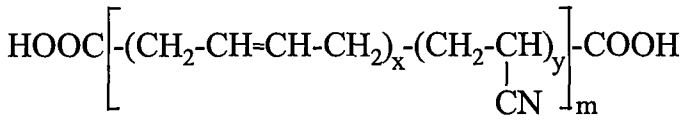
Three different types of materials are used in this study. The first one is a general rubber modified epoxy resin (RME). The second one is a rubber-modified epoxy resin with bisphenol-A (BPA) added, which is used to investigate the effect of rubber particle size, as described later. The last one is a thermoplastic modified epoxy resin (TPME), which is utilised to check the effect of morphology much more comprehensively. The appropriate unmodified epoxy resin (UME) is used as a reference material for each type.

The first two types of materials, the general RME series and the RME with BPA added series, consist of epoxy 'AY105', a diglycidyl ether of bisphenol-A (DGEBA), produced by Ciba-Geigy. Its chemical structure is as follows:

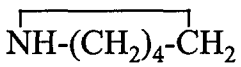


where n has the values n=0 (87.2w/w%), n=1 (11.1w/w%), n=2 (1.5w/w%) and n>2 (0.2w/w%). The epoxy equivalent weight is approximately 190g/mol.

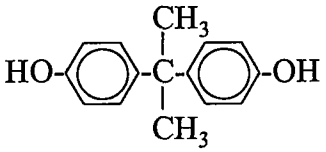
The RME also contains 'CTBN1300X8', carboxyl-terminated acrylonitrile-butadiene copolymer, produced by B.F.Goodrich. It is represented by:



The carboxyl content is 2.37w/w% and the acrylonitrile content is 17w/w%. The molecular weight is approximately 3500g/mol. The curing agent used for the general RME series and RME with BPA added series is piperidine, which is represented by:



The RME with BPA added series also contains bisphenol-A. Its chemical structure is same as the main part of DGEBA, as follows.



The thermoplastic modified epoxies (TPME) series contains epoxy 'MY9512', a tetraglycidyl 4,4'diamino diphenyl methylene (TGDDM), produced by Ciba-Geigy, as a base resin. TPME series also contains a reactively terminated polyethersulphone (PES) copolymer, and 4,4'-diamino diphenyl sulphone (DDS) is used as a curing agent.

All formulations are listed in Table 3.1 and Table 3.2. The preparation for the general RME series was started by hand mixing preheated 'AY105' and 'CTBN1300X8' for approximately 5-10 minutes. The mixture was heated again to 60-70°C in a water bath, and then mixed with an electric stirrer for 5 minutes. Then, the degassing process was done in heated vacuum oven until frothing stopped. The mixture was cooled down to 30-40°C, and then piperidine added

slowly. After a gentle hand-mix for 10 minutes, the mixture was poured into a preheated mould and cured. It was then allowed to cool down to ambient temperature. The UME material was prepared in the same way, after excluding the rubber addition process and electric stirrer process.

Table 3.1 Formulations of the general RME series and the RME with BPA added series

Description	AY105 (phr)	1300X8 (phr)	BPA (phr)	piperidine (phr)	curing condition
15phrRME120	100	15	0	5	120°C x 16h
UME120	100	0	0	5	120°C x 16h
15phrRME160	100	15	0	5	160°C x 6h
UME160	100	0	0	5	160°C x 6h
5phrRME120	100	5	0	5	120°C x 16h
5phrRME120+BPA	100	5	24	5	120°C x 16h
UME120+BPA	100	0	24	5	120°C x 16h

Note: "phr" means parts per hundred resin

Table 3.2 Formulations of the TPME series

Description	MY9512 (phr)	PES copolymer (phr)	DDS (phr)	curing condition
PES0	100	0	31.47	150°C x 4h 180°C x 4h in N_2 200°C x 3h in N_2
PES10	100	14.61	31.47	
PES20	100	32.87	31.47	
PES25	100	43.82	31.47	

For the RME with BPA added series, the preparation was started by adding BPA to preheated 'AY105' with gently stirring. The mixture was put into the oven at 120°C, and stirred continuously. It was kept until all the BPA was dissolved. Then, it was cooled down to 60-70°C, and the 'CTBN1300X8' was added. This procedure was exactly the same as for the general RME materials. For the UME with BPA added material, the rubber addition process and electric stirrer process were omitted.

For the TPME series, the preparation was started by dissolving the granules of PES copolymer in a methylene chloride/methanol (95/5 by volume). 'MY9512' and DDS were then added. The mixture was cast into the mould preheated at 150°C, and degassed for 30minutes. in a vacuum oven. Then, the materials were cured at 150°C for 4 hours, 180°C for 4 hours and 200°C for 3 hours. At both 180°C and 200°C, the curing was done in a nitrogen atmosphere. For PES0, the first process of dissolving PES copolymer was omitted, the preparation started with just the MY9512 and DDS mixture.

3.3 Fracture toughness measurements

Compact tension tests were conducted to measure the fracture toughness of the materials. The adopted procedures were in accordance with ASTM standard D5045-91a. Specimens were cut from the moulded sheets into the geometry shown in Fig.3.1.

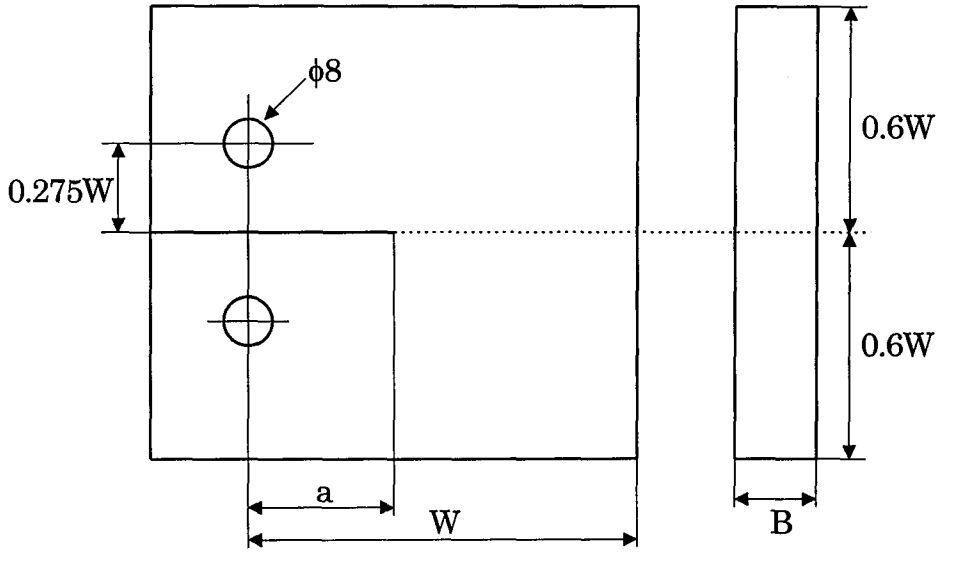


Fig.3.1 Compact tension specimen

The width, W, was 54.2mm. Then, the initial crack was introduced by tapping a razor blade into the saw-cut notch in order to cause a natural crack growth. The initial crack length was controlled in the range of $0.45<a/W<0.55$. Then, samples were tested at room temperature (23°C) using an 'Instron 1185' or 'Instron 1186' testing machine, with an appropriate crosshead speed. The load-displacement curve was obtained and the provisional toughness K_Q was calculated from the following equations:

$$K_Q=(P_Q/BW^{1/2})f(x) \quad (3.1)$$

$$f(x)=(2+x)(0.886+4.64x-13.32x^2+14.72x^3-5.6x^4)/(1-x)^{3/2} \quad (3.2)$$

$$x=a/W \ (0.2<x<0.8) \quad (3.3)$$

The validity of K_Q was checked via the following size criteria :

$$B, a, (W-a) > 2.5(K_Q/\sigma_y)^2 \quad (3.4)$$

If these criteria were satisfied, the value of K_Q was taken to be the fracture toughness, K_{Ic}.

3.4 Modulus measurements

Three point bend tests were employed to measure the elastic modulus (flexural modulus) of the materials. The adopted procedures were in accordance with ASTM standard D790M-86. Beam specimens were cut from the moulded sheets according to the ASTM specifications.

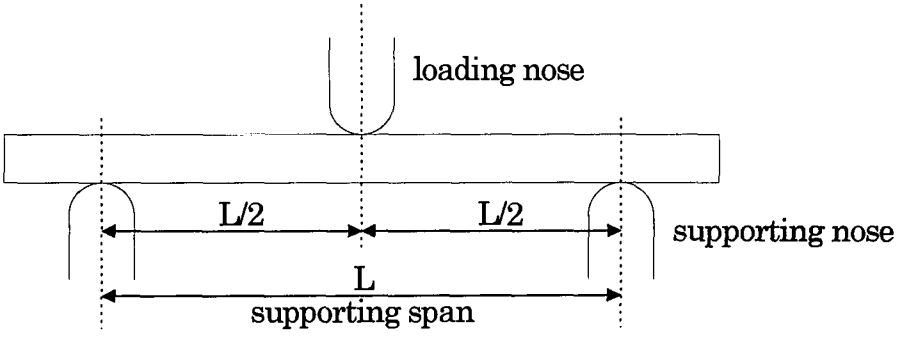


Fig.3.2 Three point bending test

The following dimensions were chosen: width 10mm (for the RME series and the RME with BPA added series) and 6.5mm (for the TPME series), depth 4mm (for the RME series and the RME with BPA added series) and 3.5mm (for the TPME series), length 75-80mm, and support span 60mm. The span-to-depth ratio was calculated as 15 for the RME series and the RME with BPA added series, and as 17.1 for the TPME series. Both values were within the ASTM requirement.

A strain rate, Z, of 0.01(mm/mm·minute) was used. The crosshead speed was set to the calculated value from the following equation:

$$R=ZL^2/6d \qquad (3.5)$$

where R is the crosshead speed (mm/minute), L is the support span (mm), d is the depth of beam (mm), and Z is the strain rate (mm/mm·minute). The elastic modulus was calculated by the following equation:

$$E=L^3m/4bd^3 \qquad (3.6)$$

where E is the modulus in bending (MPa), b is the width of beam (mm), and m is the slope of the tangent to the initial straight-line portion of the load-deflection curve (N/mm).

3.5 DSC and DMTA studies

Differential scanning calorimeter (DSC) measurements were conducted to investigate the glass transition temperature, T_g. The measurement was carried out with a heating rate of 10°C/minutes, and using a temperature range of 30°C to 160°C for the general RME series and RME with BPA added series, and 30°C to 300°C for the TPME series. Typical DSC data are shown in Fig.3.3. Heat flow changes around T_g arise due to the heat release or absorption according to the transition. The value of T_g was determined as the middle point of the changing temperature region.

It was difficult to determine the glass transition temperature of the TPME series by a DSC measurement, because its T_g is quite high and thermal

degradation started below the T_g. Thus, dynamic mechanical thermal analysis (DMTA) measurements were also done for these materials. A specimen, which had a typical size of 1.5mm x 6mm x 50mm, was subjected to an oscillating sinusoidal stress of 5Hz. The tensile mode of operation was selected, and the measurement was carried out using a heating rate of 5°C/minutes, from 30°C to 280°C. Typical DMTA data are shown in Fig.3.4. The value of T_g was determined as the temperature at which the loss factor, tanδ, possessed the maximum value.

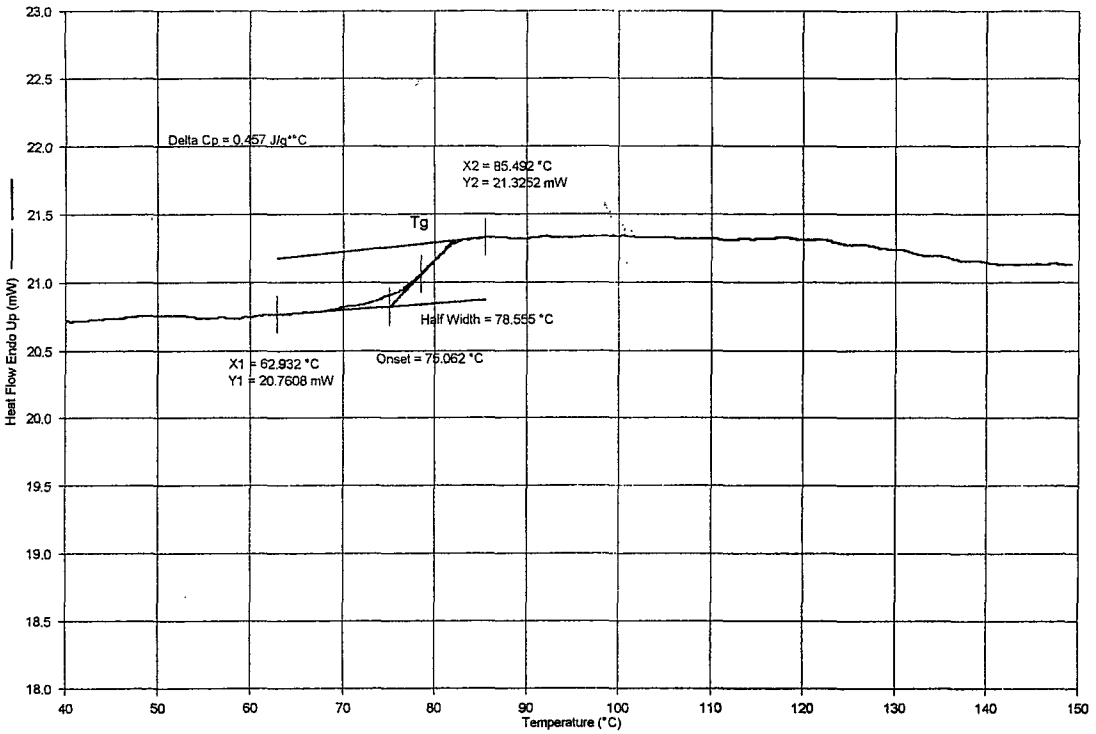


Fig.3.3 Typical DSC data (UME160)

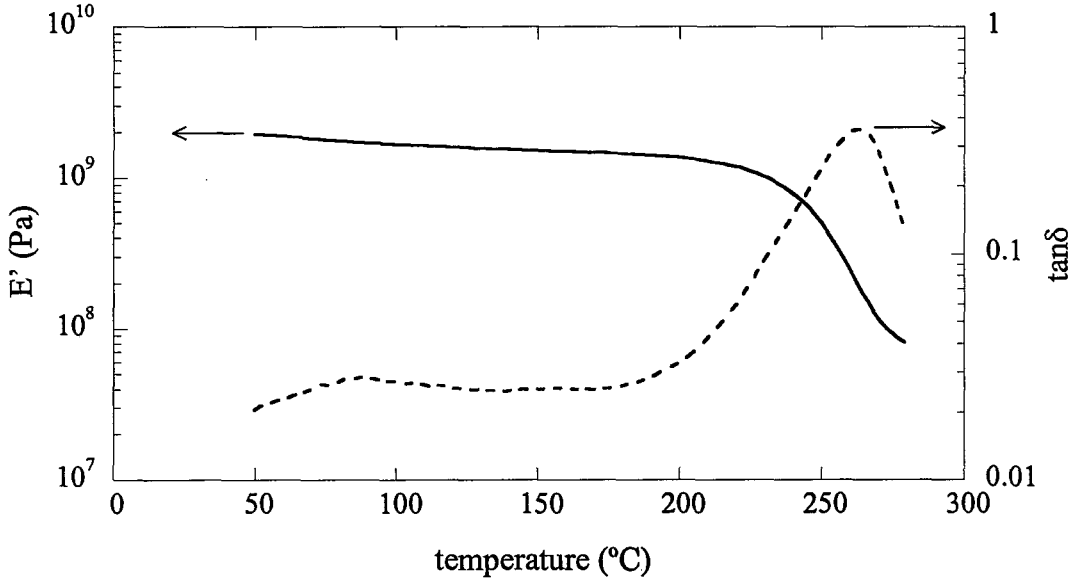


Fig.3.4 Typical DMTA data (PES0)

3.6 Fatigue crack growth rate studies

Large compact tension specimens were used to measure the fatigue crack growth rate. Specimens were cut from moulded sheets into the geometry shown in Fig.3.1. The width, W, was 128mm. The initial crack was then introduced by tapping a razor blade into the saw-cut notch in order to cause a natural crack growth, as for the static tests. The initial crack length was controlled in the range of $0.35<a/W<0.45$. Then, samples were tested using a 'Mayes' cyclic fatigue testing machine. All experiments were conducted at a room temperature of 23±3°C.

Both displacement-control and load-control tests were used for this study. The test was started under displacement-control to determine the threshold value, below which there is no fatigue crack propagation. The test was then changed to load-control, and the fatigue crack growth rate was measured until the specimen failed. A sinusoidal wave form loading was employed at a frequency of 5 Hz. The load ratio (R=minimum load/maximum load) was 0.2.

During the experiments, the crack length was measured both electrically and optically. A crack gauge was used for the electrical method. It was bonded to

the side of the specimen using an adhesive, and the crack length was measured as the electrical resistance of the gauge changed as the fatigue crack grew.

The maximum value of the stress intensity factor, K_{max}, and the range of K and ΔK were calculated from the following equations:

$$K_{max}=(P_{max}/BW^{1/2})f(x) \quad (3.7)$$

$$\Delta K=(\Delta P/BW^{1/2})f(x) \quad (3.8)$$

$$\Delta P=P_{max}-P_{min} \quad (3.9)$$

where P_{max} is the maximum load, and P_{min} is the minimum load. The function f(x) was calculated in the same manner as mentioned in equation 3.2.

There were sometimes differences between the measured crack lengths from the electrical method and the optical method, due to the effect shown in Fig.3.5. According to the standard, ASTM E647, the average crack length was taken for the calculation for the K value, via the following equation [94]:

$$a = (a_{gauge} + a_{micro})/2 \quad (3.10)$$

where a_{gauge} is the crack length measured using the crack gauge, and a_{micro} that measured optically.

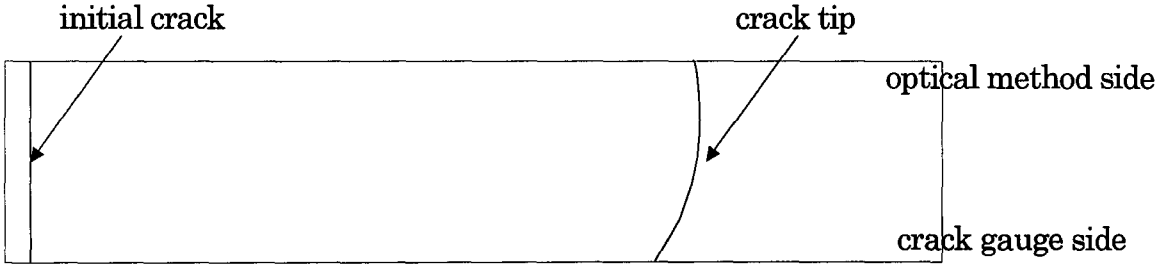


Fig.3.5 Schematic showing the fatigue fracture surface

There are two methods for calculating the fatigue crack growth rate, da/dN, from the data sets of the crack length, a, and the number of cycles, N. ASTM E647 recommends the two methods: the secant method and the incremental polynomial method [94]. The secant (or point-to-point) method simply involves calculating the slope of the straight line connecting two adjacent data points on the a versus N curve. It is expressed as follows:

$$(da/dN)_i = (a_{i+1} - a_i) / (N_{i+1} - N_i) \tag{3.11}$$

The incremental polynomial method involves fitting a second-order polynomial (parabola) to sets of (2n+1) successive data points, where n is usually 1, 2, 3 or 4. The form of the equation for the local fit is as follows:

$$\hat{a}_i = b_0 + b_1 (N_i - C_1)/C_2 + b_2 [(N_i - C_1)/C_2]^2 \tag{3.12}$$

where b_0, b_1 and b_2 are the regression parameters that are determined by the least squares method over the range of $a_{i-n} \leq a \leq a_{i+n}$. The value $\hat{a}_i$ is the fitted value of the crack length at N_i. C_1 and C_2 are the parameters which are used to scale the input data within the range of -1 to 1. The fatigue crack growth rate at N_i, $(da/dN)_i$, is obtained from the derivative of the above parabola, which is given by:

$$(da/dN)_I = b_1/C_2 + 2b_2 (N_i - C_1)/C_2^2 \tag{3.13}$$

We used the incremental polynomial method and chose n=3, i.e. 7 successive data points, for calculating the fatigue crack growth rate.

3.7 Localised heating effects

The materials having large hysteresis loop under their stress-strain curve have the possibility to generate heat during the fatigue tests, and we might have to take any such localised heat effects into account. In order to check this effect, the precise measurement of the surface temperature of the specimens were conducted during the fatigue tests, using an infrared camera system. Two materials, 15phrRME160 (which has the most possibility for any localised temperature rise ocuurring) and 15phrRME120 were studied.

As shown in Fig.3.6, the experimental set-up consisted of an infrared camera, a controller, a monitor and PC. The highest temperature resolution is 1/16°C. The measurement was carried out under a cyclic frequency of 5Hz.

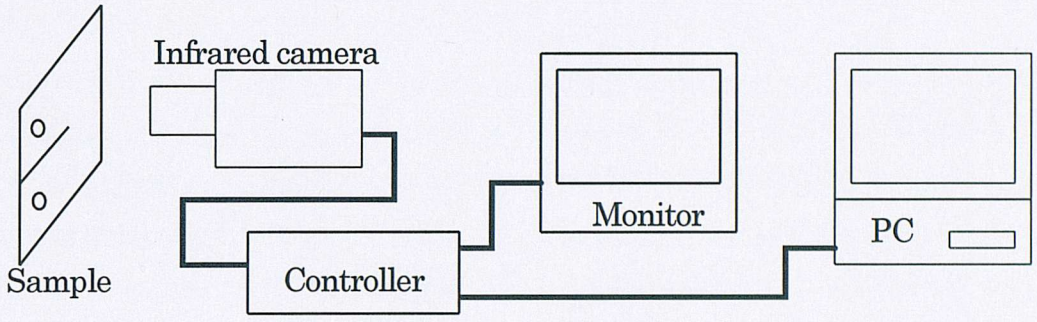


Fig.3.6 Schematic set-up of the infrared camera system

3.8 Microscopy studies

Transmission optical microscopy (TOM), scanning electron microscopy (SEM) and transmission electron microscopy (TEM) were utilised for observing the operative mechanisms in the rubber-modified and unmodified epoxy.

For TOM observation, thin sections, perpendicular to the fracture surface and parallel to the crack propagation direction, were obtained from the mid-plane of the specimen as shown in Fig.3.7, using petrographic thinning techniques [95].

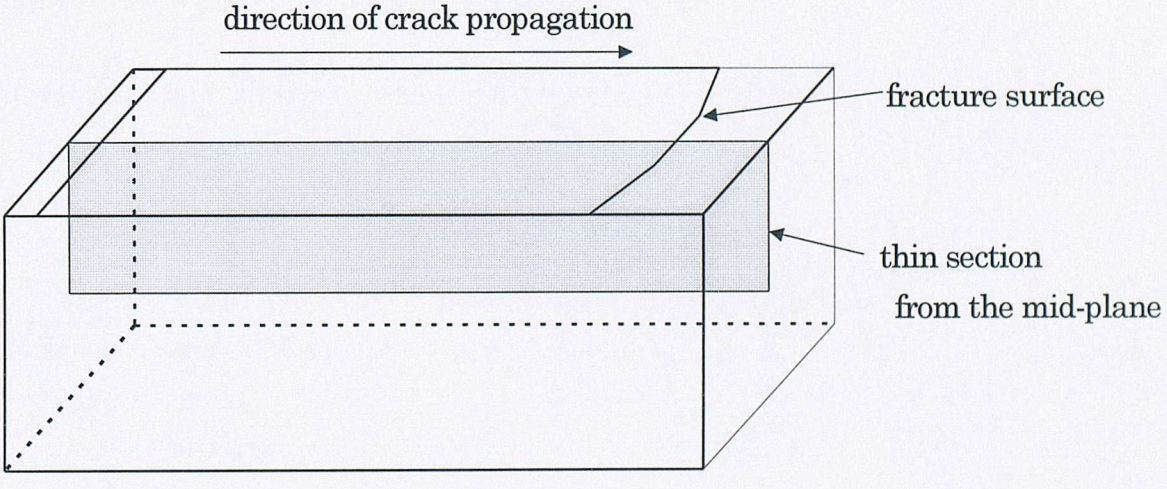


Fig.3.7 Thin section from mid-plane (plane strain region)

Tested CT specimens were cut into small samples, which included the damage zone, and embedded in a clear mounting epoxy. Then, they were reduced in thickness by cutting and polishing until the final thickness of 50-100μm was reached. These thin sections were examined by using a 'Nikon Optishot-2' microscope under both bright field and crossed polars.

SEM was also used to examine the fracture surfaces of the tested specimens. All samples were coated with a thin film of gold by sputtering before SEM examination. The instrument used was 'JEOL JSM-5300' scanning electron microscope operated at 25-30kV. In some cases, we used polished samples. These samples were polished in a similar way of petrographic techniques, and then etched with appropriate etching liquid to improve the SEM image. Potassium permanganate mixed acid (sulphuric acid and phosphoric acid) solution was used for etching the materials containing epoxy 'MY9512'. The etching procedure is as follows [96]:

(i) Dissolve a small quantity of potassium permanganate in acid mixture (5:2:2 volume of sulphuric asid:phosphoric acid:distilled water) in a ultrasonic bath. The concentration is 0.1g potassium permanganate per 10ml acid mixture.
(ii) Cool the solution down to 2-5°C, and a sample is etched for 2 minutes in the solution, agitated with a magnetic stirrer.
(iii) The sample is rinsed using ultrasonic agitation. Firstly, it is rinsed in 10:1 sulphuric acid:distilled water until any pink colouration due to the presense of potassium permanganate has disappeared. Then, the sample is rinsed 3-4 times in 100vol hydrogen peroxide and finally ethanol.

This etching was used to improve the contrast of the SEM image. The etching liquid selectively attacks PES copolymer phase, and epoxy resin phase remains intact.

For TEM observation, samples were initially trimmed to the appropriate size and shape. Then, trimmed samples were stained using osmium tetroxide solution. Osmium tetroxide stains the materials having carbon double-bonds present. Therefore, rubbery phase is selectively stained, and the TEM image is much improved.

3.9 Image analysis studies

The microstructural parameters of the secondary phase in a multiphase materials can be obtained from SEM micrographs, using the image analysis techniques. The digitised SEM picture (Bitmap Format) was converted to the PICT Format data using 'Adobe Photoshop' software. Then, the interface between the matrix and the secondary phase was manually denoted using 'Claris Draw' software, and converted the extracted image to the Raw File Format for further data processing. The data were stored in the computer, and the results such as the volume fraction and the average particle size were calculated. Although the information solely on the area fraction may be obtained directly from the SEM micrographs, it can be more easily translated to the volume fraction via the above technique [97]. Three to five SEM pictures were used for each calculation.

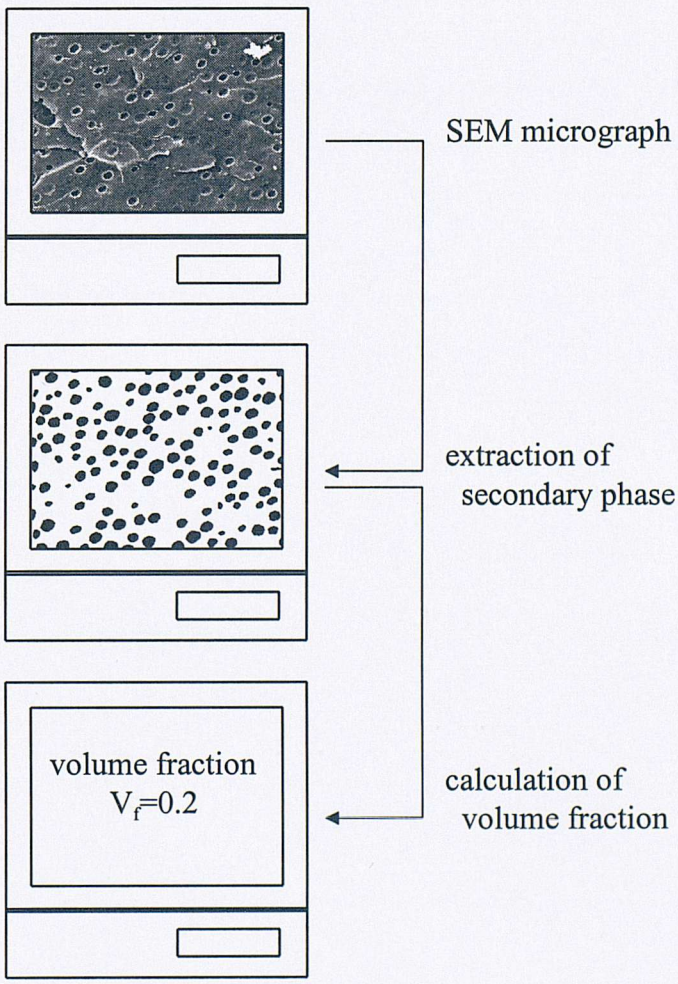


Fig.3.8 Diagram of image analysis

3.10 Concluding remarks

This Chapter has described the chemical structure and the formulations of the general RME series, the RME with BPA added series and the TPME series. The experimental techniques including the measurements of fracture toughness, moduli, fatigue crack growth rates and localised temperature rise, DSC and DMTA studies, microscopy studies and the image analysis technique have also been reviewed. The basic material properties such as static mechanical properties, glass transition temperature, crosslink density and the microstructure will be discussed in the next Chapter.

Appendix : Volume fraction and average particle size

The information obtained from the SEM micrographs is not the volume fraction of the particles but the area fraction of the particles. However, it is known from the quantitative stereology [97] that the area fraction is equal to the volume fraction. Thus, the volume fraction of the particles can also be obtained. The average particle size is calculated by the procedure described below. The average intercept area of the particles, S, is calculated. The value of S is related to the radius of the particle, r_p, via the following equation [97] :

$$S = (2/3)\pi r_p^2 \tag{3.14}$$

Thus, the average radius of the particle, r_p, is given by :

$$r_p = (3S/2\pi)^{1/2} \tag{3.15}$$

Chapter Four

Basic Material Properties

4.1 Introduction

Before discussing the fatigue behaviour of the toughened epoxy polymers, it is important to investigate their static material properties, i.e. the properties measured under a constant rate of displacement. Static mechanical properties such as modulus, yield stress, static fracture toughness, etc. are essential parameters in order to discuss the fatigue behaviour in later Chapters. Thermal properties such as the glass transition temperature are also important parameters to characterise the molecular dynamics and structure of the polymers. These basic material properties and some initial fractographic studies will be discussed in the present Chapter.

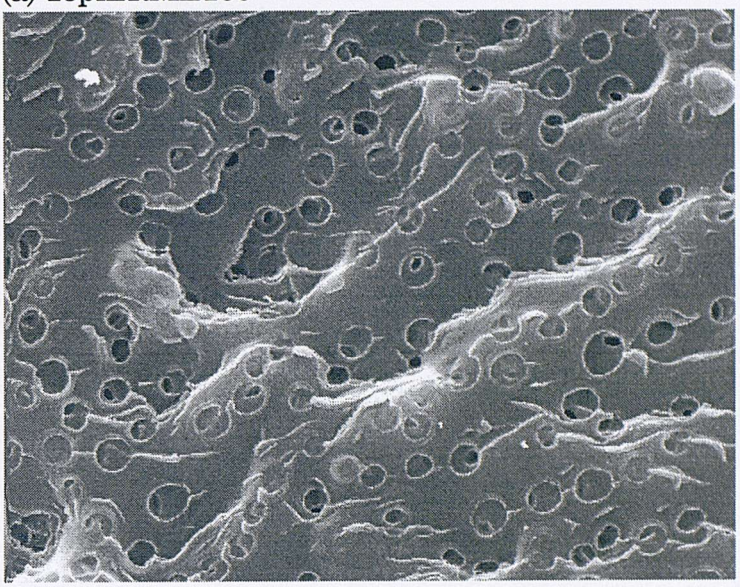
As discussed in Chapter Three, moduli were measured using three point bending tests and the static fracture toughness was measured using compact tension specimens. The glass transition temperature was measured using DSC and DMTA. Very accurate modulus measurements, via DMTA, were also undertaken to investigate the crosslink density of the epoxy matrix. The microstructures of the toughened epoxy polymers were characterised using SEM micrographs.

4.2 Microstructure

4.2.1 RME series and RME with BPA series

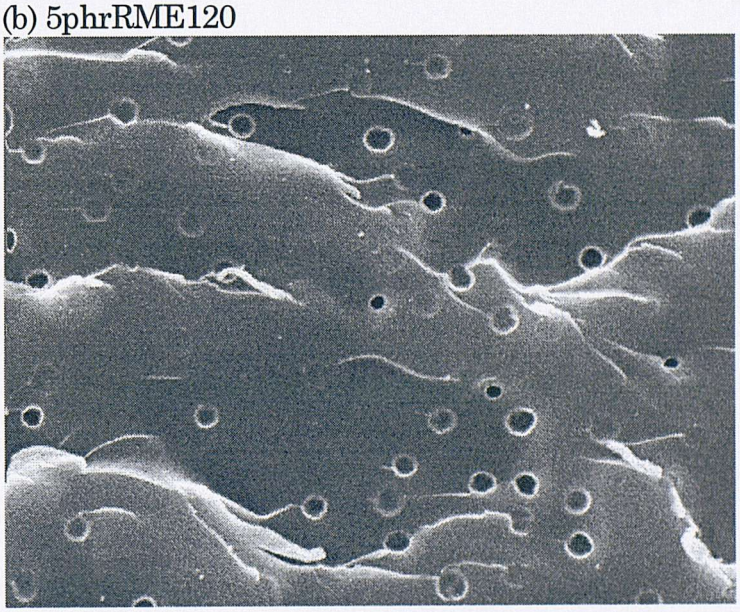
The 15phrRME160, 5phrRME120, 15phrRME120 and 5phrRME120+BPA materials have a particulate microstructure, i.e. dispersed rubber particles in a continuous epoxy matrix. Fig.4.1 shows the microstructure of 15phrRME160 and 5phrRME120. For both materials, it can be seen that spherical rubber particles are dispersed in an epoxy matrix.

(a) 15phrRME160



20μm

(b) 5phrRME120



20μm

Fig.4.1 SEM micrographs of the fracture surfaces for 15phrRME160 and 5phrRME120

Considering the particle size of the dispersed rubber phase, there is relatively little difference in the particle size with respect to the 15phrRME160, 5phrRME120 and 15phrRME120 materials. The particle radius is around 1.7μm for 15phrRME160, 1.4μm for 15phrRME120 and 1.0μm for 5phrRME120. Therefore, it may be stated that the rubber content and the curing temperature have only a very slight effect on the size of the dispersed rubber particles. This effect may be explained as follows. As the CTBN rubber is initially miscible in the DGEBA epoxy, rubber particles form during the curing process. As the curing reaction proceeds, the epoxy resin polymerises and the miscibility of the epoxy resin and the rubber decreases. Finally, phase separation occurs and dispersed rubber particles are formed. When the rubber content and/or the curing temperature is changed, the miscibility of the rubber and the epoxy resin, and their viscosities, are affected. Consequently, the speed of phase separation changes and thus the final particle size changes. That is the reason why the particle size varies for the 15phrRME160, 5phrRME120 and 15phrRME120 materials.

Several researchers have investigated the phase separation process during the curing of rubber modified epoxies [98-102]. For example, Kim and Kim [98] utilised a light scattering technique and reported that the phase separation mechanism for the DGEBA epoxy and the CTBN rubber system is the nucleation and growth of rubbery phase. Chen and Lee [101] also suggested the nucleation and growth is the phase separation mechanism for a similar DGEBA/CTBN system. Hsich [100] reported that not only nucleation and growth process, but also spinodal decomposition, are observed during the phase separation for a DGEBA/CTBN system. Spinodal decomposition is the phase separation process in which any infinitesimal composition fluctuations in the mixture leads to a phase separation. There is no sharp interfacial boundary between the separated phases in the initial stage of this type of phase separation. He also suggested that nucleation and growth gives larger rubber particles than spinodal decomposition.

The microstructure of the 5phrRME120+BPA material is basically the same as that of the 15phrRME160, 5phrRME120 and 15phrRME120 materials. However, the rubber particle size of the 5phrRME120+BPA material is extremely small, as shown in Fig.4.2. The particle radius is 0.2-0.3μm. Although it is not yet clear why the addition of BPA causes the smaller particle size, it may be that BPA changes the miscibility of the rubber and/or the speed of the chemical reaction. It

was observed that the temperature of the mixture of epoxy, BPA, rubber and curing agent rose more rapidly than that of the mixture without BPA. This observation implies that the curing reaction might be accelerated when BPA is added. Whether the phase separation mechanism is nucleation and growth or spinodal decomposition, small rubbery domains form first and then become larger. Therefore, if the curing reaction is accelerated by the addition of BPA, the epoxy resin might cure so quickly that there is not enough time for the rubber particles to become large. Thus, a small particle size would be obtained for the 5phrRME120+BPA material.

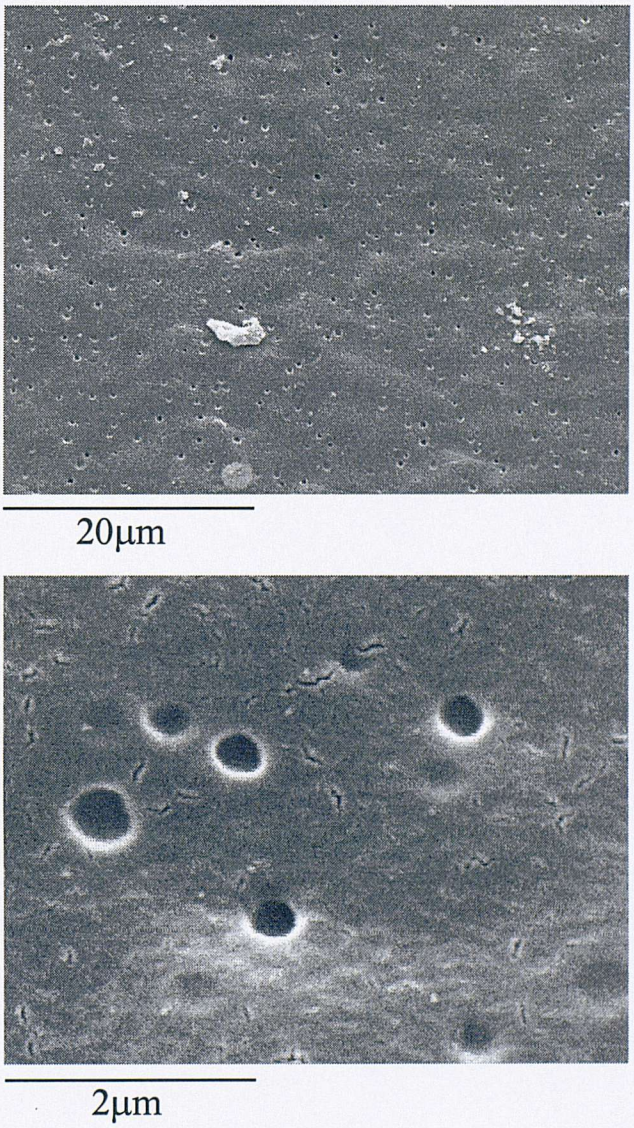


Fig.4.2 SEM micrographs of the fracture surfaces for 5phrRME120+BPA

The mean radii of rubber particles, r_p, in the 15phrRME160, 5phrRME120, 15phrRME120 and 5phrRME120+BPA materials are summarised in Table 4.1. The r_p values were calculated from between three and five SEM micrographs, each containing approximately 100 rubber particles. Fig.4.3 shows the particle size distribution for the 15phrRME160 material. The measured particle radius is scattered within the range of 0.75μm to 2.5μm, whereas the mean value is 1.7μm. As Underwood suggested [97], the measured particle radius is scattered even if all the "real" particles have a uniform radius, because the measured radius depends on which position of the particle the crack intersects. Therefore, the real particle size distribution may have a smaller scatter associated with it than that shown in Fig.4.3.

Table 4.1 Mean radius of the rubber particles

Material	r_p (μm)	σ(μm)
15phrRME160	1.7	0.30
5phrRME120	1.0	0.20
15phrRME120	1.4	0.25
5phrRME120+BPA	0.2-0.3	

Note : σ means standard deviation

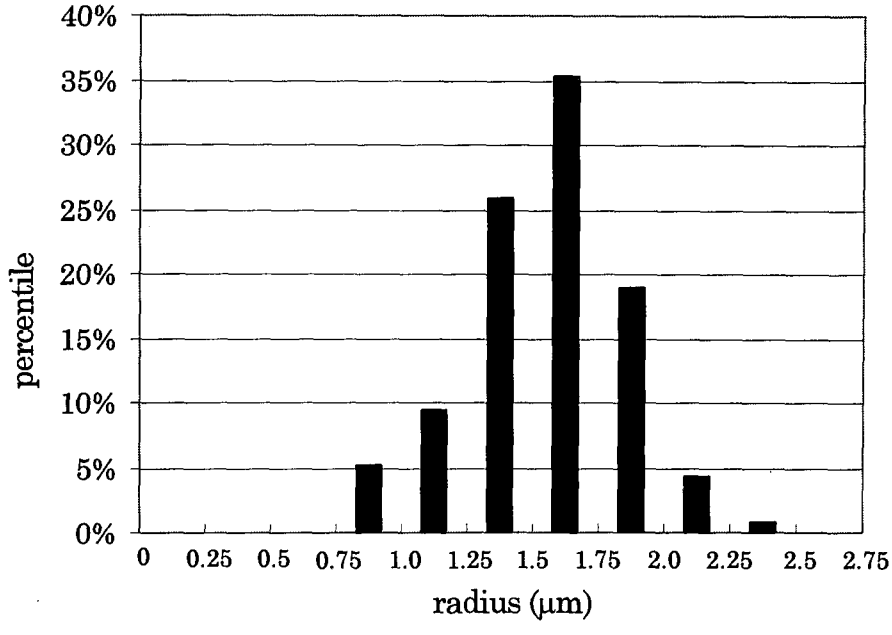


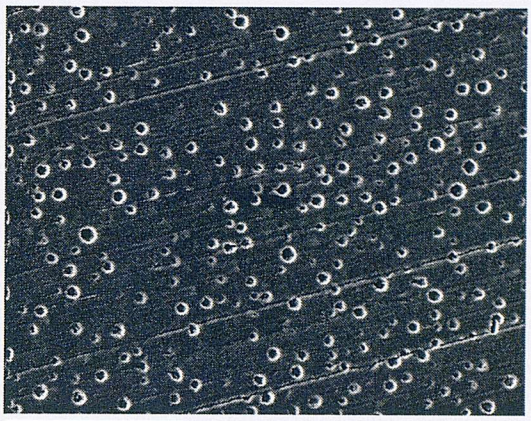
Fig.4.3 Typical particle size distribution for 15phrRME160

4.2.2 TPME series

The TPME series, which contains a polyethersulphone (PES) copolymer toughener, has a greater variety of microstructures than the RME series, or the RME with BPA added series. When the PES copolymer content is small, it is observed that the PES copolymer phase is dispersed as particles in the epoxy matrix. As the PES copolymer content increases, however, the microstructure becomes co-continuous in nature. Finally, when the PES copolymer content is relatively high, the matrix phase is inverted. Tedguy [103] also reported similar results for the microstructure of these materials. To illustrate these points, Fig.4.4 shows the microstructure of the PES10, PES20 and PES25 materials. The materials were polished using 0.25μm polishing powder, and etched, before SEM observation; according to the procedure which was discussed in Chapter Three.

As may be seen in Fig.4.4, the PES10 material (where the PES copolymer content is 14.61phr) contains dispersed PES copolymer particles of approximately 0.5μm radius. For the PES20 material (where the PES copolymer content is 32.67phr), the microstructure is co-continuous. Both the epoxy and PES copolymer domains are observed as continuous. It can be seen that the typical width of the PES copolymer domains is 15-30μm. The phase inversion is observed for the PES25 material (where the PES copolymer content is 43.82phr). The matrix is now the PES copolymer with the epoxy resin dispersed as spherical particles, with a radius of approximately 1μm.

(a) PES10



(b) PES20



(c) PES25

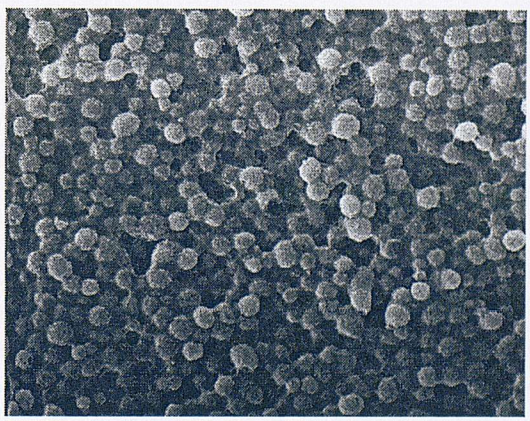


Fig.4.4 SEM micrographs of (a) PES10, (b) PES20 and (c) PES25

4.3 Glass transition temperature

4.3.1 Rubber modified epoxies

Glass transition temperature, T_g, is a basic material property which indicates the mobility of the molecules. Generally, for a given backbone structure, high T_g corresponds to a low mobility and low T_g corresponds to a high mobility. For crosslinked polymers, therefore, a high T_g often means a high crosslink density and a low T_g often means a low crosslink density. The T_g values of the epoxy matrix in the RME series, and the RME with BPA added series, were measured using DSC. These values are shown in Table 4.2.

Table 4.2 T_g of the epoxy phase and rubbery phase in the materials of the RME series and the RME with BPA added series

Material	T_g (epoxy) (°C)	T_g (rubber) (°C)
UME160	77.8	---
15phrRME160	68.5	-58(-52)
UME120	89.2	---
5phrRME120	86.1	-76
15phrRME120	84.7	-58(-55)
UME120+BPA	101.2	---
5phrRME120+BPA	98.5	-73

Note: The values of T_g(rubber) are from DMTA data
T_g(rubber) values in brackets are from DSC data of ref. [7]

The T_g value of the epoxy matrix of the material cured at 160°C is lower than that of the material cured at 120°C, when no BPA is added. This implies that the crosslink density of the epoxy matrix of the material cured at 160°C is lower than that of the material cured at 120°C. The T_g value of the epoxy matrix of the

material with BPA added is higher than that of the material without BPA. It seems, therefore, that the epoxy matrix of the material with BPA added has a higher crosslink density. However, this result is not direct evidence that the addition of BPA increases the crosslink density of epoxy matrix. BPA molecules may act as a diluent material of the epoxy matrix, and obstruct the motion of the epoxy molecules. If so, the addition of BPA can decrease the crosslink density, and increase the T_g value, simultaneously. For a more direct and precise evaluation of the crosslink density, we have to determine the average molecular weight between crosslinks, M_c. This can be measured using DMTA methods which give accurate modulus values. The M_c values and crosslink density will be discussed in detail in the next section.

The T_g value of the rubber modified epoxy is slightly reduced from that of the unmodified epoxy. This small change in the T_g value is considered to be caused by rubber molecules being dissolved in the epoxy matrix. When polymer A dissolves another polymeric material B, the T_g value of polymer A also changes. This is because the dissolved material B affects the mobility of polymer A. The T_g value of the modified polymer A is given by the following equation [104]:

$$T_g = \frac{\alpha_p (1-V_B) T_{g,A} + \alpha_d V_B T_{g,B}}{\alpha_p (1-V_B) + \alpha_d V_B} \qquad (4.1)$$

where V_B is the volume fraction of dissolved polymer B, $T_{g,A}$ is the T_g value of pure polymer A, $T_{g,B}$ is the T_g value of pure polymer B, and α_p and α_d are constants. For most cases, the following values of the constants α_p and α_d may be used [104] :

$$\alpha_p = 4.8 \times 10^{-4} /°C \qquad (4.2)$$

$$\alpha_d = 1.0 \times 10^{-3} /°C \qquad (4.3)$$

Hence, knowing T_g, $T_{g,A}$ and $T_{g,B}$, the volume fraction of dissolved polymer B may be calculated. For example, for 15phrRME160, T_g is 68.5°C, $T_{g,A}$ is 77.8°C and $T_{g,B}$ is -52°C. The calculated V_B value is around 3.5%. In the same manner, we can obtain a value of V_B of 1.0% for 5phrRME120, 1.5% for 15phrRME120 and 0.8% for 5phrRME120+BPA. Hence, the amount of CTBN rubber dissolved in the DGEBA epoxy matrix is quite small. It is reasonable, therefore, to consider that the

mechanical properties of the epoxy matrix in the rubber modified materials are virtually the same as those of the pure epoxy.

4.3.2 Thermoplastic modified epoxies (TPME)

For the TPME series, it was quite difficult to detect the T_g values using DSC. They were, therefore, measured using DMTA. Table 4.3 shows the T_g values of the TPME materials. The T_g value of the epoxy phase gradually decreases as the PES copolymer content increases, as for the rubber modified epoxies. The volume fraction of dissolved PES copolymer in the epoxy phase can be calculated in the same way as described above. It is calculated as 4.1% for PES10, 6.6% for PES20 and 9.4% for PES25. These values are slightly greater than those for the RME and the RME with BPA added series, but the amount of dissolved PES copolymer is still relatively small.

Table 4.3 T_g of the epoxy phase and PES copolymer phase in the TPME series

Material	T_g (epoxy) (°C)	T_g (PES copolymer) (°C)
PES0	263.1	---
PES10	256.5	185.4
PES20	253.8	187.6
PES25	248.9	191.6

4.4 Molecular weight between crosslinks

As mentioned before, the T_g value is only an approximate indicator of the crosslink density. In order to evaluate the crosslink density more precisely, we have to measure a more direct parameter, namely the molecular weight between crosslinks, M_c. A high M_c value corresponds to a low crosslink density, and a low M_c value corresponds to a high crosslink density. This parameter may be calculated using the rubbery equivalent modulus, E_r, which may be measured using accurate DMTA techniques. Examples of these DMTA data are shown in

Fig.4.5.

The relationship between M_c and E_r is given by the following equation [68]:

$$\log (E_r/3) = 6 + 293\rho/M_c \qquad (4.4)$$

where ρ is the density of the epoxy, 1.18g/cm^3. In the case of the unmodified epoxies, the measured modulus was used directly as the E_r value. However, in the case of the rubber modified epoxies, the Ishai-Cohen model [105] for the modulus of a particulate composite was employed to obtain the E_r value of the epoxy matrix.

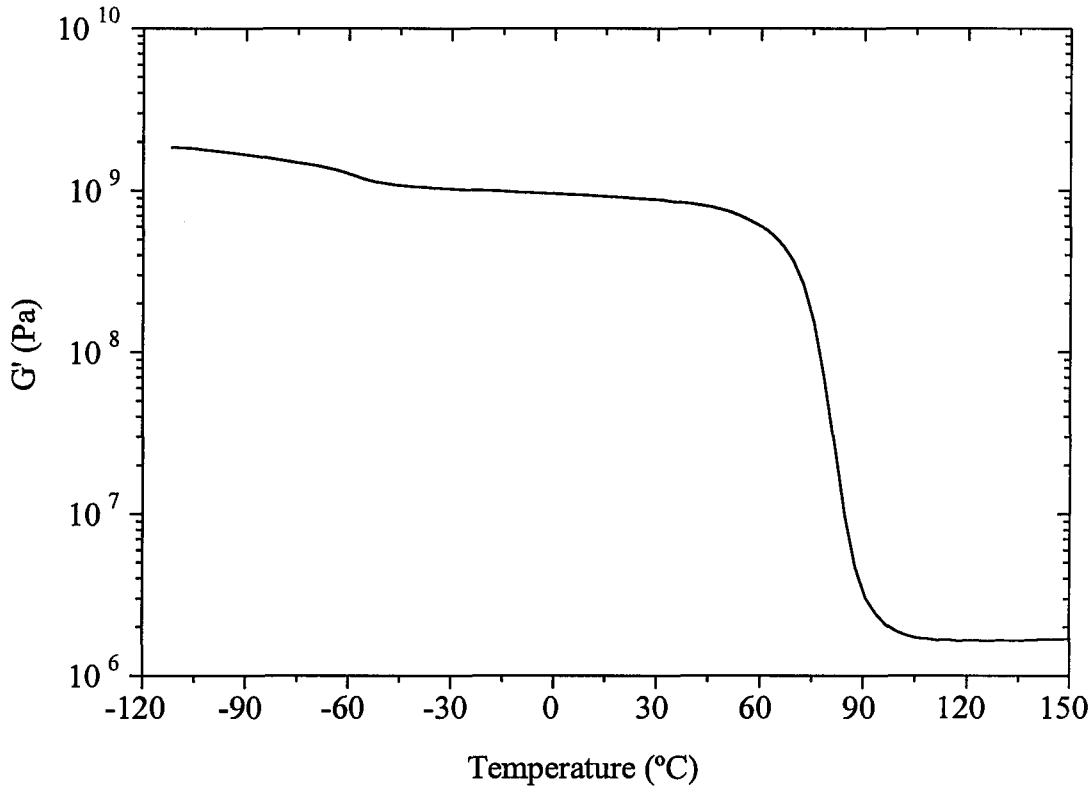


Fig.4.5 Typical data of the accurate DMTA measurements (15phrRME160)

There is another equation derived from the kinetic theory of rubber elasticity, e.g. [106]:

$$M_c = 3\rho RT/E_r \qquad (4.5)$$

where R is the gas constant. Table 4.4 shows the calculated M_c values of the epoxy matrix for the RME and the RME with BPA added series, via both equation 4.4 and 4.5.

As shown in Table 4.4, equation 4.5 gives higher M_c values than equation 4.4. However, both equations suggest that the materials cured at 120°C have the highest crosslink density, the materials with BPA added have the second highest and the materials cured at 160°C have the lowest crosslink density. It is also suggested that the variation of rubber content does not significantly affect the crosslink density of the epoxy matrix. For the TPME series, the degradation of the material occurred before a rubbery plateau modulus was observed. Thus, no data on the M_c values were obtained for the TPME series.

Table 4.4 The M_c values of the RME series and the RME with BPA added series

material	E_r (MPa)	$E_{r(epoxy)}$ (MPa)	M_c (eq.4.4) (g/mol)	M_c (eq.4.5) (g/mol)
UME160	5.7	5.7	1250	2200
15phrRME160	4.6	5.5	1310	2260
UME120	17.0	17.0	460	730
5phrRME120	14.0	16.0	480	780
15phrRME120	13.9	19.2	430	650
UME120+BPA	12.2	12.2	570	1030
5phrRME120+BPA	11.3	13.1	540	960

Table 4.5 shows the comparison between the calculated M_c values via equation 4.4 and the values of M_c reported by Kinloch et al. [56], who also used equation 4.4. There is fairly good agreement for the materials cured at 120°C. For the materials cured at 160°C, however, the calculated M_c values are far lower than the reported M_c values. It might be that the nonlinearity of equation 4.4 is one of the reasons which causes this difference. As shown in Fig.4.6, the calculated M_c value approaches infinity as the value of E_r approachs a value of 3MPa, and

equation 4.4 does not accept an E_r value below 3MPa. Therefore, if the measured E_r value is relatively low, a small error in the E_r value causes a significant difference in the calculated M_c value. For instance, a 10% error in the E_r value causes a 30% difference in the M_c value when E_r is around 5MPa, and the same error causes a 300% difference in the M_c value when E_r is around 3.5MPa.

Table 4.5 Comparison of the M_c values via equation 4.4

material	M_c (eq.4.4) (g/mol)	M_c (ref.[52]) (g/mol)
UME160	1250	4900
15phrRME160	1310	4370
UME120	460	590
15phrRME120	430	630

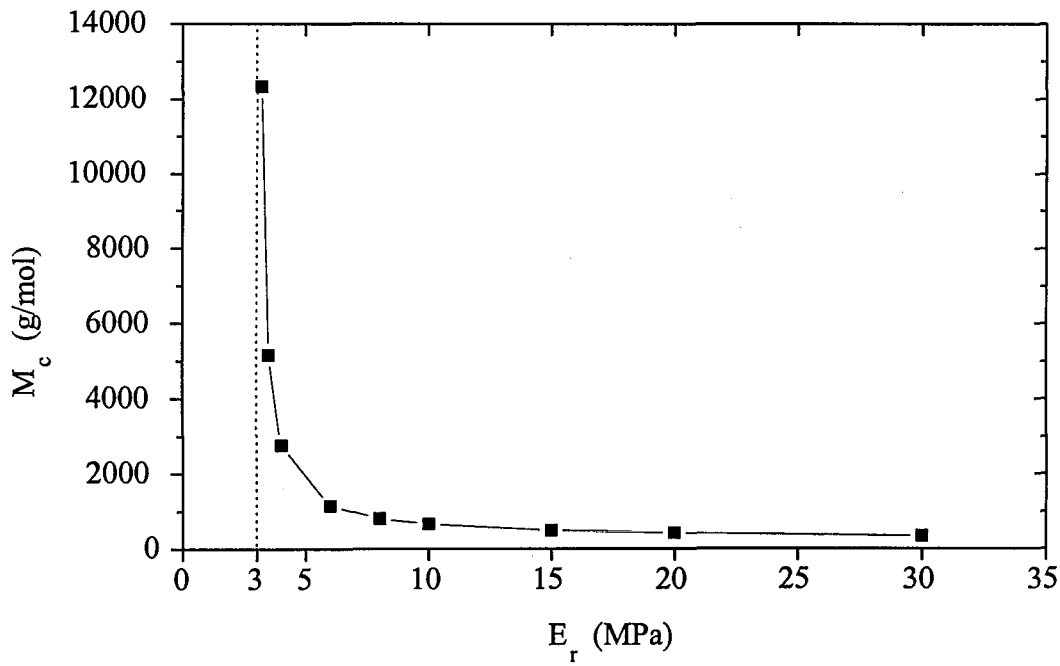


Fig.4.6 M_c as a function of E_r, calculated via equation 4.4

4.5 Mechanical properties

4.5.1 Rubber modified epoxies

Table 4.6 shows the mechanical properties of the rubber modified epoxy (RME) series and the RME with bisphenol-A (BPA) added series. The flexural moduli of all these materials are in the range of 2.43GPa to 3.35GPa. For the materials cured at 120°C, the modulus gradually decreases as the rubber content increases: 3.04GPa for UME120, 2.90GPa for 5phrRME120 and 2.43GPa for 15phrRME120. This same trend is seen for the materials cured at 160°C: the modulus is 3.35GPa for UME160 and 2.56GPa for 15phrRME160. The trend is considered to be due to the presence of the rubbery phase. The modulus of the rubbery phase is far smaller than that of the epoxy matrix, and the modulus of the rubber modified epoxy therefore decreases with an increasing volume fraction of rubbery phase.

Table 4.6 Mechanical properties of the materials of the RME series and the RME with BPA added series

Material	E (GPa)	K_{Ic} (MPa·m$^{1/2}$)	G_{Ic} (kJ/m^2)
UME160	3.35	1.20 (1.29)	0.38
15phrRME160	2.56	4.03 (4.23)	5.57
UME120	3.04	0.81 (0.88)	0.19
5phrRME120	2.90	2.22	1.49
15phrRME120	2.43	2.47 (2.64)	2.20
UME120+BPA	2.76	0.88	0.25
5phrRME120+BPA	2.77	3.01	2.87

Note: *G_{Ic} was calculated from the equation, $G=K^2(1-\nu^2)/E$*
Poisson's ratio was estimated as 0.35
The K_{Ic} values in bracket are from ref. [56]
For K_{Ic} values the peak load was used, except for 15phrRME160

The modulus of the material cured at 120°C is lower than that of the material cured at 160°C: 3.04GPa for UME120 and 3.35GPa for UME160; 2.43GPa for 15phrRME120 and 2.56GPa for 15phrUME160. The addition of BPA causes a slight decrease of modulus.

The measured K_{Ic} values of UME160, 15phrRME160, UME120 and 15phrRME120 agree well with those reported by Kinloch et al. [56]. The fracture toughness, K_{Ic}, of the rubber modified epoxies are all larger than those of the unmodified epoxies. For the materials cured at 120°C, the value of K_{Ic} increases from 0.81MPa·$m^{1/2}$ for UME120 to 2.47MPa·$m^{1/2}$ for 15phrRME120, by the addition of 15phr rubber. The value of K_{Ic} also increases from 1.20MPa·$m^{1/2}$ for UME160 to 4.03MPa·$m^{1/2}$ for 15phrRME160, in case of the materials cured at 160°C. As shown in Table.4.6, the fracture toughness of 5phrRME120 is also greatly increased from that of the UME120 material. The addition of only 5phr rubber is sufficient to cause a significant improvement of the K_{Ic} value.

Similar results were obtained for the materials with BPA added. The K_{Ic} value, 3.01 MPa·$m^{1/2}$, for the 5phrRME120+BPA material is significantly improved from that of the UME120+BPA material. This improvement of fracture toughness is given by the additional toughening mechanisms, such as shear yielding and void growth, which are activated by the introduction of rubber particles. These mechanisms will be discussed in more detail later.

4.5.1.1 Effect of the volume fraction of rubber

Fig.4.7 shows the derived G_{Ic} values plotted against the volume fraction of rubber, which is measured using image analysis of the SEM pictures. As shown in Fig.4.7, the relationship between G_{Ic} and V_{fr} is not linear, whereas Kinloch and Hunston [58] reported a linear relationship between these parameters. There is a difference in the measured V_{fr} values between this study and the report by Kinloch and Hunston. For instance, the measured V_{fr} value in this study is 7% for 5phrRME120 and 21% for 15phrRME120, whereas Kinloch and Hunston reported 10% for 5phrRME120 and 17% for 15phrRME120. It is considered that this difference in the measured V_{fr} values causes the different relationship between G_{Ic} and V_{fr}. However, the results in this study agree with the results reported by Kinloch and Hunston [58] and Bucknall and Yoshii [57] in that the G_{Ic} value

generally increases with increasing volume fraction of rubber, V_{fr}, as shown in Fig.4.8. As discussed in Chapter Two, the volume fraction of rubber is not the only material parameter which affects the fracture toughness. There are other parameters such as the crosslink density of the matrix epoxy, etc. Therefore, the results can not be explained simply by the effect of the volume fraction of rubber. However, it may be suggested that as a general trend the fracture toughness increases with increasing the volume fraction of rubber.

Fig.4.7 also demonstrates that the materials cured at 160°C have the greatest difference in the G_{Ic} values between the rubber modified epoxy and the unmodified epoxy, the materials with BPA added cured at 120°C have the second greatest, and the materials cured at 120°C have the smallest difference. This suggests that when the epoxy matrix is more ductile, it can respond more readily to the presence of the rubbery particles.

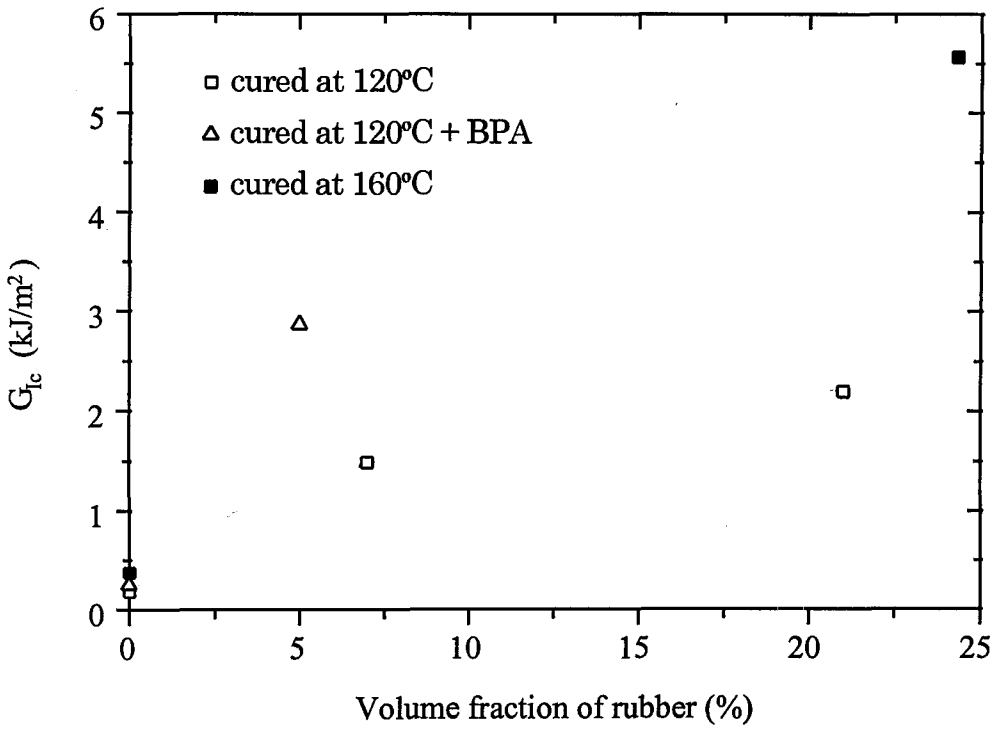


Fig.4.7 The G_{Ic} values plotted against the volume fraction of rubber

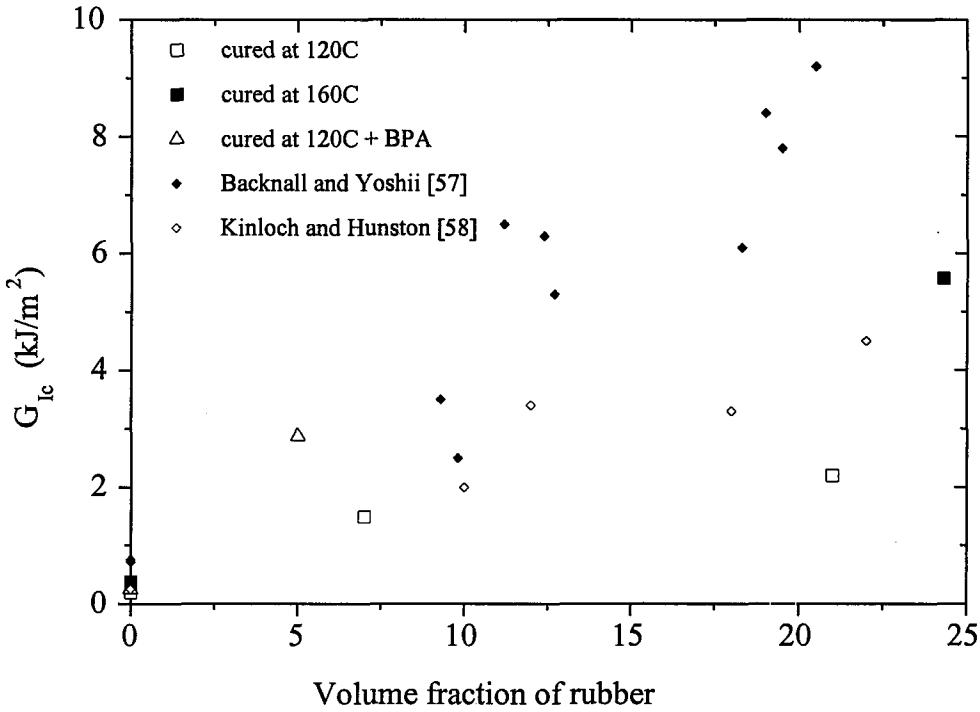


Fig.4.8 Effect of the volume fraction of rubber on the G_{Ic} values

4.5.1.2 Effect of crosslink density

Table 4.6 also demonstrates that the change of curing temperature from 120°C to 160°C improves K_{Ic} by approximately one and half times. For the unmodified epoxy, the value of K_{Ic} increases from 0.81MPa·m$^{1/2}$ to 1.20MPa·m$^{1/2}$, and for the 15phr rubber modified epoxy, it increases from 2.47MPa·m$^{1/2}$ to 4.03MPa·m$^{1/2}$. This improvement of fracture toughness is considered to be due to the decrease in the crosslink density of the matrix epoxy. As the crosslink density decreases, the ductility of the matrix epoxy increases and hence the matrix epoxy becomes more able to undergo plastic deformation. Hence, the materials having the lower crosslink density possess the higher fracture toughness.

The addition of BPA also increases the fracture toughness. The K_{Ic} value increases from 0.81MPa·m$^{1/2}$ for UME120 to 0.88MPa·m$^{1/2}$ for UME120+BPA, and it also increases from 2.22MPa·m$^{1/2}$ for 5phrRME120 to 3.01MPa·m$^{1/2}$ for 5phrRME120+BPA. Kinloch et al. [56] also reported that the addition of BPA increased the fracture toughness of rubber modified epoxy. The reason for the

improvement of fracture toughness can be considered as follows: As mentioned in Chapter Three, the chemical structure of BPA is the same as the main part of the matrix epoxy resin, DGEBA. Hence, BPA can be considered as an additional part of the matrix resin. Therefore, the addition of BPA causes the increase of the molecular ratio, epoxy resin : curing agent (piperidine). The ratio, epoxy resin : curing agent, is increased from approximately 9:1 to 10.5:1 by adding 24phr BPA, as detailed in Appendix A. In other words, the number of epoxy resin molecules per curing agent molecule increases. When the other conditions for the chemical curing reaction are same as the materials without BPA, the addition of BPA causes a decrease in the crosslink density of the epoxy. Thus, the addition of BPA improves the fracture toughness.

Fig.4.9 plots the K_{Ic} values against the $M_c^{1/2}$ values. The values of the average molecular weight between crosslinks, M_c, were calculated from the rubbery equivalent modulus of the epoxy matrix, as discussed in section 4.4. This graph shows that the K_{Ic} value increases with increasing M_c value, and the relationship between K_{Ic} and $M_c^{1/2}$ is approximately linear. Similar results on the relationship between K_{Ic} and $M_c^{1/2}$ were reported by Pearson and Yee [55]. As they suggested, the epoxy which has the low crosslink density, i.e. the higher M_c value, exhibits greater ductility than the epoxy which has the higher crosslink density, i.e. the lower M_c value. Consequently, the former has greater toughenability than the latter. Hence, for rubber modified epoxies, the material with a low crosslink density has a much greater fracture toughness.

Fig.4.10 plots both the data measured in the present study and the reported data by Pearson and Yee [55], Karger-Kocsis and Friedrich [54] and Huang [7], for CTBN rubber modified epoxies. Although only an approximate comparison can be made due to the differences in the materials and test conditions used for the measurements of these data, the data can be represented by a linear relationship. Strictly speaking, some scatter can be seen within the plotted data. This scatter may arise from differences in the rubber content, the curing agent used, the test conditions, or the method for the calculation of M_c values, etc.

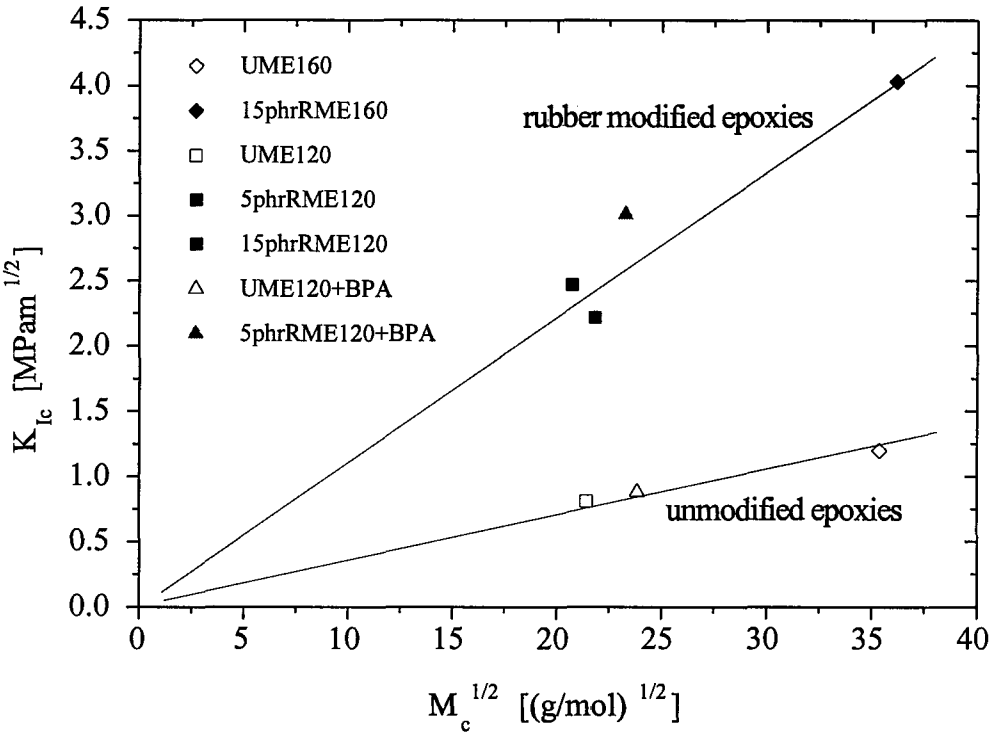


Fig.4.9 Effect of crosslink density on the fracture toughness

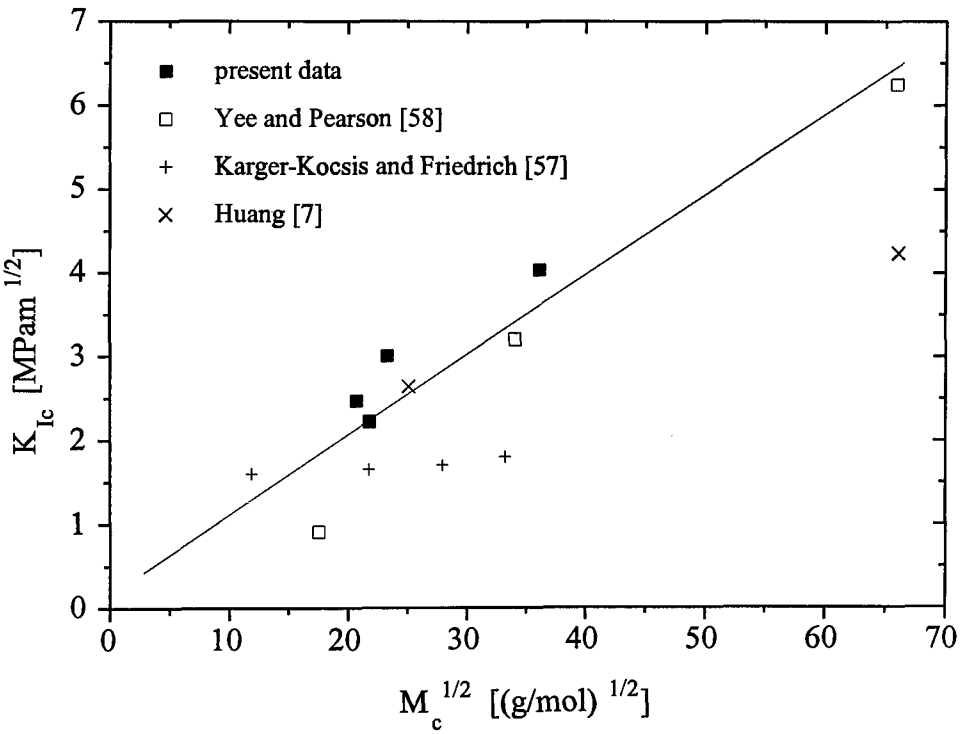


Fig 4.10 Effect of crosslink density for CTBN rubber modified epoxies

4.5.2 Thermoplastic modified epoxies

Table 4.7 shows the mechanical properties of the thermoplastic modified epoxy (TPME) series.

Table 4.7 Mechanical properties of the TPME materials

Material	E (GPa)	K_{Ic} (MPa·m$^{1/2}$)	G_{Ic} (kJ/m^2)
PES0	3.90	0.50	0.06
PES10	3.74	0.61	0.09
PES20	3.67	1.01	0.24
PES25	3.56	1.16	0.33

Note: The moduli of PES20 and PES25 are the values from ref. [103].

The flexural moduli of all the TPME materials lie in the range from 3.56GPa to 3.90GPa, which are all higher than those of the DGEBA epoxy based materials. The flexural modulus decreases slightly with increasing amounts of PES copolymer.

The fracture toughness, K_{Ic}, of the epoxy is increased by the addition of PES copolymer. Further, the value of K_{Ic} increases as the content of PES copolymer increases. However, the K_{Ic} value of PES10, which contains 14.61phr PES copolymer, is only 0.61MPa·m$^{1/2}$. A maximum K_{Ic} value of 1.16MPa·m$^{1/2}$ was measured for the PES25 material which contains 43.82phr PES copolymers. These measured K_{Ic} values show excellent agreement with those reported by Tudgey [103].

Fig.4.11 shows both the measured K_{Ic} values and those reported by Tudgey [103]. One interpretation of the data suggests that an increase of the PES copolymer content gives a relatively small increase of the K_{Ic} value, when the PES copolymer content is lower than about 23phr. However, there is a relatively large increase of the K_{Ic} value when the PES copolymer content is increased to more

than about 23phr. As discussed later, the morphology changes greatly between these levels of PES content. Although the microstructure at PES copolymer contents of less than 23phr consists of dispersed particles of PES, the microstructure is co-continuous for the PES20 material (32.67phr). Finally, the microstructure is converted to epoxy particle dispersed phase for the PES25 material (43.82phr). Hence, it can be considered that the change of morphology is one reason for a significant increase in fracture toughness at PES copolymer contents of greater than 23phr. However, a second interpretation is that a linear fit to the data shown in Fig.4.11 is also a reasonable description of the results.

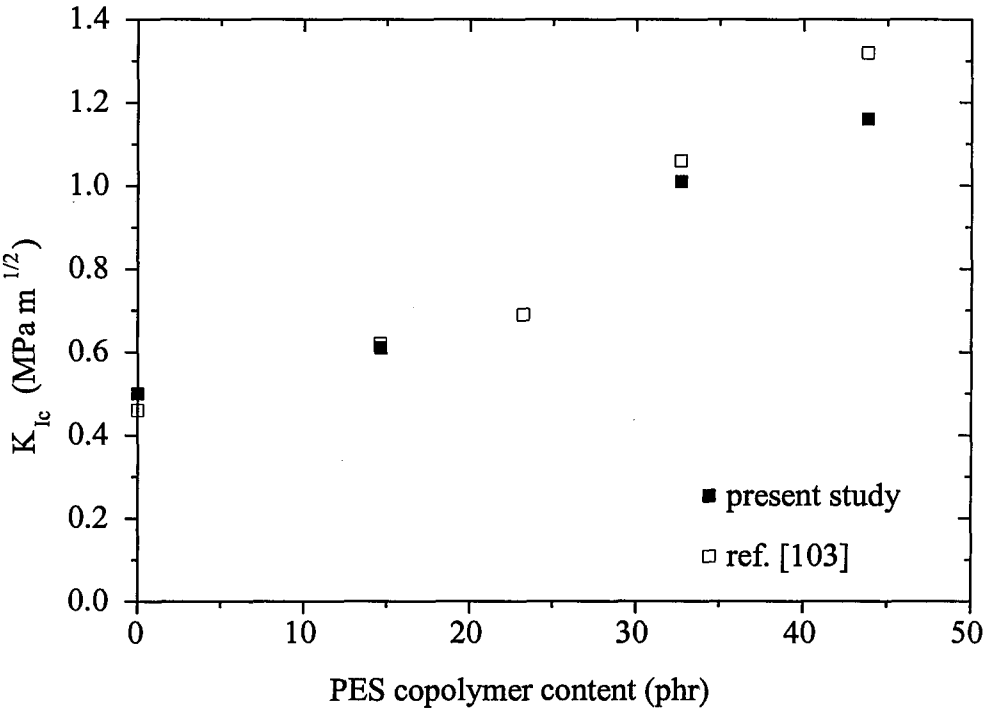


Fig.4.11 The K_{Ic} values of the TPME materials, as a function of PES copolymer content

4.6 Concluding remarks

The basic properties of the materials used in this study, such as modulus, static fracture toughness, crosslink density, dispersed particle size, etc. have been discussed. The microstructure of the materials was also reviewed.

For the rubber modified epoxies, the fracture toughness increases with increasing the rubber content, and the 15phrRME160 material has the highest fracture toughness. The crosslink density of the matrix epoxy also affects the fracture toughness; the materials having the lower crosslink density have the higher fracture toughness. The average radius of the dispersed rubber particles is in the range from 1.0μm to 1.7μm, except for the 5phrRME120+BPA material which has extremely small rubber particles.

For the thermoplastic modified epoxies, the fracture toughness increases as the PES copolymer content increases. The microstructure of the thermoplastic modified epoxies changes from a PES copolymer particle dispersed phase to a co-continuous phase with increasing PES copolymer content. Finally, the matrix phase is inverted.

The following Chapters will discuss the fatigue behaviour of the above materials. Firstly, the fatigue behaviour of the rubber modified epoxies will be discussed.

Appendix : Ishai-Cohen model

When a two-phase material has a particulate microstructure, with soft particles (modulus E_p) which are dispersed in a hard matrix, the modulus of the two-phase material, E_c, is lower than that of the matrix material, E_m. The ratio (E_c/E_m) of E_c and E_m is given by the following equation [105]:

$$E_c/E_m = 1 + V_f/\{m/(m-1) - V_f^{1/3}\} \qquad (4.6)$$

where V_f is the volume fraction of the soft particles and m is the ratio of the modulus of the particles and the matrix, i.e. E_p/E_m.

Chapter Five

Fatigue Crack Propagation in Rubber Modified Epoxies

5.1 Introduction

As mentioned in Chapter One and Chapter Two, despite the successes in toughening epoxies with rubbers, there are relatively few studies concerning their fatigue behaviour. Very recently, Azimi et al. [51,74,93,107] reported the fatigue behaviour of some rubber modified epoxies. However, the relationships between the fatigue behaviour and material properties are not yet well understood.

In the present study, the fatigue crack propagation behaviour has been measured, from the threshold region to near the fracture toughness, K_{Ic}. The relationships between the fatigue crack growth rate and the microstructural parameters, such as the crosslink density, rubber content and particle size, are discussed in this Chapter. The concept of a K-transition is introduced and discussed in connection with the toughening mechanisms. The surface temperature of the fatigue specimens was also measured to verify whether any localised heating effect should be taken into account.

Fatigue tests were performed in both a constant displacement mode and a constant load mode. The constant displacement mode was firstly chosen to determine the threshold values. Then, the testing mode was changed to constant load mode until final failure of the specimen occurred. The fatigue crack growth rate was measured using the compact tension specimens with crack gauges, which enabled the crack length to be measured electrically, as discussed in section 3.6. The crack length was also measured optically using a travelling microscope. The incremental polynomial method was employed to calculate the fatigue crack growth rate, as recommended in the ASTM standard [94]. The surface temperature of some of the specimens being tested was monitored using an infrared camera. Details of the testing method are described in section 3.7.

5.2 Effect of crosslink density

5.2.1 Introduction

Several researchers [43,54-56] have investigated the influence of the crosslink density on the fracture toughness for rubber modified epoxies. Pearson and Yee [55] suggested a linear relationship between the K_{Ic} values and the square root values of the average molecular weight between crosslinks, M_c. There are, however, few studies on the effect of crosslink density on the fatigue resistance. Hwang et al. [48] and Karger-Kocsis and Friedrich [54] reported that the fatigue resistance increases with increasing M_c value. However, their results [48,54] included not only the effect of crosslink density but also the effect of other microstructural parameters, such as the rubber content, etc. Thus, the quantitative relationship between the fatigue behaviour and the value of M_c for rubber modified epoxies is not yet well understood.

5.2.2 Experimental results

The crosslink density of the matrix epoxy can be varied by changing the curing conditions. In this study, we selected two different curing conditions, 120°Cx16hours and 160°Cx6hours to investigate the effect of crosslink density. In order to evaluate only the effect of the crosslink density, it is desirable that the materials have the same microstructural features except the crosslink density. Therefore, two sets of materials were chosen for this purpose. The first set is UME160 and UME120, and the second one is 15phrRME160 and 15phrRME120. The crosslink density of the matrix epoxy for these materials is shown in Table 5.1. High molecular weight between crosslinks, M_c, corresponds to low crosslink density, and low M_c corresponds to high crosslink density, as discussed in Chapter Four.

Table 5.1 The crosslink density of the matrix epoxy for the UME160, UME120, 15phrRME160 and 15phrRME120 materials

Material	M_c (g/mol)
UME160	1250
UME120	460
15phrRME160	1310
15phrRME120	430

The fatigue crack growth rates of UME160 and UME120, both of which are unmodified epoxies, are shown in Fig.5.1 plotted against K_{max}, and in Fig.5.2 plotted against ΔK. The M_c value is 1250g/mol for UME160 and 460g/mol for UME120. This means that the UME160 material has a lower crosslink density than the UME120 material. As shown in Fig.5.1 and Fig.5.2, the fatigue crack growth rate of UME160 is lower than that of UME120, for a given value of K_{max}. In other words, the UME160 material has better fatigue resistance than UME120.

Similar results were obtained for the rubber modified epoxies. The fatigue crack growth rates of 15phrRME160 and 15phrRME120 are shown in Fig.5.3 plotted against K_{max}, and in Fig.5.4 plotted against ΔK. The M_c value is 1310g/mol for 15phrRME160 and 430g/mol for 15phrRME120, i.e. 15phrRME160 has a lower crosslink density than 15phrRME120. As for the unmodified epoxies, the fatigue crack growth rate of 15phrRME160 is lower than that of 15phrRME120 over the whole range of K_{max} or ΔK values. Thus, the rubber modified epoxy possessing a lower crosslink density has a smaller fatigue crack growth rate than the rubber modified epoxy possessing a higher crosslink density.

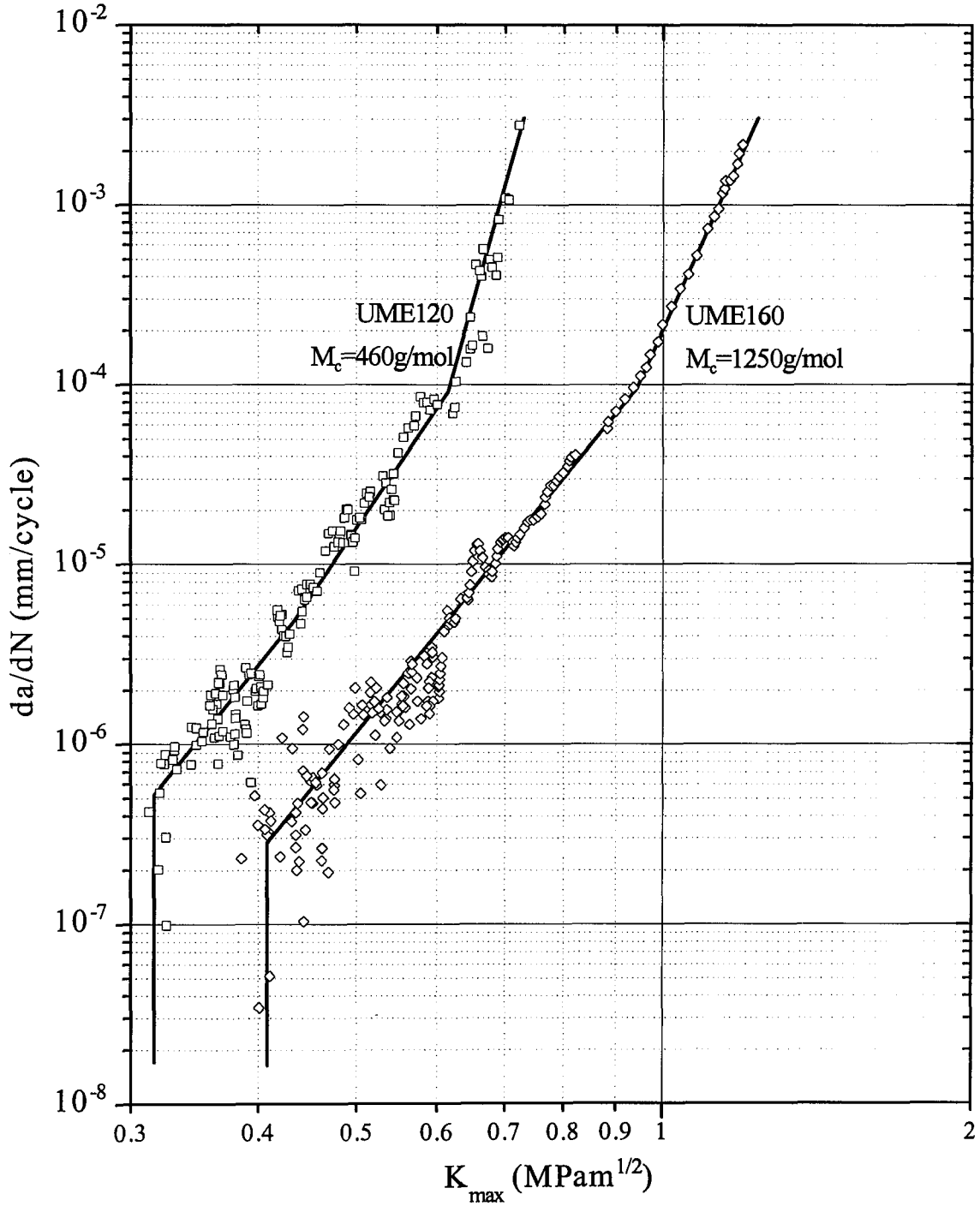


Fig.5.1 Fatigue crack growth rate for UME160 and UME120 plotted against K_{max}

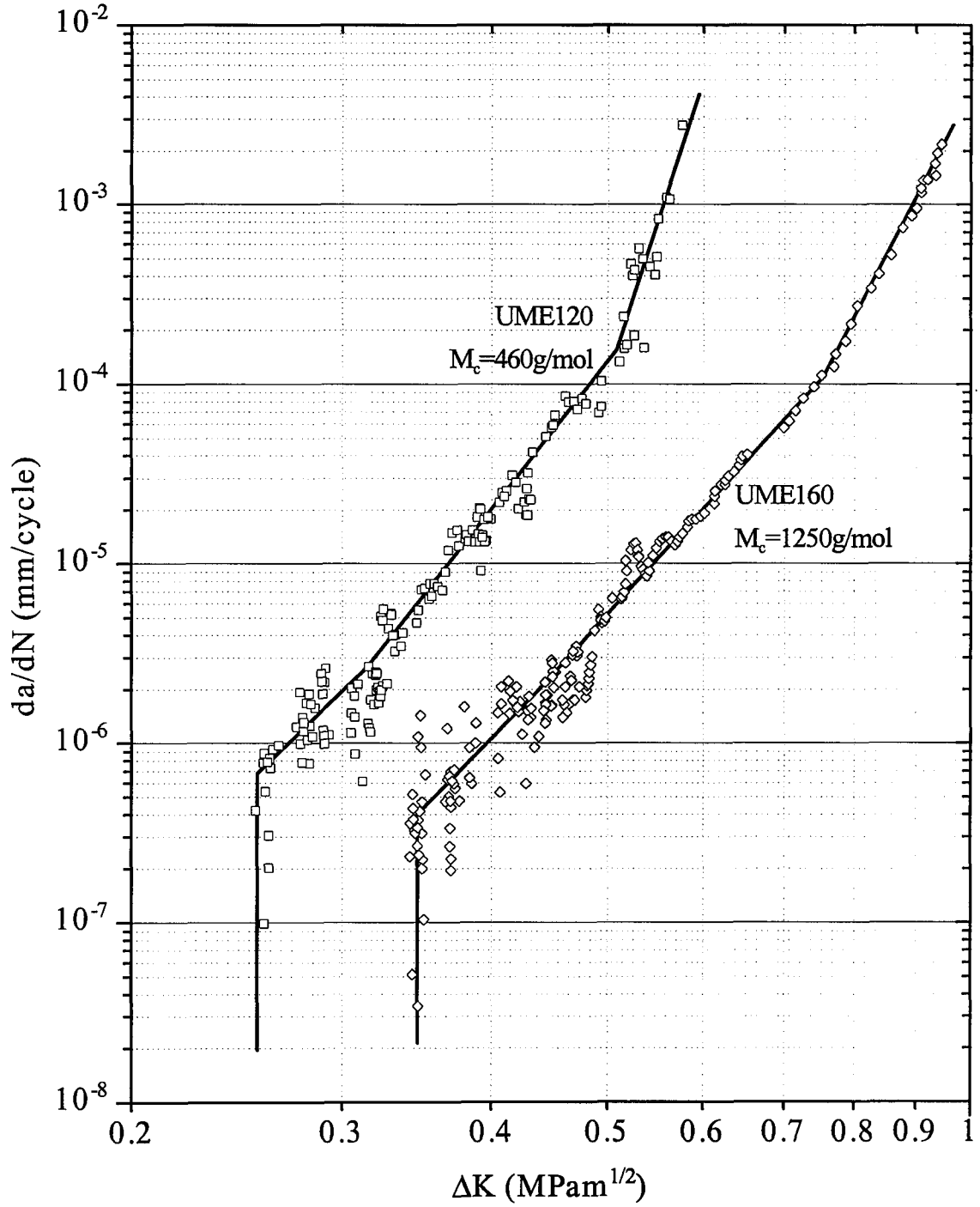


Fig.5.2 Fatigue crack growth rate for UME160 and UME120 plotted against ΔK

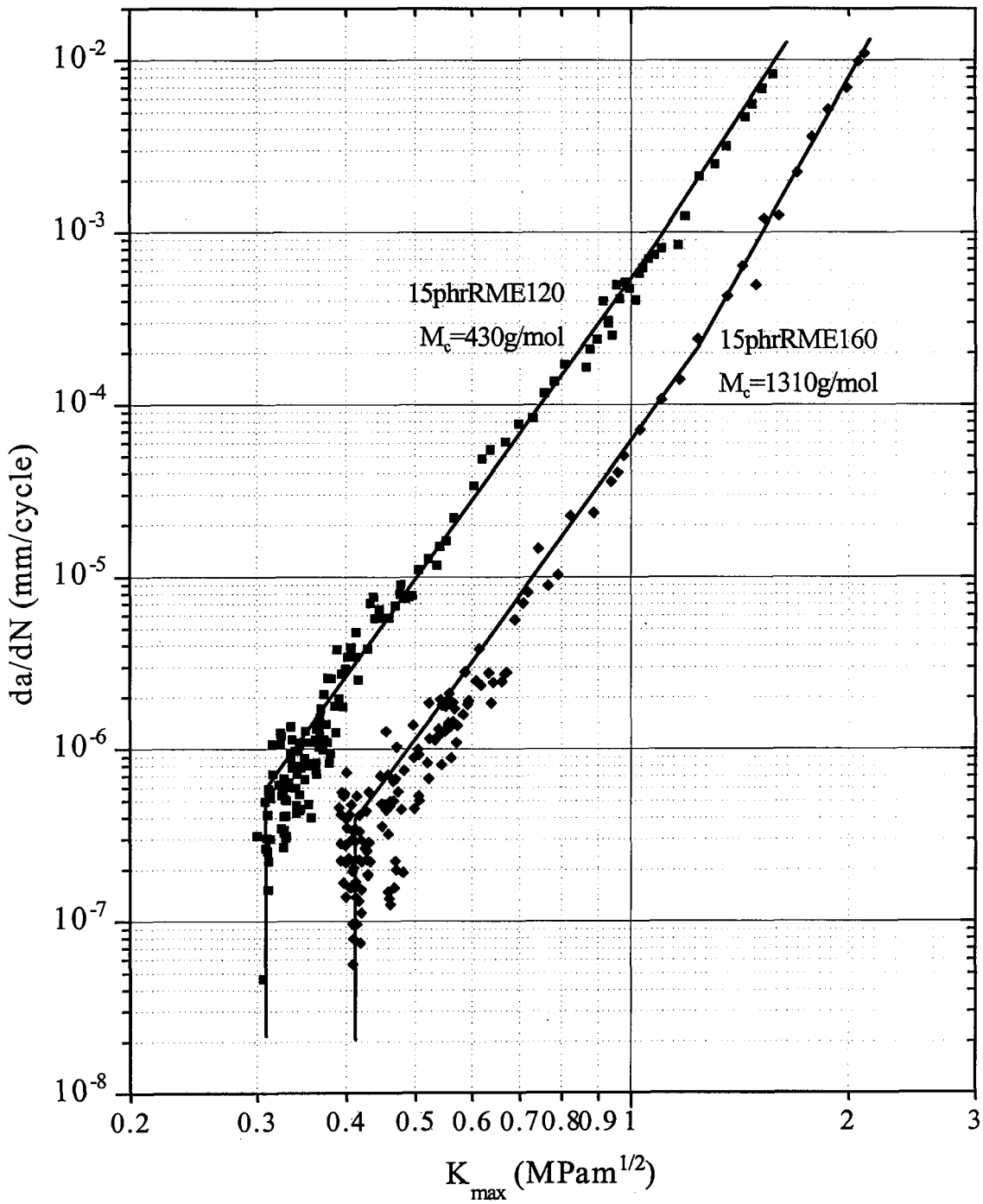


Fig.5.3 Fatigue crack growth rate for 15phrRME160 and 15phrRME120 plotted against K_{max}

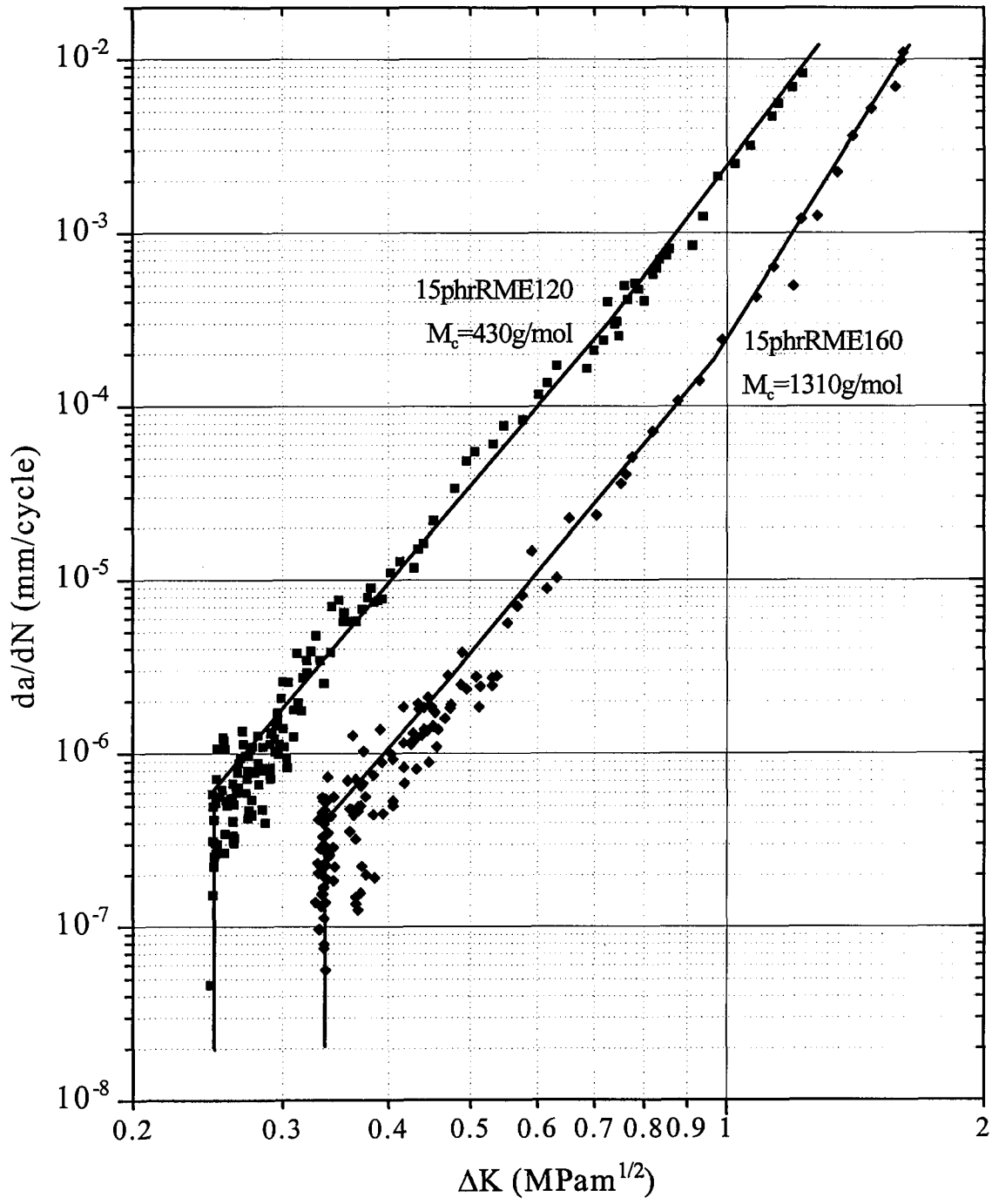


Fig.5.4 Fatigue crack growth rate for 15phrRME160 and 15phrRME120 plotted against ΔK

5.2.3 Values of ΔK and K_{max} and M_c values

The experimental results suggest that the fatigue crack growth rate becomes lower as the crosslink density of the matrix epoxy decreases. These results on the effect of crosslink density can be explained as follows. Generally, the epoxy which has the lower crosslink density has a greater ductility than the epoxy which has the higher crosslink density. The former, consequently, has a greater ability for plastic deformation than the latter. Lu [35] investigated the deformability using the plane strain compression test for the various unmodified epoxies and the rubber modified epoxies, which have various crosslink densities. He suggested that the material having a lower crosslink density can undergo more plastic deformation. He also reported that the fracture toughness of the epoxy possessing the lower crosslink density was more greatly improved by the addition of rubber particles than the epoxy with the higher crosslink density. He concluded that a less crosslinked epoxy system has the greater deformability, and consequently the more potential for toughening.

As shown in Fig.5.5, the increase in the M_c value results in an increase in the fracture strain, i.e. an increase in the ability for plastic deformation. Crack propagation which is accompanied by more plastic deformation obviously dissipates more energy per unit crack propagation. Hence, the epoxy having the lower crosslink density would be expected to have a lower fatigue crack growth rate, than the epoxy having the higher crosslink density.

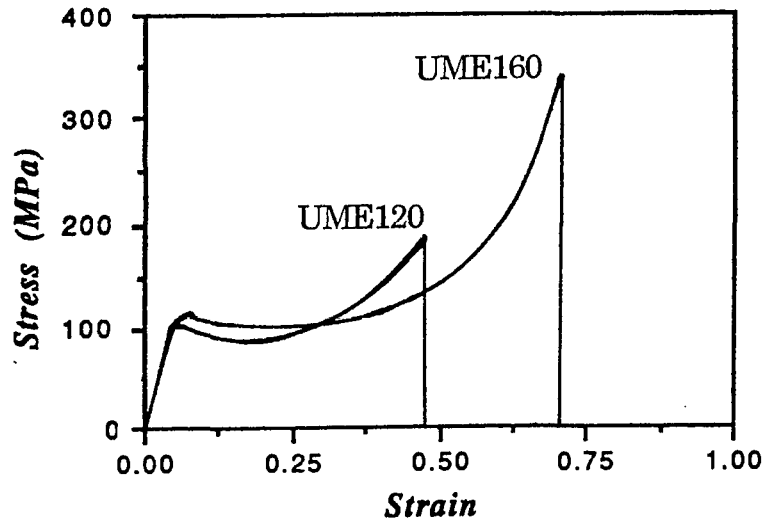


Fig.5.5 Stress-strain curve for the UME160 and UME120 materials [7] (plane strain compression test)

Strictly speaking, the difference between the 15phrRME160 material and the 15phrRME120 material is not only in the crosslink density of the matrix epoxy, but also in the rubber particle size. As discussed in section 4.2.1, the approximate radius of rubber particles in 15phrRME160 is 1.7μm, and that in 15phrRME120 is 1.4μm. As discussed in detail later (see section 5.5), this slight change in the radius of the rubber particles does have a small effect on the fatigue crack growth curve. However, the effect of particle size is minimal compared with the effects due to the crosslink density. Therefore, the differences in the crack growth rate curves between the 15phrRME160 and 15phrRME120 materials are entirely caused by the effect of the crosslink density. In fact, the fatigue crack growth curve of the 15phrRME160 material is shifted from that of 15phrRME120 in almost same way as that of UME160 is shifted from that of UME120. Both UME160 and UME120, of course, contain no rubber particles, and consequently the particle size has no effect on their fatigue crack growth rate curves.

Hwang et al. [43] and Karger-Kocsis and Friedrich [54] have also investigated the influence of the crosslink density of the epoxy on the fatigue resistance, as discussed in section 2.5.3.1. Fig.5.6 plots the ΔK^* values, i.e. the ΔK values for da/dN=7.5x10^{-4}mm/cycle, against the square root of the average molecular weight between crosslinks, M_c, for the data of the unmodified epoxies from ref. [43], ref. [54] and the present study. This graph shows a very good correlation between the ΔK^* and $M_c^{1/2}$ values. The ΔK^* value increases linearly with an increase in the $M_c^{1/2}$ value. These results imply that the viscoelastic nature of the epoxy polymer plays an important role during the fatigue crack propagation. The epoxy having a lower crosslink density has more ability for plastic deformation, and consequently dissipates more energy during the fatigue crack propagation. Hence, the epoxy having a lower crosslink density has the better fatigue resistance than the epoxy having a higher crosslink density.

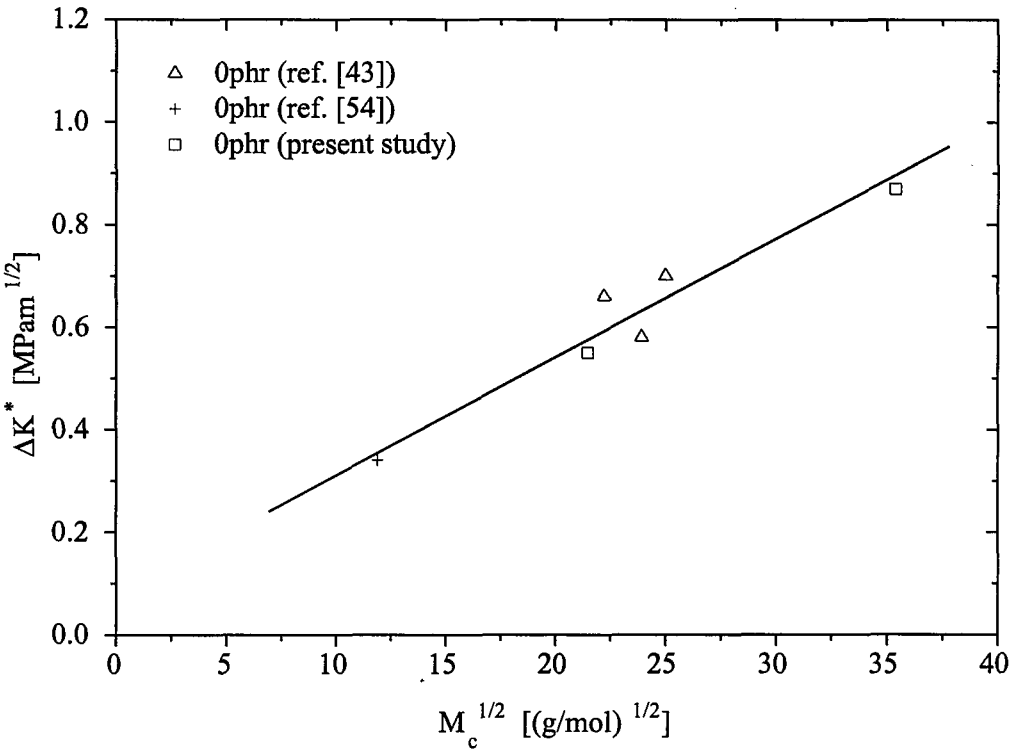


Fig.5.6 Relationship between ΔK (for da/dN=7.5x10⁻⁴mm/cycle) and $M_c^{1/2}$ for unmodified epoxies*

Fig.5.7 plots the values of ΔK at da/dN = 7.5x10⁻⁴mm/cycle, i.e. ΔK*, against the $M_c^{1/2}$ values, for both the rubber modified epoxies and the unmodified epoxies, from ref. [43] and the present study. This graph shows that there is good agreement between the results in the present study and that of ref. [43]. A linear relationship between ΔK* and $M_c^{1/2}$ is found to exist, especially for the unmodified epoxies (0phr). However, there is some difference between the results from ref. [43] and the results in the present study, for the rubber modified epoxies (15phr). The data from ref. [43] are located below the line for the rubber modified epoxies in the present study, and close to the line for the unmodified epoxies (0phr). The results in the present study suggest that the presence of the rubber particles itself also has a beneficial effect on the fatigue resistance, whereas the results by Hwang et al. [43] suggest that the increase in the ΔK* values in the rubber modified epoxies is mainly due to the increase in the M_c values, and that there is relatively small toughening effect arising from the rubber particles. However, as discussed in detail later in section 5.3, it is not believed by the present author that there is only a small toughening effect caused by the rubber particles. The results of Hwang et al.

[43] may arise from an overestimation of the M_c values. As discussed in section 4.5, the Ishai-Cohen model [105] was applied to calculate the rubbery equivalent modulus, E_r, of the matrix epoxy in the present study, in order to avoid the underestimation of the modulus of the matrix in a particulate microstructure. However, Hwang et al. [43] did not apply this model, and this may cause the underestimation of the E_r values and hence cause the overestimation of the M_c values. The correct M_c values for the rubber modified epoxies (15phr) in ref. [43] should be lower. Thus, the data points for the rubber modified epoxies (15phr) in ref. [43] should be somewhat shifted to the left, and be close to the line for the rubber modified epoxies (15phr). The recalculated M_c values in ref. [43] using the same model as for the present study are shown in Fig.5.7a. This clearly shows two different lines for the rubber modified epoxies (15phr) and the unmodified epoxies (0phr). This also shows a good agreement between the results from ref. [43] and the results in the present study.

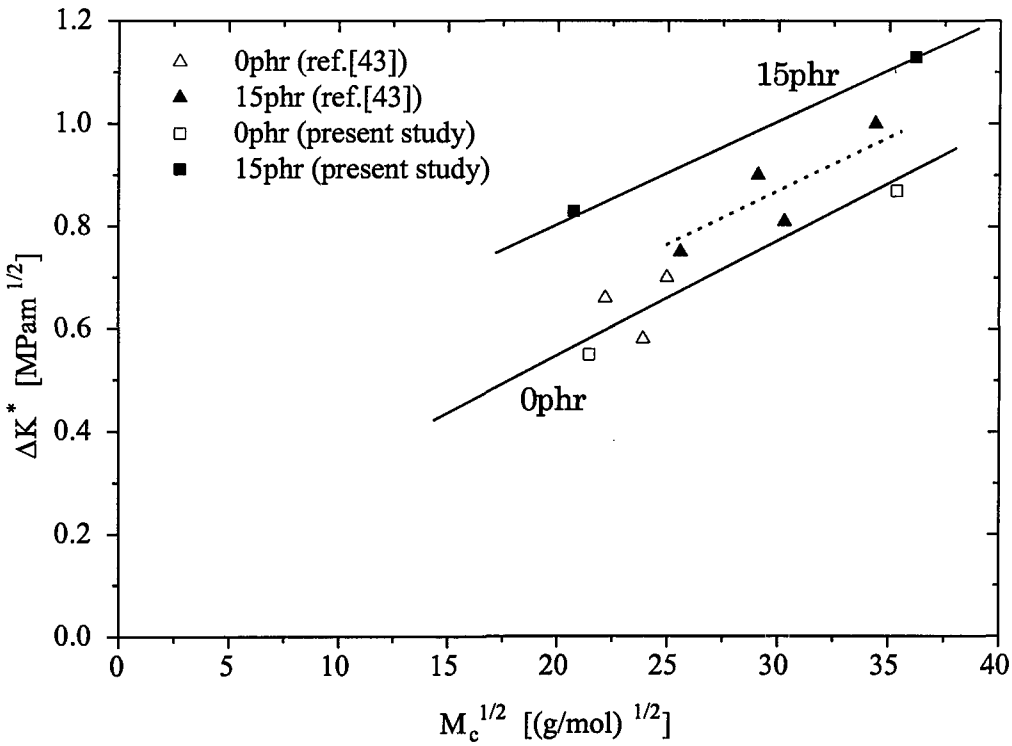


Fig.5.7 Relationship between ΔK^* (for $da/dN=7.5x10^{-4}$mm/cycle) and $M_c^{1/2}$

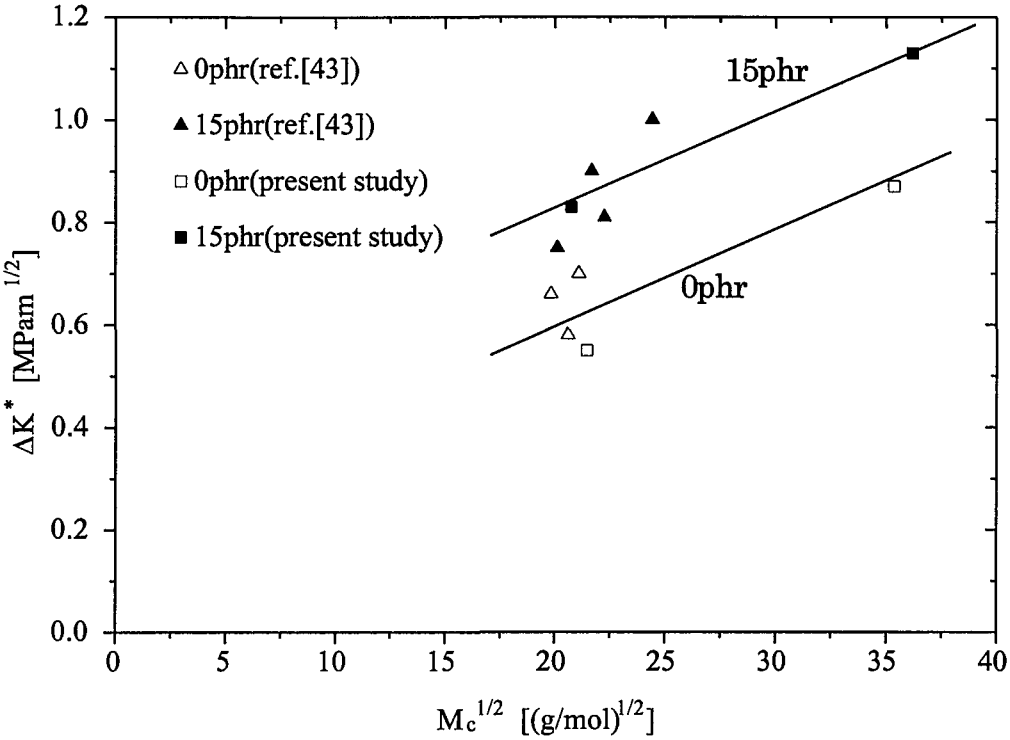


Fig.5.7a Relationship between ΔK (for da/dN=7.5x10⁻⁴mm/cycle) and $M_c^{1/2}$ (M_c values in ref. [43] are recalculated)*

A comparison with the data from ref. [54] with the present results is given in Fig.5.8. Fig.5.8 plots the values of ΔK at da/dN = 1x10⁻³mm/cycle, i.e. ΔK**, against the square root of the average molecular weight between crosslinks, M_c, for both the data from ref. [54] and the present study. There is excellent agreement between the results in the present study and that of ref. [54] for the unmodified epoxies (0phr). However, there are some differences between the results from ref. [54] and the results in the present study, for the rubber modified epoxies (15phr). A similar explanation for the differences in the data of the rubber modified epoxies may be given, as for the results by Hwang et al. [43]. Namely, that the M_c values of the rubber modified epoxies in ref. [54] may also have been overestimated. The recalculated M_c values in ref. [54] using the same model as for the present study are shown in Fig.5.8a. This clearly shows two different lines for the rubber modified epoxies (15phr) and the unmodified epoxies (0phr). It is also shown that there is an excellent agreement between the results from ref. [54] and the results in the present study.

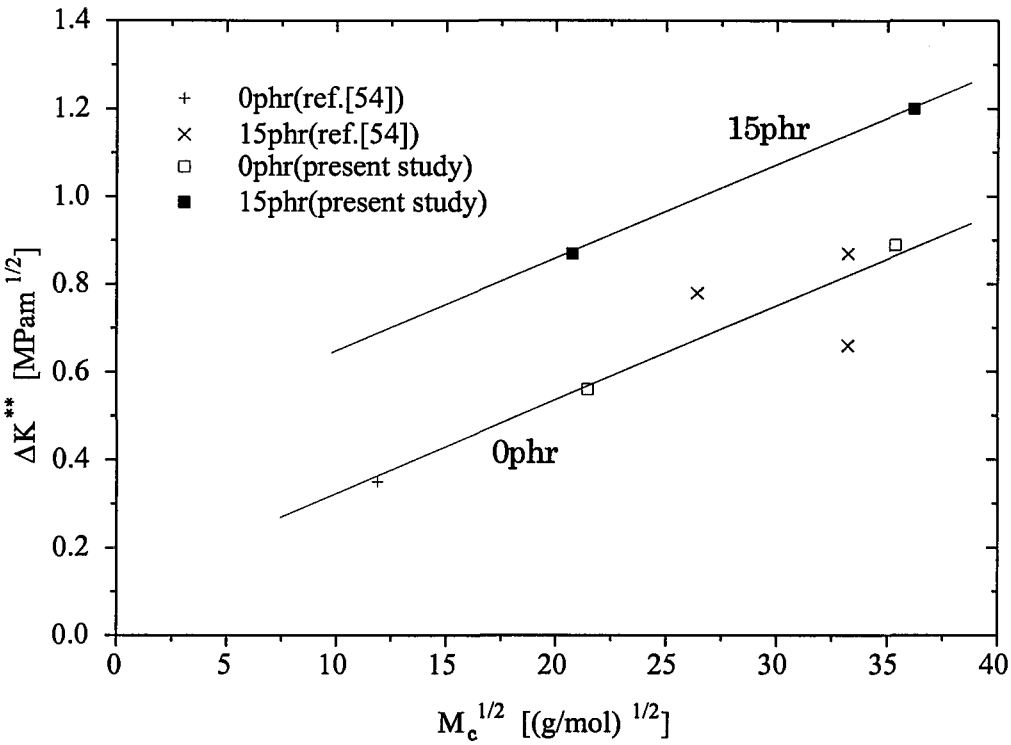


Fig.5.8 Relationship between ΔK^{**} (for da/dN=1x10^{-3}mm/cycle) and $M_c^{1/2}$

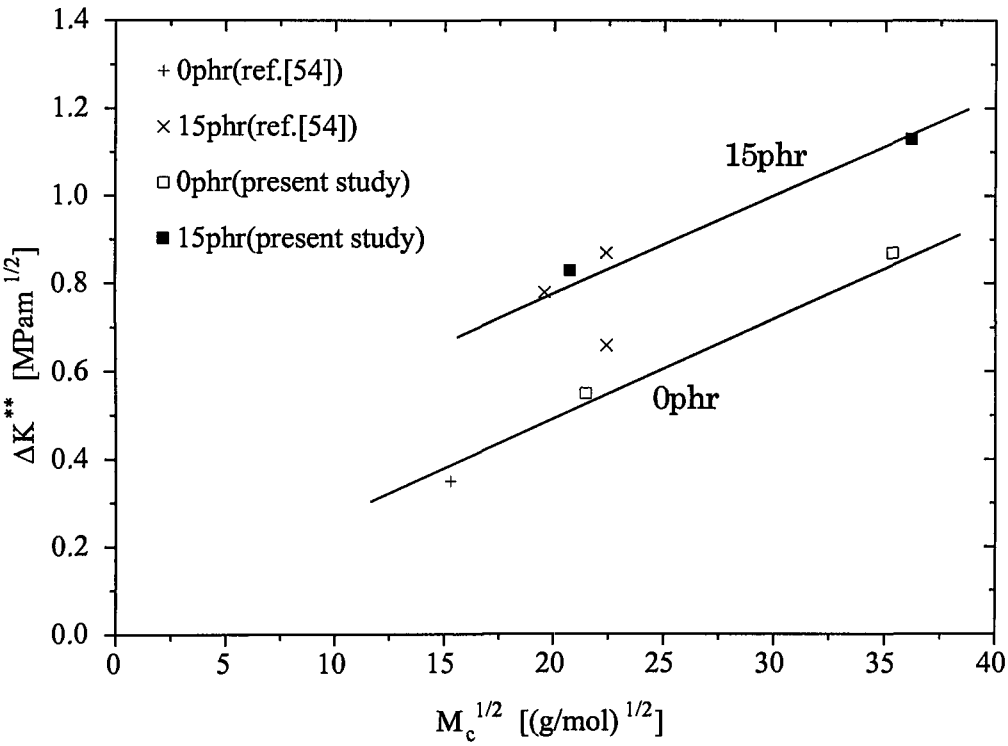


Fig.5.8a Relationship between ΔK^{**} (for da/dN=1x10^{-3}mm/cycle) and $M_c^{1/2}$ (M_c values in ref. [54] are recalculated)

5.2.4 Values of K_{th} and M_c values

The threshold K_{max} value, K_{th}, below which no fatigue crack propagation is observed, is 0.41MPa·m$^{1/2}$ for UME160 and 0.31MPa·m$^{1/2}$ for UME120, as shown in Table 5.2. Thus, the threshold value of the epoxy having the lower crosslink density is higher than that of the epoxy possessing the higher crosslink density. This means that the threshold value is increased as the crosslink density decreases. For the rubber modified epoxies, the threshold K_{max} value, K_{th}, is 0.41MPa·m$^{1/2}$ for 15phrRME160 and 0.31MPa·m$^{1/2}$ for 15phrRME120. As for the unmodified epoxies, the threshold K_{max} value, K_{th}, increases as the crosslink density decreases. Fig.5.9 plots the K_{th} values against the $M_c^{1/2}$ values. This graph implies that the K_{th} values also have a linear correlation with the $M_c^{1/2}$ values. These novel results demonstrate that the material properties of the matrix epoxy determine the fatigue behaviour in the threshold region. Therefore, the intrinsic higher ductility of the epoxy matrices with a higher M_c value, is reflected in a better fatigue resistance in the threshold region; and the consequently higher K_{th} values, regardless of the rubber content.

Table 5.2 The threshold values of UME160, UME120, 15phrRME160 and 15phrRME120

Material	M_c (g/mol)	K_{th} (MPa·m$^{1/2}$)	ΔK_{th} (MPa·m$^{1/2}$)	K_{th}/K_{Ic}	$\Delta K_{th}/K_{Ic}$
UME160	1250	0.41	0.34	0.34	0.28
UME120	460	0.31	0.25	0.38	0.31
15phrRME160	1310	0.41	0.33	0.10	0.08
15phrRME120	430	0.31	0.25	0.12	0.10

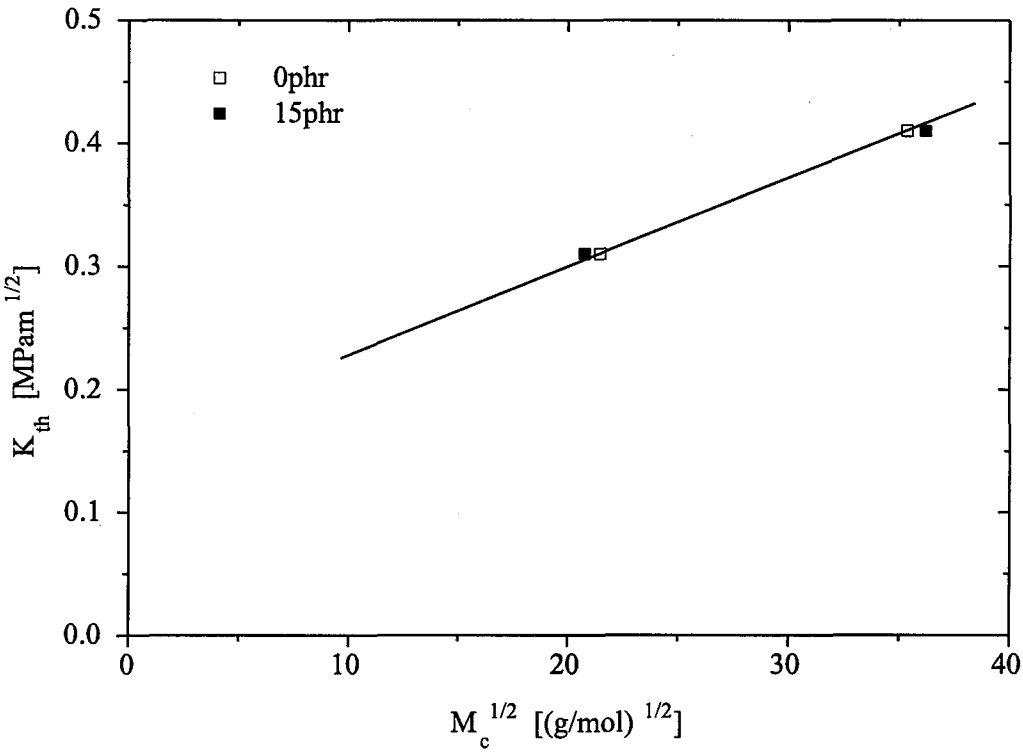


Fig.5.9 Influence of the M_c values on the K_{th} values

5.2.5 K_{max}/K_{Ic} plots and M_c values

The fatigue crack growth rate is also plotted against the normalised K_{max} value, K_{max}/K_{Ic}, as shown in Fig.5.10 and Fig.5.11. These graphs indicate that the fatigue crack growth rate data of both UME160 and UME120 lie on almost the same line, including the threshold region, despite of the difference in the crosslink density and as do the data of both 15phrRME160 and 15phrRME120.

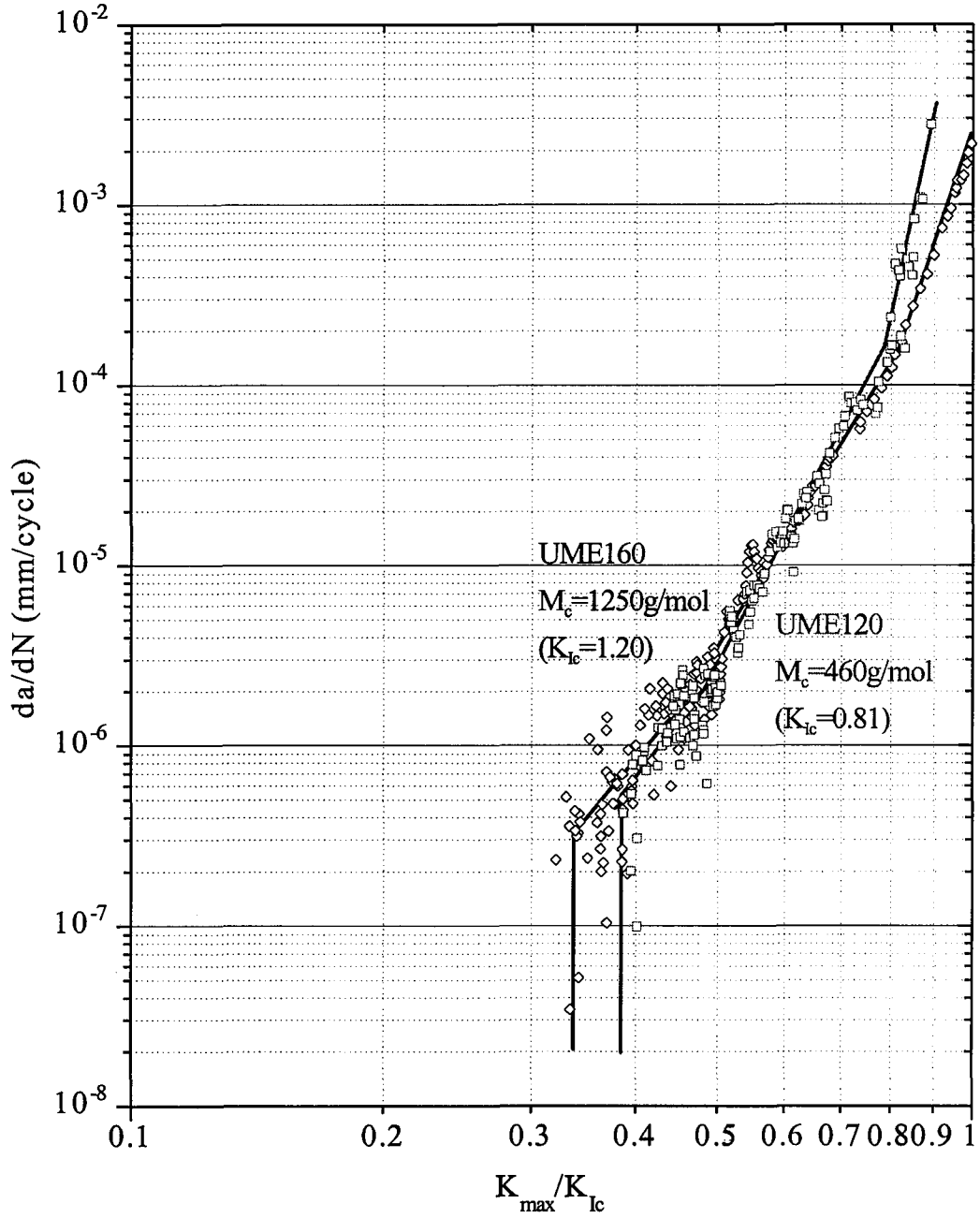


Fig.5.10 Fatigue crack growth rate for UME160 and UME120 plotted against K_{max}/K_{Ic}

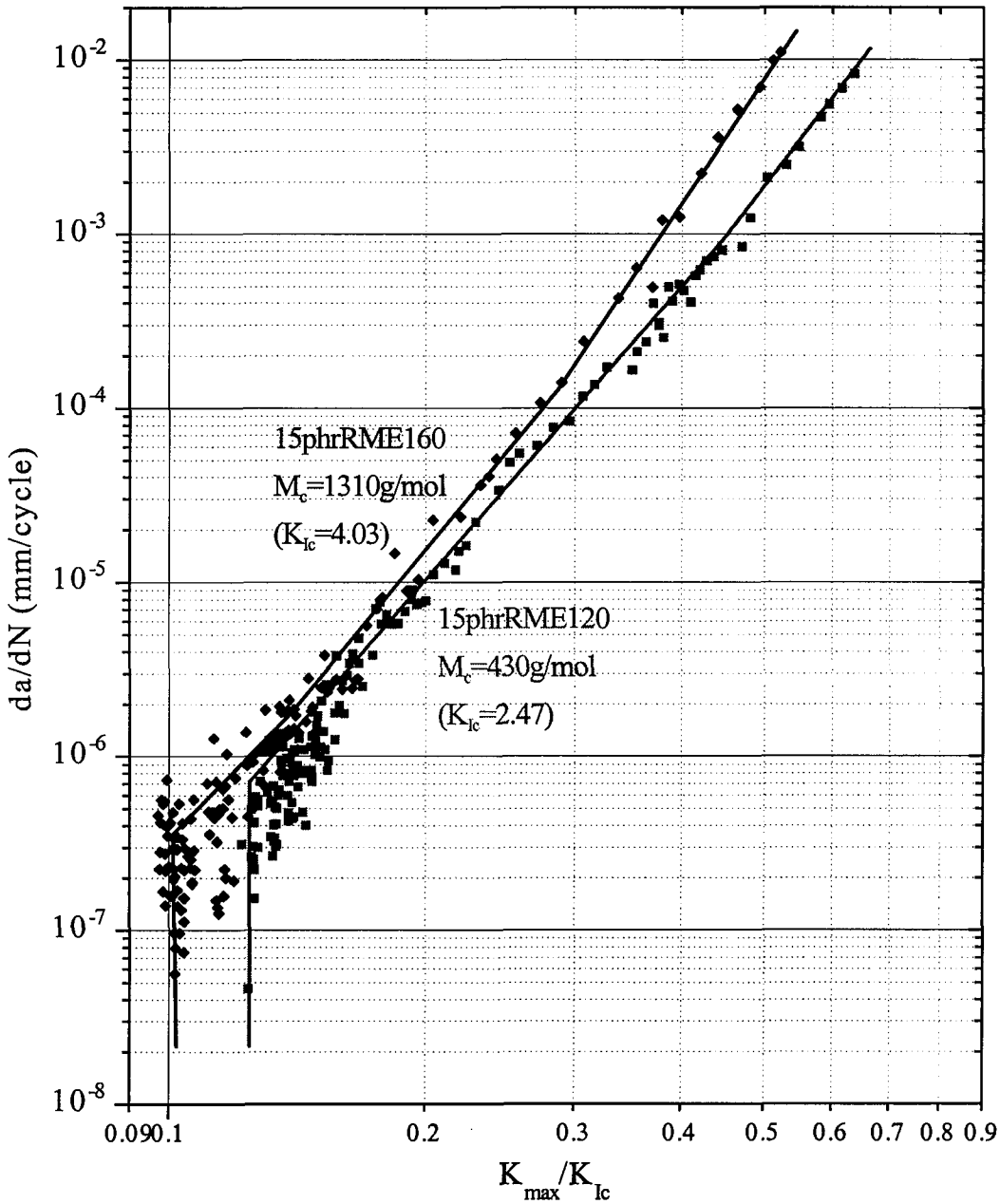


Fig.5.11 Fatigue crack growth rate for 15phrRME160 and 15phrRME120 plotted against K_{max}/K_{Ic}

Fig.5.10 and Fig.5.11 suggest that when the data are plotted against the normalised K_{max} value, K_{max}/K_{Ic}, the crosslink density of the matrix epoxy hardly affects on the fatigue crack growth rate curve. As there have been very few studies on this area, only a speculation may be given for these results, as follows. As shown in Fig.5.9, the K_{th} values have a linear correlation with the $M_c^{1/2}$ values. Thus it can be expressed as:

$$K_{th} \approx A\, M_c^{1/2} \tag{5.1}$$

where A is a constant. Furthermore, as discussed in Chapter Four, the K_{Ic} values are also in correlation with the $M_c^{1/2}$ values, thus:

$$K_{Ic} \approx B\, M_c^{1/2} \tag{5.2}$$

where B is a constant. From equation 5.1 and 5.2, the normalised threshold value, K_{th}/K_{Ic}, can be given by :

$$K_{th}/K_{Ic} \approx A/B \equiv C \tag{5.3}$$

where C is a constant. This is why the materials having the same rubber content have the nearly same K_{th}/K_{Ic} value. Meanwhile, the fatigue crack growth rate approaches to infinite as the applied K_{max} value approaches to the K_{Ic} value. That is,

$$da/dN \rightarrow +\infty \text{ when } K_{max}/K_{Ic} \rightarrow 1 \tag{5.4}$$

Namely, when the fatigue crack growth rates are plotted against K_{max}/K_{Ic}, the starting point of the fatigue curve, i.e. K_{th}/K_{Ic}, is the same and the fatigue curve approaches to the same value, $+\infty$, as K_{max}/K_{Ic} approaches to unity. Hence, the whole fatigue curve should be the same.

5.3 Effect of rubber content

5.3.1 Introduction

There are few studies on the influence of the rubber content on the fatigue resistance of rubber modified epoxies. As discussed in section 2.5.3.2, Karger-Kocsis and Friedrich [92] and Azimi et al. [51,83] reported that the fatigue resistance increases with increasing the rubber content. Azimi et al. [51,83] also suggested that the improvement of the fatigue resistance due to the presence of rubber particles is limited in a relatively high-K region, as discussed in section 2.5.1. The results from these studies will be compared with the results from the present work later in this section.

To evaluate the effect of rubber content, the following materials were used in the present study :

(i) the material cured at 160°C : UME160 and 15phrRME160
(ii) the material cured at 120°C : UME120 and 15phrRME120

5.3.2 The materials cured at 160°C

The fatigue crack growth rates of the first group of materials, i.e. UME160 and 15phrRME160, are shown in Fig.5.12 and Fig.5.13. The values of da/dN are plotted against K_{max} in Fig.5.12, and ΔK in Fig.5.13. The fatigue crack growth rate in the 15phrRME160 material is smaller than that of the UME160 material when the value of K_{max} or ΔK is relatively large, i.e. approximately $K_{max} > 0.58 MPa \cdot m^{1/2}$, or $\Delta K > 0.46 MPa \cdot m^{1/2}$. However, when the value of K_{max} or ΔK is relatively small, there is little difference in the fatigue crack growth rate between the 15phrRME160 and UME160 materials. Furthermore, the 15phrRME160 material has almost the same threshold value, K_{th} or ΔK_{th}, as the UME160 material. The threshold value, K_{th}, is approximately $0.41 MPa \cdot m^{1/2}$ ($\Delta K_{th} \sim 0.33 MPa \cdot m^{1/2}$) for both materials. Thus, the 15phrRME160 material has the better fatigue resistance than the UME160 material in the high-K region, but the 15phrRME160 material does not have a superior fatigue resistance in the relatively low-K region, near the threshold value.

These results suggest that the toughening mechanisms which originate from the addition of rubber particles are not effective when the value of K is relatively small. The material property of the epoxy resin dominates the fatigue behaviour in this region, despite of the presence of rubber particles. On the other hand, the results in that the fatigue crack growth rate of the rubber modified epoxy is smaller than that of the unmodified epoxy in the high-K region suggest that the toughening mechanisms dissipate more energy during the fatigue crack propagation in the this region.

As shown in Table 5.1, there is a small difference in the measured M_c value between the two materials: 1310g/mol for 15phrRME160 and 1250g/mol for UME160. However, the difference is almost certainly within the measurement error, and thus both materials virtually have the same crosslink density. (Indeed, if there were a real difference in crosslink density between them, each material should have a different threshold value, as discussed in the previous section on the effect of crosslink density. The fact that there is little difference in the threshold values confirms that there is virtually no difference in the crosslink density.)

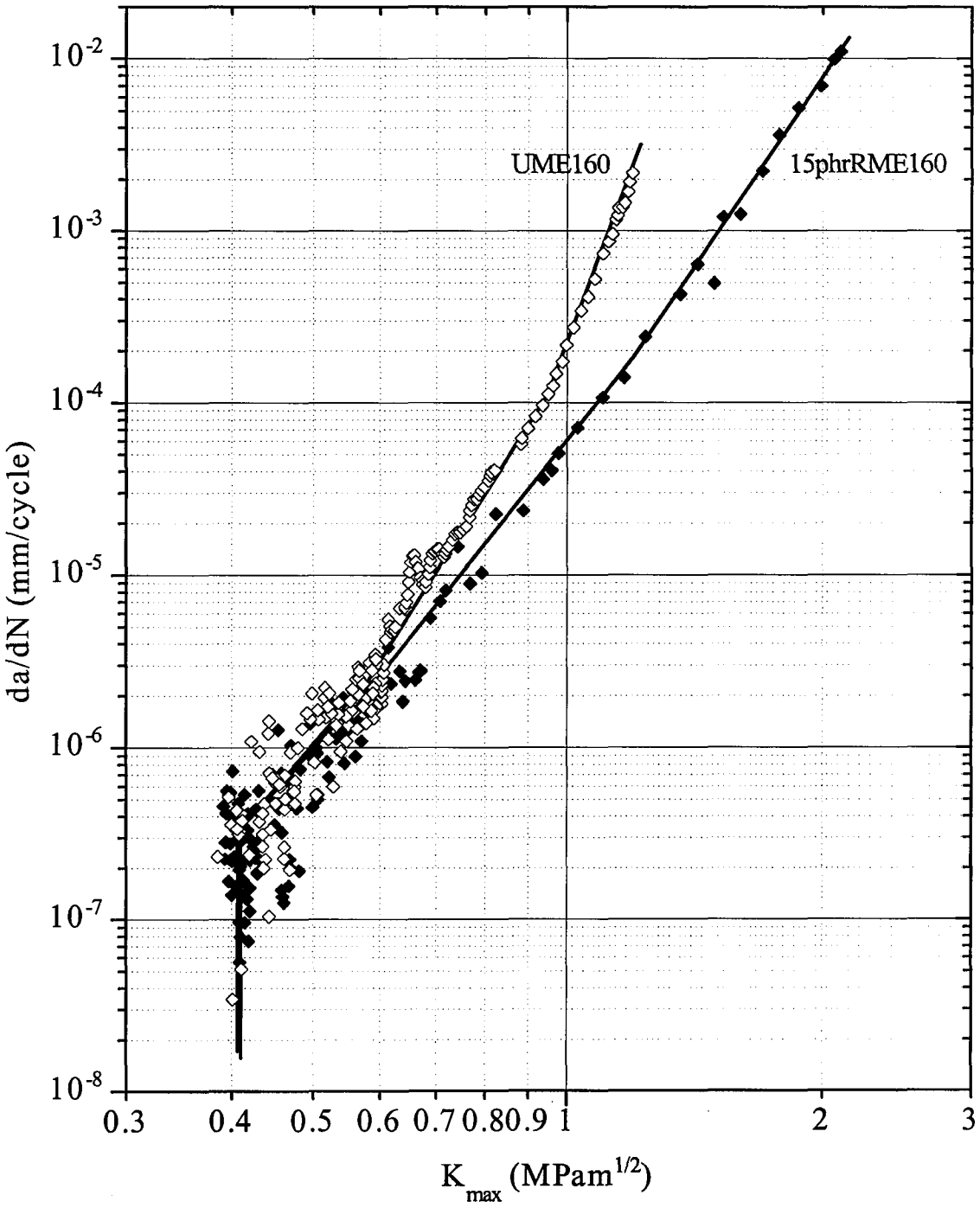


Fig.5.12 Fatigue crack growth rate for UME160 and 15phrRME160 plotted against K_{max}

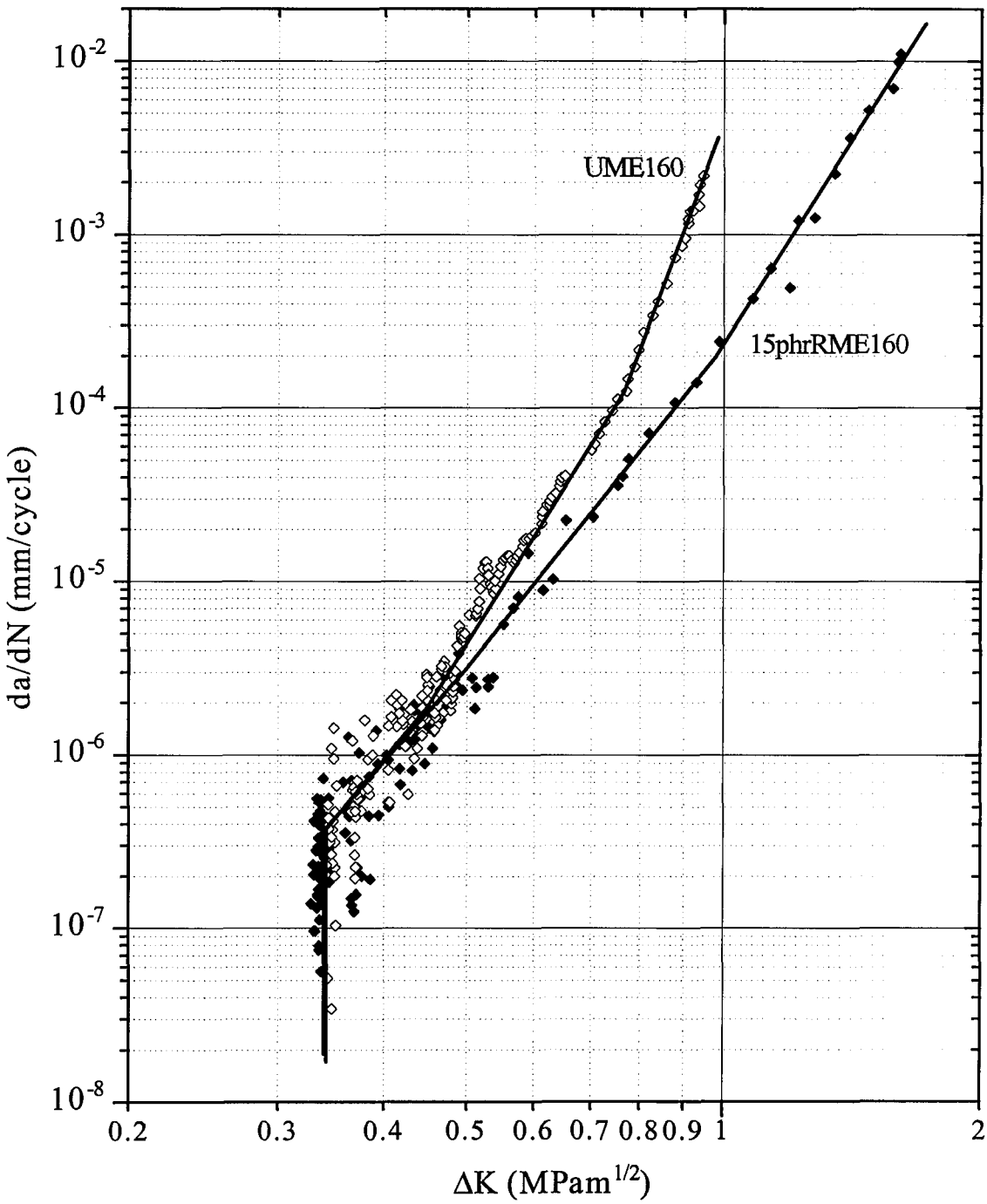


Fig.5.13 Fatigue crack growth rate for UME160 and 15phrRME160 plotted against ΔK

5.3.3 The materials cured at 120°C

Fig.5.14 and Fig.5.15 show the fatigue crack growth rates of the second group of materials, i.e. UME120 and 15phrRME120. The values of da/dN are plotted against K_{max} in Fig.5.14, and ΔK in Fig.5.15. Comparing the data of UME120 with that of 15phrRME120, the fatigue crack growth rate in 15phrRME120 is smaller than that in UME120, in the relatively high-K region. However, there is little difference in the fatigue crack growth rate between 15phrRME120 and UME120, in the relatively low-K region. This is a similar result as for the 15phrRME160 and UME160 materials. Hence, again, the toughening mechanisms due to the rubber particles are not active when the value of K is relatively small. On the other hand, in the relatively high-K region, the rubber particles reduce the fatigue crack growth rate of the rubber modified epoxy because of the additional energy dissipation induced by the presence of the rubber particles.

There is also a small difference in the measured M_c values between these two materials: 430g/mol for the 15phrRME120 material and 460g/mol for the UME120 material. This difference, however, should also be considered to be within experimental error, as for the 15phrRME160 and UME160 materials.

In summary, the rubber modified epoxies are not toughened by the addition of rubber particles in the relatively low-K region, and the toughening effect of rubber particles is effective only above a certain value of K_{max} (or ΔK). Azimi et al. [51,74] investigated the influence of the rubber content on the fatigue crack propagation of rubber modified epoxies, and reported similar results. As they suggested, it is important to introduce a concept of K-transition for a better understanding of this phenomena. This will be discussed in details in section 5.4.

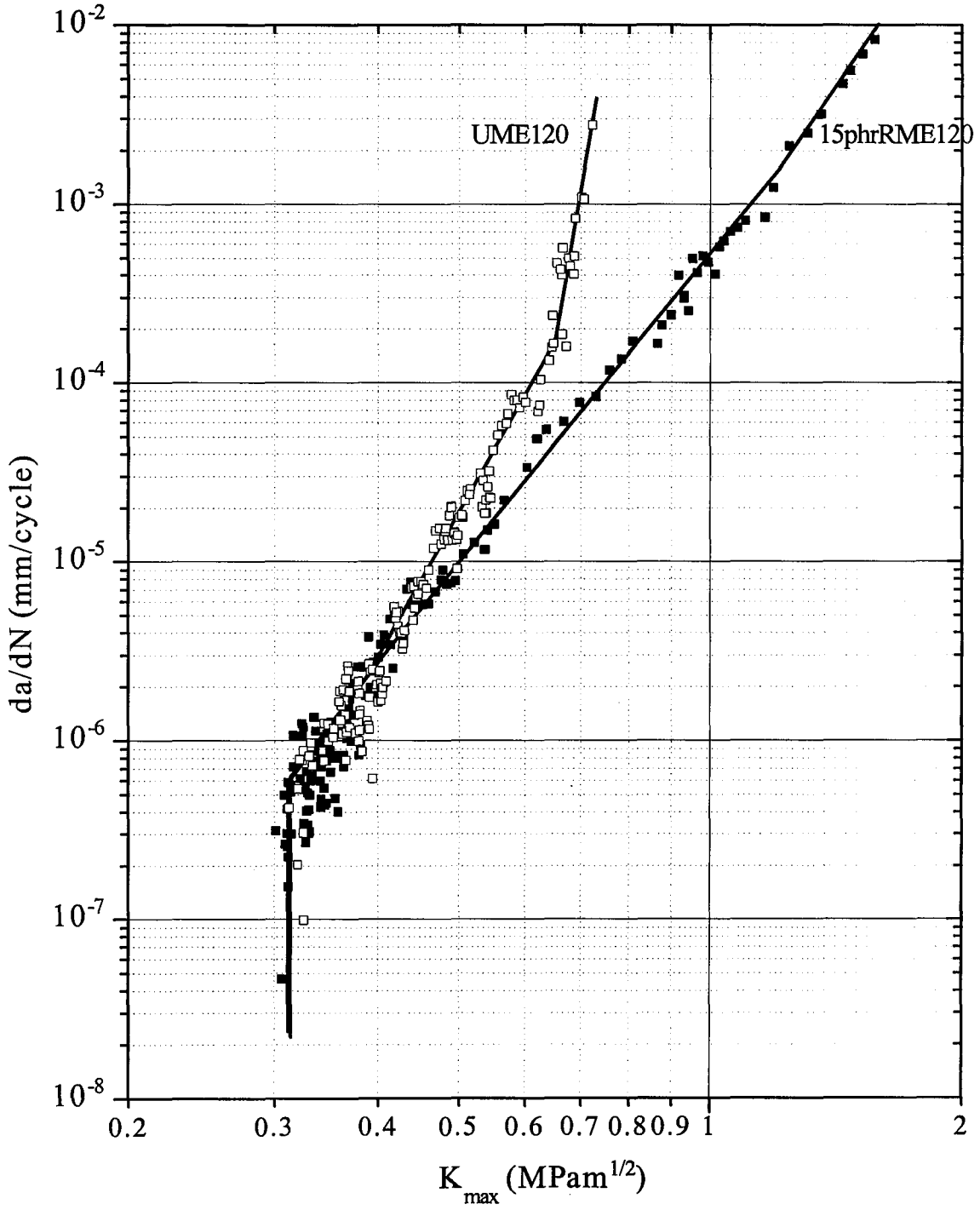


Fig.5.14 Fatigue crack growth rate for UME120 and 15phrRME120 plotted against K_{max}

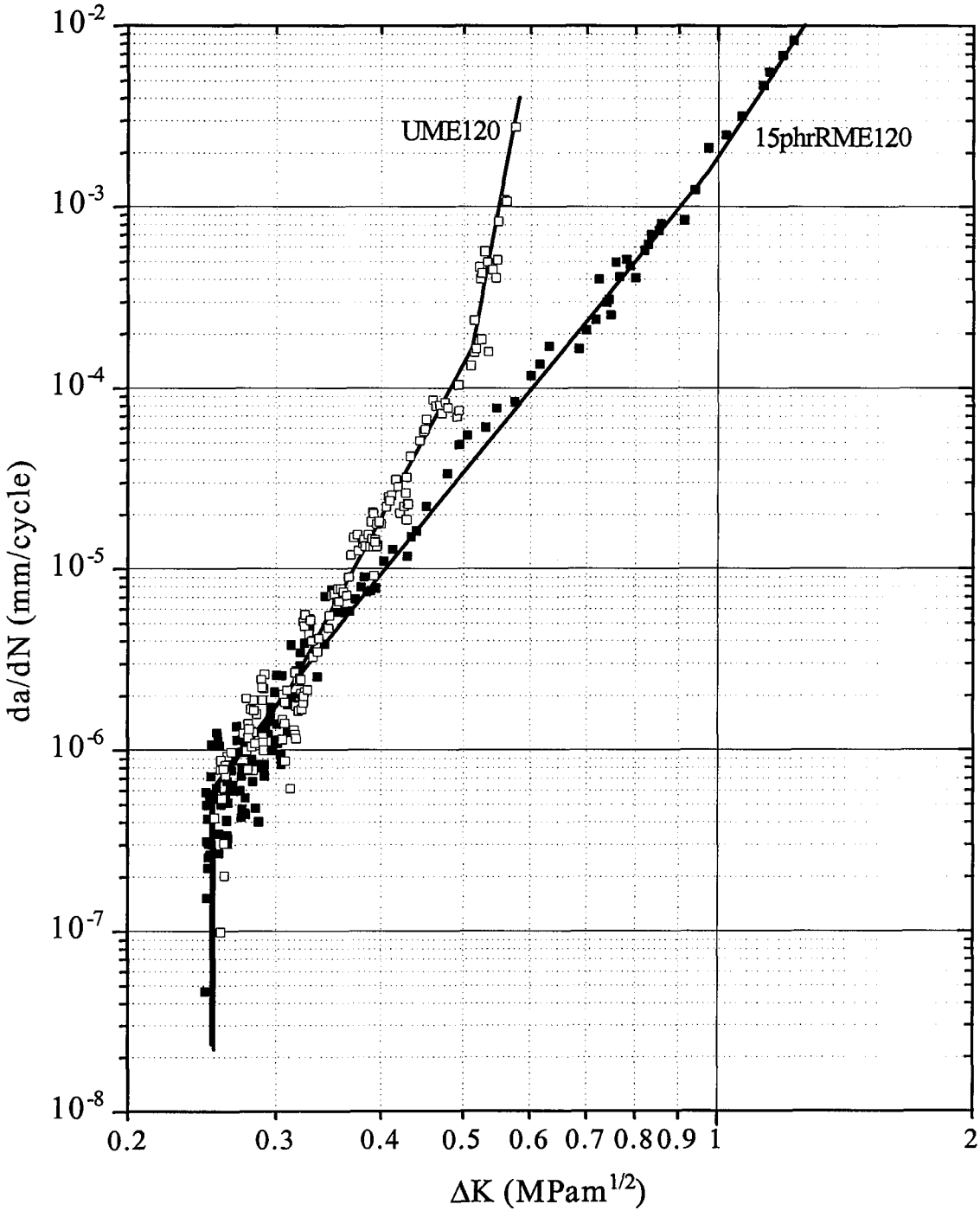


Fig.5.15 Fatigue crack growth rate for UME120 and 15phrRME120 plotted against ΔK

5.3.4 Discussion

In order to assess the effect of rubber content on the fatigue crack growth rate in the relatively high-K region, the ΔK values at da/dN=1x10^{-3} mm/cycle (termed ΔK**) are plotted against the rubber content in Fig.5.16, as Karger-Kocsis and Friedrich did [54]. Fig.5.16 also includes the results reported by Azimi [51]. This graph suggests that the ΔK** value increases with increasing the rubber content. In other words, the fatigue resistance increases as the rubber content increases. The graph also shows that only a small amount of rubber, 5phr, is needed to improve the fatigue resistance; and that the addition of more rubber gives only a small increase in fatigue resistance, especially in the high crack growth rate region.

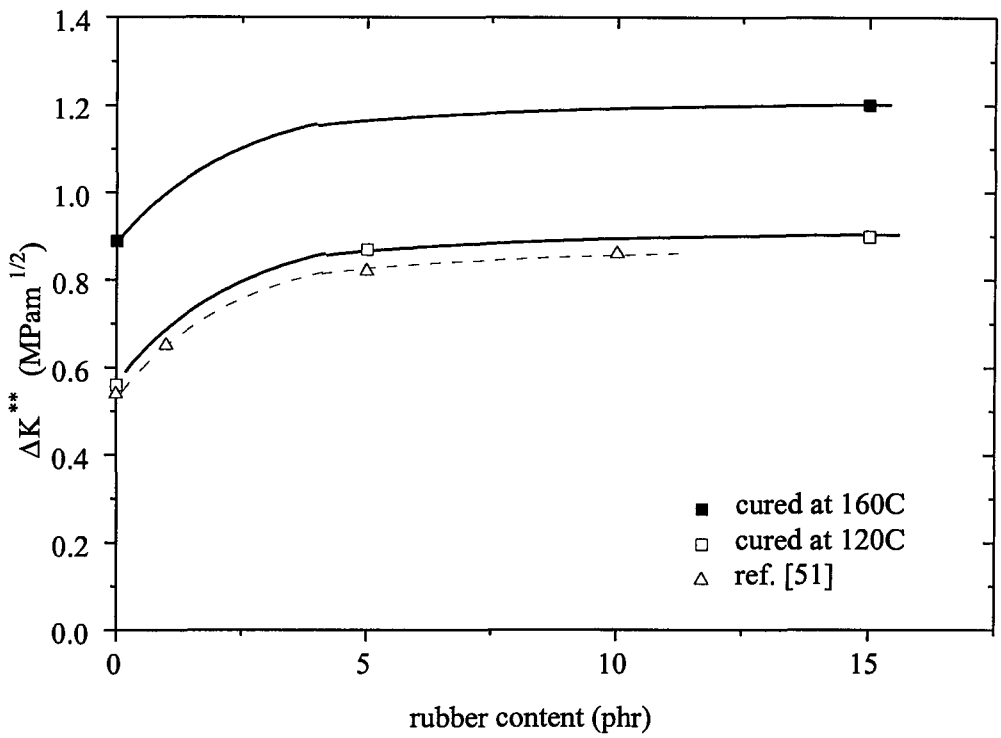


*Fig.5.16 Effect of rubber content on the ΔK** value (da/dN = 1x10^{-3}mm/cycle)*

The results reported by Azimi [51] show a very good agreement with the results of the materials cured at 120°C. Azimi used a similar DGEBA epoxy as used in the present study, and the CTBN rubber, curing agent and curing temperature

in Azimi's study are all the same for the materials cured at 120°C in the present study. Thus, it can be expected that the material properties of the epoxies in Azimi's study are very close to those of the epoxies cured at 120°C. Hence, this may cause the very good agreement between these materials.

Fig.5.17 plots the slope, m, of the Paris Law against the rubber content. The Paris Law is expressed by the following equation:

$$da/dN = A\,(\Delta K)^m \qquad (5.5)$$

where A and m are constants. The constant m indicates the slope of the fatigue curve in Paris Law plot. A large m value means a steep fatigue curve and a high sensitivity for the K value, whereas a small m value means a gentle fatigue curve and a low sensitivity for the K value. Generally speaking, a smaller m value is preferable for a better fatigue resistance, as shown in Fig. 5.18.

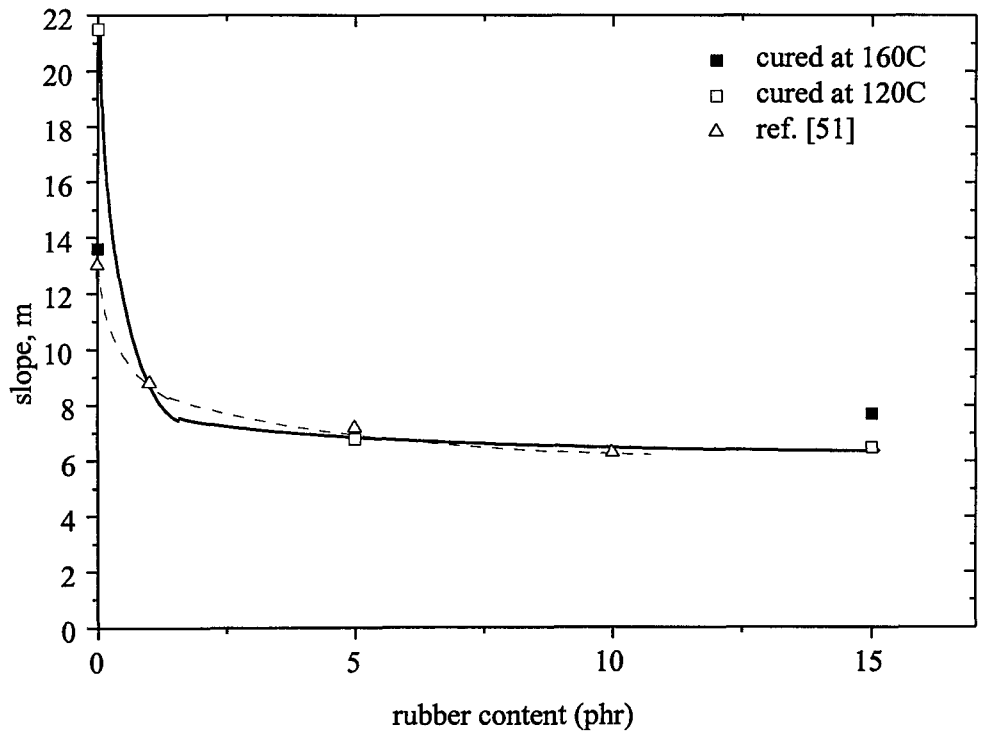


Fig.5.17 Influence of the rubber content on the slope, m, of the Paris Law

As shown in Fig.5.17, the slope, m, is strongly affected by the rubber content. The fatigue curve is relatively steep for the unmodified epoxy in Paris Law plot, and it becomes gentle with increasing the rubber content. This means that the material becomes less sensitive to the K value as the rubber content is increased. These results are in accordance with the results by Azimi et al. [51,74]. They also reported that the slope, m, is not depend on the rubber particle size.

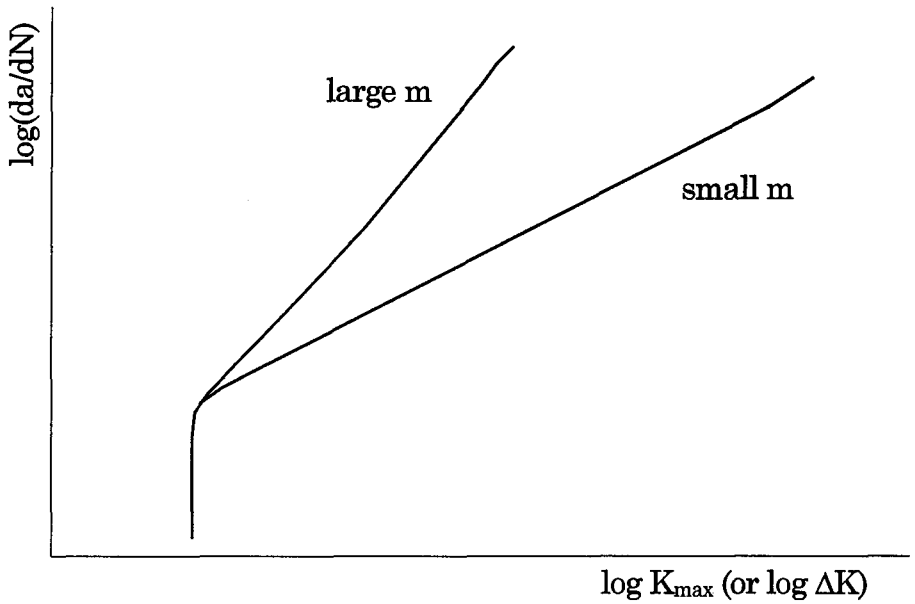


Fig.5.18 Schematic graph of the fatigue curves with a large m and a small m

The fatigue crack growth rate plotted against the normalised K_{max} value, K_{max}/K_{Ic}, is shown in Fig.5.19 and Fig.5.20. Fig.5.19 shows the fatigue data for 15phrRME160 and UME160, and Fig.5.20 shows the data for 15phrRME120 and UME120. For both groups of materials, the fatigue crack growth curve shifts from right to left (i.e. high K_{max}/K_{Ic} to low K_{max}/K_{Ic}) with the rubber content increasing from 0phr (unmodified epoxy) to 15phr. This means that the rubber modified epoxy, which contains 15phr rubber, has a higher fatigue crack growth rate than the unmodified epoxy, at the same value of K_{max}/K_{Ic}. In other words, the K_{max}/K_{Ic} value necessary for a certain amount of fatigue crack growth rate is smaller for the rubber modified epoxy than for the unmodified epoxy. This can be understood qualitatively as follows.

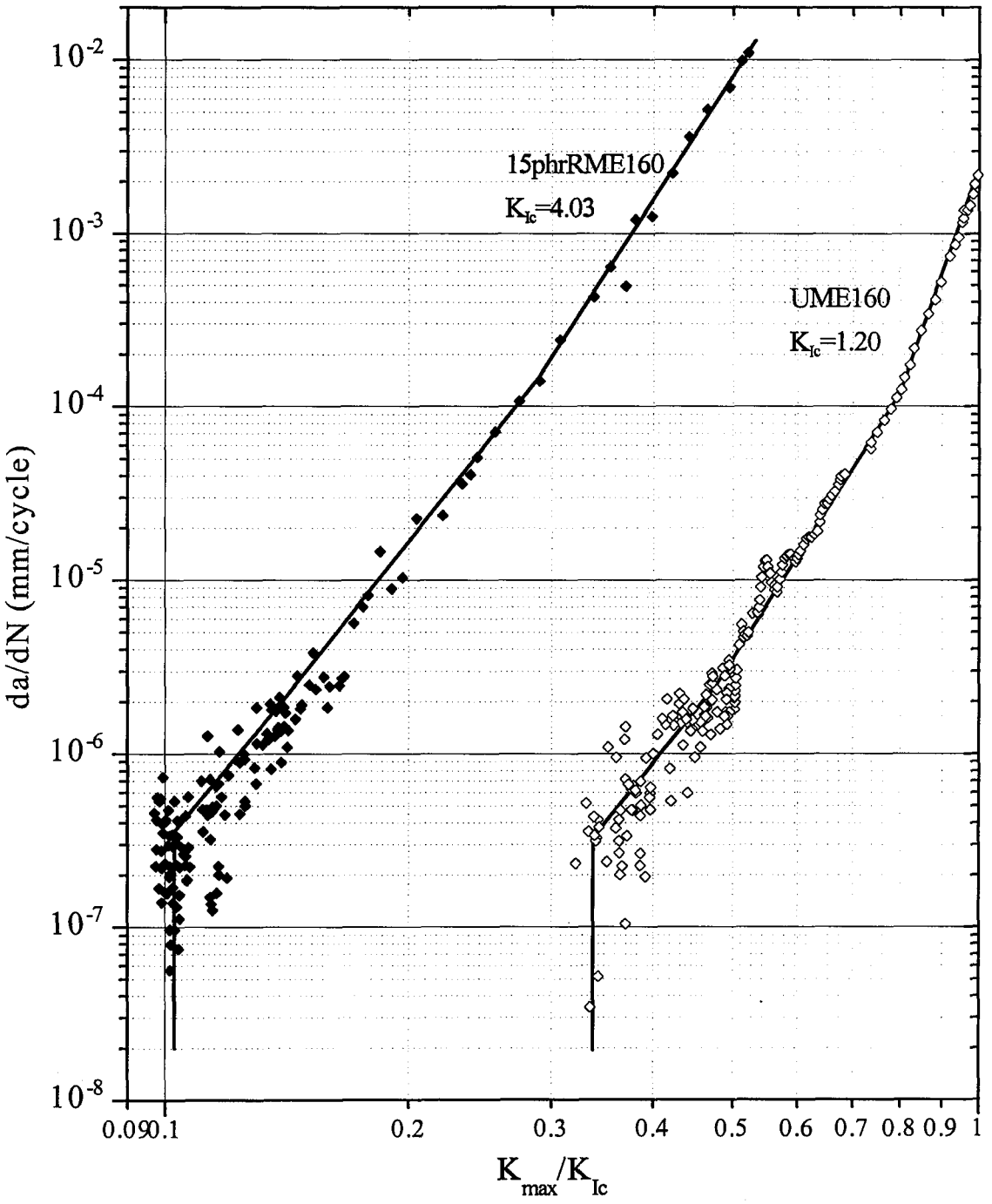


Fig.5.19 Fatigue crack growth rate for 15phrRME160 and UME160 plotted against K_{max}/K_{Ic}.

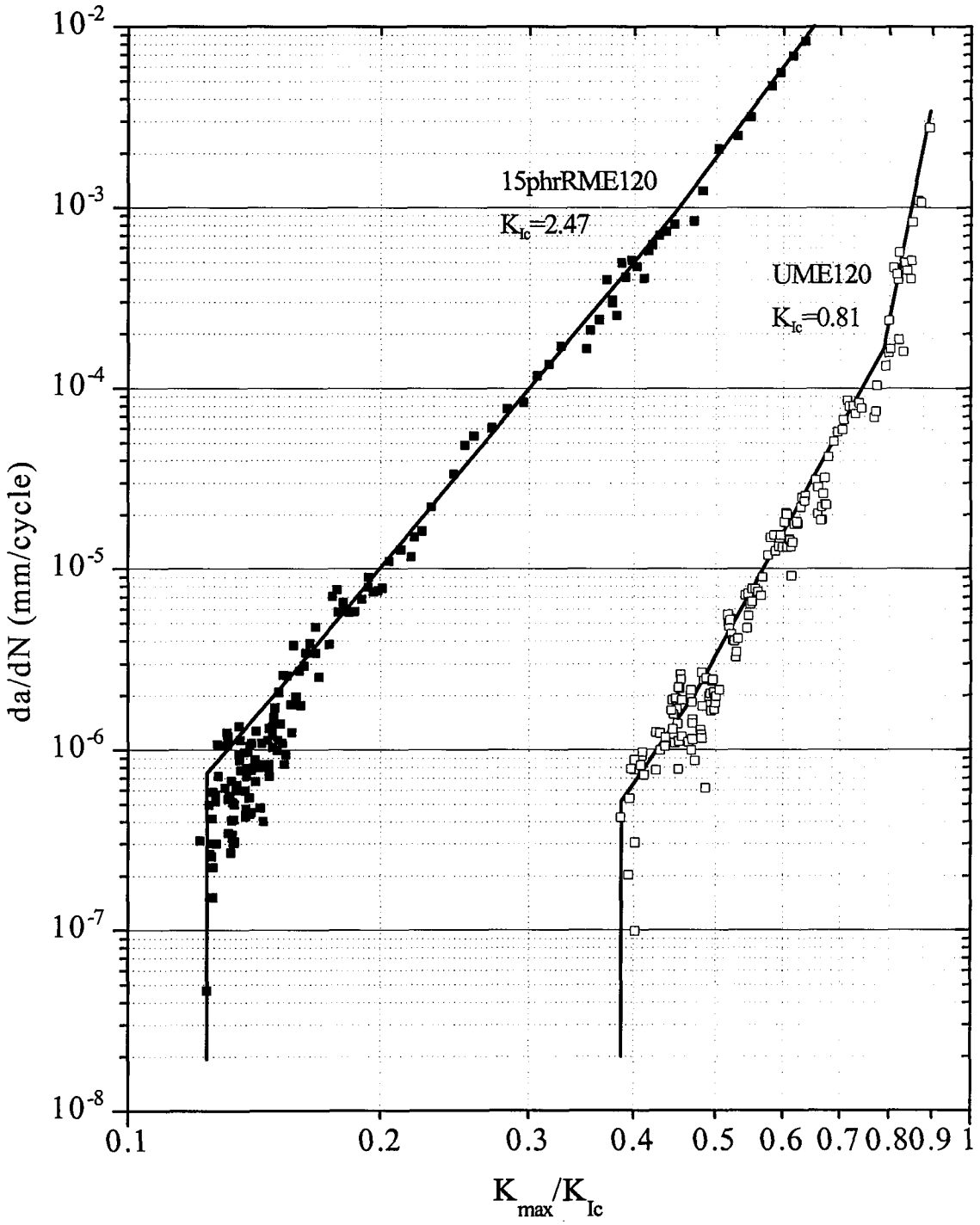


Fig.5.20 Fatigue crack growth rate for 15phrRME120 and UME120 plotted against K_{max}/K_{Ic}.

Imagine two materials A and B; material A as a rubber modified epoxy and material B as an unmodified epoxy. Both A and B have the same threshold value, $K_{th,A}$ and $K_{th,B}$, but the K_{Ic} value of A, $K_{Ic,A}$, is greater than that of B, $K_{Ic,B}$. Thus,

$$K_{th,A} = K_{th,B} \tag{5.6}$$

$$K_{Ic,A} > K_{Ic,B} \tag{5.7}$$

The normalised threshold values, $(K_{th}/K_{Ic})_A$ and $(K_{th}/K_{Ic})_B$, are related to each other as follows:

$$(K_{th}/K_{Ic})_A \equiv K_{th,A}/K_{Ic,A} < (K_{th}/K_{Ic})_B \equiv K_{th,B}/K_{Ic,B} \tag{5.8}$$

In the threshold region, therefore, the fatigue data of material A (rubber modified epoxy) is located in the lower K_{max}/K_{Ic} region than that of material B (unmodified epoxy). As the fatigue crack growth rate increases, the necessary K_{max} value also increases. Finally, when the K_{max} value equals the K_{Ic} value, the fatigue crack growth rate becomes infinite. Consequently, in the very high fatigue crack growth rate region, the normalised K_{max} value, K_{max}/K_{Ic}, of both materials approaches to unity.

$$K_{max}/K_{Ic} \rightarrow 1 \text{ when } da/dN \rightarrow +\infty \tag{5.9}$$

Therefore, the fatigue curves of martial A and B can be drawn schematically as shown in Fig.5.21. The fatigue data of material A is located at lower values of K_{max}/K_{Ic} than that of material B. The difference between them decreases with increasing K_{max}/K_{Ic} value, and the fatigue crack growth rates for both materials approach to infinity, as the K_{max}/K_{Ic} value approaches unity. This is why the rubber modified epoxy has a higher fatigue crack growth rate than the unmodified epoxy, at a given K_{max}/K_{Ic} value. It is also the reason why the fatigue crack growth curve shifts from right to left (i.e. high K_{max}/K_{Ic} to low K_{max}/K_{Ic}) with increasing rubber content.

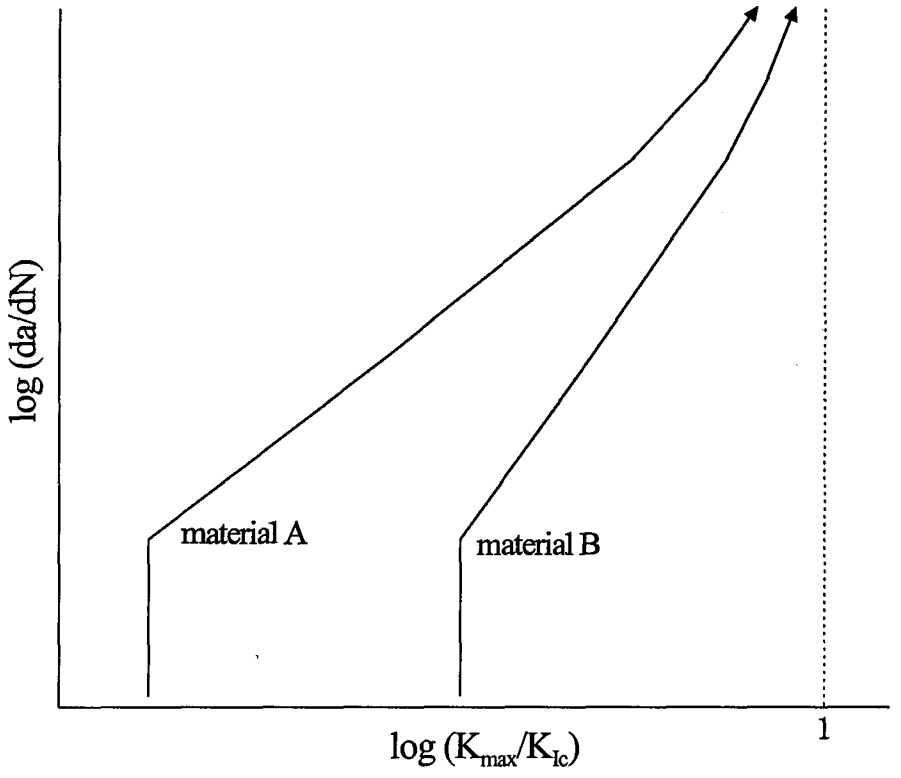


Fig.5.21 Schematic fatigue curves of material A and B

The fatigue data for the present epoxy materials together with data for similar materials, which contain 1phr, 5phr and 10phr rubber, measured by Azimi et al. [107] are plotted in Fig.5.22. It can be seen from the results given in Fig.5.22 that there is a steady shift in the fatigue curves as the rubber content is increased.

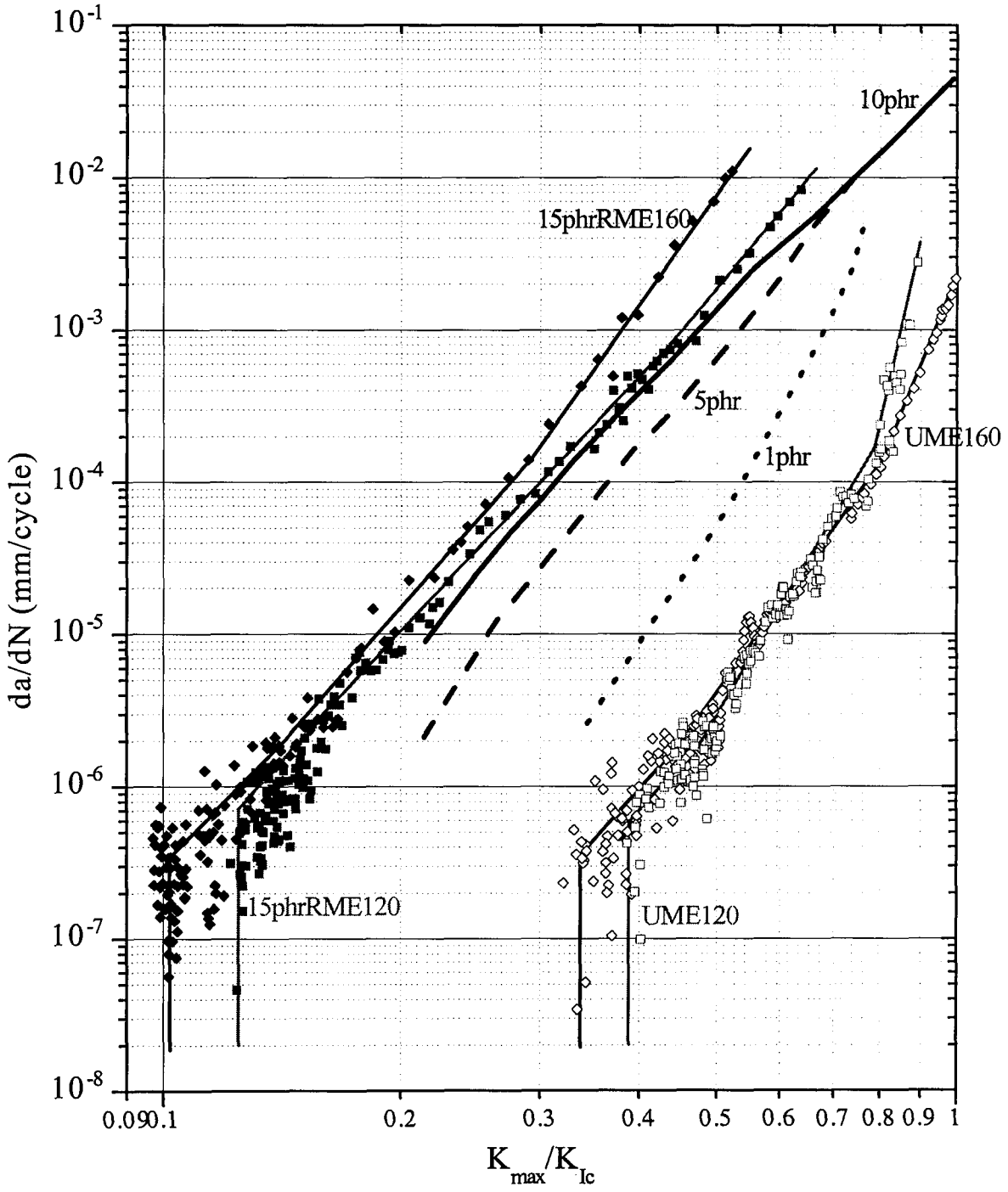


Fig.5.22 Variation of fatigue crack growth rate plotted against K_{max}/K_{Ic} (Data of 1phr, 5phr and 10phr are from ref. [107])

5.4 K-transition value

The results in the previous section suggest that a rubber modified epoxy is not toughened by the additional rubber particles in the relatively low K region of the da/dN versus K_{max}, or ΔK, curve; and that the toughening mechanisms activated by the rubber particles are effective only above a certain K value. Thus, the concept of a K-transition value is helpful for a more quantitative understanding of the results.

Fig.5.23 shows the experimental definition of the K-transition value. A K-transition value, K_T, can be experimentally defined as a critical value of the stress intensity factor, K_{max}, at which a difference in the fatigue crack growth rate curve between the rubber modified epoxy and the unmodified epoxy starts to be observed. Indeed, Fig.5.23 shows that the value of K_T can be clearly defined since there is little difference in the fatigue crack growth rate between the rubber modified epoxy and the unmodified epoxy below K_T, whereas the rubber modified epoxy has significantly better fatigue resistance than the unmodified epoxy above K_T.

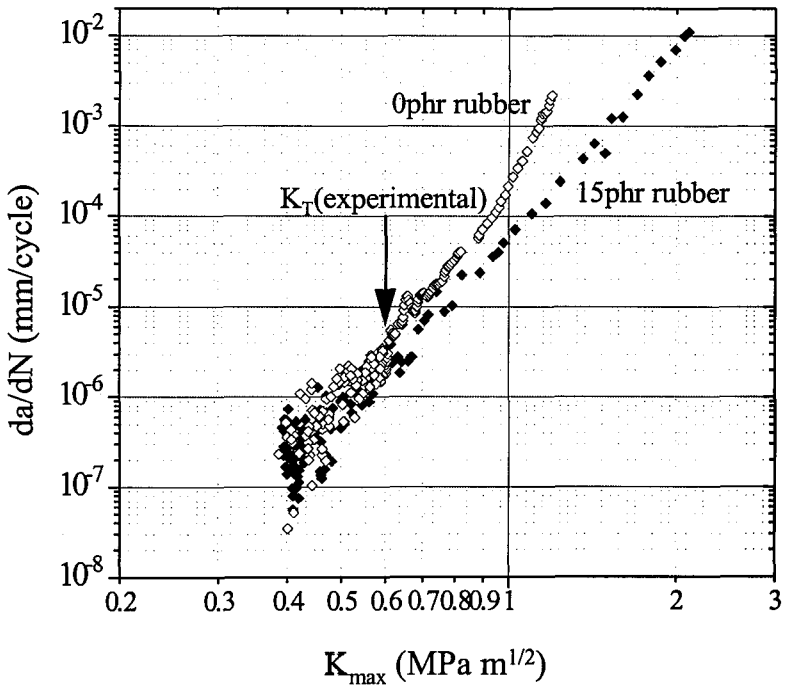


Fig.5.23 Experimental definition of a K-transition value

Theoretically, it is suggested that the K_T value is a stress intensity factor where the plastic zone size is the same as the size of the rubber particles. As shown in Fig.5.24, when the K_{max} value is smaller than K_T, the size of plastic zone is smaller than that of rubber particles. Hence, the plastic deformation is now restricted to a very limited region around the crack tip, and consequently the additional energy dissipation mechanisms associated with the presence of rubber particles can not become active. On the other hand, when the K_{max} value is greater than K_T, the plastic zone is large enough to engulf the rubber particles in the vicinity of the crack tip. Thus, the rubber particles can cause further plastic deformation of the epoxy matrix and, therefore, more energy is dissipated during crack propagation.

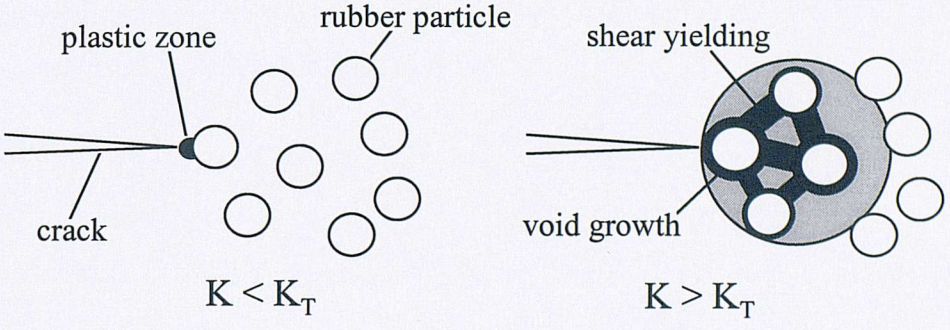


Fig.5.24 Schematic drawing of the plastic deformation near crack tip

The plastic zone radius, r_y, can be estimated using LEFM by the following equation, as discussed in section 2.2.4:

$$r_y = (K/\sigma_{yt})^2/6\pi \qquad (5.10)$$

where σ_{yt} is tensile yield stress. When the plastic zone size is equal to the size of the rubber particles, the following condition is achieved:

$$r_y \equiv r_p \qquad (5.11)$$

where r_p is the radius of the rubber particle. Thus, the value of K_T can be calculated by substituting equation 5.10 into equation 5.11, as follows:

$$K_T = (6\pi r_p)^{1/2} \sigma_{yt} \tag{5.12}$$

The calculated K_T values are 0.59 MPa·m$^{1/2}$ for 15phrRME160, and 0.46 MPa·m$^{1/2}$ for 15phrRME120. From the SEM observations, 1.7μm is used as the radius of the rubber particle, r_p, for 15phrRME160, and 1.4μm for 15phrRME120, as shown in Table 4.1 in section 4.2.1. It should also be noted that for these calculations, we have to use the tensile yield stress of the epoxy matrix, σ_{yt}, as the yield stress, and take the strain rate of the fatigue tests into account, which may be far higher than that used in the static tests.

In the fatigue tests, a sinusoidal wave form loading is employed at a frequency of 5Hz, as discussed in section 3.6. The maximum displacement of the crosshead is approximately 1mm. Therefore, the crosshead displacement, x, can be expressed by the following equation:

$$x = x_0 \sin(2\pi ft) \tag{5.13}$$

where x_0 is 1mm and f is 5Hz. The crosshead speed, $|dx/dt|$, is as follows:

$$|dx/dt| = |2\pi f x_0 \cos(2\pi ft)| \tag{5.14}$$

The mean value of the crosshead speed can be given by:

$$|dx/dt|_{mean} = (2/\pi)\, 2\pi f x_0 = 4 f x_0 = 1200(\text{mm/min.}) \tag{5.15}$$

Thus, the equivalent crosshead speed in the fatigue tests is about 1000mm/min. The compressive yield stress, σ_{yc}, at this crosshead speed is estimated by extrapolating the yield stress data by Huang [7]. Then, the tensile yield stress, σ_{yt}, is calculated using the following relationship:

$$\sigma_{yt} \sim 0.78 \sigma_{yc} \tag{5.16}$$

Finally, the values of σ_{yt} used for the calculations are, therefore, 105MPa for the 15phrRME160 material, and 90MPa for the 15phrRME120 material, as summarised in Table.5.4.

Table.5.4 Theoretically calculated K_T values

Material	σ_{yt} (MPa)	r_p (μm)	K_T (theoretical) (MPa·m$^{1/2}$)
15phrRME160	105	1.7	0.59
15phrRME120	90	1.4	0.46

As shown in Fig.5.25, these K_T values explain the behaviour of the fatigue crack growth rate curves very well for both the materials cured at 160°C and at 120°C. For a given cure temperature (i.e. for a given M_c value for the epoxy matrix), the rubber modified epoxies have better fatigue resistance than the unmodified epoxies above the K_T values, and there are no differences in the fatigue resistance between the materials below the K_T values.

Equation 5.12 also predicts that the material which has smaller rubber particles will have the smaller K_T value, and consequently the better fatigue resistance. As shown schematically in Fig.5.26, the value of K_T decreases, upon decreasing the particle size. Therefore, the fatigue crack growth rate curve moves downwards. Although it is not certain what happens when the theoretical K_T becomes smaller than the value of K_{th}, it is assumed that the 'real' K_T is approaches the value of K_{th}. This is because the K_{th} value itself is considered to be governed by the material properties of the matrix epoxy, and is not affected by the rubber particles.

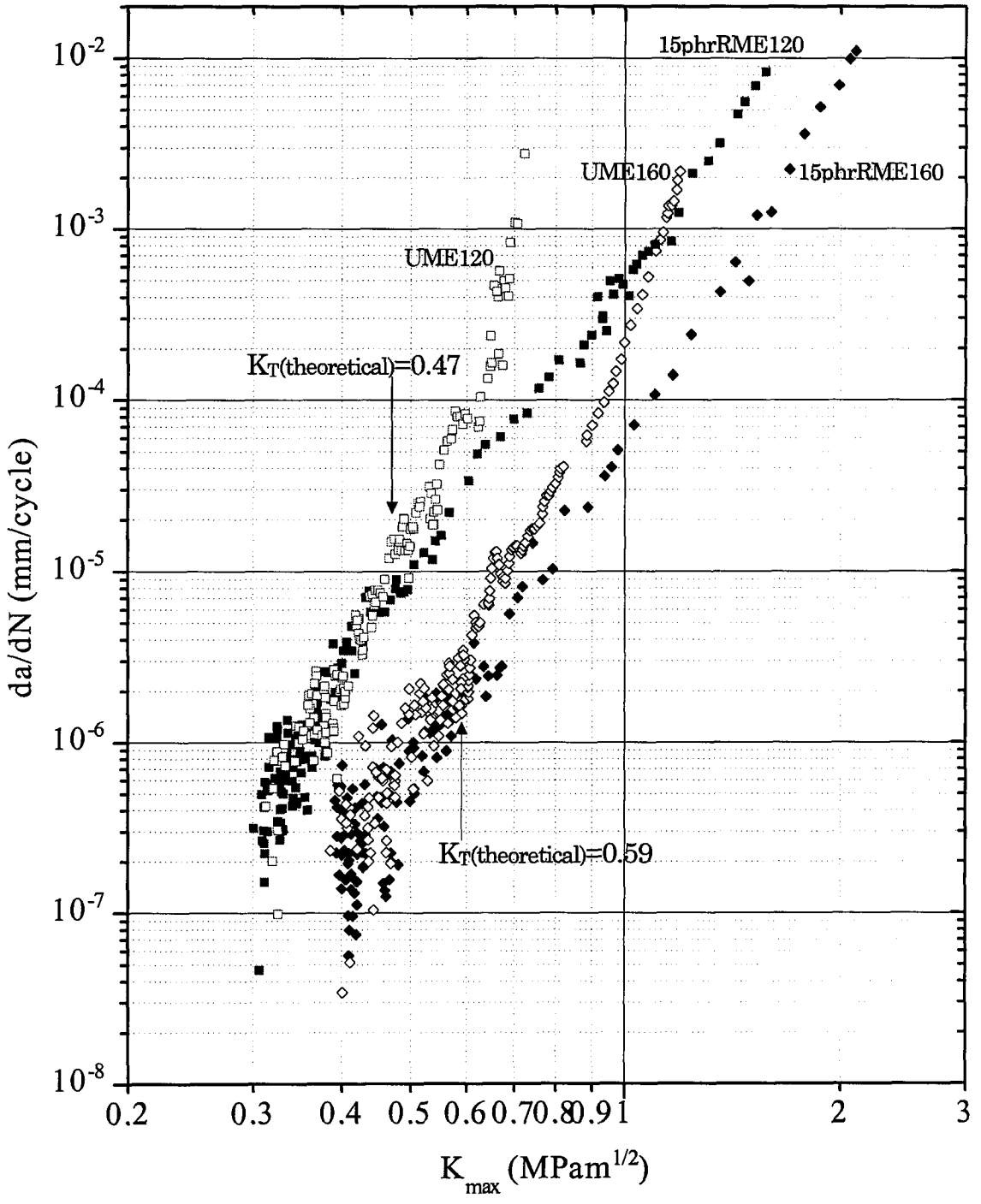


Fig.5.25 The calculated K_T values and experimental fatigue data for 15phrRME160 and UME160, and 15phrRME120 and UME120

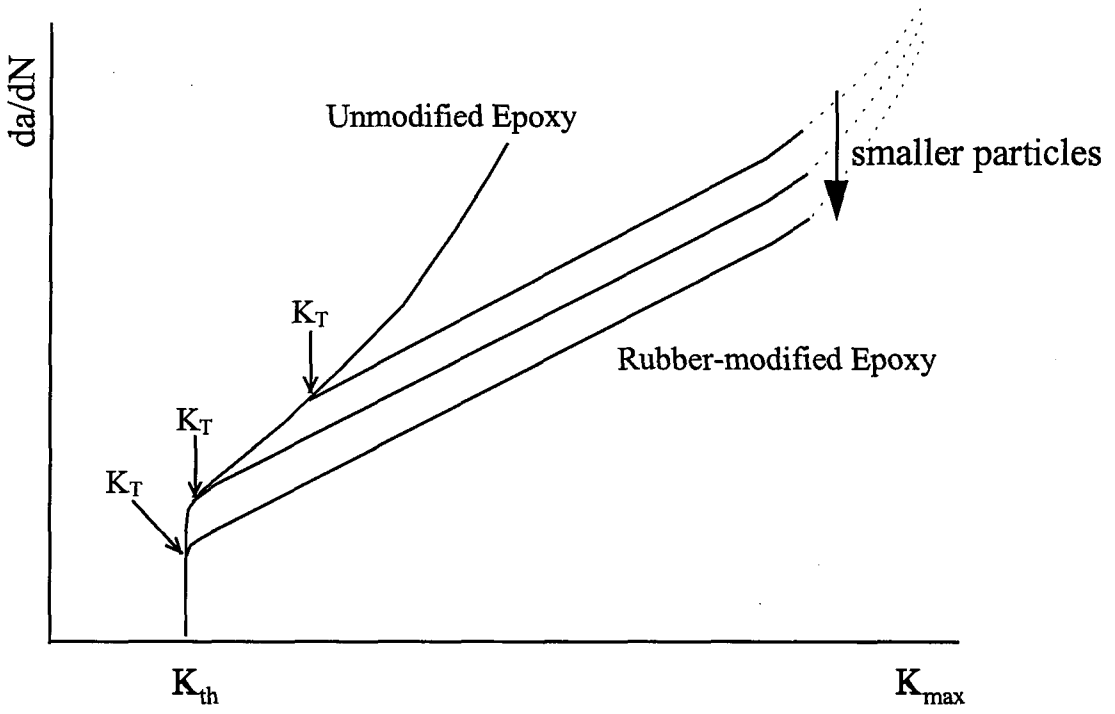


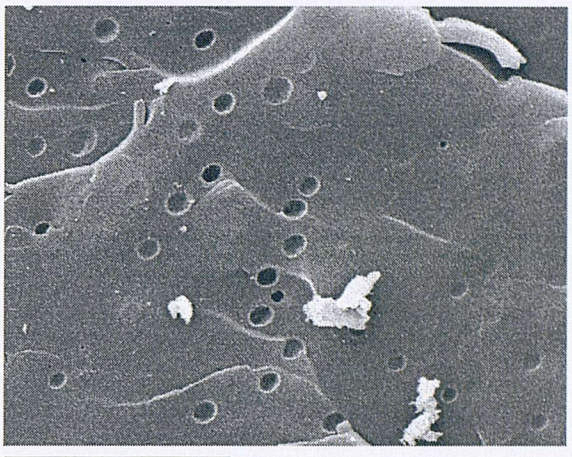
Fig.5.26 Expected effect of particle size on the fatigue crack growth rate

5.5 Effect of particle size

5.5.1 Introduction

As mentioned in section 5.4, the rubber particle size is expected to change the K-transition value, K_T, and consequently affect the fatigue crack growth rate. In order to check this predicted effect of particle size, we investigated the fatigue crack growth rates for the following materials: 5phrRME120 and 5phrRME120+BPA. The particle radius of the 5phrRME120 material is about 1.0μm, and the 5phrRME120+BPA material has much smaller rubber particles, the radius of which is 0.2-0.3μm, as shown in Fig.5.27. The fatigue crack growth rates for the UME120 and UME120+BPA materials, both of which contain no rubber particles, were also measured as reference materials.

5phrRME120 (r_p=1.0μm)



20μm

5phrRME120+BPA (r_p=0.2-0.3μm)



20μm

Fig.5.27 Microstructure of the 5phrRME120 and 5phrRME120+BPA materials

5.5.2 5phrRME120 and 5phrRME120+BPA

Fig.5.28 clearly shows that the 5phrRME120+BPA material has a better fatigue resistance than the 5phrRME120 material. As expected from the discussion in the previous section, the fatigue crack growth rate curve shifts downwards with decreasing particle size. However, it should be noted that not only the particle size but also the crosslink density of the matrix epoxy are different between the two materials, as shown in Table 5.5. Thus, both the effect of particle size and crosslink density have to be considered.

Table 5.5 Material properties of the 5phrRME120, 5phrRME120+BPA, UME120 and UME120+BPA materials

Material	M_c (g/mol)	r_p (μm)
5phrRME120	480	1.0
5phrRME120+BPA	540	0.2-0.3
UME120	460	---
UME120+BPA	570	---

The M_c value is 480g/mol for 5phrRME120, and 540g/mol for 5phrRME120+BPA. Thus, the 5phrRME120+BPA material has a lower crosslink density than the 5phrRME120 material. As discussed in section 5.3, the material having the lower crosslink density should have the better fatigue resistance than the material having the higher crosslink density. Now, to evaluate the effect of M_c on the fatigue behaviour, the fatigue growth rate of the UME120 and UME120+BPA materials may be compared. Fig.5.29 shows the fatigue data for the UME120 and UME120+BPA materials. It can be seen that the fatigue crack growth rate of UME120+BPA is lower than that of UME120 at any given K_{max} value. This means the change in crosslink density, due to the addition of BPA, improves the fatigue resistance, including the threshold value, K_{th}.

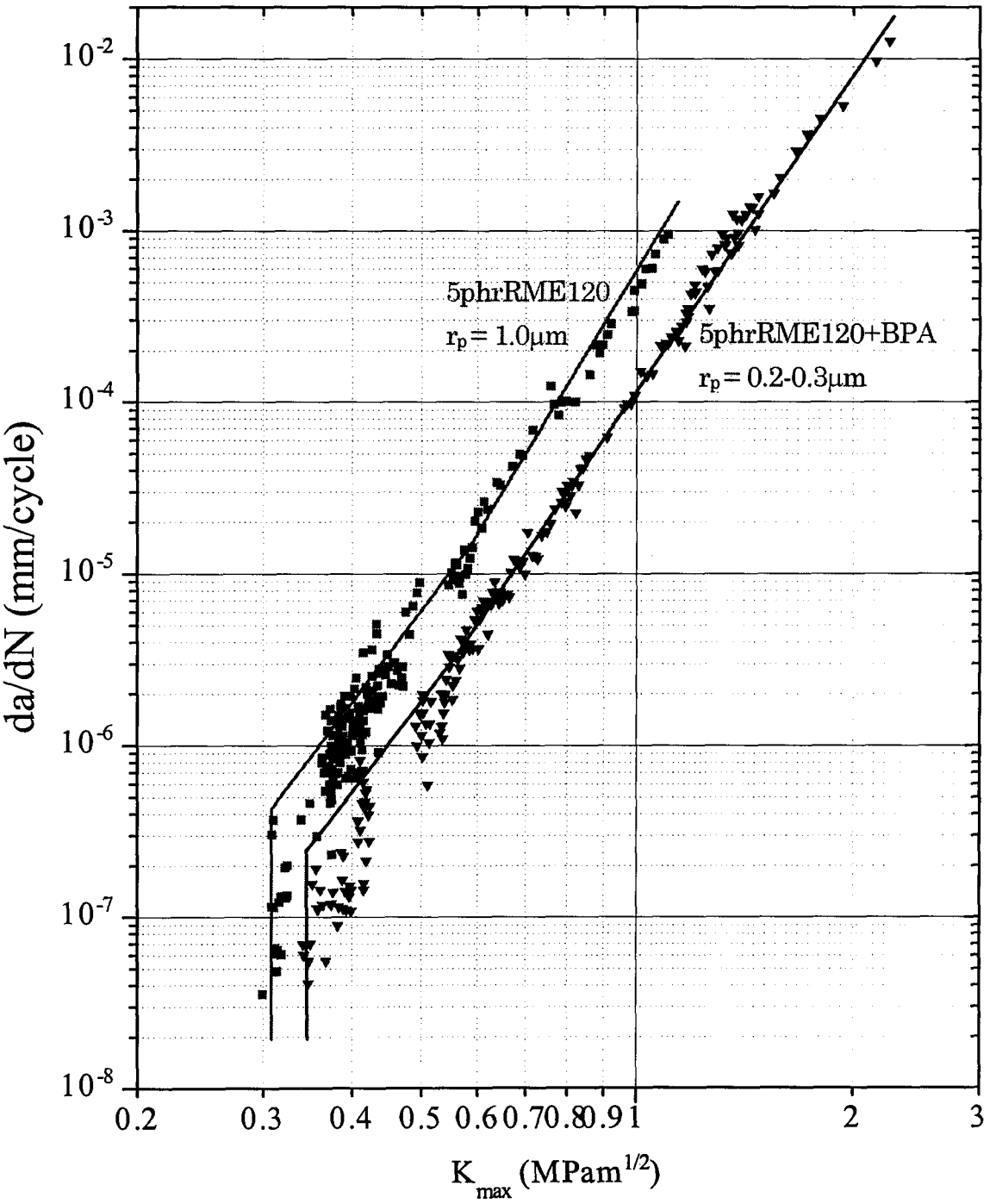


Fig.5.28 Fatigue crack growth rate for 5phrRME120 and 5phrRME120+BPA plotted against K_{max}

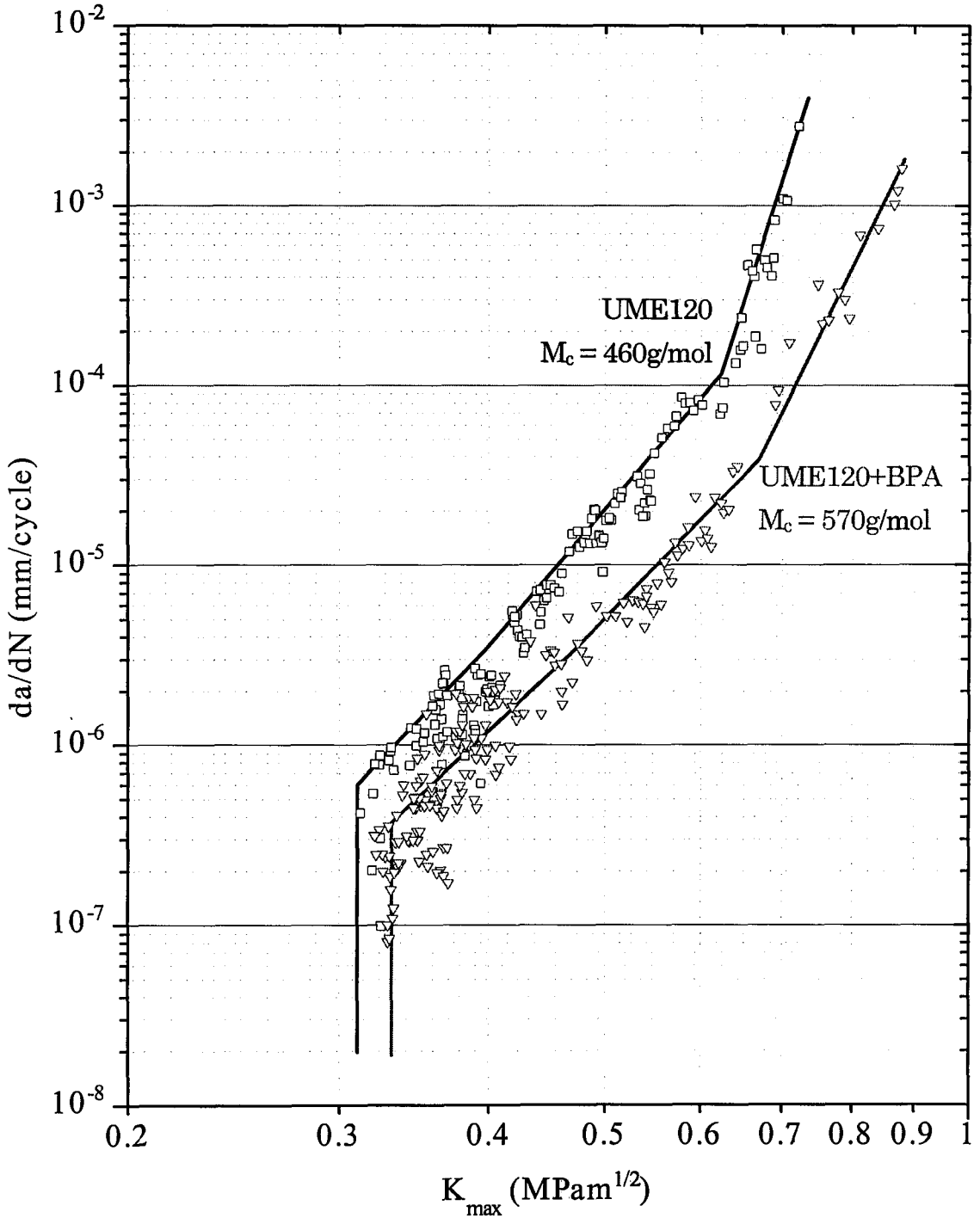


Fig.5.29 Fatigue crack growth rate for UME120 and UME120+BPA plotted against K_{max}

5.5.3 Interpretation of the experimental results

Fig.5.30 shows the fatigue crack growth rate of all four materials of interest: 5phrRME120, 5phrRME120+BPA, UME120 and UME120+BPA. It should be noted that since there is little difference in the threshold values between the UME120 and 5phrRME120 materials, the difference in the crosslink density (460g/mol for UME120 and 480g/mol for 5phrRME120) between these two materials is virtually negligible. The same comment may be made for the difference in the crosslink density (570g/mol for UME120+BPA and 540g/mol for 5phrRME120+BPA) between the UME120+BPA and 5phrRME120+BPA materials.

As Fig.5.30 is rather 'busy', a schematic graph is shown in Fig.5.31. In order to evaluate the effect of crosslink density and particle size separately, we may consider an imaginary 5phr rubber modified epoxy which has the same crosslink density (i.e. M_c=540g/mol or 570g/mol) as the UME120+BPA and 5phrRME120+BPA materials and the same rubber particle size (i.e. 1.0μm) as the 5phrRME120 material. Table 5.6 summarises the M_c values and the rubber particle size, r_p, for all the materials of interest.

Table 5.6 M_c and r_p values for UME120, UME120+BPA, 5phrRME120, 5phrRME120+BPA and the imaginary rubber modified epoxy material

	M_c=460-480g/mol	M_c=540-570g/mol
unmodified	UME120	UME120+BPA
r_p=0.2-0.3μm		5phrRME120+BPA
r_p=1.0μm	5phrRME120	Imaginary material

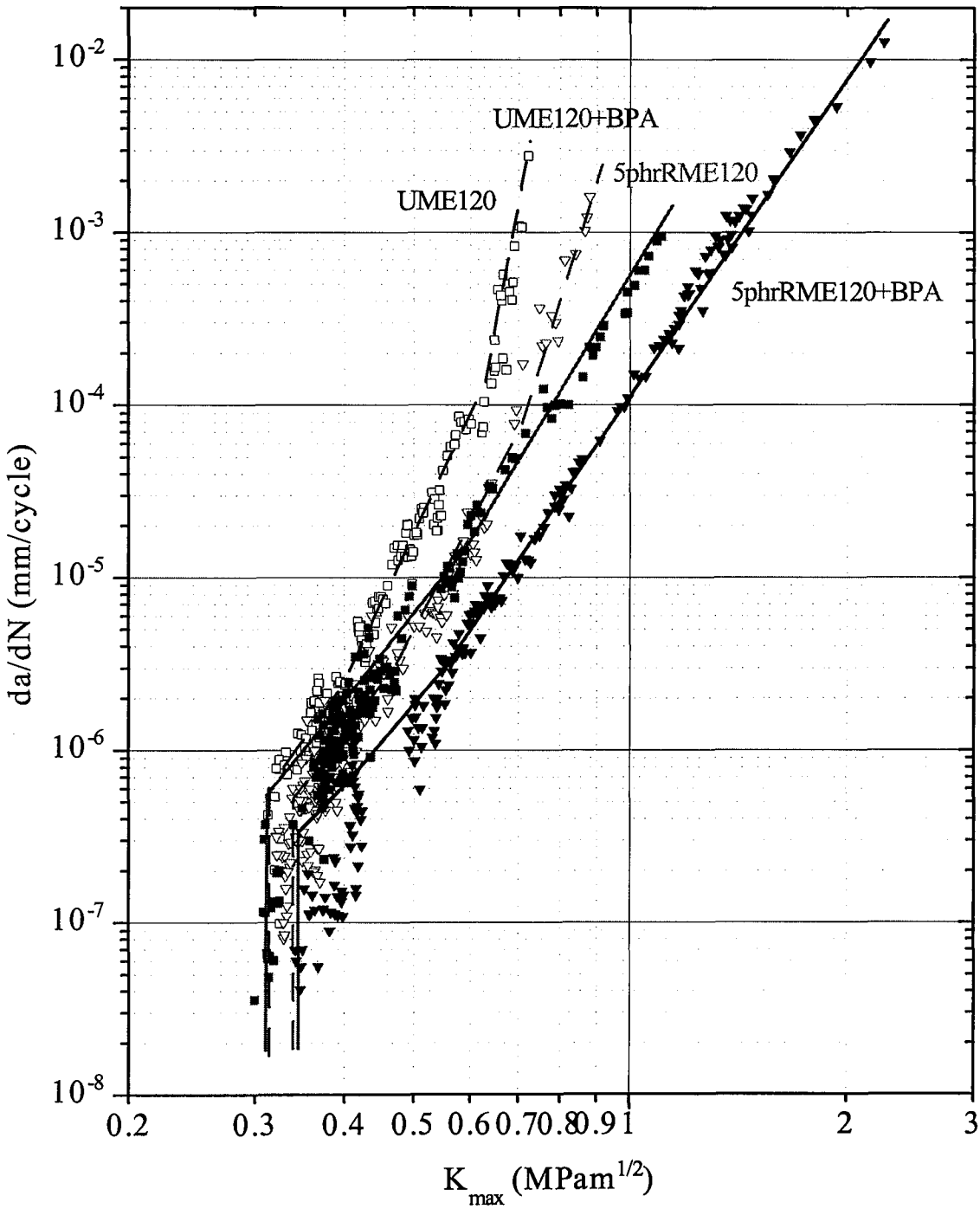


Fig.5.30 Fatigue crack growth rate for 5phrRME120, 5phrRME120+BPA, UME120 and UME120+BPA plotted against K_{max}

The improvement in the fatigue resistance from fatigue curve(1), UME120, to fatigue curve(3), 5phrRME120, is caused by the addition of 5phr rubber particles with a radius of 1.0μm. The improvement in the fatigue resistance from UME120+BPA to the imaginary rubber modified epoxy material should be similar to the improvement from UME120 to 5phrRME120. Thus, the fatigue curve of the imaginary rubber modified epoxy material may be represented by the fatigue curve(5).

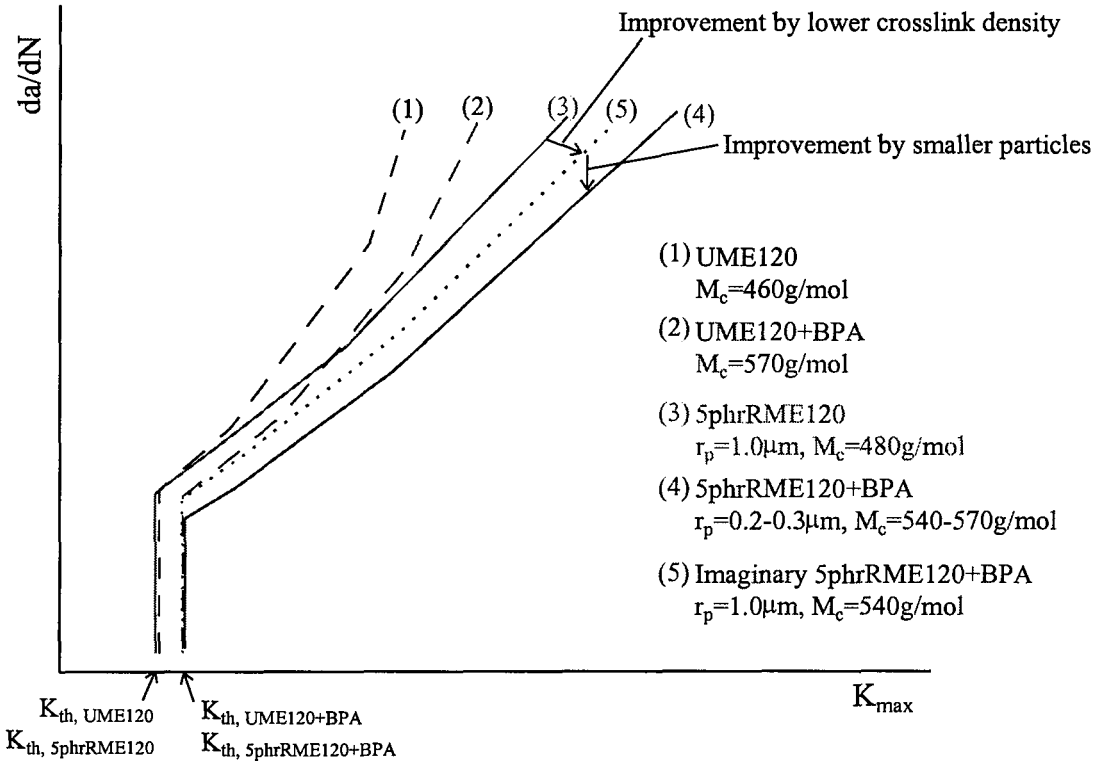


Fig.5.31 Schematic graph of fatigue data for UME120, UME120+BPA, 5phrRME120, 5phrRME120+BPA and the imaginary rubber modified epoxy

Thus, as shown in Fig.5.31, the improvement in the fatigue resistance from fatigue curve(3) (5phrRME120) to fatigue curve(5) (the imaginary rubber modified epoxy material) is considered to arise from the change in the crosslink density from M_c=460-480g/mol to M_c=540-570g/mol. The improvement in the fatigue resistance from fatigue curve(5) (the imaginary rubber modified epoxy material) to fatigue curve(4) (5phrRME120+BPA) is considered to arise from the change in the rubber particle size from r_p=1.0μm to r_p=0.2-0.3μm. Therefore, it may be considered that the difference in fatigue resistance between 5phrRME120 (i.e. fatigue curve(3)) and

5phrRME120+BPA (i.e. fatigue curve(4)) is partly caused by the change in the crosslink density of the matrix epoxy, and partly caused by the change in rubber particle size. Hence, it may be concluded that the reduction of the rubber particle size indeed improves the fatigue resistance. These results are in accordance with the studies by Azimi et al. [51,74]. They also reported that the rubber modified epoxy with smaller particles (about 0.2μm in radius) has a better fatigue resistance than the rubber modified epoxy with larger particles (about 1.5μm in radius).

5.5.4 5phrRME120 and 15phrRME120

There is another example of the effect of particle size in the fatigue curves for the 5phrRME120 and 15phrRME120 materials. The approximate particle radius is 1.0μm for 5phrRME120, and 1.4μm for 15phrRME120; and the measured M_c value is 460g/mol for UME120 and 480g/mol for 5phrRME120 and 15phrRME120. Thus, it may be considered that there is virtually no difference in the crosslink density between these materials. If the rubber particle size in the 5phrRME120 material is 1.4μm (i.e. the same for the 15phrRME120 material), the K-transition value, K_T, of the 5phrRME120 material should be the same as for the 15phrRME120 material. Thus, the fatigue curves should be as shown in Fig.5.32. Hence, the fatigue curve of the 5phrRME120 material should be located between those of the UME120 and 15phrRME120 materials, and it should have somewhat more gentle gradient than that of the 15phrRME120 material, since the slope of the fatigue curve is dependent on the rubber content.

However, the 5phrRME120 material has a smaller rubber particle than 15phrRME120 in reality. The K-transition value, K_T, of 5phrRME120 should therefore be smaller than that of the 15phrRME120 material (i.e. the calculated K_T value is approximately $0.39MPa{\cdot}m^{1/2}$ for the 5phrRME120 material and $0.46MPa{\cdot}m^{1/2}$ for the 15phrRME120 material). Thus, the fatigue curve of the 5phrRME120 material is expected to be shifted slightly downwards from that in Fig.5.32, as schematically shown in Fig.5.33. Hence, the 5phrRME120 material should have the best fatigue resistance among these three materials of interest (i.e. UME120, 5phrRME120 and 15phrRME120) near threshold region, and the fatigue curve of the 5phrRME120 material crosses with that of the 15phrRME120 material at a higher K region. The measured fatigue crack growth rates for the UME120, 5phrRME120 and 15phrRME120 materials are shown in Fig.5.34.

These experimental results suggest that the above interpretation is indeed correct. These results also suggest that the rubber modified epoxy having smaller rubber particles possesses a better fatigue resistance than the rubber modified epoxy having larger rubber particles, and that the rubber particle size affects the fatigue resistance via the change in the K-transition values.

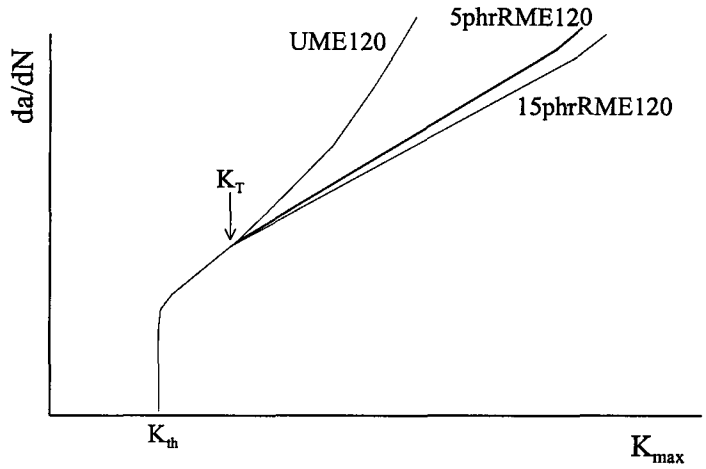


Fig.5.32 Schematic graph of the expected fatigue crack growth rate for UME120, 5phrRME120 and 15phrRME120 (if both the 5phrRME120 and 15phrRME120 materials have same particle size)

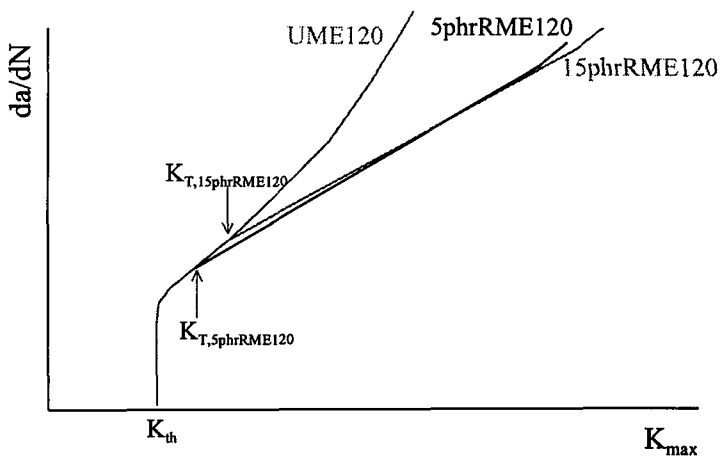


Fig.5.33 Schematic graph of the expected fatigue crack growth rate for UME120, 5phrRME120 and 15phrRME120 (when the 5phrRME120 material has the smaller rubber particles than the 15phrRME120 material)

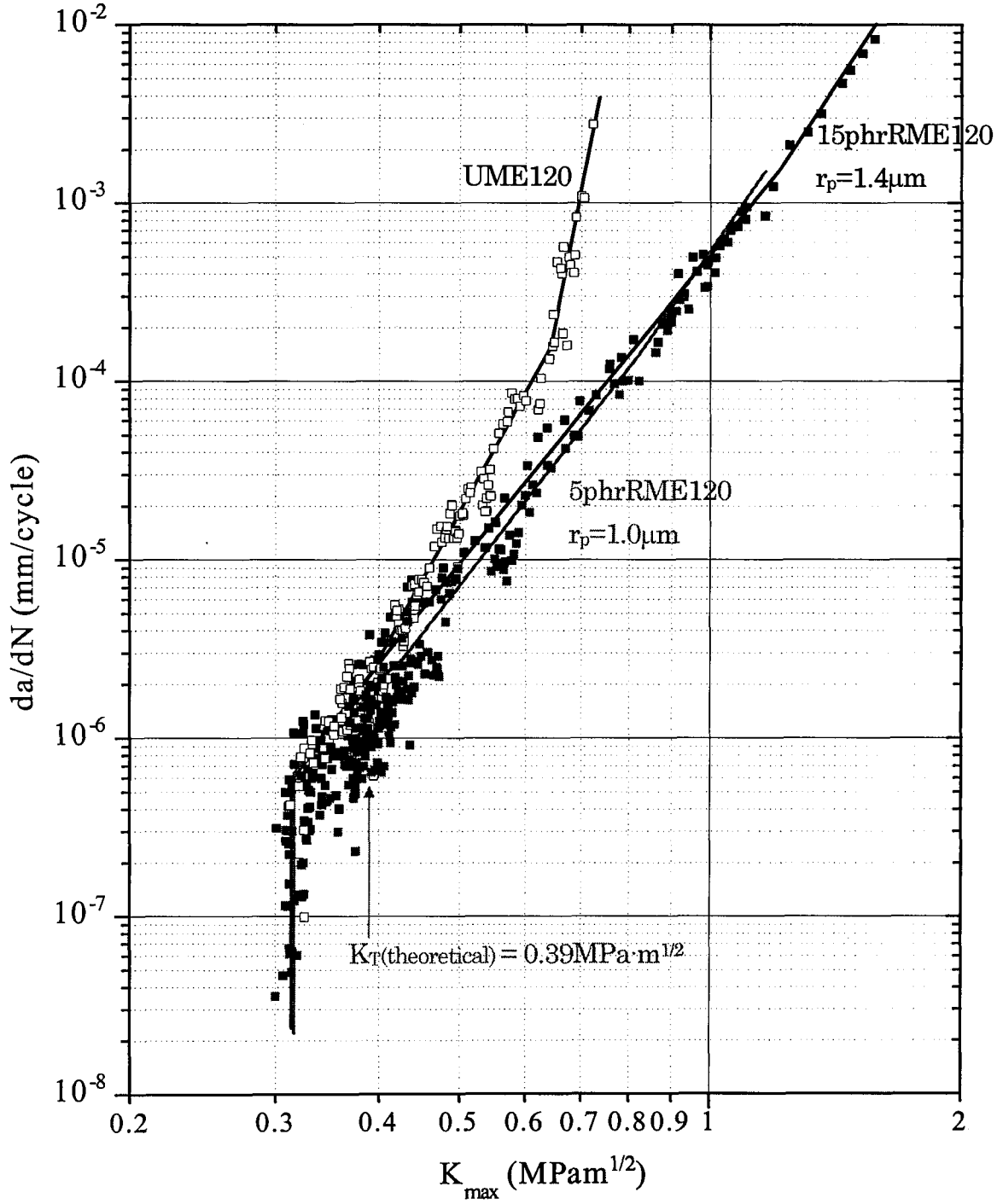


Fig.5.34 Fatigue crack growth rate for UME120, 5phrRME120 and 15phrRME120 plotted against K_{max}

5.6 Localised heating effects

The measurement of the surface temperature of the specimens during the fatigue tests was undertaken using the infrared camera system, as discussed in section 3.7. The aim of the work was to evaluate the localised temperature rise caused by the heat generated due to energy dissipation during the fatigue test. Materials dissipate energy during the process of crack propagation. Some of the dissipated energy changes into heat, and raises the material's temperature locally in the vicinity of the crack tip. Thus, if any significant localised temperature rise is detected, then we have to take thermal effects into account when the toughening mechanisms are discussed. The material which might cause the most heat generation is considered to be 15phrRME160 in the present study. This is because the 15phrRME160 material has the highest fracture toughness and also has the best fatigue resistance. This means that the 15phrRME160 material might dissipate the most energy, i.e. generate the most heat, of all the materials used in the present study.

The measured surface temperatures of the 15phrRME160 material during the fatigue tests are shown in Fig.5.35. The measured area is about 45mm x 45mm, and the crack propagates from left to right. No difference in the surface temperature was detected until the K_{max} value reached 1.2MPa·m$^{1/2}$, and then the surface temperature near the crack tip started to increase. However, the maximum value of the rise in the measured surface temperature was less than 1°C. If we consider the temperature range at which the fatigue tests were done, i.e. 23±3°C, this measured temperature rise is very small. Consequently, the thermal effects for the toughening mechanisms may be neglected.

Fig.5.36 shows a graph of the surface temperature rise of 15phrRME160 and 15phrRME120 plotted against K_{max}. The detected temperature rise for 15phrRME120 is also very small, and interestingly the value is almost same as that of 15phrRME160, at the same K_{max} value. So again, it may be concluded that thermal effects during the fatigue crack growth in these materials may be neglected.

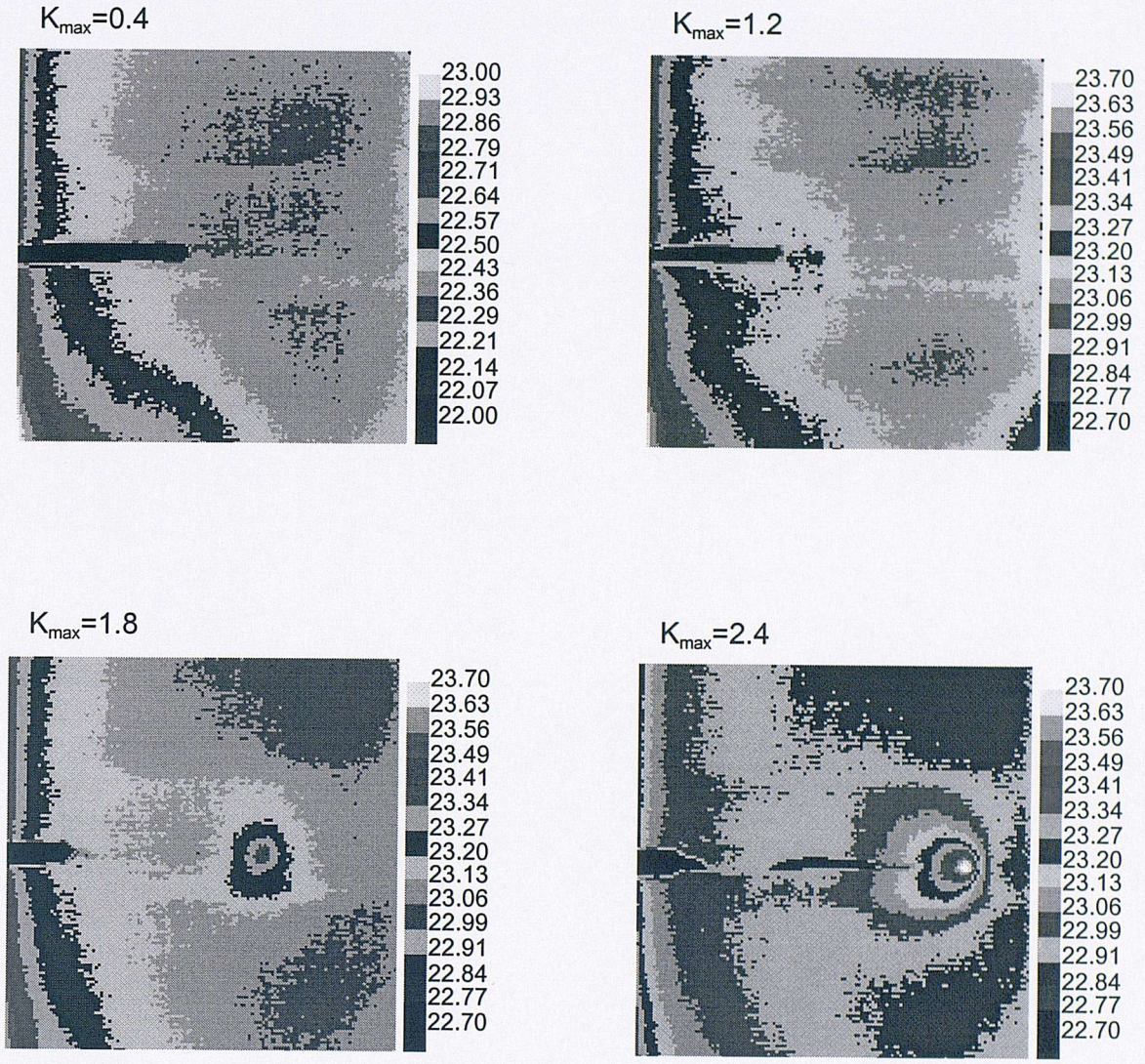


Fig.5.35 Surface temperature of 15phrRME160 specimen during the fatigue test (f=5Hz)

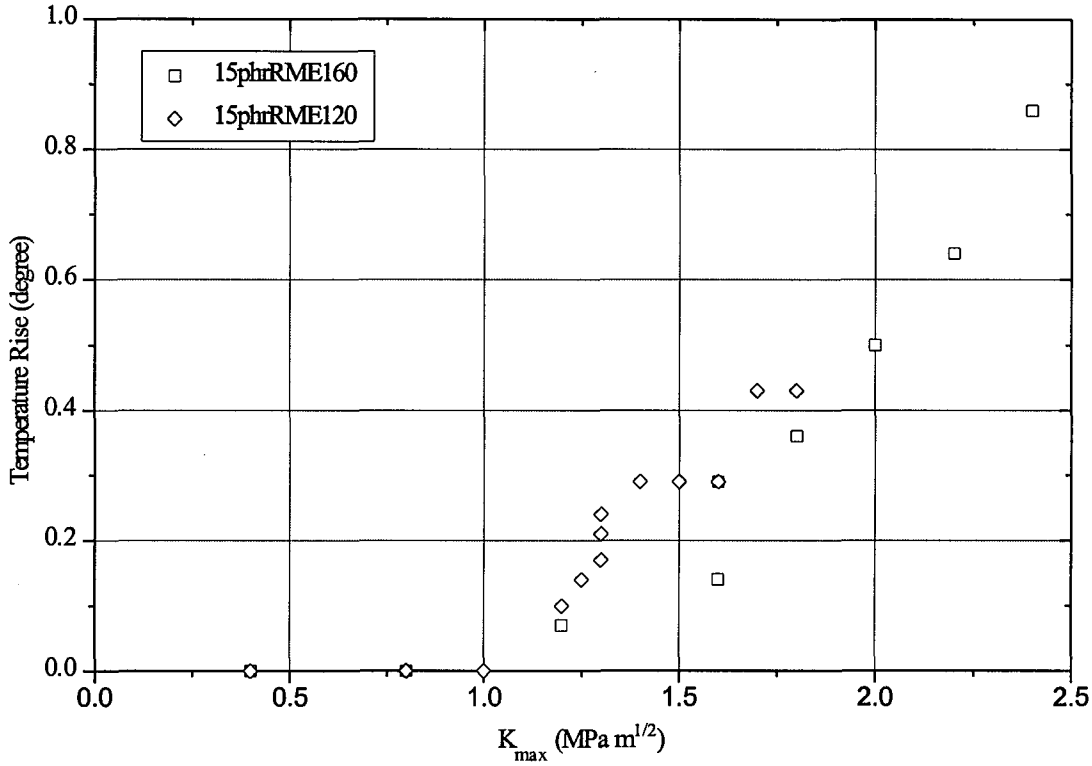


Fig.5.36 Temperature rise for 15phrRME160 and 15phrRME120

5.7 Concluding remarks

In this Chapter, three major effects of material properties on the fatigue crack growth rate in rubber modified epoxy polymers were investigated, i.e. the effect of crosslink density of the matrix epoxy, rubber content and rubber particle size.

The crosslink density of the matrix epoxy affects the fatigue curve including the threshold value, K_{th}. When the crosslink density of the matrix is relatively low, the complete fatigue curve shifts to the higher K region, and the lower the crosslink density then the better the fatigue resistance.

The rubber content affects the fatigue resistance when the applied K value is relatively large. Generally, the gradient of the fatigue curve becomes less steep as the rubber content increases. However, there is virtually no effect on the threshold value, K_{th}, or close to the threshold region. In other words, a rubber modified epoxy has a better fatigue resistance than an unmodified epoxy only

above a certain K value. The critical value of the stress intensity factor at which the difference between the rubber modified epoxy and the unmodified epoxy starts to appear may be defined as the K-transition value, K_T.

The size of rubber particles affects the fatigue curve through affecting the K_T value. The K_T value decreases with decreasing particle size. Consequently, the fatigue curve shifts towards the lower crack growth rate, i.e. the fatigue resistance is getting better, as the particle size decreases. However, the threshold value is not affected by the size of rubber particles.

Thus, it can be concluded that the material having the lowest crosslink density of matrix epoxy, the highest rubber content and the smallest particle size should have the best fatigue resistance.

The local temperature rise of the specimen during the fatigue test is relatively low, and consequently the localised heating effect in the vicinity of crack tip is virtually negligible. Thus, it may be concluded that thermal heating effects do not influence the toughening mechanisms during the fatigue tests on the epoxy materials in the present study.

In the next Chapter, fractographic studies will be discussed. Transmission optical microscopy, TOM, scanning electron microscopy, SEM, and transmission electron microscopy, TEM, were employed to investigate the micromechanisms of crack growth in the present study.

Chapter Six

Fractographic Studies and Rubber Toughening Mechanisms

6.1 Introduction

The toughening caused by dispersed rubber particles in epoxy matrices with respect to static and fatigue loading conditions have been discussed in Chapter Four and Chapter Five. It has shown that the toughening behaviour is influenced by the microstructural properties such as the crosslink density of the matrix epoxy, rubber particle size, etc.

In this Chapter, fractographic studies on the rubber modified epoxies will be discussed in order to clarify the fracture processes and the rubber toughening mechanisms. Fractography is the science of studying fracture surfaces in order to determine the source of the fracture and the relation between the crack propagation and the microstructure of the material [108]. The fracture surface and the crack tip area have been carefully studied using transmission optical microscopy (TOM), scanning electron microscopy (SEM) and transmission electron microscopy (TEM). Most fractographic studies have been done using SEM in the present study. TOM and TEM were utilised as supplementary methods for the SEM observations.

6.2 Results of the static fracture tests

6.2.1 SEM observations

Fig.6.1 shows the SEM micrographs of the fracture surfaces for the 15phrRME160 material. It may be observed that the rubber particles are cavitated and thus 'apparent' voids are formed in slow (stable) crack growth region. It should be noted that the term 'void' corresponds to a cavitated rubber particle and hence contains both an outer rubber layer and inner cavity. The rubber particles remain intact in the fast (unstable) crack growth region (Due to very little plastic

deformation of the epoxy matrix surrounding the particles, the interface between the rubber particles and the matrix is rather indistinct. However, many particles can be seen when the micrograph, Fig.6.1(b), is carefully observed.). Furthermore, the size of the void in the slow crack growth region, where the toughening mechanisms which involve plastic deformation are very active, is significantly larger than the initial size of the rubber particles. Similar observations have been reported by many authors [7,43,64,109] for the rubber modified epoxies.

The SEM micrographs of the 15phrRME120, 5phrRME120 and 5phrRME120+BPA materials are shown in Fig.6.2, Fig.6.3 and Fig.6.4. For all these materials, the rubber particles are cavitated and the voids are formed in the slow crack growth region, and the rubber particles remain intact in the fast crack growth region, as shown for the 15phrRME160 material. It is also observed that the size of the voids larger than the initial size of the rubber particles.

These observations suggest that the cavitation of the rubber particles occurs and that plastic void growth follows the cavitation for all the above materials, namely for the 15phrRME160, 15phrRME120, 5phrRME120 and 5phrRME120+BPA materials.

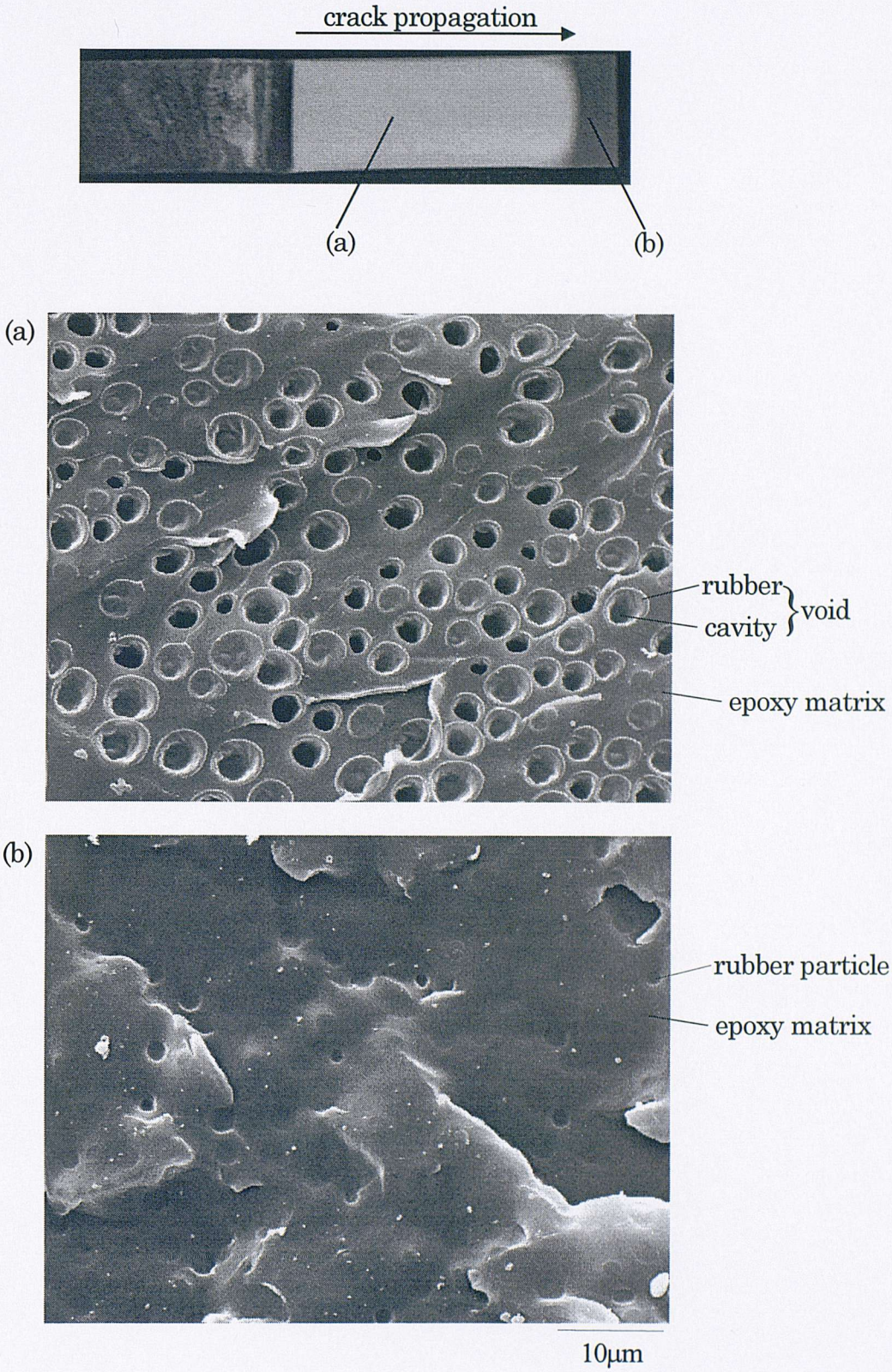


Fig.6.1 SEM micrographs of fracture surface of 15phrRME160 from a static fracture test (K_{Ic}=4.03MPam$^{1/2}$, crosshead speed 0.1mm/min.)
(a) slow crack growth region, (b) fast crack growth region

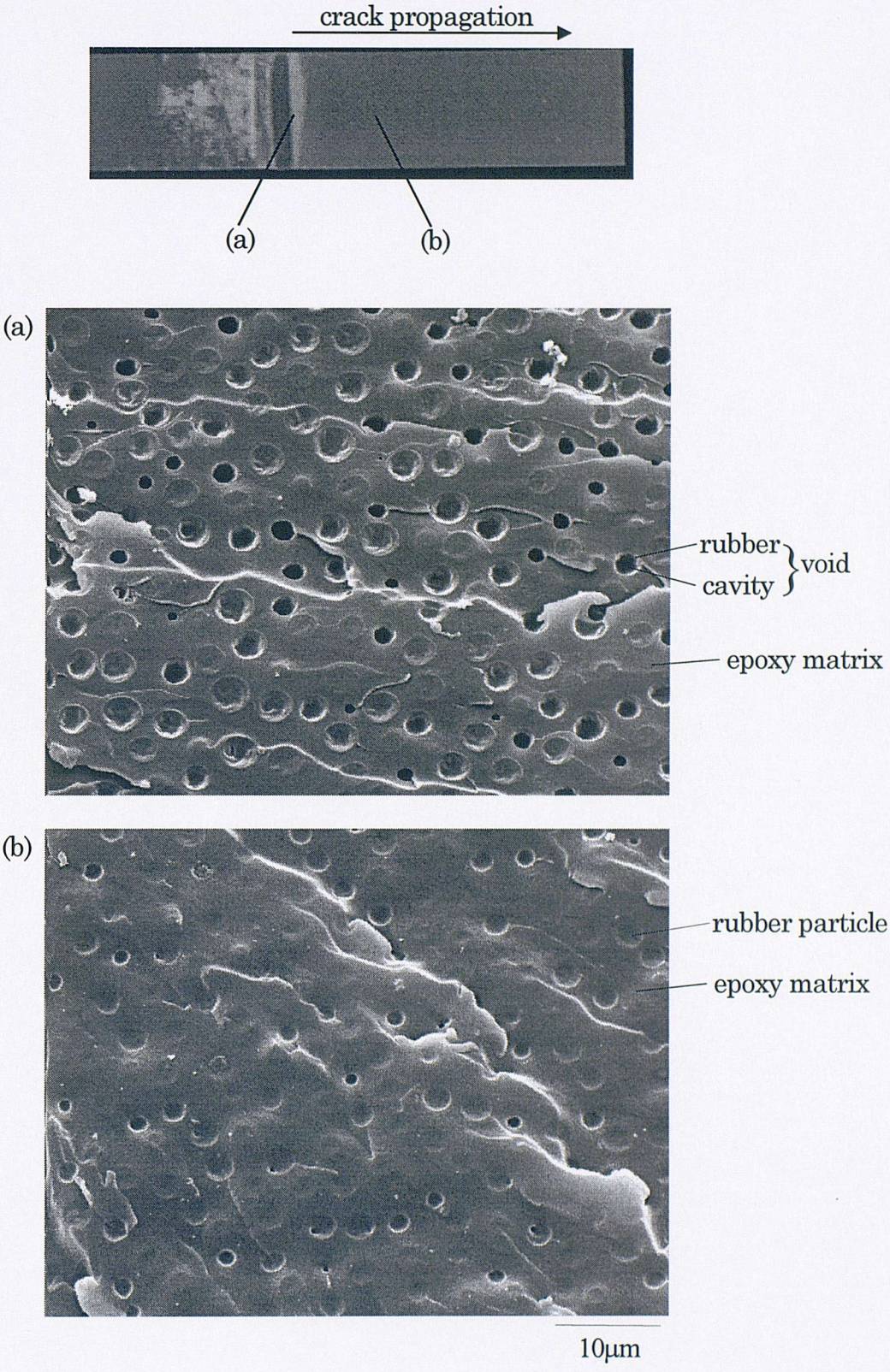


Fig.6.2 SEM micrographs of fracture surface of 15phrRME120 from a static fracture test (K_{Ic}=2.47MPam$^{1/2}$, crosshead speed 0.1mm/min.)
(a) slow crack growth region, (b) fast crack growth region

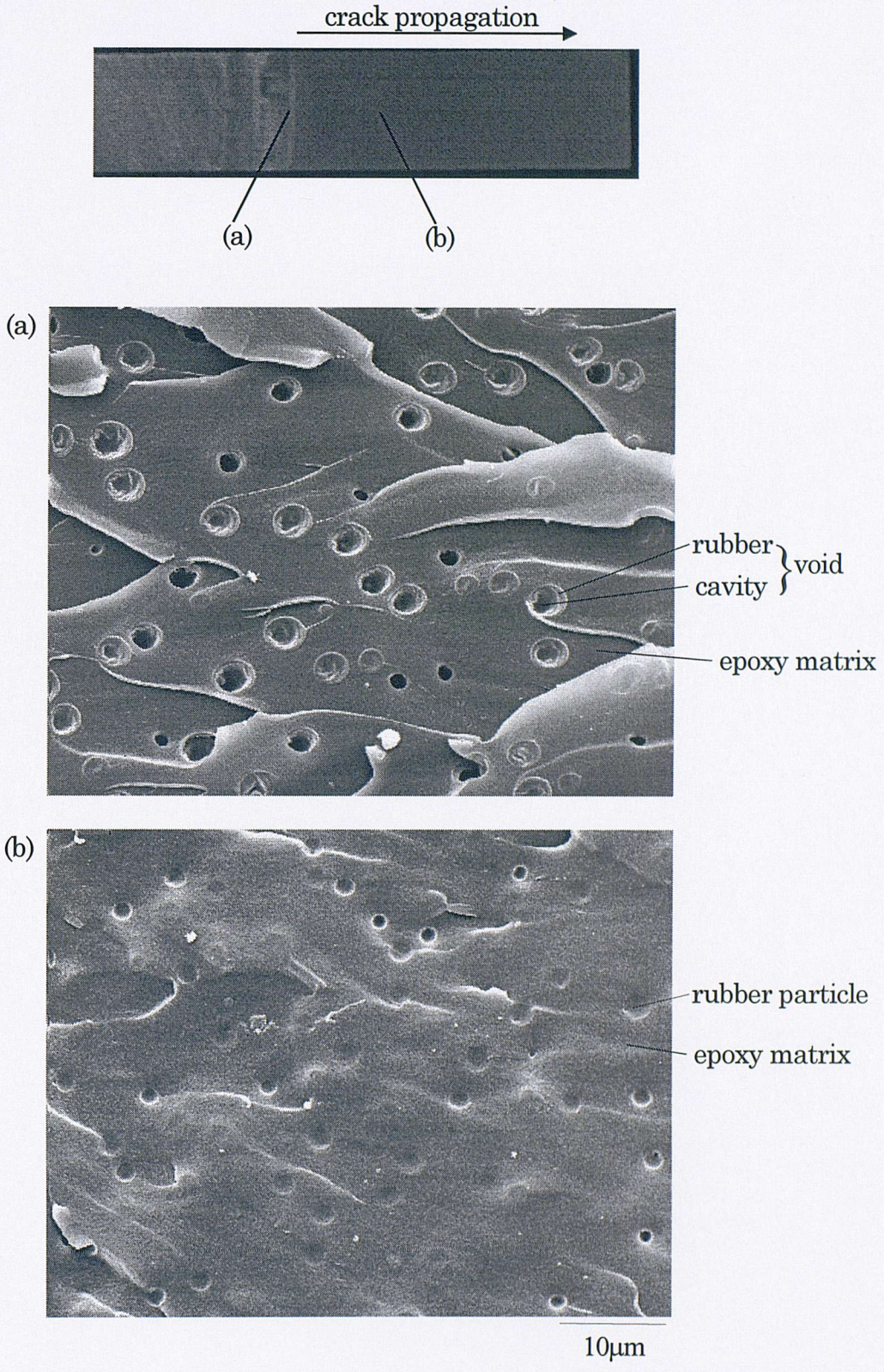


Fig.6.3 SEM micrographs of fracture surface of 5phrRME120 from a static fracture test (K_{Ic}=2.20MPam$^{1/2}$, crosshead speed 0.1mm/min.)
(a) slow crack growth region, (b) fast crack growth region

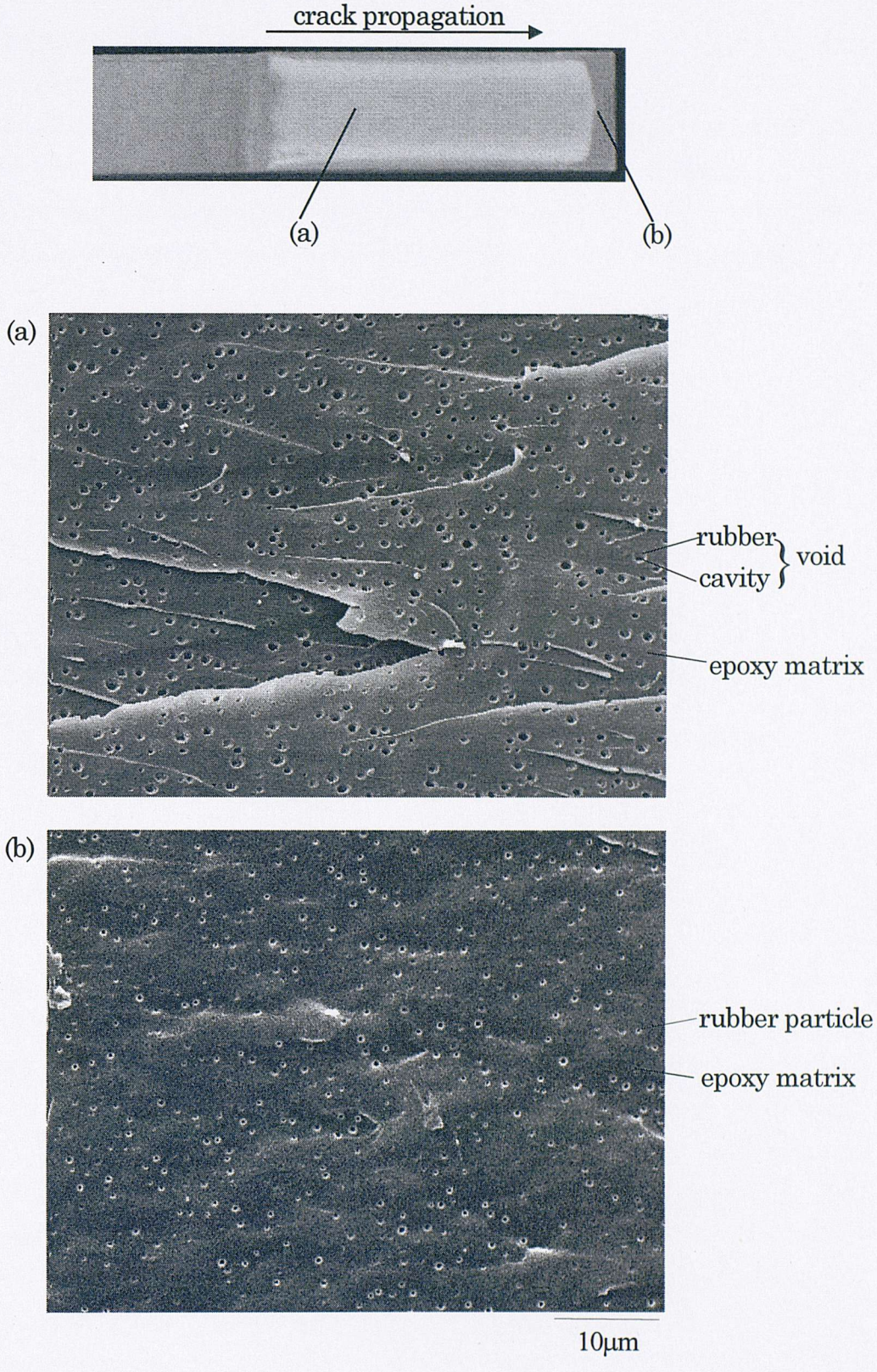


Fig.6.4 SEM micrographs of fracture surface of 5phrRME120+BPA from a static fracture test (K_{Ic}=3.01MPam$^{1/2}$, crosshead speed 0.1mm/min.)
(a) slow crack growth region, (b) fast crack growth region

6.2.2 Volume fraction of voids

The volume fraction of rubber particles, V_{fr}, and the volume fraction of void, V_{fv}, can be calculated from the SEM micrographs using an image analysis technique, as discussed in section 3.9. The V_{fr} and V_{fv} values for the 15phrRME160, 15phrRME120, 5phrRME120 and 5phrRME120+BPA materials are summarised in Table 6.1.

Table 6.1 Volume fraction of rubber particles and voids

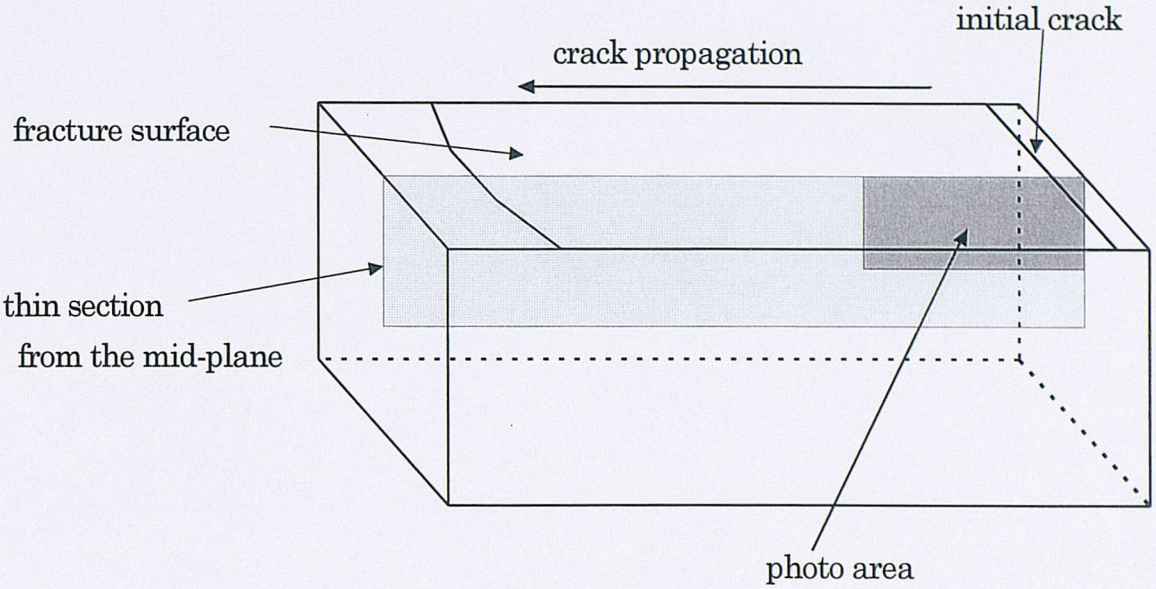
Material	V_{fr}	V_{fv}	V_{fv}/V_{fr}
15phrRME160	0.24±0.02	0.39±0.03	1.63
15phrRME120	0.21±0.02	0.27±0.02	1.29
5phrRME120	0.07±0.01	0.12±0.01	1.71
5phrRME120+BPA	0.05±0.01	0.10±0.02	2.00

For the 15phrRME160 material, the V_{fr} value is 0.24 and the V_{fv} value is 0.39. The ratio of V_{fv} and V_{fr}, V_{fv}/V_{fr}, is approximately 1.63. This means that the voids grow 63% by volume during the fracture process. For the 15phrRME120 material, the V_{fr} value is 0.21 and the V_{fv} value is 0.27, and the value of V_{fv}/V_{fr} is approximately 1.29 and so the voids grow only 29% by volume. These results suggest that the more plastic void growth occurs, and hence more energy is dissipated by the void growth mechanism, in the 15phrRME160 material than in the 15phrRME120 material. This difference in the amount of plastic void growth between 15phrRME160 and 15phrRME120 is considered to arise from the difference in the stress-strain curves of the matrix epoxies, which reflects difference in the crosslink densities of the epoxy materials. As Huang and Kinloch suggested [110], voids grow easily until strain hardening of the matrix epoxy occurs. The critical strain at which strain hardening starts is higher in 15phrRME160 than in 15phrRME120, as discussed in section 5.2.3. Thus, the 15phrRME160 material has the greater ability to plastically deform, such as in plastic void growth, than the 15phrRME120 material. This may be why the amount of void growth is greater in the 15phrRME160 material than in the 15phrRME120 material.

The ratio of V_{fv} and V_{fr}, V_{fv}/V_{fr}, is approximately 1.71 for the 5phrRME120 and 2.00 for the 5phrRME120+BPA material. These values are greater than those for the 15phrRME160 and 15phrRME120 materials. This implies that void growth mechanism has a greater importance in the toughening process in the 5phrRME120 and 5phrRME120+BPA materials, than in the 15phrRME160 and 15phrRME120 materials. This difference in the importance of void growth may arise from the difference in the rubber particle size. The 5phrRME120 and 5phrRME120+BPA materials have smaller rubber particles than the 15phrRME160 and 15phrRME120 materials, as discussed in section 4.2.1. Therefore, the K-transition values, at which toughening mechanisms which involve plastic deformation become active, are lower in the former materials than in the latter materials. This means that the toughening mechanisms which involve plastic deformation, such as the void growth mechanism, is activated even at a relatively small applied load. This may be a reason why the values of V_{fv}/V_{fr} for the 5phrRME120 and 5phrRME120+BPA materials are larger than those for the 15phrRME160 and 15phrRME120 materials.

6.2.3 TOM observations

The TOM micrographs of the mid-plane, parallel to the crack propagation and perpendicular to the fracture surface, are shown in Fig.6.5 (15phrRME160) and Fig.6.6 (15phrRME120). For both materials, a birefringent zone can be observed near the crack surface. The birefringent zone corresponds to the stress whitening zone, and suggests the presence of cavitation of the rubber particles with/without the shear yielding of the matrix epoxy between the cavitated particles. The cavitation of the rubber particles reduces the triaxial constraint and this reduction may then facilitate localised shear yielding in the epoxy matrix between the cavitated particles, as suggested by many authors [9-11,35,111]. Thus, the presence of the birefringent zone indicates, indirectly, that the shear yielding mechanism is active during the fracture process for both the 15phrRME160 and 15phrRME120 materials.



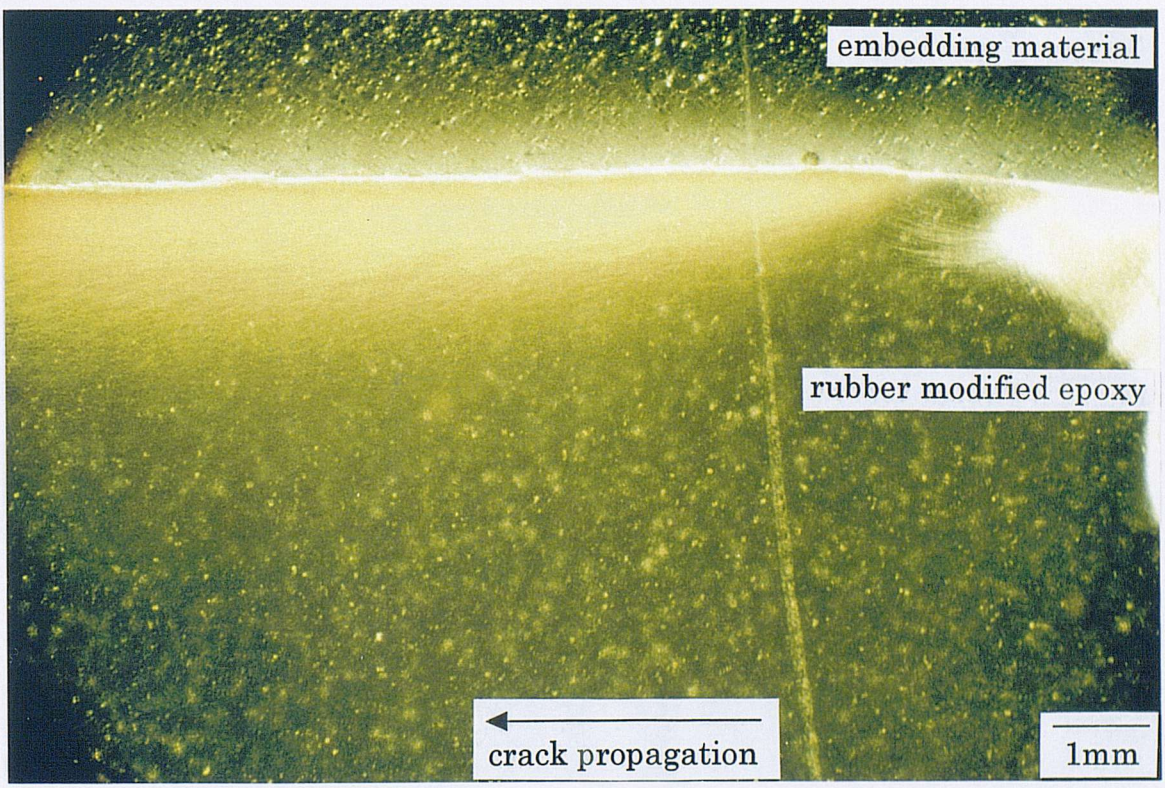
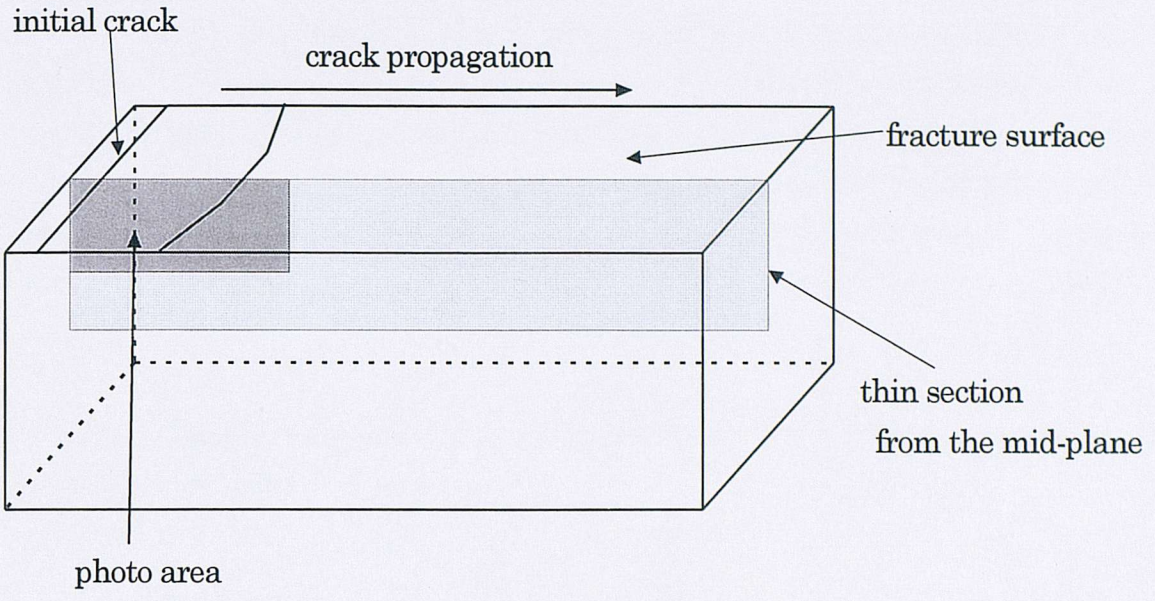


Fig.6.5 TOM micrographs, under crossed polars, of 15phrRME160 from a static fracture test (thin section parallel to the crack propagation and perpendicular to the fracture surface)



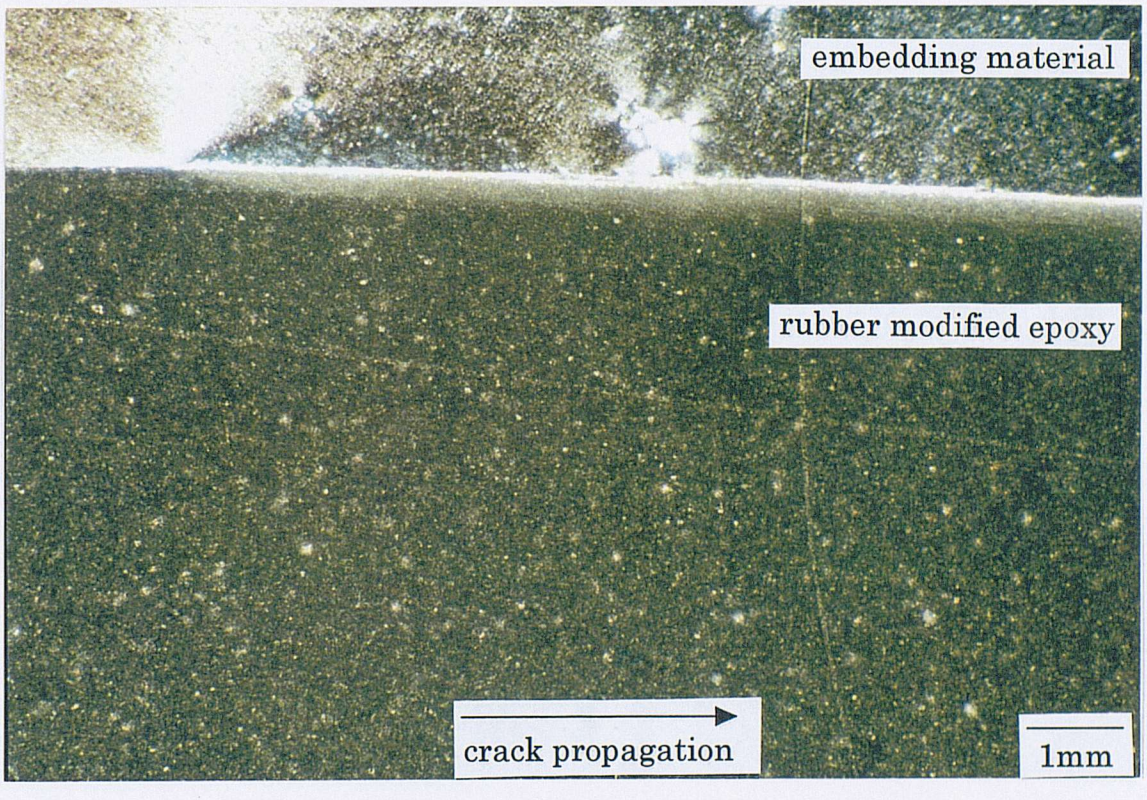


Fig.6.6 TOM micrographs, under crossed polars, of 15phrRME120 from a static fracture test (thin section parallel to the crack propagation and perpendicular to the fracture surface)

The birefringent zone size, r_b, is 1.2-1.4mm for the 15phrRME160 material and 0.15-0.20mm for the 15phrRME120 material. Thus, the birefringent zone in the 15phrRME160 material is far larger than that in the 15phrRME120 material. This implies that the amount of cavitation and localised shear yielding is greater in the 15phrRME160 material than in the 15phrRME120 material. Table 6.2 summarises the birefringent zone size, r_b, and the plastic zone size, r_y, for these materials.

Table 6.2 The birefringent zone size and the plastic zone size for the 15phrRME160 and 15phrRME120 materials

Material	r_b (μm)	r_y (μm)	r_b/r_y
15phrRME160	1200-1400	165	7.3-8.5
15phrRME120	150-200	87	1.7-2.3

Note : $r_y = (K_{Ic}/\sigma_{yt})^2/6\pi$

For both materials, the birefringent zone size, r_b, is far greater than the plastic zone size, r_y, as schematically shown in Fig.6.7. This implies that the stress criteria for cavitation of the rubber particles is lower than that for yielding, i.e. plastic deformation, of the matrix epoxy. Thus, it is suggested that cavitation of the rubber particles firstly occurs, and then toughening mechanisms which involve plastic deformation, such as shear yielding and plastic void growth, follow.

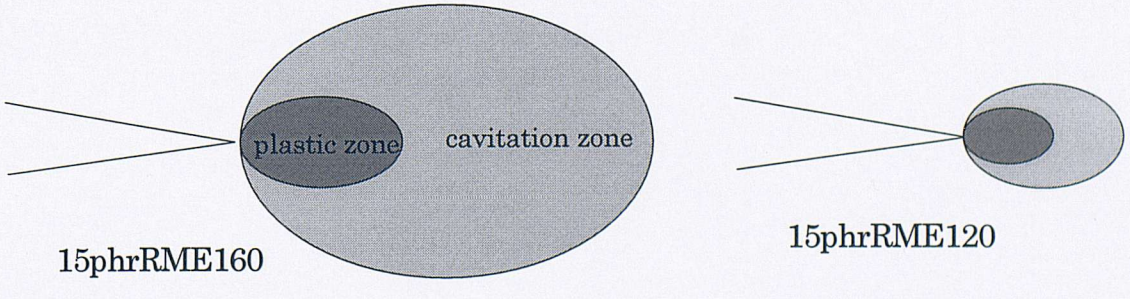


Fig.6.7 Schematic drawing of the cavitation zone and the plastic zone

The difference in the extent of the birefringent zone between these materials is considered to be caused by three factors. The first factor is the rubber particle size. It has been suggested by Lazzeri and Bucknall [61] that the relatively large rubber particles cavitate at a lower stress than the smaller rubber particles. Since the 15phrRME160 material has larger rubber particles than the 15phrRME120 material, as discussed in section 4.2.1, the rubber particles in the 15phrRME160 material may cavitate more readily than those in the 15phrRME120 material.

The second factor is the crosslink density of the matrix epoxy. Fu [35] studied the effect of the crosslink density of the epoxy matrix on the fracture behaviour of the rubber modified epoxies, and suggested that the rubber modified epoxy system with a lightly crosslinked epoxy matrix enables the rubber particles to cavitate more easily. Therefore, the 15phrRME160 material, which has a lower crosslink density than the 15phrRME120 material, demonstrates a larger cavitation zone.

The last factor is the modulus of the matrix epoxy. Liang et al. [112] investigated the effect of the material properties on the stress criteria for the cavitation of the dispersed particles. They suggested that the high modulus of the matrix material should be beneficial for the cavitation of the particles. Thus, the higher modulus for the 15phrRME160 material, compared to the 15phrRME120 material, may cause the larger cavitation zone.

In summary, all the above factors cause a positive effect on the cavitation of the rubber particles in the 15phrRME160 material, and they may explain why 15phrRME160 has an extremely large birefringent zone.

6.2.4 TEM observations

The TEM micrographs of the 15phrRME160 material in static fracture are shown in Fig.6.8. The micrographs were taken near the crack surface (Fig.6.8(a)) and at a point approximately 1mm below the crack surface (Fig.6.8(b)). The area in Fig.6.8(a) is within the plastic zone, and the area in Fig.6.8(b) is outside the plastic zone but within the birefringent zone (close to the edge of the birefringent zone).

As shown in Fig.6.8(a), the cavitated rubber particles near the crack surface are not spherical but somewhat elongated, whereas most rubber particles remain intact outside the plastic zone, as shown in Fig.6.8(b). This means that the plastic shear deformation of the matrix epoxy indeed occurs near the crack surface. It is also shown that the cavitated rubber particles, i.e. voided rubber particles, near the crack surface are dilated. This proves that void growth mechanism is active near the crack surface.

Fig.6.9 shows the TEM micrographs of the 5phrRME120+BPA material, which was taken near the crack surface. The cavitated rubber particles are observed as for the 15phrRME160 material. It is also observed that the cavitated rubber particles are elongated This proves that localised shear yielding also occurs during the fracture process, as for the 15phrRME160 material.

It should be noted that the thickness of the TEM sections is approximately 100nm.

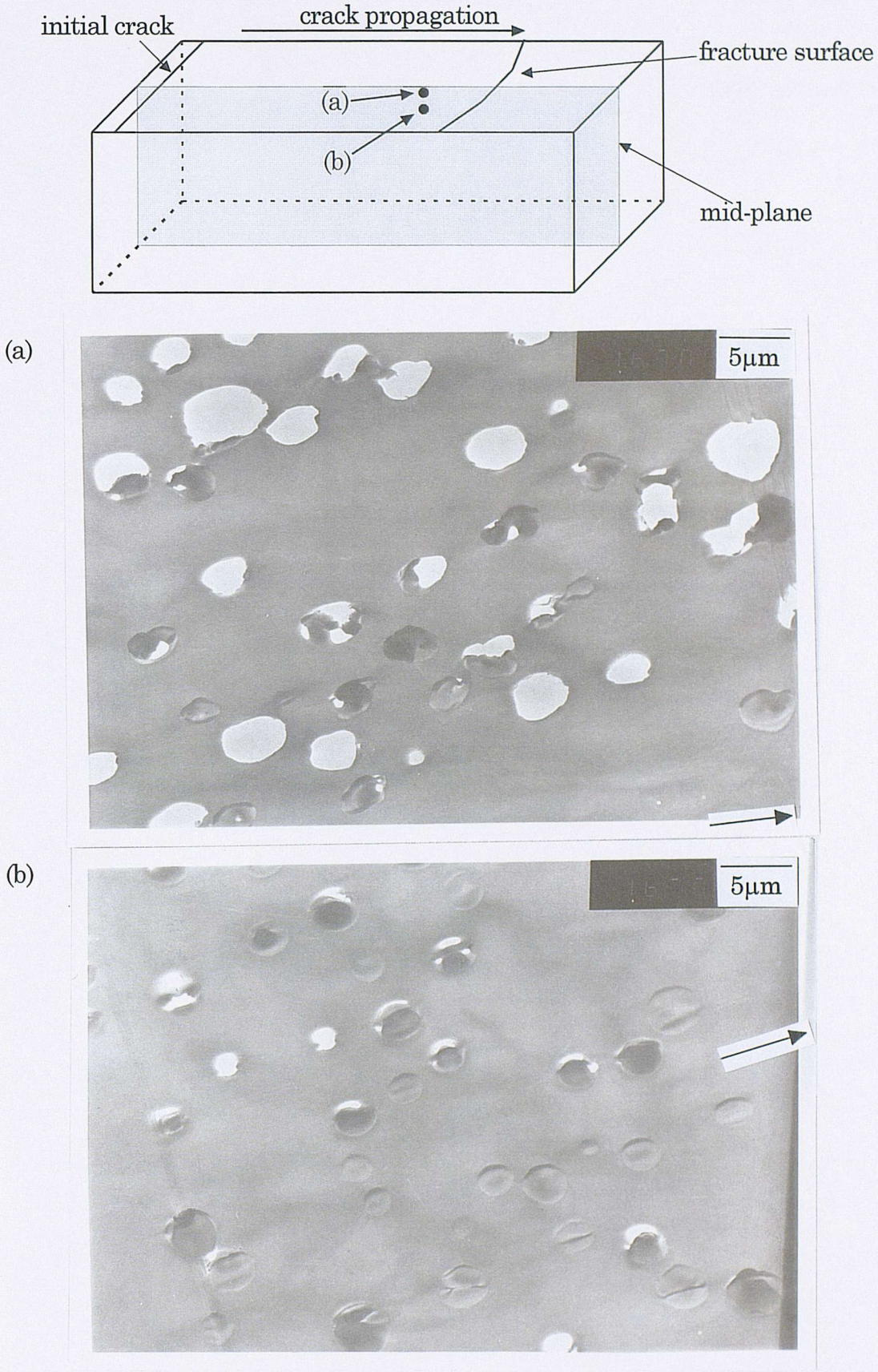
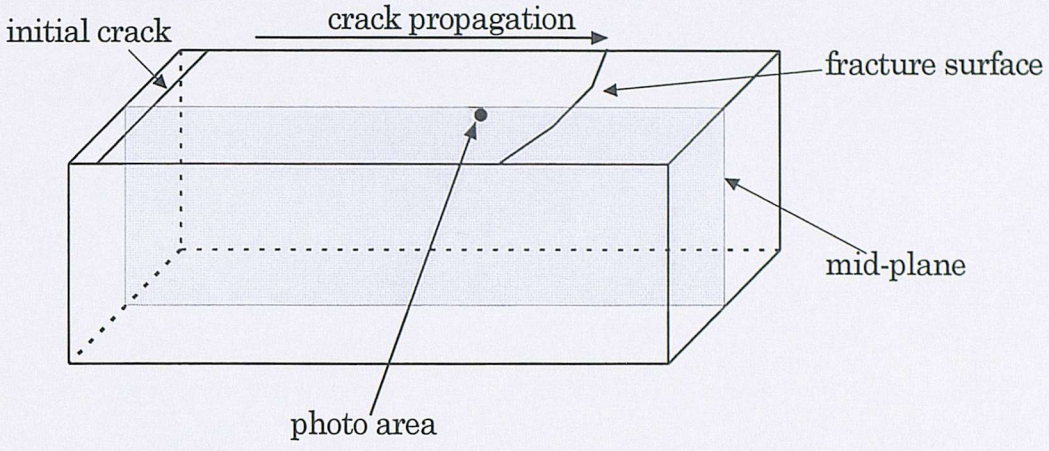


Fig.6.8 TEM micrographs of 15phrRME160: (a) near the crack surface , (b) 1mm below the crack surface (arrow indicates the crack propagation direction)



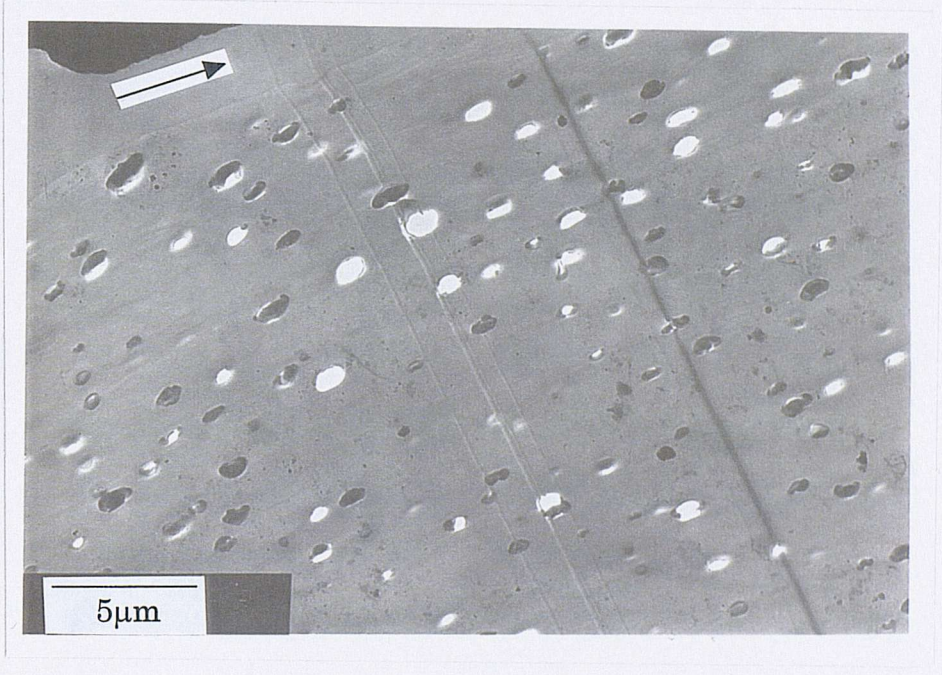


Fig.6.9 TEM micrographs of 5phrRME120+BPA (near the crack surface : arrow indicates the crack propagation direction)

6.3 Fatigue fracture

6.3.1 SEM observations

6.3.1.1 15phrRME160

The SEM micrographs of the fatigue surfaces at K_{max}=0.61, 1.4 and 3.3MPam$^{1/2}$ in the 15phrRME160 material are shown in Fig.6.10. As for the SEM micrographs from a static test, the cavitation of the rubber particles can be seen in all micrographs shown in Fig.6.10. It is also observed that the size of the cavitated rubber particle increases with increasing K_{max} value. This suggests that the amount of plastic dilatation of the epoxy matrix surrounding the rubber particles increases, and hence the energy dissipated due to the void growth mechanism during the fatigue crack propagation increases with an increase in the K_{max} value.

Table 6.3 summarises the volume fraction of void, V_{fv}, in the 15phrRME160 material. The measured volume fraction of void at K_{max}=0.61MPam$^{1/2}$ is approximately 0.245, which is slightly higher than the initial volume fraction of rubber, V_{fi}=0.24. These results imply that the epoxy matrix surrounding the rubber particles dilates plastically by a small amount. In other words, the void growth mechanism is active but the amount of the energy dissipation due to the void growth mechanism is rather small. The volume fraction of void, V_{fv}, steadily increases with an increase in the K_{max} value. The value of V_{fv} is 0.25 for K_{max}=1.0MPam$^{1/2}$, 0.30 for K_{max}=2.2MPam$^{1/2}$ and 0.37 for K_{max}=3.3MPam$^{1/2}$; and the ratio of V_{fv} and V_{fr}, V_{fv}/V_{fr}, eventually attains a value of 1.54, which means that the voids dilate over 50% by volume, at K_{max}=3.3MPam$^{1/2}$. These results also indicate that the amount of the plastic dilatation of the epoxy matrix surrounding the rubber particles increases, and hence the energy dissipated due to the void growth mechanism during the fatigue crack propagation increases, with an increase in the K_{max} value.

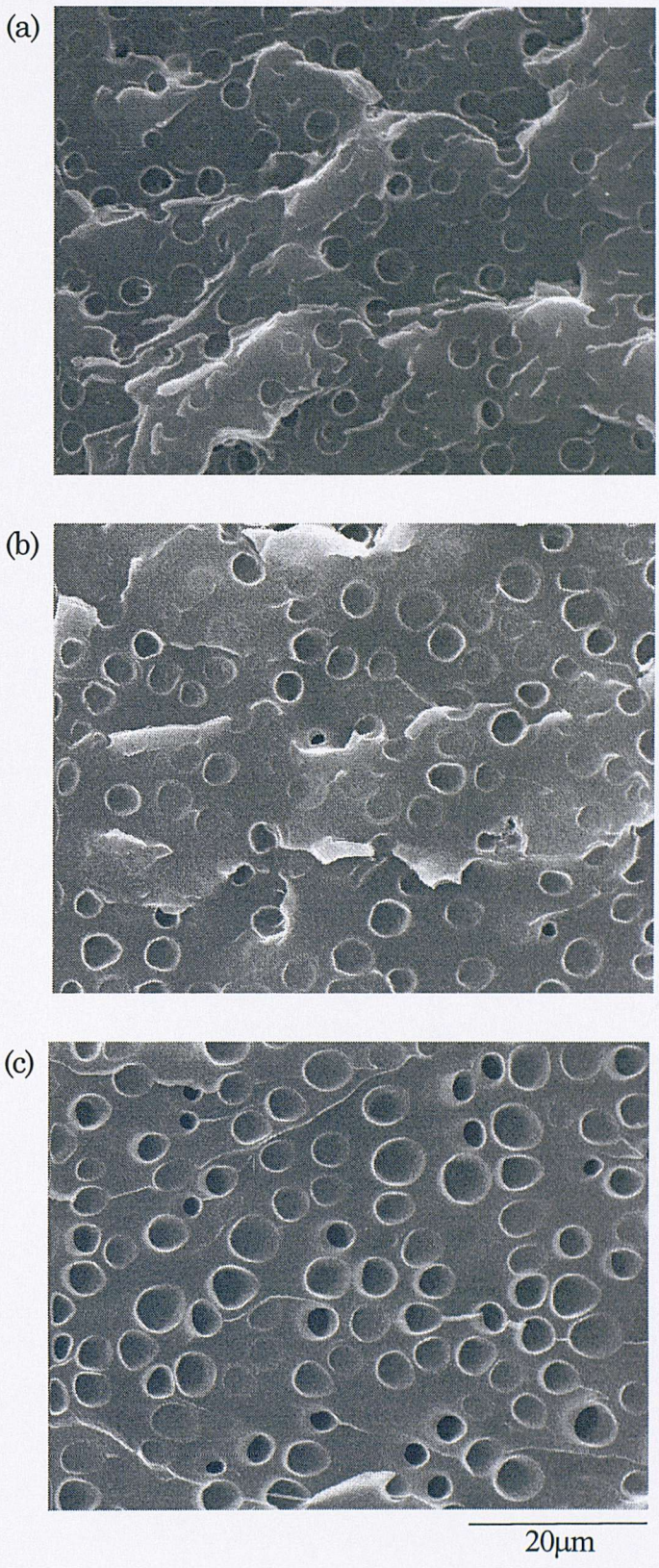


Fig.6.10 SEM micrographs of fracture surface of 15phrRME160 from a fatigue test (a) K_{max}=0.61MPam$^{1/2}$ (b) K_{max}=1.4MPam$^{1/2}$ (c)K_{max}=3.3MPam$^{1/2}$

Table 6.3 Volume fraction of void at various K_{max} values for 15phrRME160

K_{max}(MPam$^{1/2}$)	V_{fv}	V_{fv}/V_{fr}
0.61	0.245±0.02	1.02
1.0	0.25±0.02	1.04
2.2	0.30±0.03	1.25
3.3	0.37±0.03	1.54

Note : V_{fr}=0.24

The K-transition value, at which the toughening mechanisms which involve plastic deformation become active, is approximately 0.59MPam$^{1/2}$ for the 15phrRME160 material, as discussed in section 5.4. Now, it may be expected that the amount of void growth would not be so significant when the applied K_{max} value is relatively low, close to the K-transition value. Thus, the observed results are in agreement with the concept, and value, of the K-transition. In that, the measured volume fraction of void, V_{fv}, is very close to the initial volume fraction of rubber, V_{fr}, at the values of K_{max}=0.61MPam$^{1/2}$ and that the V_{fv} value increases with an increase of the applied K_{max} value.

A more quantitative analysis on the toughening mechanisms in the 15phrRME160 material will be discussed later in Chapter Seven.

6.3.1.2 15phrRME120

The SEM micrographs of the fracture surfaces of the 15phrRME120 material after a fatigue test are shown in Fig.6.11. As for the 15phrRME160 material, the cavitation of the rubber particles can be seen in all micrographs shown in Fig.6.11. It is also observed that the size of the cavitated rubber particle increases with increasing K_{max} value. This again suggests that the amount of plastic dilatation of the epoxy matrix surrounding the rubber particles increases, and hence the energy dissipated due to the void growth mechanism during the fatigue crack propagation increases, with an increase in the K_{max} value.

At a relatively low K_{max} value (0.3MPam$^{1/2}$), the rubber particles are cavitated, but little dilatation of the epoxy matrix surrounding the particles can be

observed. This suggests that the void growth mechanism is hardly active at this K_{max} level. Indeed, there is little difference between the volume fraction of voids at K_{max}=0.3MPam$^{1/2}$ and the initial volume fraction of rubber, V_{fr}=0.21, as shown in Table 6.4. Since the estimated K-transition value for this material is approximately 0.46MPam$^{1/2}$, as discussed in section 5.4, the toughening mechanisms such as void growth and shear yielding are not yet active at K_{max}=0.3MPam$^{1/2}$. Thus, these observations are consistent with the concept of the K-transition.

At relatively high K_{max} values (i.e. 0.9MPam$^{1/2}$ and 1.6MPam$^{1/2}$), the size of the cavitated rubber particles is greater than the initial rubber particle size. The matrix epoxy surrounding the particles is plastically dilated and consequently the void growth mechanism is active and dissipates energy in these conditions. It is also observed that the size of the cavitated particles increases with increasing K_{max} value. This implies that the toughening effect due to the void growth mechanism increases as the K_{max} value increases, as for the 15phrRME160 material. However, the amount of the dilatation appears to be rather small, compared with the 15phrRME160 material. As shown in Table 6.4, the ratio of volume fraction of void and rubber, V_{fv}/V_{fr}, at K_{max}=1.6MPam$^{1/2}$ is approximately 1.17, which is rather less than the V_{fv}/V_{fr} value at a high K_{max} value for the 15phrRME160 material. Thus, the energy dissipated by the void growth mechanism in the 15phrRME120 material is considered to be smaller than that in the 15phrRME160 material.

Table 6.4 Volume fraction of void at various K_{max} values for 15phrRME120

K_{max}(MPam$^{1/2}$)	V_{fv}	V_{fv}/V_{fr}
0.3	0.21±0.01	1.00
0.5	0.21±0.01	1.00
0.9	0.215±0.02	1.02
1.6	0.245±0.02	1.17

Note : V_{fr}=0.21

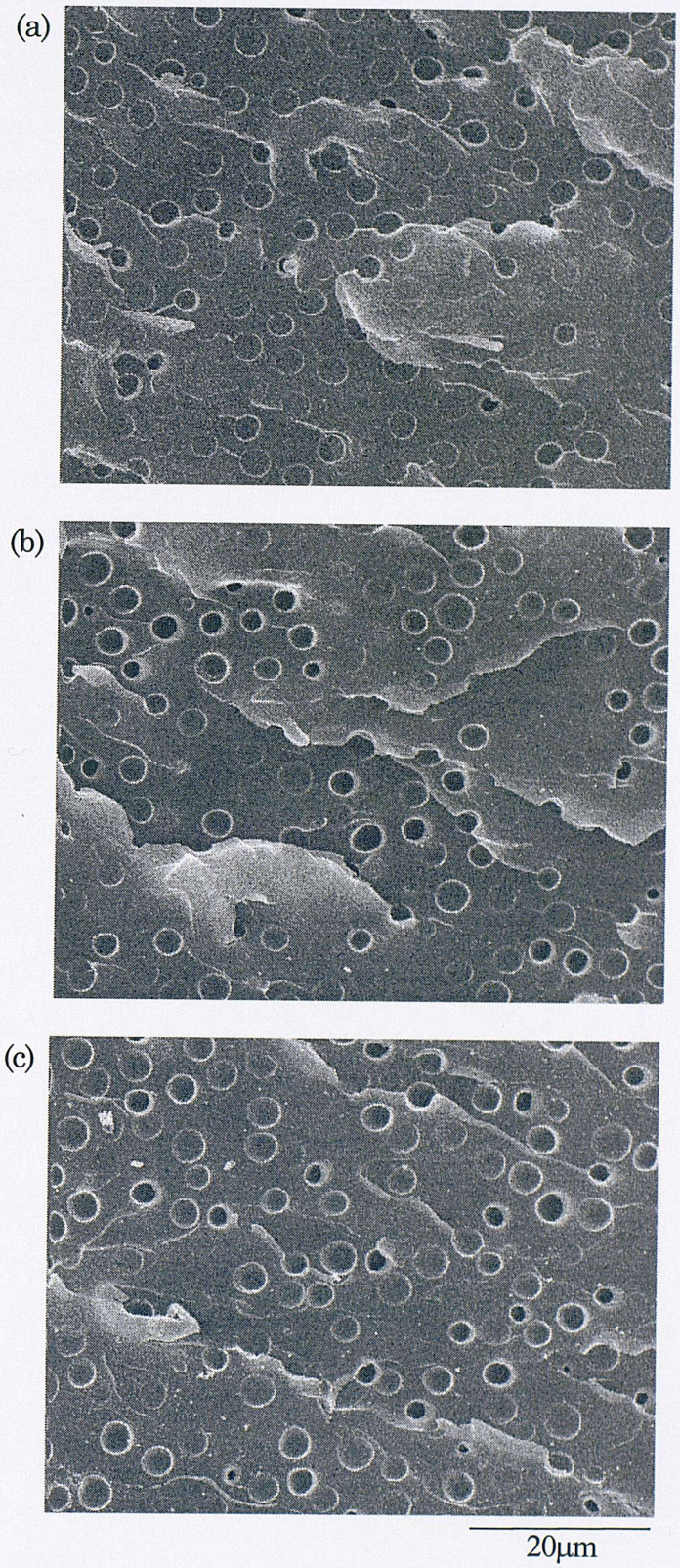


Fig.6.11 SEM micrographs of fracture surface of 15phrRME120 from a fatigue test (a) K_{max}=0.3MPam$^{1/2}$ (b) K_{max}=0.9MPam$^{1/2}$ (c)K_{max}=1.6MPam$^{1/2}$

As discussed in section 6.2.2, voids grow easily until strain hardening of the matrix epoxy occurs. The critical strain at which strain hardening starts is higher in 15phrRME160 than in 15phrRME120, as discussed in section 5.2.3. Thus, the 15phrRME160 material has the greater ability to plastically deform, such as in plastic void growth, than the 15phrRME120 material. This is a qualitative explanation of why the values of V_{fv}/V_{fr} for the 15phrRME120 material are smaller than those for the 15phrRME160 material.

A more quantitative analysis on the toughening mechanisms in the 15phrRME120 material will also be discussed later in Chapter Seven.

6.3.1.3 5phrRME120 and 5phrRME120+BPA

Fig.6.12 shows the SEM micrographs of the fracture surfaces of the 5phrRME120 material after a fatigue test. These micrographs suggest the same trend as seem for the 15phrRME160 and 15phrRME120 materials. Indeed, the cavitation of the rubber particles can be seen in all micrographs shown in Fig.6.12. It is also observed that the size of the cavitated rubber particle increases with increasing K_{max} value. It is therefore again suggested that the amount of plastic dilatation of the epoxy matrix surrounding the rubber particles increases, and hence the energy dissipated due to the void growth mechanism during the fatigue crack propagation increases, with an increase in the K_{max} value.

The SEM micrographs of the 5phrRME120+BPA material from a fatigue test are shown in Fig.6.13. The micrographs show that both the cavitation of the rubber particles and the dilatation of the surrounding epoxy matrix already occur at a relatively low K_{max} value (i.e. 0.4MPam$^{1/2}$), unlike the other materials, namely 15phrRME160, 15phrRME120 and 5phrRME120. As discussed in section 5.4, the K-transition value, K_T, at which the toughening mechanisms become active, can be estimated by the following equation:

$$K_T = (6\pi r_p)^{1/2}\sigma_{yt} \qquad (6.1)$$

where r_p is the radius of the rubber particle and σ_{yt} is the tensile yield stress. As discussed in section 4.2.1, the rubber particle radius is 0.2-0.3μm for the 5phrRME120+BPA material.

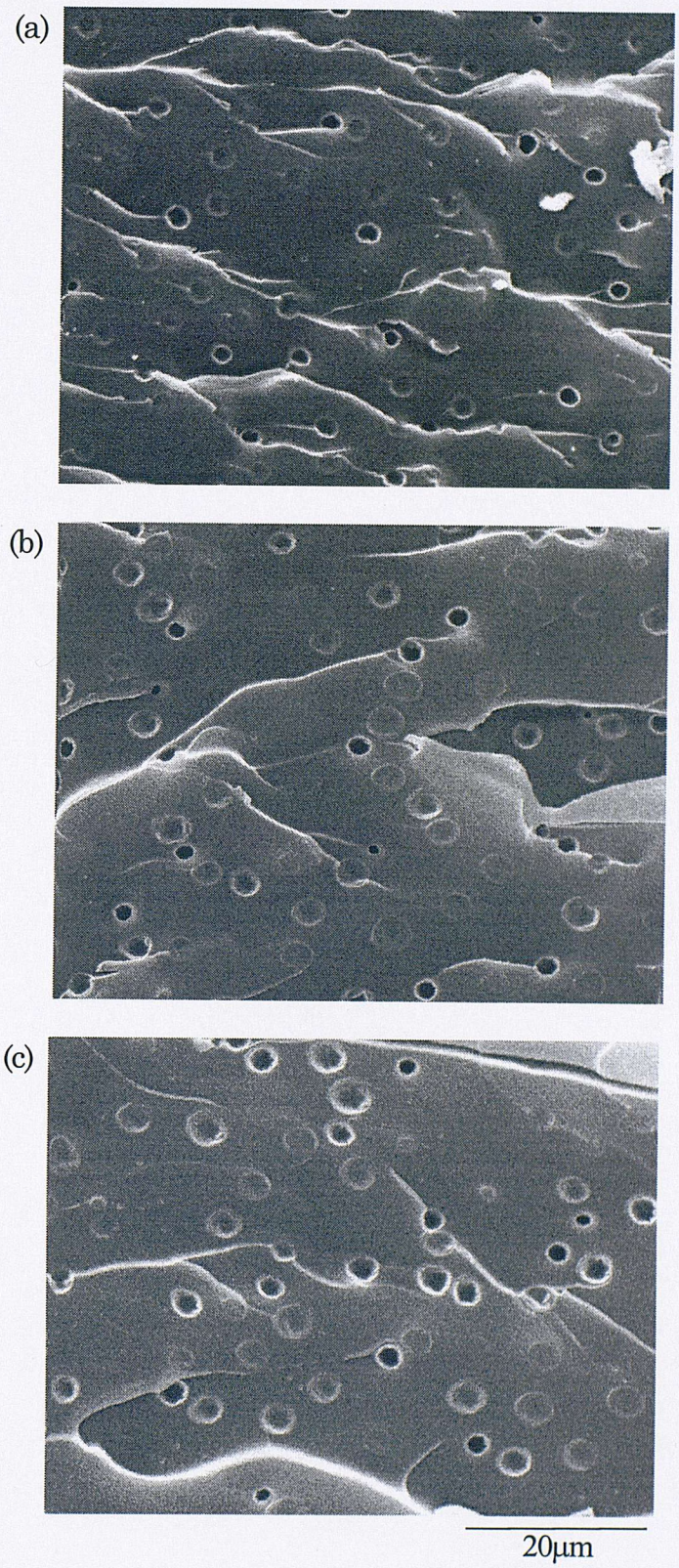


Fig.6.12 SEM micrographs of fracture surface of 5phrRME120 from a fatigue test (a) K_{max}=0.4MPam$^{1/2}$ (b) K_{max}=0.8MPam$^{1/2}$ (c)K_{max}=1.1MPam$^{1/2}$

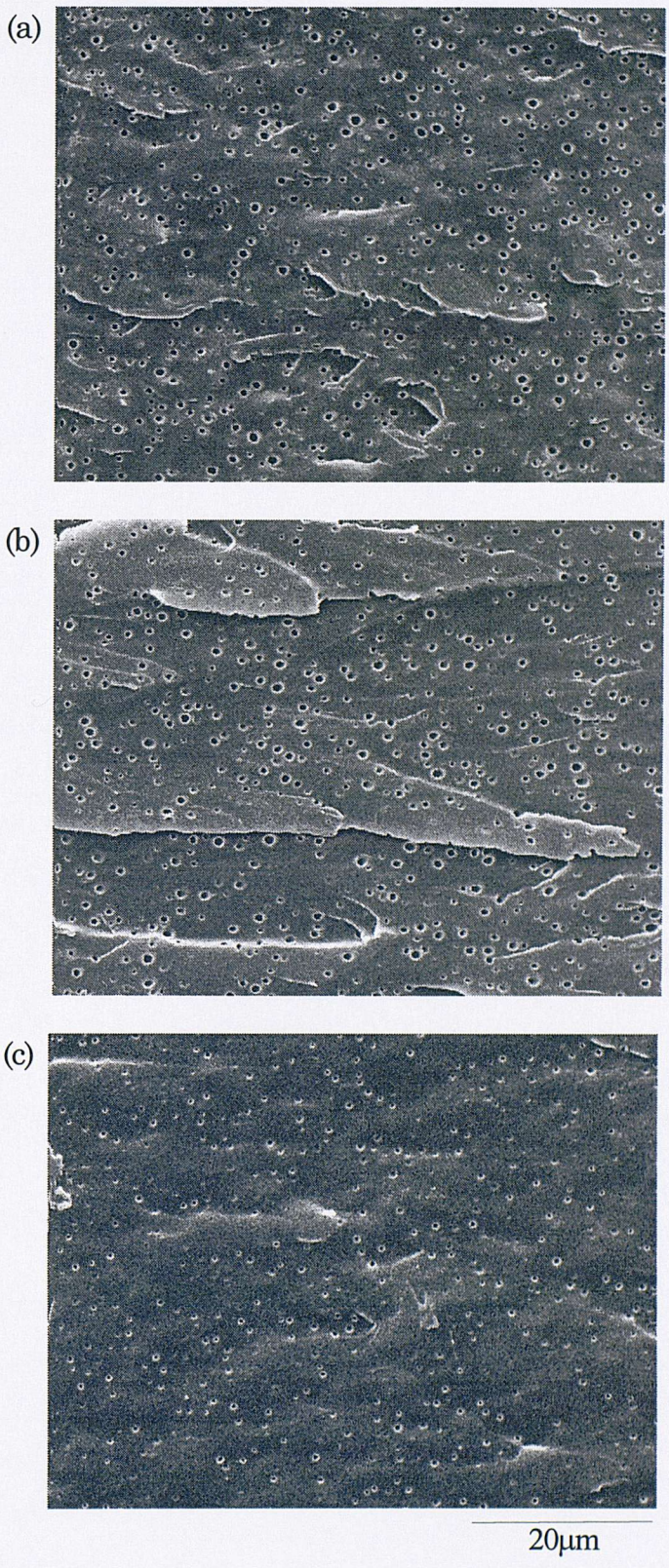


Fig.6.13 SEM micrographs of fracture surface of 5phrRME120+BPA from a fatigue test: (a) K_{max}=0.4MPam$^{1/2}$ (b) K_{max}=1.8MPam$^{1/2}$ (c) fast crack growth region

Assuming the σ_{yt} value for the 5phrRME120+BPA material is almost the same as that of the 5phrRME120 or 15phrRME120 material, the estimated K_T value is 0.20-0.25MPam$^{1/2}$. This value is smaller than the experimentally measured threshold value of the 5phrRME120+BPA material, namely 0.34MPam$^{1/2}$. Thus, it may be expected that the rubber toughening mechanisms such as void growth and shear yielding, are somewhat active even in the region of about K_{max}=0.4MPam$^{1/2}$. This may be the reason why cavitation of the rubber particles and plastic void growth can be observed even in this region.

6.3.2 TOM observations

Fig.6.14 and Fig.6.15 show the TOM micrographs of the mid-plane section of the 15phrRME160 material after fatigue testing. As shown in Fig.6.14, virtually no birefringent zone is observed in a low K_{max} region (i.e. K_{max}~0.4MPam$^{1/2}$). Since the birefringent zone corresponds to the area where the rubber particles are cavitated, these observations mean that the cavitation of the rubber particles with (or without) the shear yielding of the matrix epoxy between the particles does not occur in this region. As discussed in section 5.3.2, in this region there is little difference in the fatigue resistance between the 15phrRME160 and UME160 materials. Thus, it can be concluded that there is no evidence of the toughening effect originating from the presence of the rubber particles. Furthermore, as discussed in section 5.4, the estimated K_T value is 0.59MPam$^{1/2}$ for this material. Hence, it is also expected from this conclusion that the toughening mechanisms which involve plastic deformation are not yet active in this low K region. Hence, these observations are all consistent with the experimental results from the fatigue tests, and the concept of K-transition.

On the other hand, at a high K_{max} region (i.e. K_{max}=2.2-3.3MPam$^{1/2}$), a birefringent zone can be clearly observed near the fatigue crack surface. The measured birefringent zone size is 0.3-0.35mm, which is smaller than the birefringent zone size measured from the static fracture test (i.e. 1.2-1.4mm). The ratio of the birefringent zone size and the plastic zone size, r_b/r_y, is 5.0-9.7, as shown in Table 6.5. Despite the absolute differences in the birefringent zone size between the fatigue and static fractures, it is of interest to note that the r_b/r_y ratio in the fatigue fracture is similar to that in the static fracture, namely 7.3-8.5.

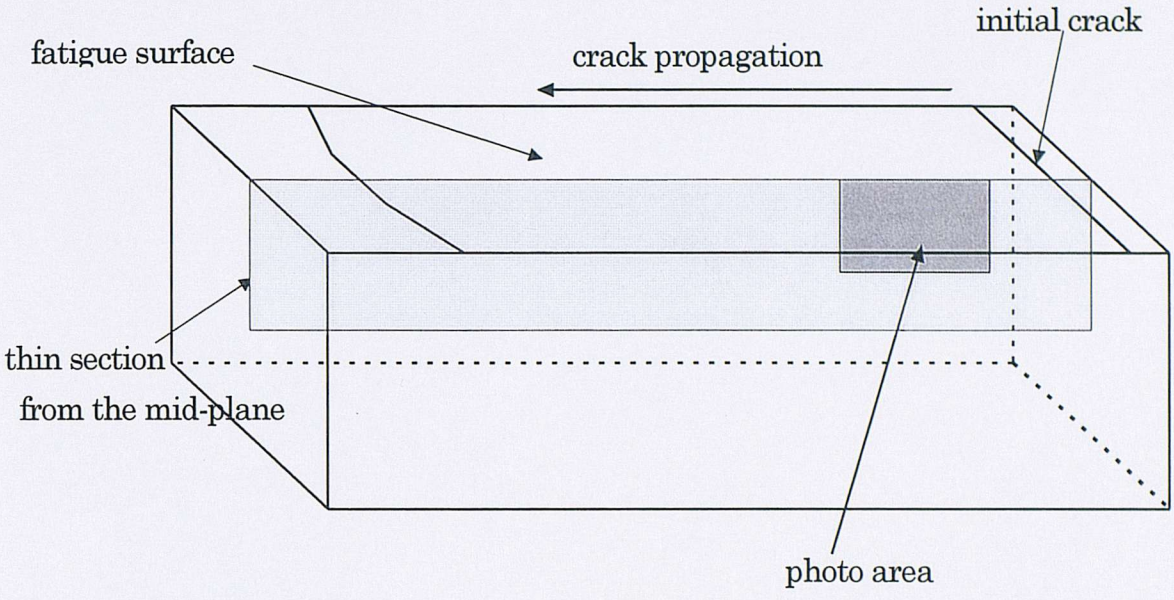
As discussed in section 5.4, the loading rate in the fatigue test is far higher than that in the static test. A higher loading rate causes an increase in the yield stress of the epoxy matrix. Thus, according to the LEFM equation, i.e. $r_y=(K_{max}/\sigma_{yt})^2/6\pi$, the plastic zone size, r_y, becomes smaller in fatigue fracture. A higher loading rate also causes an increase in the modulus of the rubber particles. As Bucknall et al. have suggested [26], an increase in the shear modulus of rubber particles makes it more difficult for the rubber particles to cavitate. Therefore, the birefringent zone size, r_b, may also become smaller in fatigue fracture. Hence, the r_b/r_y ratio may be not significantly affected by the change in the loading rate. This may be why the r_b/r_y ratio in the fatigue fracture studies is similar to that observed in the static fracture tests.

If these r_b/r_y ratios are applied to the estimate the r_b/r_y ratio at a relatively low K_{max} value, then the r_b value at K_{max}=0.4MPam$^{1/2}$ should be approximately 5-10μm, since the calculated plastic zone size, r_y, is 1μm as shown in Table 6.5. The birefringent zone with an extent of 5-10μm is too small to be detected. Thus, this may be the reason why no birefringent zone is observed from the region of K_{max}=0.4MPam$^{1/2}$, as shown in Fig.6.14.

Table 6.5 Birefringent zone size of 15phrRME160 measured from fatigue tests

K_{max} (MPam$^{1/2}$)	r_b (μm)	r_y (μm)	r_b/r_y
0.4	not detected	1	not obtained
2.2-3.3	300-350	31-70	5.0-9.7

Note : $r_y = (K_{max}/\sigma_{yt})^2/6\pi$



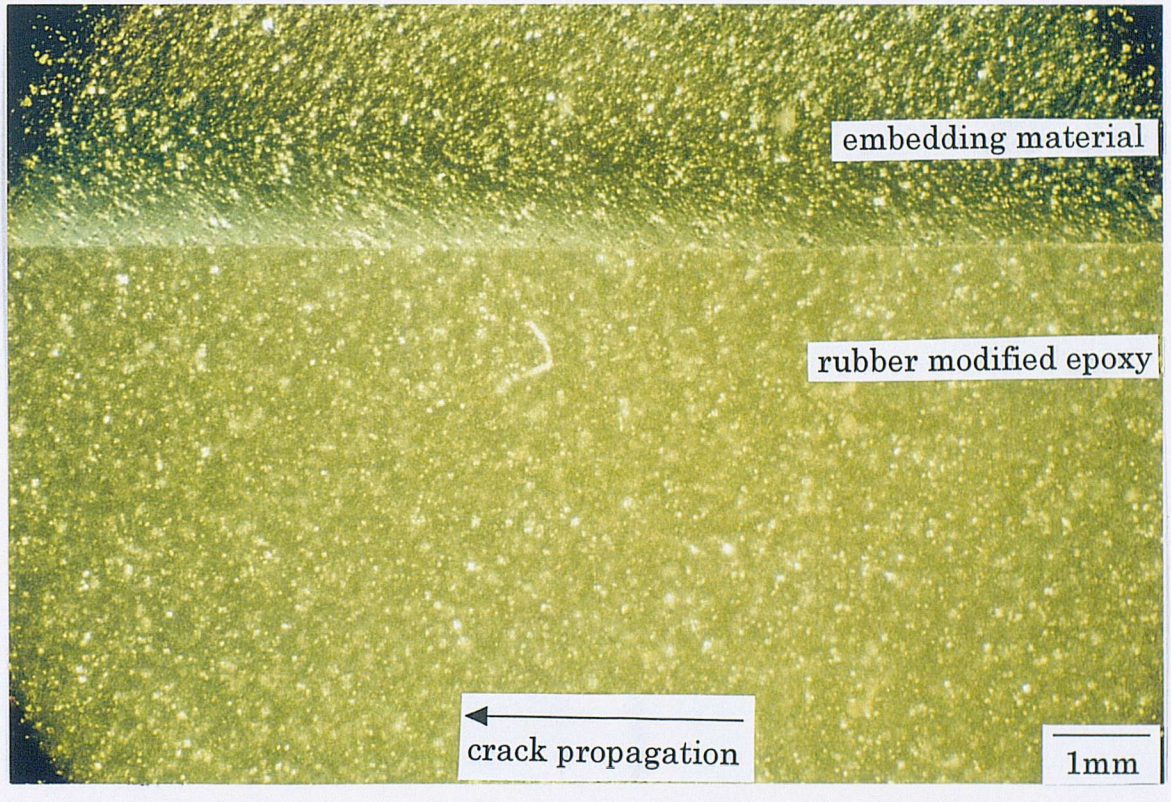
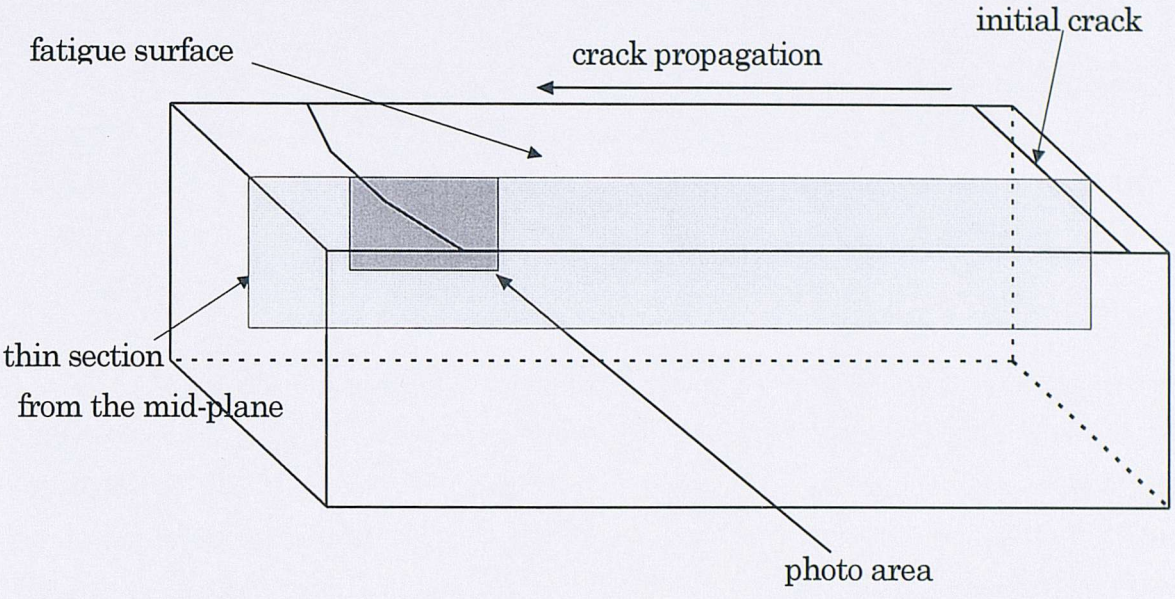


Fig.6.14 TOM micrographs, under crossed polars, of 15phrRME160 from a fatigue test (thin section parallel to the crack propagation and perpendicular to the fracture surface), K_{max}~0.4MPam$^{1/2}$



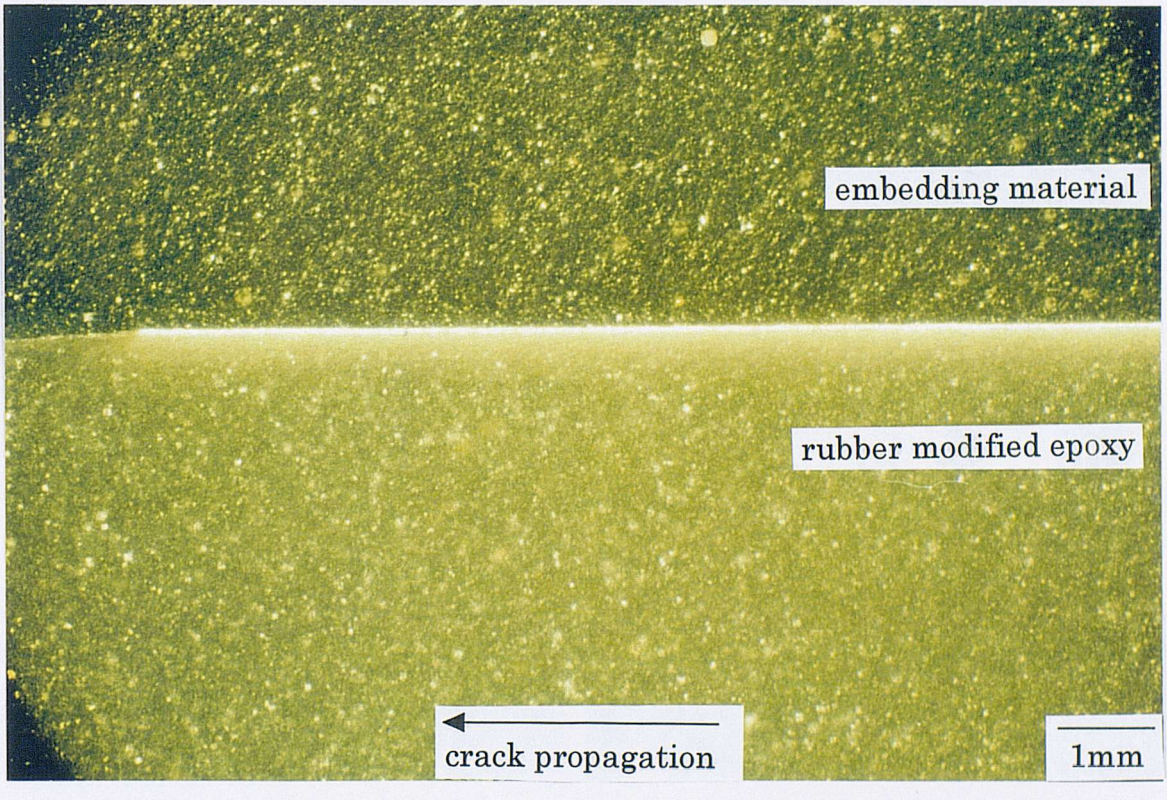


Fig.6.15 TOM micrographs, under crossed polars, of 15phrRME160 from a fatigue test (thin section parallel to the crack propagation and perpendicular to the fracture surface), K_{max}*=2.2-3.3MPam*$^{1/2}$

6.3.3 TEM observations

The TEM micrographs of a mid-plane section of the 15phrRME160 materials after a fatigue test are shown in Fig.6.16 and Fig.6.17. As shown in Fig.6.16, at K_{max}~0.4MPam$^{1/2}$, it can be seen that almost all rubber particles remain intact. This suggests that any toughening mechanisms which involves plastic deformation are not active.

On the other hand, elongated rubber particles near the crack surface can be observed at K_{max}~3.0MPam$^{1/2}$, as shown in Fig.6.17 (the fatigue fracture surface is just above the upper edge of the photo area). This means that plastic shear deformation of the matrix epoxy occurs during the fatigue crack propagation in this region. It is also observed that the cavitated particle size is greater than the initial rubber particle size, 1.7μm. This observation reveals that the void growth mechanism is active in this region.

The above observations are in agreement with the results obtained from the SEM and TOM observations. Further, these results also prove the validity of the concept of the K-transition, in that there is no evidence of the toughening mechanisms which involve plastic deformation being active below the K-transition value, 0.59MPam$^{1/2}$.

It should be noted again that the thickness of the TEM sections is approximately 100nm.

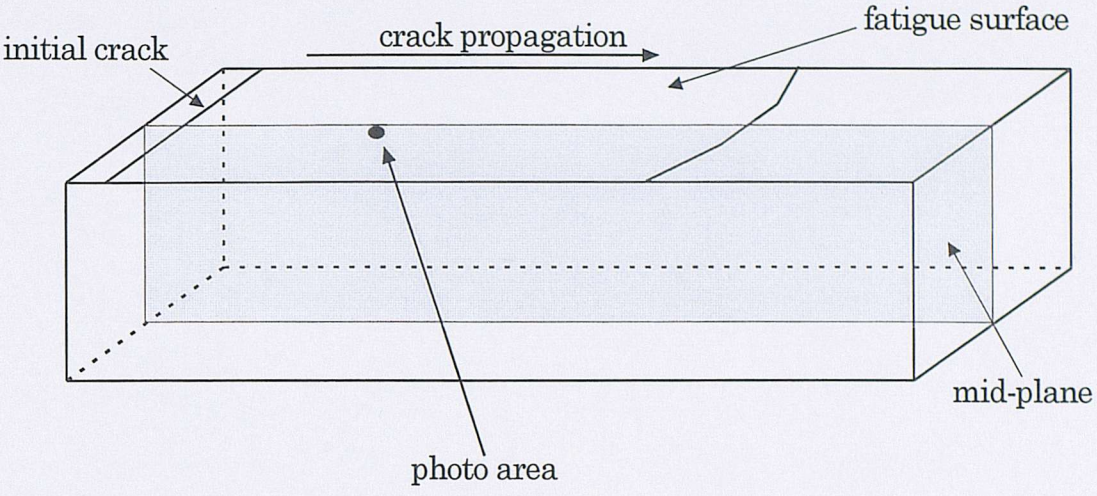
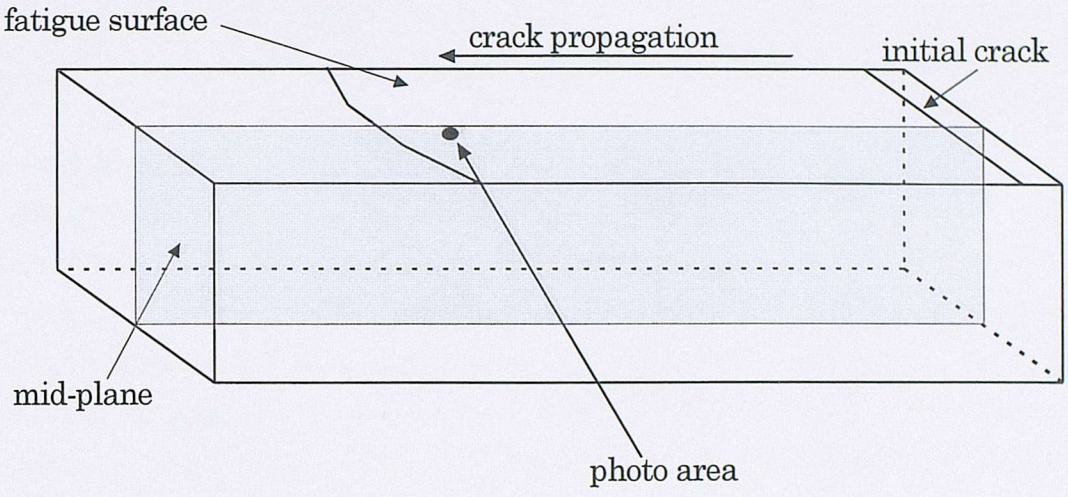




Fig.6.16 TEM micrographs of 15phrRME160; K_{max}~0.4MPam$^{1/2}$ (arrow indicates the crack propagation direction)



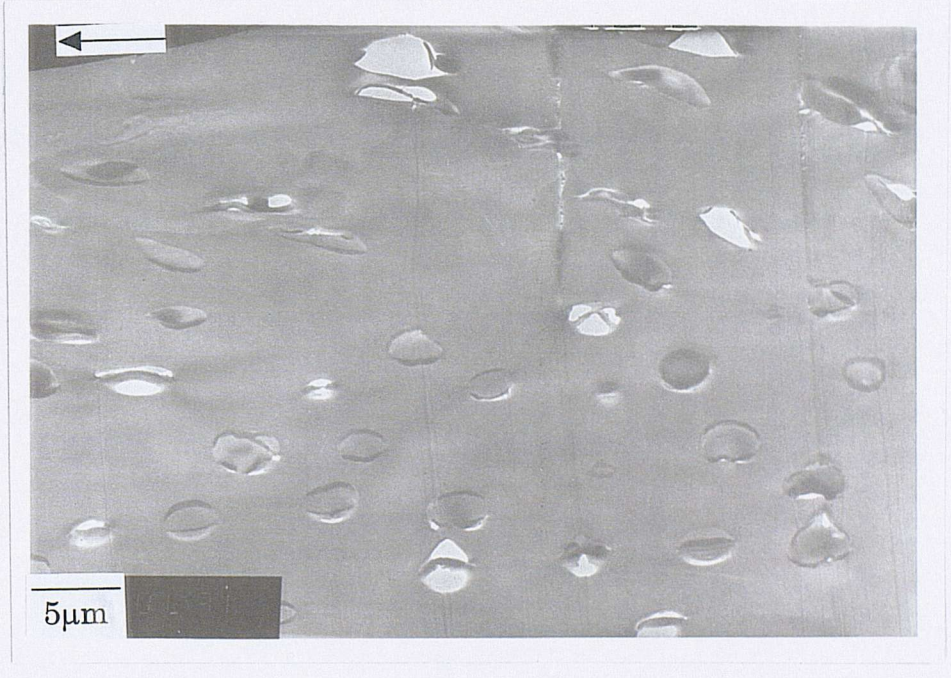


Fig.6.17 TEM micrographs of 15phrRME160; K_{max}~3.0MPam$^{1/2}$ (arrow indicates the crack propagation direction)

6.4 Concluding remarks

In the present Chapter, the fracture surfaces of the rubber modified epoxies were investigated using SEM, TOM and TEM. The toughening effects caused by the presence of the rubber particles were also discussed. For both static and fatigue fracture, cavitation of the rubber particles was observed in the vicinity of the crack surface. It is confirmed that plastic void growth and shear yielding are the main toughening mechanisms. In fatigue conditions, the validity of the concept of K-transition was also proved via the SEM and TOM observations. There is little evidence of the toughening effects, caused by the presence of the rubber particles, being active below the K-transition value. Whereas considerable plastic deformation due to the void growth and shear yielding mechanisms is observed far above the K-transition value.

In the next Chapter, the toughening mechanisms arising from the presence of rubber particles will be theoretically modelled. A quantitative analysis for the energy dissipation during the fatigue crack propagation will be employed for the 15phrRME160 and 15phrRME120 materials.

Chapter Seven

Modelling of Rubber Toughening Mechanisms

7.1 Introduction

The fatigue behaviour of the rubber modified epoxies and their toughening mechanisms were discussed in the previous Chapters. However, our understanding is still qualitative and it is highly desirable to develop a mathematical model to quantify the toughening mechanisms, especially in fatigue fracture.

Several models have been proposed to explain the toughening effect due to the introduction of rubbery particles in static fracture. Kunz-Douglass et al. [53] developed a model which is based on the energy dissipation during the stretching and bridging of the crack surfaces by rubber particles. However, rubber bridging plays just a secondary role in the rubber toughening of epoxy polymers. Furthermore, this model could not explain the stress whitening observed in rubber modified materials.

Kinloch [113] calculated the fracture energy dissipated by the localised shear yielding mechanism inside the plastic zone. However, the contributions of void growth and rubber bridging were not taken into account.

Recently, Huang et al. [7, 47, 48] extended Kinloch's model [113] to calculate the energy dissipation during the fracture. They also described the contributions to the increases in the fracture energy due to void growth and rubber bridging separately, and succeeded in estimating the fracture energy.

In the present Chapter, the above models will be modified so that they may be applied to the fatigue condition. The calculations will be compared with the experimental results.

7.2 Development of the theoretical model

The dissipated energy, G, of the rubber modified epoxy during the fatigue crack propagation can be expressed as:

$$G = G_0 + \Delta G \tag{7.1}$$

where G_0 is the contribution of the intrinsic fracture energy, i.e. the fracture energy of the unmodified epoxy, and ΔG is the dissipated energy caused by the additional toughening mechanisms. In this study, we considered shear yielding, void growth and rubber bridging as the main toughening mechanisms. These three mechanisms are schematically represented in Fig.7.1.

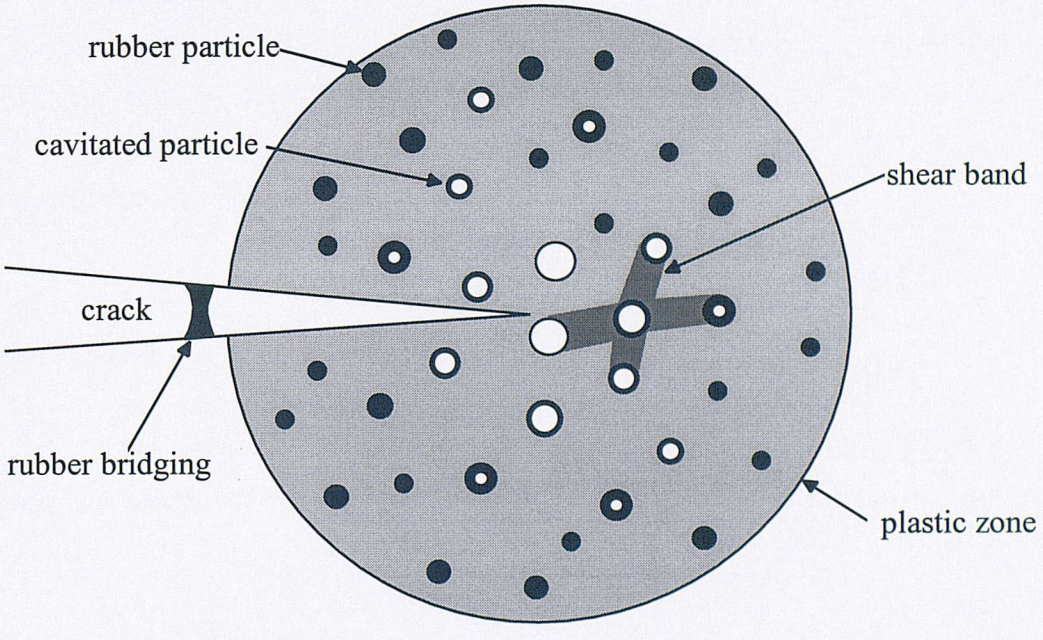


Fig.7.1 Schematic drawing of the toughening mechanisms of rubber modified epoxy polymers [7]

The dissipated energy caused by the toughening mechanisms, ΔG, can be divided into three terms as follows:

$$\Delta G = \Delta G_s + \Delta G_v + \Delta G_r \tag{7.2}$$

where ΔG_s is the contribution from shear yielding, ΔG_v is the contribution from void growth, and ΔG_r is the contribution from rubber bridging. The values of ΔG_s and ΔG_v are related to the size of the plastic zone, and can be calculated by the following equations, as detailed in Appendix B:

$$\Delta G_s = 2 \int_0^{r_y} U_s(r)\, dr \tag{7.3}$$

$$\Delta G_v = 2 \int_0^{r_y} U_v(r)\, dr \tag{7.4}$$

where r_y is the radius of the plastic zone, r is the distance from the crack tip, $U_s(r)$ is the dissipated energy density for the shear yielding mechanism, and $U_v(r)$ is the dissipated energy density for the void growth mechanism. Thus, we firstly have to evaluate the size of the plastic zone in order to calculate the dissipated energy due to these two mechanisms. The contribution of rubber bridging will be explained later in details in Section 7.6.

7.3 The size of the plastic zone

Linear elastic fracture mechanics suggests that the radius of the plastic zone can be calculated by the following equations.

$$r_y = (K/\sigma_y)^2/6\pi \quad \text{(plane strain)} \tag{7.5}$$

$$r_y = (K/\sigma_y)^2/2\pi \quad \text{(plane stress)} \tag{7.6}$$

where σ_y is the yield stress. This means that the radius of the plastic zone is inversely proportional to the square of the yield stress. Therefore, the relationship on the radius of the plastic zone between the rubber modified epoxy and the unmodified epoxy can be approximately assumed to be given by the following equation:

$$r_y/r_{yu} = (\sigma_{yu}/\sigma_c)^2 \tag{7.7}$$

where r_y is the plastic zone radius of the rubber modified epoxy, r_{yu} is the plastic zone radius of the unmodified epoxy, σ_{yu} is the uniaxial yield stress of the unmodified epoxy, and σ_c is the critical stress of the rubber modified epoxy for yielding. It should be noted that σ_c is not the same as the uniaxial yield stress of the rubber modified epoxy. This is because the stress field around the rubber particle is not uniform and yielding occurs when the von Mises stress at any place reaches the uniaxial yield stress [7]. If we use the following definition:

$$\sigma_{yu}/\sigma_c \equiv K_{vm} \tag{7.8}$$

where K_{vm} is the maximum concentration factor of the von Mises stress, equation 7.7 can be expressed as:

$$r_y/r_{yu} = K_{vm}^2 \tag{7.9}$$

This factor can be calculated from the finite element method, and the values calculated by Huang using two dimensional plane strain model are used in the present study [7,47].

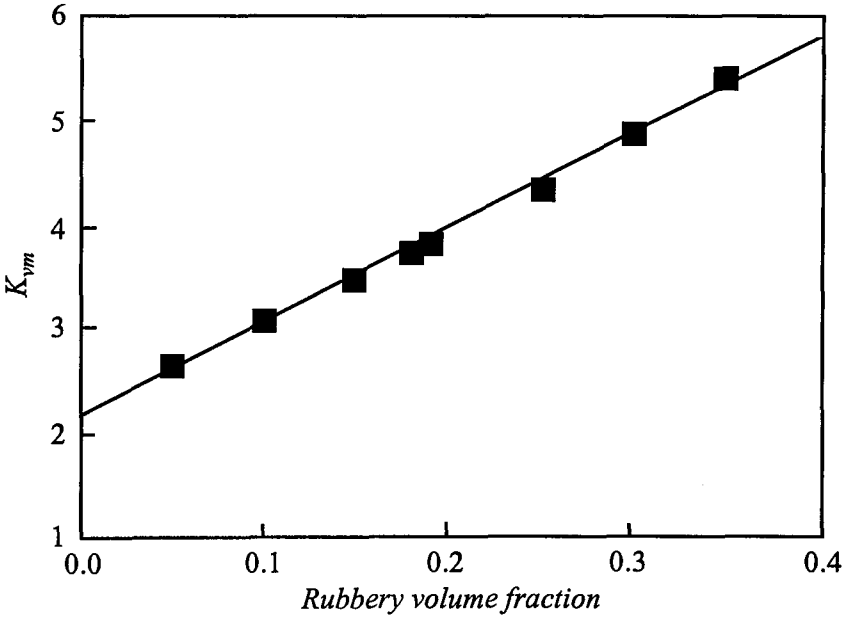


Fig.7.1 von Mises stress concentration factor as a function of rubbery volume fraction

The yielding of glassy polymers is generally dependent on the hydrostatic stress. Strictly, therefore, the von Mises criterion is not satisfied, and it should be modified as described by the following equation, as mentioned in Chapter Two:

$$\tau_{vm} = \tau_0 - \mu_m p \tag{7.10}$$

where τ_{vm} is the von Mises shear stress, τ_0 is the yield stress under pure shear, μ_m is a constant and p is the hydrostatic stress. As the maximum concentration factor of von Mises stress, K_{vm}, was calculated under uniaxial loading, the following relationship can be satisfied:

$$\sigma_1 >> \sigma_2, \sigma_3 \tag{7.11}$$

From the definition of the von Mises stress and the hydrostatic stress,

$$\sigma_{vm} = \{(\sigma_1 - \sigma_2)^2/2 + (\sigma_2 - \sigma_3)^2/2 + (\sigma_3 - \sigma_1)^2/2\}^{1/2} \approx \sigma_1 \tag{7.12}$$

$$p \equiv (\sigma_1 + \sigma_2 + \sigma_3)/3 \approx \sigma_1/3 \approx \sigma_{vm}/3 \tag{7.13}$$

and the von Mises stress, σ_{vm}, and the von Mises shear stress, τ_{vm}, are related to each other through the following equation:

$$\sigma_{vm}^2 = 3\tau_{vm}^2 \tag{7.14}$$

The hydrostatic stress, p, can be expressed as:

$$p = 3^{1/2}\tau_{vm}/3 = \tau_{vm}/3^{1/2} \tag{7.15}$$

Therefore the criterion 7.10 can be modified as:

$$\tau_{vm} = \tau_0/(1+ \mu_m/3^{1/2}) \tag{7.16}$$

This means that the effective yield stress is reduced by $1/(1+ \mu_m/3^{1/2})$. In other words, the stress required for shear yielding is reduced by $1/(1+ \mu_m/3^{1/2})$. Therefore, the relative size of the plastic zone will be increased. Hence, the relationship of the radius of the plastic zone compared between the rubber modified epoxy and the unmodified epoxy, i.e. equation 7.9, should be modified as:

$$r_y / r_{yu} = K_{vm}^2 (1 + \mu_m / 3^{1/2})^2 \qquad (7.17)$$

As shown in Fig.7.1, the value of K_{vm} is a function of rubbery volume fraction. If there is no cavitation or debonding of rubber particles, the initial volume fraction of rubber particles, V_{fr}, can be used for the calculation of the K_{vm} value. However, cavitation of the rubber particles often occurs and the voids, i.e. the cavitated rubber particles, continue growing in the fracture process. The voids also cause stress concentration of the same value as the rubber particles. Therefore, the volume fraction of voids, V_{fv}, which is greater than V_{fr}, should be used to calculate the K_{vm} value.

7.4 The contribution of shear yielding

For the calculation of the contribution of shear yielding mechanism, ΔU_s, the dissipated energy density function for the shear yielding, $U_s(r)$ was estimated by the following equation [7, 48]:

$$U_s(r) = V_{fs}(r)\, W_s(r) \qquad (7.18)$$

where $V_{fs}(r)$ is the volume fraction of the matrix epoxy in which shear yielding occurs, and $W_s(r)$ is the shear plastic energy density of the matrix epoxy.

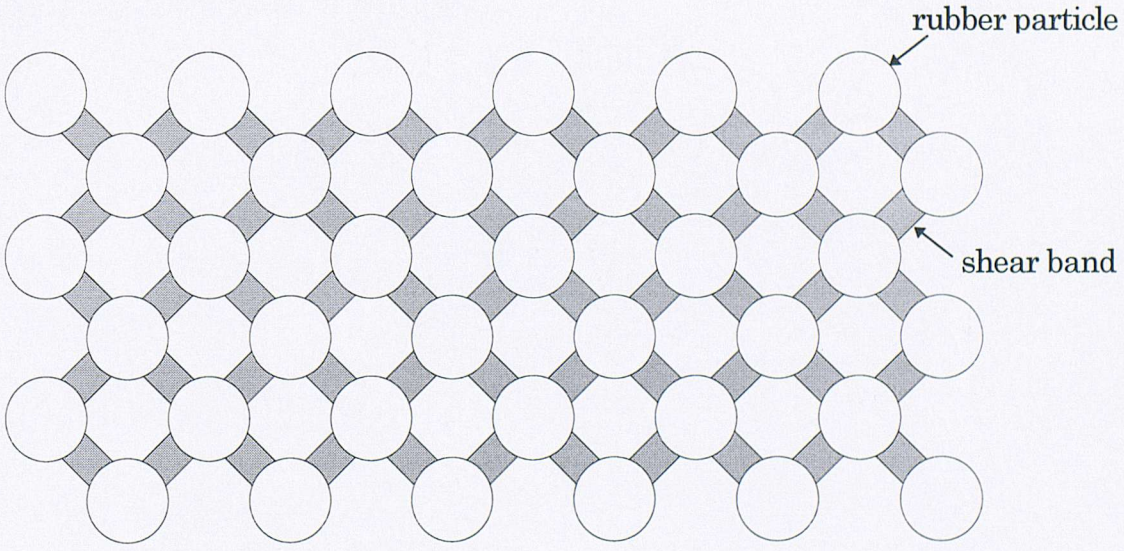


Fig. 7.2 Simple cubic array of the rubber particles and shear bands

For the assessment of the volume fraction of shear yielding, $V_{fs}(r)$, a simple cubic array for the rubber particle distribution model was assumed, as shown in Fig.7.2. Fig.7.3 also shows the three dimensional illustration of the geometric relationships.

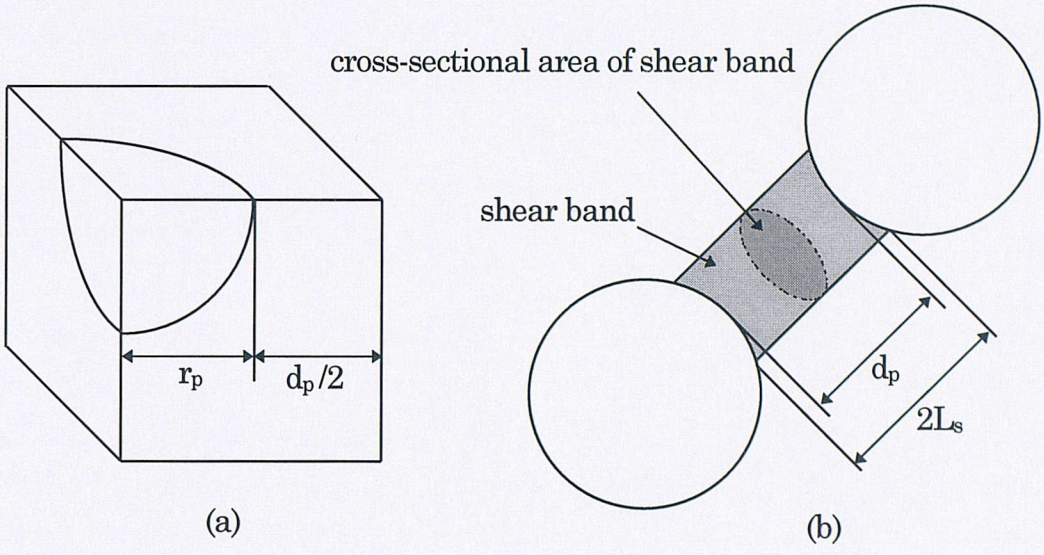


Fig.7.3 Geometric relationship (a) basic element of simple cubic array (b) particles and localised shear band

As illustrated in Fig.7.3 (a), one eighth of the particle is included in a basic element. The volume fraction of the particles (i.e. either rubber particles or voids), V_f, is given by the following equation:

$$V_f = \frac{(4\pi r_p^3/3)/8}{(r_p + d_p/2)^3} \tag{7.19}$$

where r_p is the radius of the particle and d_p is the interfacial particle-to-particle distance. Therefore:

$$d_p = [(4\pi/3V_f)^{1/3} - 2]\, r_p \tag{7.20}$$

The number of the particles per unit volume, N_v, can be defined by the following equation:

$$N_v = V_f/(4\pi r_p^3/3) = 3V_f/(4\pi r_p^3) \tag{7.21}$$

Then, it is assumed that the cross-sectional area of the shear band can be given by the following equation, as in the case of the rigid particle toughened polymers [114]:

$$S(r) = \alpha(r)\pi r_p^2 \tag{7.22}$$

where $\alpha(r)$ is the scaling factor that is assumed to be a function of the distance from the crack tip. Kinloch [113] suggested that it is represented by the following equation:

$$\alpha(r) = 1 - r/r_y \tag{7.23}$$

As shown in Fig.7.4, the scaling factor, $\alpha(r)$, becomes a unity when r approaches to zero (i.e. the cross-sectional area of shear band is the same as that of the particles when r=0). The value of $\alpha(r)$ decreases steadily with increasing r, and becomes zero at the boundary of the plastic zone. This means that the cross-sectional area of shear band becomes smaller as the distance from the crack tip increases, and completely disappears at the boundary of the plastic zone.

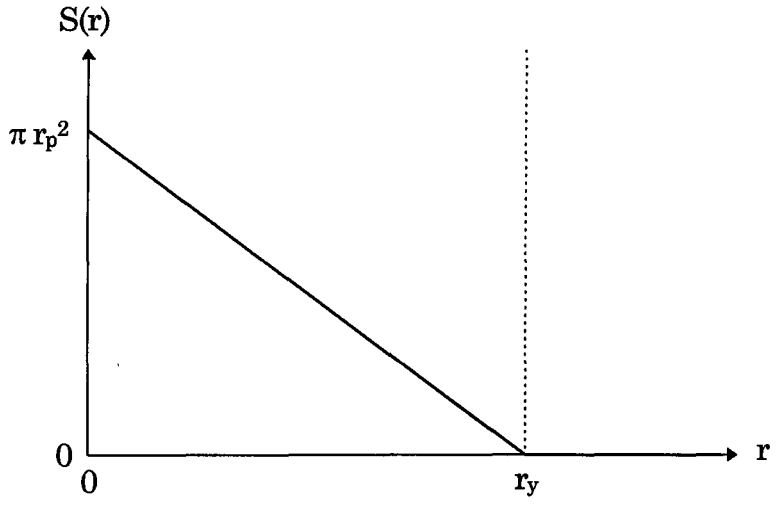


Fig.7.4 Cross-sectional area of shear band, as a function of distance from the crack tip

The length of a shear band, $2L_s$, as defined in Fig.7.3(b), can be expressed as follows:

$$2L_s = 2r_p + d_p - 2\,[1-\alpha(r)]^{1/2} r_p \qquad (7.24)$$

As a shear band is located between two particles, the volume of the shear band per one particle, V_s, is half the volume of the shear band shown in Fig.7.3(b). The values of V_s can be calculated by the following equation:

$$V_s = n_s \{S(r)L_s - (\pi/3)\,(L_s - d_p/2)^2\,[3r_p - (L_s - d_p/2)]\} \qquad (7.25)$$

where n_s is the number of shear bands per one particle and is equal to four, as shown in Fig.7.2. The volume of the shear band per one particle, V_s, is also a function of the distance from the crack tip; $V_s(r)$. By substituting equations 7.20, 7.22 and 7.24 into 7.25, the following equation may be obtained:

$$V_s(r) = (2\pi/3)\, r_p^2 \{3(4\pi/3V_f)^{1/3}\,\alpha(r) + 4\,[1-\alpha(r)]^{3/2} - 4\} \qquad (7.26)$$

Thus, the volume fraction of the matrix epoxy in which shear yielding occurs, $V_{fs}(r)$, can be calculated as follows:

$$V_{fs}(r) = N_v V_s(r) = (V_f/2)\{3(4\pi/3V_f)^{1/3}\,\alpha(r) + 4\,[1-\alpha(r)]^{3/2} - 4\} \qquad (7.27)$$

As suggested in section 7.3, the cavitation of the rubber particles occurs and the voids, i.e. cavitated rubber particles, continue growing in the fracture process. Therefore, the volume fraction of voids, V_{fv}, should be used as the volume fraction of the particles.

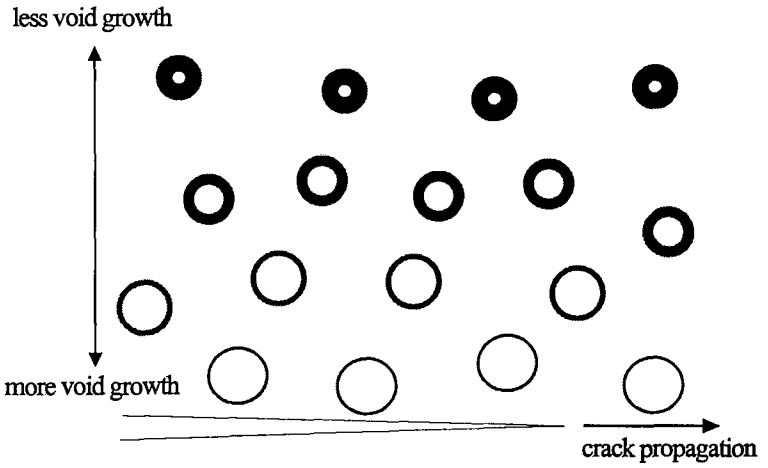


Fig. 7.5 Schematic drawing of the distribution of voids in plastic zone

As shown in Fig.7.5, it is natural to think that the volume fraction of voids is not a constant, but is dependent upon the distance from the crack tip, r. The volume fraction of voids should be the same as the volume fraction of rubber particles far from the crack surface, and should be at a maximum close to the crack tip. It may be assumed that the volume fraction of voids is simply represented by the following equation:

$$V_{fv}(r) = V_{fv0} - (V_{fv0} - V_{fr})\, r / r_y \qquad (7.28)$$

where V_{fv0} is the volume fraction of voids visible from studying the fracture surface, which is measured by SEM observation, and V_{fr} is the volume fraction of rubber particles. As shown in Fig.7.6, $V_{fv}(r)$ is equal to V_{fv0} at r=0, i.e. at the crack tip. Its value gradually decreases with increasing r, and $V_{fv}(r)$ equals to the volume fraction of rubber particles, V_{fr} at $r=r_y$, i.e. at the boundary of the plastic zone.

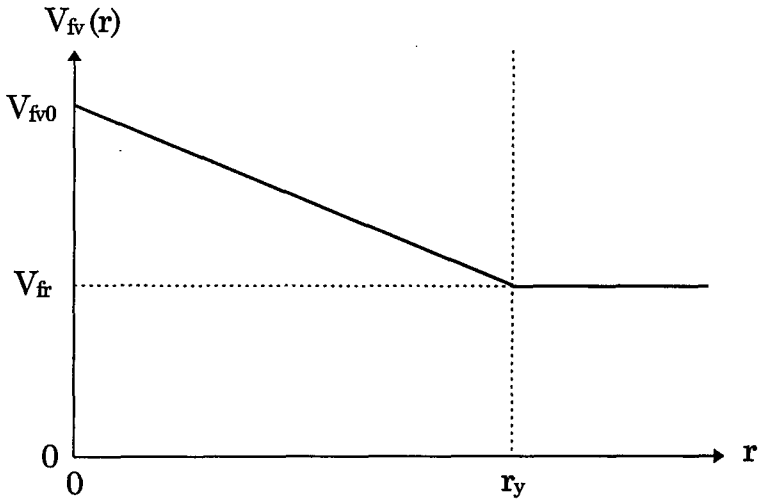


Fig.7.6 Volume fraction of voids, as a function of distance from the crack tip

Thus, equation 7.27 can be modified as follows:

$$V_{fs}(r) = [V_{fv}(r)/2]\{3\,[4\pi/3V_{fv}(r)]^{1/3}\,\alpha(r) + 4\,[1-\alpha(r)]^{3/2} - 4\} \qquad (7.29)$$

Next, an estimate of the shear plastic energy density of the matrix epoxy, $W_s(r)$, is required for the calculation of the dissipated energy by the shear yielding

mechanism. Assuming that the material is perfectly elastic-plastic, the shear plastic energy density can be expressed as follows:

$$W_s(r) = \tau_y \gamma(r) \tag{7.30}$$

where τ_y is the shear yield stress of the matrix epoxy, and $\gamma(r)$ is the shear plastic strain of the matrix epoxy. For a perfectly elastic-plastic material, the components of the strain tensor are proportional to the inverse of r within the plastic zone [7, 48]. Therefore, as an approximation, the shear plastic strain of the matrix epoxy, $\gamma(r)$, inside the plastic zone can be assumed as follows:

$$\gamma(r) = \gamma_f \alpha(r) \tag{7.31}$$

where γ_f is the fracture strain of the matrix epoxy. This means that the shear plastic strain has the maximum value of γ_f at the crack tip and decreases steadily towards zero at the boundary of the plastic zone, as shown in Fig.7.7.

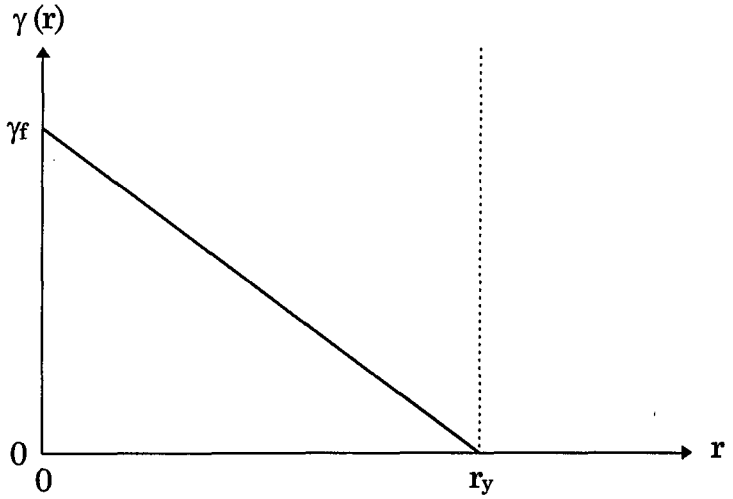


Fig.7.7 Estimated shear plastic strain inside the plastic zone, as a function of distance from the crack tip

The shear yield stress of the matrix epoxy, τ_y, can be deduced as follows [7, 48]:

$$\tau_y = \sigma_{yc}/2 \tag{7.32}$$

where σ_{yc} is the compressive yield stress of the matrix epoxy. By substituting equations 7.31 and 7.32 into 7.30, the shear plastic energy density can be obtained as follows:

$$W_s(r) = \sigma_{yc}\gamma_f\alpha(r)/2 \tag{7.33}$$

Thus, the dissipated energy density of shear yielding, $U_s(r)$, can be estimated by substituting equations 7.29 and 7.33 into 7.18, to give:

$$U_s(r) = [\sigma_{yc}\gamma_f\alpha(r)V_{fv}(r)/4]\{3[4\pi/3V_{fv}(r)]^{1/3}\alpha(r) + 4[1-\alpha(r)]^{3/2} - 4\} \tag{7.34}$$

The dissipated energy by the shear yielding mechanism, ΔG_s, is now given by the following equation:

$$\begin{aligned}\Delta G_s &= 2\int_0^{r_y} U_s(r)\,dr \\ &= (\sigma_{yc}\gamma_f/2)\int_0^{r_y} \alpha(r)V_{fv}(r)\{3[4\pi/3V_{fv}(r)]^{1/3}\alpha(r) + 4[1-\alpha(r)]^{3/2} - 4\}\,dr\end{aligned} \tag{7.35}$$

7.5 The contribution of void growth

The dissipated energy by the void growth mechanism is given by the following equation, as suggested in section 7.2:

$$\Delta G_v = 2\int_0^{r_y} U_v(r)\,dr \tag{7.36}$$

where $U_v(r)$ is the dissipated energy density of void growth. For the calculation of ΔG_v, we have to evaluate the energy density, $U_v(r)$. When a void grows from a volume of V_0 to V_1, the energy density of void growth is given by the following equation [7, 48]:

$$U_v(r) = \int_{V_0}^{V_1} p \, d\theta \tag{7.37}$$

where p is the local hydrostatic stress and θ is the volumetric strain. The increase of the volumetric strain during void growth, $d\theta$, can be expressed as follows:

$$d\theta = V_f \, dV/V \tag{7.38}$$

where V_f is the volume fraction of voids and V is the average volume of voids. Assuming the following relationships:

$$V_f = V_{fr} \text{ when } V = V_0 \tag{7.39}$$

$$V_f = V_{fv}(r) \text{ when } V = V_1 \tag{7.40}$$

i.e. V_f has the value of the volume fraction of rubber particle, V_{fr}, before the void growth, and it has the value of the volume fraction of voids, $V_{fv}(r)$ after the void growth. The value of V_f can be expressed by the following equation:

$$V_f = V_{fr} + \frac{V_{fv}(r) - V_{fr}}{V_1 - V_0} (V - V_0) \tag{7.41}$$

The hydrostatic stress, p, in the plastic zone can be represented by the equation [7, 48]:

$$p \approx \sigma_{yt}/2 \tag{7.42}$$

where σ_{yt} is the tensile yield stress. By substituting equations 7.38, 7.41 and 7.42 into 7.37, energy density, $U_v(r)$, is given by :

$$U_v(r) = \int_{V_0}^{V_1} (\sigma_{yt}/2) \{V_{fr} + \frac{V_{fv}(r) - V_{fr}}{V_1 - V_0} (V - V_0)\} \, dV/V$$

$$= (\sigma_{yt}/2) [V_{fv}(r) - V_{fr} + (V_{fr} - \frac{V_{fv}(r) - V_{fr}}{(V_1/V_0) - 1}) \log (V_1/V_0)] \tag{7.43}$$

From 7.39 and 7.40, the following relationship is valid:

$$V_1 / V_0 = V_{fv}(r) / V_{fr} \tag{7.44}$$

Therefore, equation 7.43 can be modified as follows:

$$U_v (r) = (\sigma_{yt} /2) [V_{fv} (r) - V_{fr}] \tag{7.45}$$

The dissipated energy by the void growth mechanism, ΔG_v, can be calculated as follows:

$$\begin{aligned} \Delta G_v &= \sigma_{yt} \int_0^{r_y} [V_{fv} (r) - V_{fr}] \, dr \\ &= (\sigma_{yt} /2) (V_{fv0} - V_{fr}) \, r_y \end{aligned} \tag{7.46}$$

From equation 7.17, r_y is given by :

$$r_y = K_{vm}^2 (1+ \mu_m /3^{1/2})^2 \, r_{yu} \tag{7.47}$$

Furthermore, the following relationship is valid between the tensile yield stress and the compressive yield stress [48]:

$$\sigma_{yt} = \sigma_{yc} (3^{1/2} - \mu_m) / (3^{1/2} + \mu_m) \tag{7.48}$$

Thus, equation 7.46 can be rewritten as:

$$\Delta G_v = (1/2) (1- \mu_m^2 /3) (V_{fv0} - V_{fr}) \, r_y \, \sigma_{yc} \, K_{vm}^2 \tag{7.49}$$

7.6 The contribution of rubber bridging

The dissipated energy by the rubber bridging mechanism in static fracture has been proposed by Kunz-Douglass et al. [53] to be given by :

$$\Delta G_{r,static} = 4\Gamma_t (T) \, V_{fr} \tag{7.50}$$

where $\Gamma_t (T)$ is the tearing energy of the rubber particles and V_{fr} is the volume fraction of rubber particles. The tearing energy, $\Gamma_t (T)$, of the CTBN1300X8 rubber at room temperature is approximately 460J/m^2, as shown in Fig.7.8

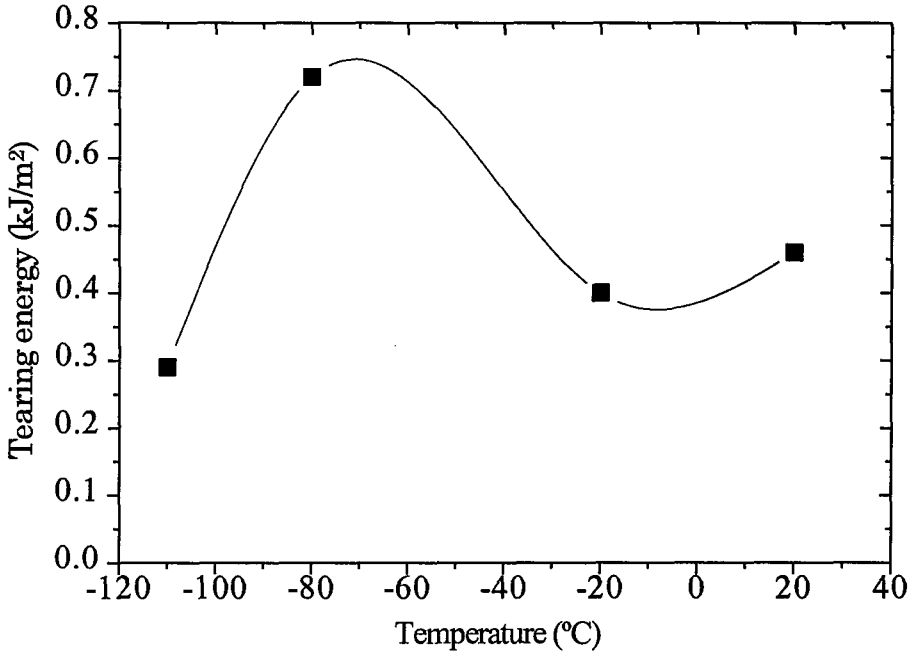


Fig. 7.8 Tearing energy of CTBN rubber (data from ref. [115])

As Kunz-Douglass's model was proposed to explain the static fracture energy, the model has now been modified for fatigue fracture, as follows:

$$\Delta G_r = 4\Gamma_t(T)\, V_{fr}\, f_r\, (da/dN) \qquad (7.51)$$

where f_r (da/dN) is a scaling factor. The scaling factor is dependent on the fatigue crack growth rate, da/dN, and is in the range of zero to one. This means that the dissipated energy in fatigue fracture is smaller than that in static fracture, and that the scaling factor indicates the ratio of the tearing energy which is dissipated at a certain fatigue crack growth rate to that of the static tearing energy. This ratio should be the same as the ratio of the energy dissipated at the certain fatigue crack growth rate in the dynamic tearing test of pure rubber and the static tearing energy. That is:

$$f_r\,(da/dN) = \Delta G_r / \Delta G_{r,static} = T_r / \Gamma_t(T) \qquad (7.52)$$

where T_r is the energy dissipated at the certain fatigue crack growth rate in the dynamic tearing test of pure rubber.

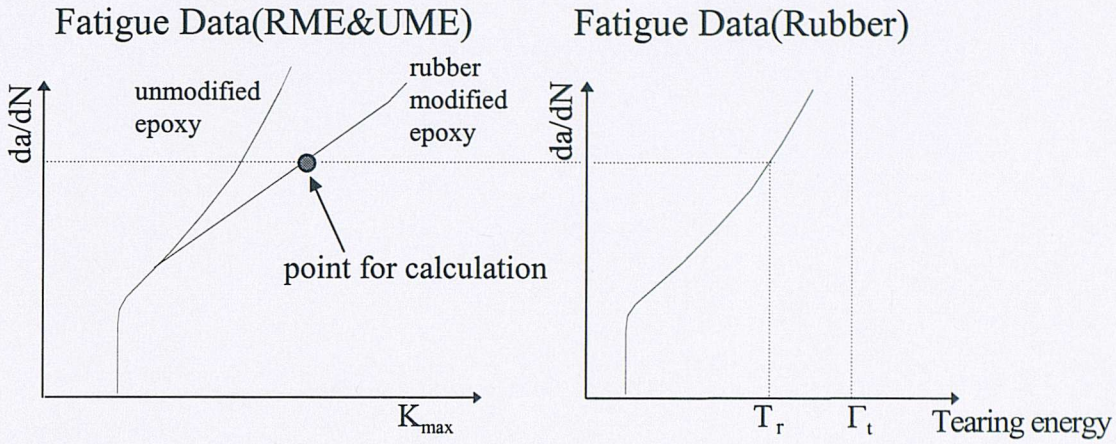


Fig.7.9 Method to evaluate the scaling factor of the rubber bridging mechanism

Fig.7.9 shows schematically how the scaling factor, $f_r(da/dN)$ was estimated. Firstly, the T_r value, at which pure rubber has the same fatigue crack growth rate as that of interest for the rubber modified epoxy, may be read from the fatigue data. Then, the value of $f_r(da/dN)$ can be evaluated as a ratio of T_r and Γ_t, as shown in equation 7.52.

7.7 The contribution of unmodified epoxy

The last term, the contribution of the intrinsic fracture energy, i.e. the dissipated energy originating from the unmodified epoxy, G_0, must be evaluated to calculate the total dissipated energy. As for the contribution of rubber bridging, the contribution of unmodified epoxy, G_0, can be assumed as follows:

$$G_0 = G_{Icu}\, f_u\,(da/dN) \qquad (7.53)$$

where G_{Icu} is the fracture energy of the unmodified epoxy and $f_u(da/dN)$ is the scaling factor. The scaling factor is dependent of the fatigue crack growth rate, da/dN, and is in the range of zero to one. In other words, the dissipated energy in fatigue fracture is smaller than that in static fracture. The procedure for the evaluation of the scaling factor, $f_u(da/dN)$, is similar to that for $f_r(da/dN)$, as shown in Fig.7.10.

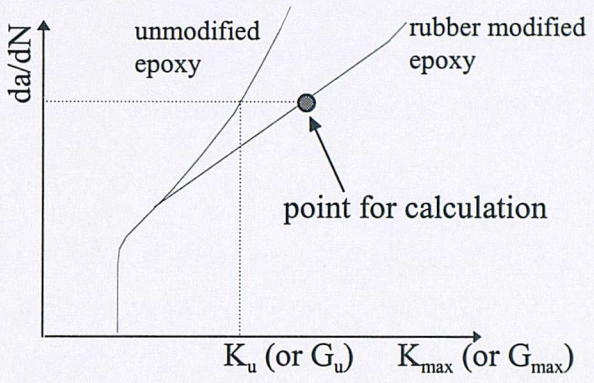


Fig. 7.10 Method to evaluate the scaling factor, $f_u(da/dN)$

Firstly, the K_u value (or G_u value), at which the unmodified epoxy has the same fatigue crack growth rate as that of interest for the rubber modified epoxy, may be read from the fatigue data. The scaling factor, $f_u(da/dN)$, can be evaluated as a ratio of G_u and G_{Icu}, the fracture energy of the unmodified epoxy, as follows:

$$f_u\,(da/dN) = G_u / G_{Icu} = (K_u / K_{Icu})^2 \qquad (7.54)$$

where K_{Icu} is the fracture toughness of the unmodified epoxy.

The radius of the plastic zone for the unmodified epoxy, r_{yu}, also can be calculated using the K_u value. From LEFM, the value of r_{yu} is given by the following equation:

$$r_{yu} = (K_u/\sigma_{yu})^2/6\pi \qquad (7.55)$$

where σ_{yu} is the yield stress of the unmodified epoxy. The value of r_{yu} is related to the radius of the plastic zone for the rubber modified epoxy, r_y, through equation 7.47. The value of r_y is also used for the calculation of the contribution of shear yielding, ΔG_s, and void growth, ΔG_v.

7.8 Application of the theoretical model

The mathematical model described in the previous sections was applied to the 15phrRME160 and 15phrRME120 materials. The calculation procedure is as follows:

(i) calculate the volume fraction of rubber, V_{fr}, and the volume fraction of void, V_{fv}, from the SEM micrographs; equation 7.28;
(ii) calculate the scaling factors, $f_u(da/dN)$ and $f_r(da/dN)$, from the fatigue crack growth rate data; equations 7.52 and 7.54;
(iii) estimate the plastic zone size of the unmodified epoxy, r_{yu}, using the K_u value; equation 7.55;
(iv) estimate the von Mises stress concentration factor, K_{vm}, by FEA; Fig.7.1;
(v) calculate the dissipated energy, ΔG_s, ΔG_v, ΔG_r and G_0, using the above parameters and the material properties, σ_{yc} (compressive yield stress of the matrix epoxy), γ_f (shear fracture strain of the matrix epoxy) and Γ_t (tearing energy of rubber); equations 7.35, 7.49, 7.51 and 7.53.

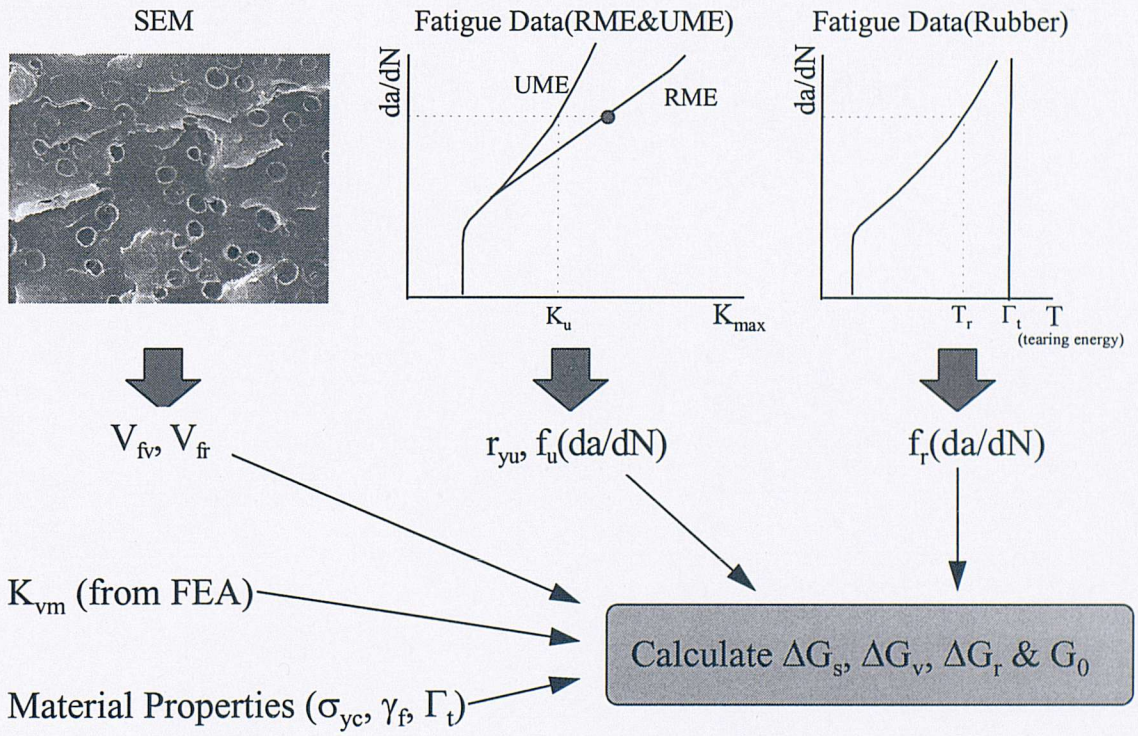


Fig.7.11 Procedures for the calculation of the energy terms

The material properties used for the calculation are shown in Table 7.1. It should be noted that the rate of loading (and of unloading) in the fatigue tests is far higher than that in the static tests (The rate of loading is estimated to be approximately 1000mm/min in the fatigue tests, as discussed in section 5.4). Therefore, the material properties under fatigue loadings are different in value from those in the static tests. The values of σ_{yc} and γ_f were estimated by extrapolating Huang's data in static tests (where the loading rate was in the range of 0.2mm/min to 20mm/min) [7]. The rate dependency of the modulus was measured using DMTA, in order to estimate the approximate modulus value in the fatigue tests. The Γ_t value in the fatigue tests was assumed to be the same as under the static loading conditions.

Table 7.1 The material properties for the calculation

Material	σ_{yc}(MPa)	γ_f	Γ_t(J/m^2)	E(GPa)
15phrRME160 (static)	116	0.71	460	2.56
15phrRME160 (fatigue)	142	0.63	460	2.67
15phrRME120 (static)	103	0.53	460	2.43
15phrRME120 (fatigue)	126	0.47	460	2.51

7.8.1 15phrRME160

For the 15phrRME160 material, five calculation points were chosen; K_{max}=0.61, 1.0, 2.2, 3.3 and 4.03(static)MPam$^{1/2}$. These correspond to G_{max} values of 0.12, 0.33, 1.59, 3.58 and 5.57kJ/m^2. Table 7.2 shows the volume fraction of the rubber and voids measured from the SEM micrographs and the calculated r_{yu} values.

The calculated energies dissipated by each mechanism and the total dissipated energy, G_{calc}, are plotted against the measured G_{max} value in Fig.7.12. The dissipated energy terms arising from shear yielding, void growth and rubber bridging increase with increasing the measured G_{max} value. The dissipated energy by shear yielding, ΔG_s, has the largest contribution to the total dissipated energy,

and the dissipated energy by void growth, ΔG_v, has the second largest contribution. The contribution of rubber bridging is rather small compared to the other two mechanisms, i.e. shear yielding and void growth.

Table 7.2 The values of V_{fr}, V_{fv0} and r_{yu} for 15phrRME160

K_{max} (MPam$^{1/2}$)	G_{max} (kJ/m^2)	da/dN (mm/cycle)	V_{fr}	V_{fv0}	r_{yu} (μm)
0.61	0.12	$2x10^{-6}$	0.24	0.245	1.47
1.0	0.33	$6x10^{-5}$	0.24	0.25	3.00
2.2	1.59	$1x10^{-2}$	0.24	0.30	5.15
3.3	3.58	$1x10^{-1}$	0.24	0.37	6.09
4.03(static)	5.57	---	0.24	0.39	9.23

Note : K_{max} means the measured K_{max} value.
G_{max} means the measured G_{max} value.

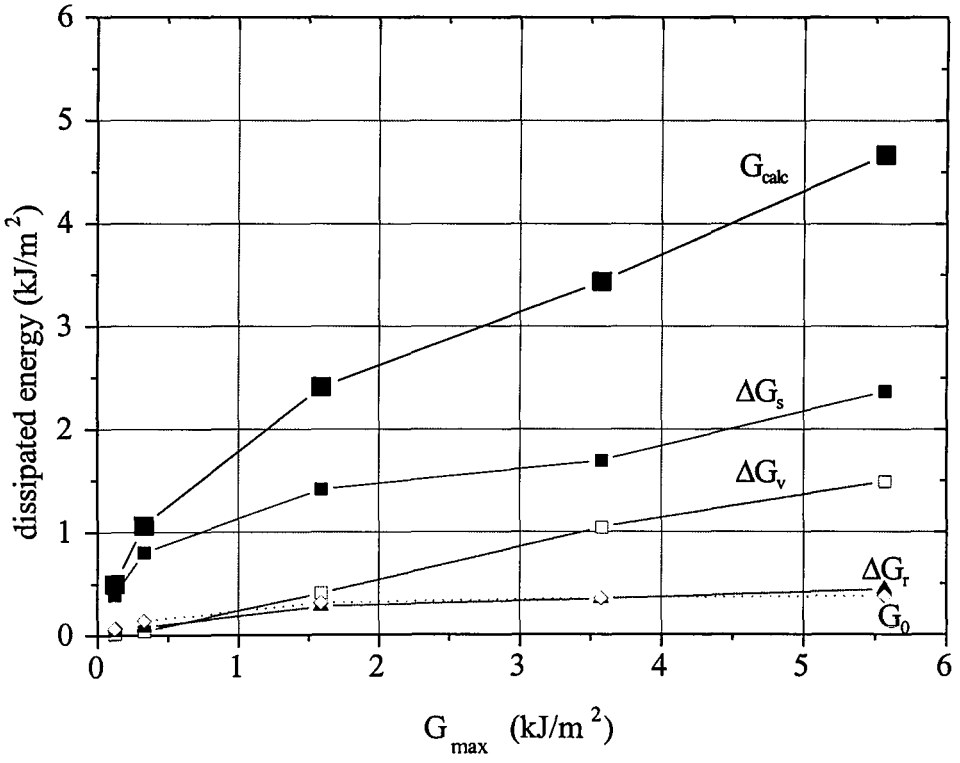


Fig.7.12 Calculated dissipated energy terms plotted against measured G_{max} for 15phrRME160 (ΔG_s: shear yielding, ΔG_v: void growth, ΔG_r: rubber bridging, G_0: unmodified epoxy, G_{calc}: total dissipated energy)

Table 7.3 summarises the calculated dissipated energies. The discussions below could be phrased in terms of comparisons of K_{max}, or G_{max}, and the former approach has been adapted. The K_{calc} value was calculated via the relationship between K and G, i.e. $G=(1-\nu^2)K^2/E$. Comparing the measured K_{max} values with the calculated values, K_{calc}, there is a fairly good agreement between them when K_{max} is relatively large. However, the K_{calc} values are rather higher than the measured K_{max} values, when K_{max} is relatively small. In other words, the dissipated energy is overestimated when K_{max} is relatively small. It is suggested that this is caused by an overestimation of the contribution from the shear yielding mechanism. This suggestion arises from the observation at K_{max}=0.61MPa·m$^{1/2}$ (G_{max}=0.12kJ/m^2). For the 15phrRME160 material, the K-transition value, where the toughening mechanisms, such as shear yielding and void growth, start to be active, is approximately 0.59MPa·m$^{1/2}$, as discussed in section 5.4. Therefore, the dissipated energy arising from these toughening mechanisms should still be small at K_{max}=0.61MPa·m$^{1/2}$, since this K_{max} value is very close to the K-transition value. However, the calculated dissipated energy by the shear yielding mechanism is not small compared to the G_0 value, which is the dissipated energy originating from the unmodified epoxy, as shown in Table 7.3. Hence, it might be necessary to modify the theoretical model to be consistent with the concept of the K-transition value.

Table 7.3 Dissipated energy due to each mechanism for 15phrRME160

K_{max}	G_{max}	ΔG_s	ΔG_v	ΔG_r	G_0	G_{calc}	K_{calc}
0.61	0.12	0.39	0.01	0.04	0.06	0.50	1.23
1.0	0.33	0.80	0.04	0.08	0.14	1.06	1.80
2.2	1.59	1.41	0.41	0.28	0.31	2.41	2.71
3.3	3.58	1.69	1.04	0.35	0.36	3.44	3.24
4.03(static)	5.57	2.37	1.49	0.44	0.38	4.67	3.70

Note : units for G_{max}, ΔG_s, ΔG_v, ΔG_r, G_0 and G_{calc} are kJ/m^2
units for K_{max} and K_{calc} are MPam$^{1/2}$

7.8.2 15phrRME120

For the 15phrRME120 material, five calculation points were chosen; K_{max}=0.3, 0.5, 0.9, 1.6 and 2.47(static)MPam$^{1/2}$. The corresponding G_{max} values are 0.03, 0.09, 0.28, 0.89 and 2.20kJ/m^2. Table 7.4 shows the volume fraction of rubber and void measured from SEM micrographs and the calculated r_{yu} values.

Table 7.4 The values of V_{fr}, V_{fv0} and r_{yu} for 15phrRME120

K_{max} (MPam$^{1/2}$)	G_{max} (kJ/m^2)	da/dN (mm/cycle)	V_{fr}	V_{fv0}	r_{yu} (μm)
0.3	0.03	1x10^{-8}	0.21	0.21	0.49
0.5	0.09	1x10^{-5}	0.21	0.21	1.14
0.9	0.28	3x10^{-4}	0.21	0.215	2.43
1.6	0.89	1x10^{-2}	0.21	0.245	3.04
2.47(static)	2.20	---	0.21	0.27	5.39

Note : K_{max} means the measured K_{max} value
G_{max} means the measured G_{max} value

The calculated energies dissipated by each mechanisms and the total dissipated energy, G_{calc}, are plotted against the measured G_{max} value in Fig.7.13. The dissipated energy terms arising from shear yielding, void growth and rubber bridging increase with increasing the measured G_{max} value. The dissipated energy by shear yielding, ΔG_s, has the largest contribution to the whole dissipated energy, as for the 15phrRME160 material However, the dissipated energy by void growth, ΔG_v, does not have such a large contribution to the total dissipated energy, when compared with the 15phrRME160 material.

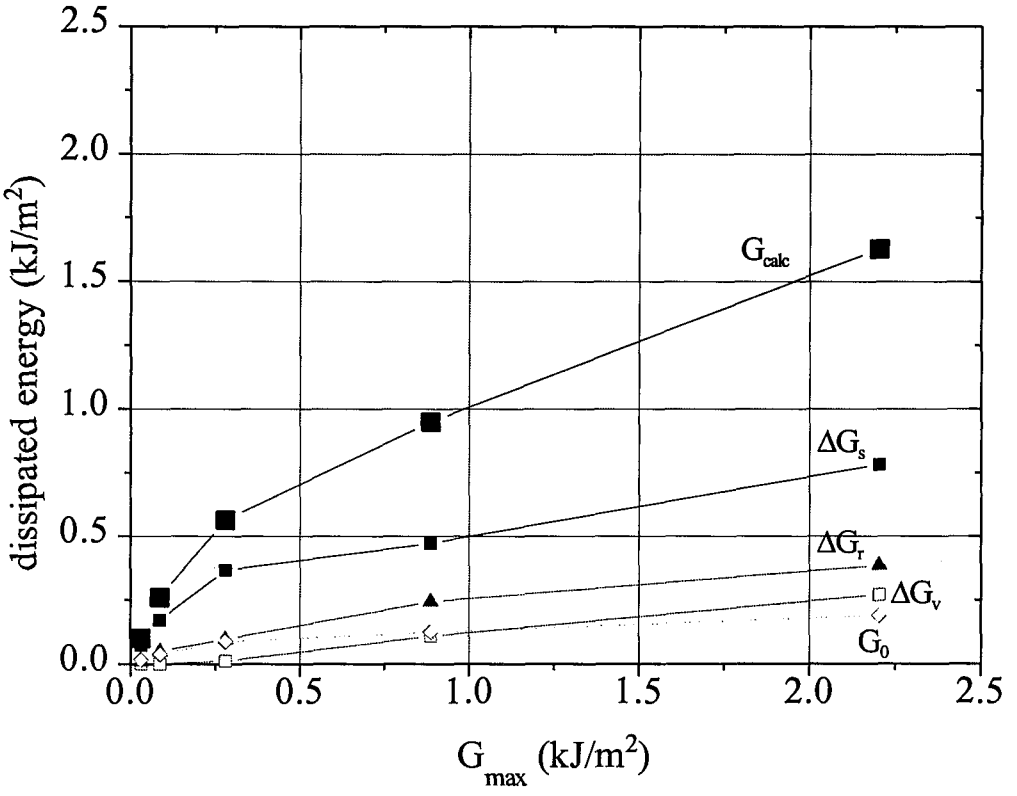


Fig.7.13 Calculated dissipated energy terms plotted against measured G_{max} for 15phrRME120 (ΔG_s: shear yielding, ΔG_v: void growth, ΔG_r: rubber bridging, G_0: unmodified epoxy, G_{calc}: total dissipated energy)

Table 7.5 summarises the calculated dissipated energies. As for the 15phrRME160 material, there is a fairly good agreement between the K_{max} and K_{calc} values when K_{max} is relatively high. However, the K_{calc} values again are rather higher than the measured K_{max} values, when K_{max} is relatively small. Therefore, the dissipated energy is overestimated when K_{max} is relatively small. It is suggested again that this is caused by an overestimation of the shear yielding mechanism, as for the 15phrRME160 material. This suggestion again arises from the observations at K_{max}=0.3MPa·m$^{1/2}$ (G_{max}=0.03kJ/m^2) and K_{max}=0.5MPa·m$^{1/2}$ (G_{max}=0.09kJ/m^2). For the 15phrRME120 material, the K-transition value, where the toughening mechanisms, such as shear yielding and void growth, start to be active, is approximately 0.46MPa·m$^{1/2}$, as discussed in section 5.4. Therefore, the dissipated energy arising from these toughening mechanisms should be still very small at K_{max}=0.3MPa·m$^{1/2}$ and K_{max}=0.5MPa·m$^{1/2}$. However, the calculated dissipated energy by the shear yielding mechanism is not small compared to the G_0

value, which is the dissipated energy originating from the unmodified epoxy, as shown in Table 7.5. Hence, again, it might be necessary to modify the theoretical model to be consistent with the concept of the K-transition value.

Table 7.5 Dissipated energy due to each mechanism for 15phrRME120

K_{max}	G_{max}	ΔG_s	ΔG_v	ΔG_r	G_0	G_{calc}	K_{calc}
0.3	0.03	0.07	0.00	0.01	0.02	0.10	0.54
0.5	0.09	0.17	0.00	0.05	0.04	0.26	0.86
0.9	0.28	0.37	0.01	0.10	0.09	0.54	1.27
1.6	0.89	0.47	0.11	0.24	0.12	0.94	1.64
2.47(static)	2.20	0.78	0.27	0.39	0.19	1.63	2.12

Note : units for G_{max}, ΔG_s, ΔG_v, ΔG_r, G_0 and G_{calc} are kJ/m^2
units for K_{max} and K_{calc} are $MPam^{1/2}$

7.9 Modification of the theoretical model

The results for both the 15phrRME160 and 15phrRME120 materials suggest that the theoretical model may overestimate the dissipated energy by the shear yielding mechanism, especially when the K_{max} value is relatively small. The calculated dissipated energy by the shear yielding mechanism at a relatively low K_{max} value is too large from the viewpoint of the K-transition.

In the theoretical model, it is assumed that the size (i.e. the cross-sectional area) of the shear band is given by the following equation, as discussed in section 7.4:

$$S(r) = \pi r_p^2(1-r/r_y) \qquad (7.56)$$

where S(r) is the cross-sectional area of the shear band, r_p is the radius of the rubber particle, r is the distance from the crack tip, and r_y is the plastic zone radius. This equation means that the shear band has the same size as the rubber particle near the crack, and the shear band disappears at the boundary of the

plastic zone. This equation also suggests that the shear band size at r=0 is always the same as the rubber particle size, regardless of the plastic zone size (i.e. regardless of the K_{max} value). This suggestion is not consistent with the concept of the K-transition. The shear band size should be smaller than the rubber particle size (even at r=0) when the K_{max} value is relatively small.

From the viewpoint of the K-transition, equation 7.56 may be modified as follows:

$$S(r) = \pi r_p^2(1-r/r_y)\, f(r_y) \tag{7.57}$$

$f(r_y)$ is a scaling factor and a function of the plastic zone size, r_y, which is given by:

$$f(r_y) = \begin{cases} 0 & (r_y < r_p) \\ [1/\{(c-1)r_p\}]r_y - 1/(c-1) & (r_p \le r_y \le cr_p) \\ 1 & (cr_p < r_y) \end{cases} \tag{7.58}$$

where c is a parameter. The shape of the function $f(r_y)$ is shown in Fig.7.14. Equations 7.57 and 7.58 mean that the shear band does not exist when the plastic zone is smaller than the rubber particle, and that even when the plastic zone is larger than the rubber particle the shear band size at r=0 is smaller than the rubber particle size, except when the plastic zone is far larger than the rubber particle (i.e. when $cr_p < r_y$). The parameter c is assumed to be fifty from the FEA results by Huang [7].

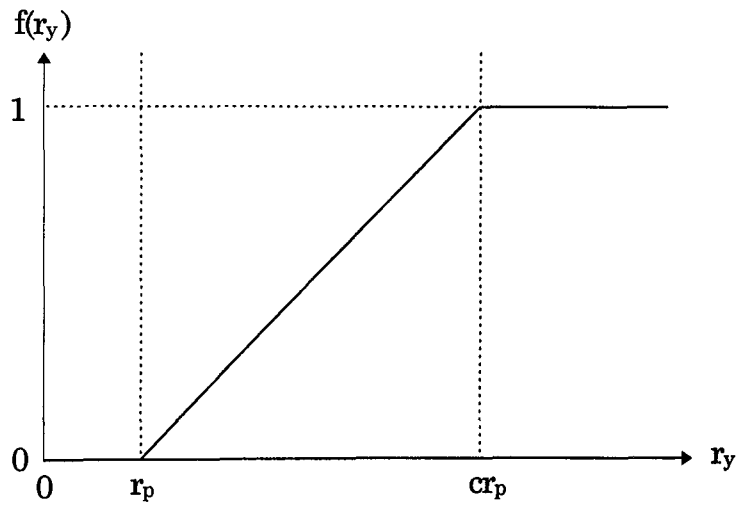


Fig.7.15 Shear band scaling function f(ry)

This modified model is consistent with the concept of K-transition. When the plastic zone is smaller than the rubber particle, the shear band does not form and consequently the shear yielding mechanism is not active. The results calculated using this modified model will be discussed in the next section.

7.10 Application of the modified theoretical model

7.10.1 15phrRME160

Fig.7.16 shows the calculated dissipated energy for the 15phrRME160 material, using the modified theoretical model. The general trend is the same as for the results using the previous model shown in Fig.7.12. The shear yielding mechanism has the largest contribution to the total dissipated energy.

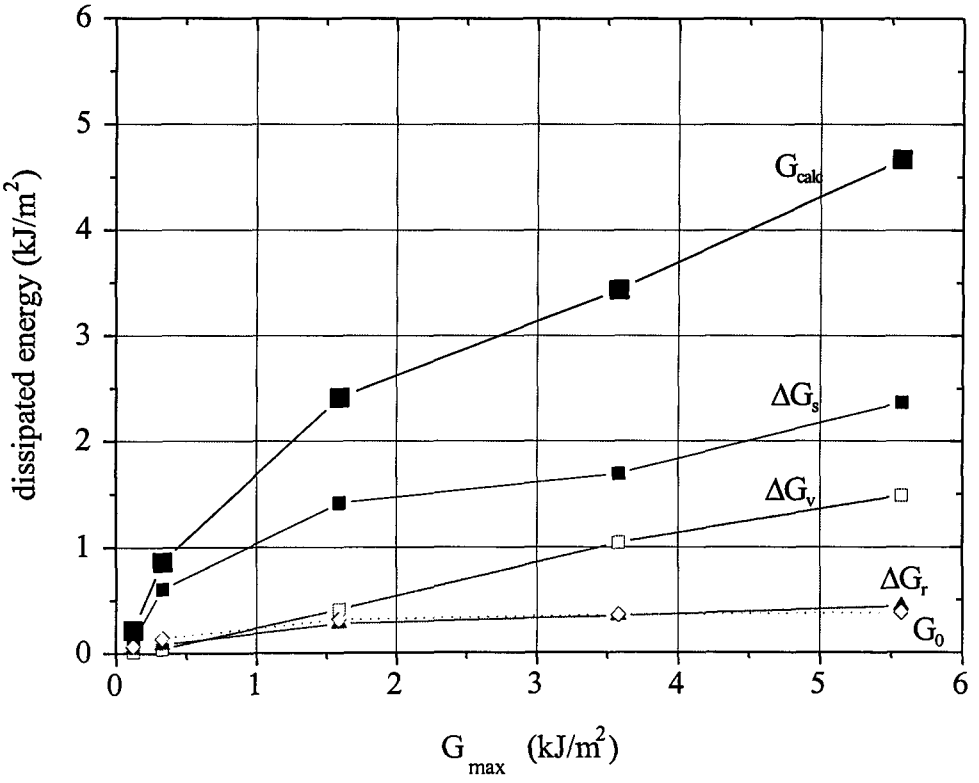


Fig.7.16 Calculated dissipated energy terms plotted against measured G_{max} for 15phrRME160, using the modified model (ΔG_s: shear yielding, ΔG_v: void growth, ΔG_r: rubber bridging, G_0: unmodified epoxy, G_{calc}: total dissipated energy)

Table 7.6 Dissipated energy due to each mechanism for 15phrRME160 (modified model)

K_{max}	G_{max}	ΔG_s	ΔG_v	ΔG_r	G_0	G_{calc}	K_{calc}
0.61	0.12	0.11	0.01	0.04	0.06	0.22	0.81
1.0	0.33	0.60	0.04	0.08	0.14	0.87	1.63
2.2	1.59	1.41	0.41	0.28	0.31	2.41	2.71
3.3	3.58	1.69	1.04	0.35	0.36	3.44	3.24
4.03(static)	5.57	2.37	1.49	0.44	0.38	4.67	3.70

Note : units for G_{max}, ΔG_s, ΔG_v, ΔG_r, G_0 and G_{calc} are kJ/m^2
units for K_{max} and K_{calc} are $MPam^{1/2}$

Table 7.6 summarises the calculated dissipated energies. Comparing the measured K_{max} values with the calculated K values, then the K_{calc} values are still rather larger than the measured K_{max} values when K_{max} is relatively small. However, the K_{calc} values are much closer to the measured K_{max} values, compared to the results using the previous model. When K_{max} is relatively large, there is a good agreement between the K_{max} and K_{calc} values.

Table 7.7 shows the contribution of each mechanism to the total dissipated energy. The shear yielding mechanism has the largest contribution, approximately a half of the total dissipated energy. The contribution of the shear yielding mechanism reaches the maximum value in the intermediate K_{max} region (i.e. K_{max}=1.0MPam$^{1/2}$), and it is slightly lower in the low K_{max} region and in the high K_{max} region. The contribution of the void growth mechanism is very small when the K_{max} value is relatively small, but it increases with an increase of the K_{max} value. In the low K_{max} region, the toughening mechanisms such as shear yielding and void growth are not highly active, since the plastic zone size is relatively small. Therefore, the contribution of shear yielding is relatively lower. In the high K_{max} region, as the void growth mechanism becomes more important, the contribution of shear yielding is lower again. This may explain why the contribution of shear yielding possesses through a maximum value in the intermediate K_{max} region. The contribution of the rubber bridging mechanism is lower than 16% of the total dissipated energy, in any K_{max} region. Thus, the rubber bridging mechanism

makes only a minor contribution to the total dissipated energy.

Table 7.7 Contribution of each mechanism for 15phrRME160 (modified model)

K_{max} (MPam$^{1/2}$)	G_{max} (kJ/m^2)	$\Delta G_s/G_{calc}$	$\Delta G_v/G_{calc}$	$\Delta G_r/G_{calc}$	G_0/G_{calc}
0.61	0.12	0.40	0.05	0.16	0.29
1.0	0.33	0.70	0.05	0.09	0.16
2.2	1.59	0.59	0.17	0.11	0.13
3.3	3.58	0.49	0.30	0.10	0.10
4.03(static)	5.57	0.51	0.32	0.09	0.08

7.10.2 15phrRME120

Fig.7.17 shows the calculated dissipated energies for the 15phrRME120 material, using the modified theoretical model. The general trend is the same as for the 15phrRME160. The shear yielding mechanism has the largest contribution to the total dissipated energy. However, the dissipated energy arising from the void growth mechanism, ΔG_v, does not possess a large contribution to the total dissipated energy, compared to the 15phrRME160 material.

Table 7.8 summarises the calculated dissipated energies. Comparing the measured K_{max} values with the calculated K values, K_{calc}, there is a good agreement between them in any K_{max} region. At K_{max}=0.3MPam$^{1/2}$, (which is below the K-transition value, i.e 0.46MPam$^{1/2}$), the dissipated energies from the shear yielding and void growth mechanisms are calculated to be very small. The intrinsic dissipated energy originating from the unmodified epoxy, G_0, is dominant in this region.

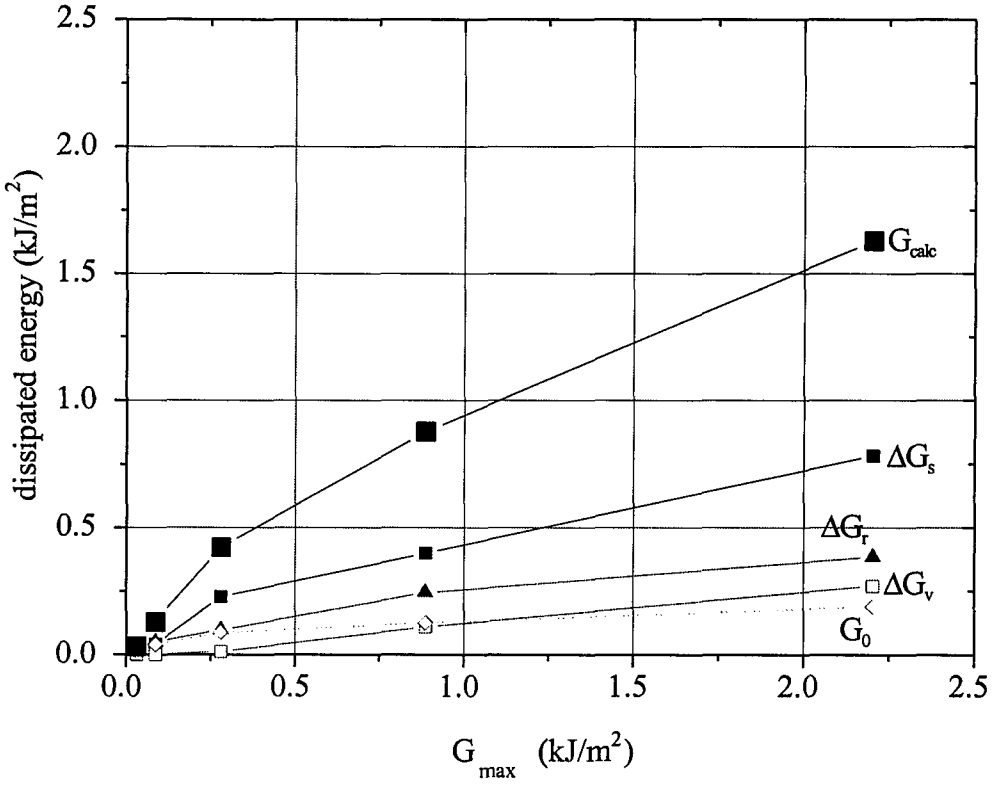


Fig.7.17 Calculated dissipated energy terms plotted against measured K_{max} for 15phrRME120, using the modified model (ΔG_s: shear yielding, ΔG_v: void growth, ΔG_r: rubber bridging, G_0: unmodified epoxy, G_{calc}: total dissipated energy)

Table 7.8 Dissipated energy due to each mechanism for 15phrRME120 (modified model)

K_{max}	G_{max}	ΔG_s	ΔG_v	ΔG_r	G_0	G_{calc}	K_{calc}
0.3	0.03	0.01	0.00	0.01	0.02	0.03	0.31
0.5	0.09	0.04	0.00	0.05	0.04	0.13	0.61
0.9	0.28	0.23	0.01	0.10	0.09	0.42	1.10
1.6	0.89	0.40	0.11	0.24	0.12	0.87	1.58
2.47(static)	2.20	0.78	0.27	0.39	0.19	1.63	2.12

Note : units for G_{max}, ΔG_s, ΔG_v, ΔG_r, G_0 and G_{calc} are kJ/m^2
units for K_{max} and K_{calc} are MPam$^{1/2}$

Table 7.9 shows the contribution of each mechanism to the total dissipated energy. When the K_{max} value is relatively high, the shear yielding mechanism has the largest contribution, approximately a half of the total dissipated energy. However, the contribution arising from the shear yielding mechanism is not dominant when the K_{max} value is relatively small. Instead, the dissipated energy arising from the rubber bridging mechanism and the unmodified epoxy is dominant in this region, especially when the K_{max} value is smaller than the K-transition value (i.e. 0.46MPam$^{1/2}$). These results are in agreement with the concept of K-transition in that the toughening mechanisms such as shear yielding and void growth are not active below the K-transition value. The contribution of the void growth mechanism is very small when the K_{max} value is relatively small, but it increases with an increase of the K_{max} value. However, the contribution of the void growth mechanism is not so large as for the 15phrRME160 material, even when the K_{max} value is relatively high. Indeed, the rubber bridging mechanism has a greater contribution to the total dissipated energy than the void growth mechanism for this material.

Table 7.9 Contribution of each mechanism for 15phrRME120 (modified model)

K_{max} (MPam$^{1/2}$)	G_{max} (kJ/m^2)	$\Delta G_s/G_{calc}$	$\Delta G_v/G_{calc}$	$\Delta G_r/G_{calc}$	G_0/G_{calc}
0.3	0.03	0.18	0.00	0.30	0.52
0.5	0.09	0.31	0.00	0.38	0.30
0.9	0.28	0.54	0.03	0.23	0.21
1.6	0.89	0.46	0.12	0.28	0.14
2.47(static)	2.20	0.48	0.17	0.24	0.12

The above results for the 15phrRME160 and 15phrRME120 materials also reflect the ability of the matrix to undergo plastic deformation on the energy dissipated from the toughening mechanisms. As discussed in section 5.2.3, due to the lower crosslink density, the 15phrRME160 material is relatively ductile and can undergo more plastic deformation than the 15phrRME120 material. Thus, the toughening mechanisms such as shear yielding and void growth make a more

dominant contribution to the total dissipated energy for the 15phrRME160 material. On the other hand, the 15phrRME120 material has a higher crosslink density, and its ductility is lower than that of the 15phrRME160 material. Therefore, the ability of the matrix epoxy to undergo plastic deformation is relatively low. Hence, the contribution of the shear yielding and void growth mechanisms is relatively low, and the contribution of rubber bridging mechanism is somewhat higher, compared to the 15phrRME160 material.

7.11 Concluding remarks

In the present Chapter, a theoretical model has been developed to quantify the dissipated energy arising from the toughening mechanisms, such as shear yielding, void growth and rubber bridging, in fatigue conditions. The calculated results using the model are in good agreement with the experimental results. The model also suggests that the shear yielding mechanism is the dominant toughening mechanism for both the 15phrRME160 and 15phrRME120 materials. However, the importance of the shear yielding mechanism is relatively low in the low K_{max} region, since the toughening mechanisms which involve plastic deformation are not sufficiently active due to the relatively small size of the plastic zone. The contribution of void growth increases steadily with an increase in the K_{max} value. The contribution of rubber bridging is relatively small for the 15phrRME160 material, but the rubber bridging mechanism does play a greater role in the 15phrRME120 material than in the 15phrRME160 material.

Chapter Eight

Fatigue Behaviour of Thermoplastic Modified Epoxies

8.1 Introduction

In the previous Chapters, we discussed the fatigue behaviour of the rubber modified epoxies. The fatigue behaviour of the rubber modified epoxies is affected by the material properties and the microstructural parameters. The influence of the crosslink density of the epoxy matrix, the volume fraction of rubber and the rubber particle size were studied in detail, as discussed in Chapter Five. However, the microstructure of the rubber modified epoxies used in the present study is always particulate, and other microstructures, such as co-continuous and phase-inverted microstructure, can not be achieved in the rubber modified epoxies.

In order to investigate the effect of the microstructure on the fatigue behaviour of the toughened epoxies more comprehensively, the thermoplastic (PES copolymer) modified epoxies were employed. As discussed in section 4.2.2, these thermoplastic modified epoxies have a wide variety of microstructures. Dispersed thermoplastic-rich particles and an epoxy-rich matrix are obtained when the amount of the added PES copolymer is relatively small, as for the rubber modified epoxies. However, the microstructure changes to be co-continuous with an increasing amount of added PES copolymer. Finally, phase-inversion with dispersed epoxy-rich particles and a thermoplastic-rich matrix is obtained when a relatively large amount of PES copolymer is added.

The fatigue behaviour of several types of PES copolymer modified epoxies will be discussed to investigate the influence of the microstructure. The SEM results of the fatigue fracture surface will also be shown in this Chapter.

8.2 Fatigue behaviour

The microstructures of the PES copolymer modified epoxies in this study are as summarised in Table 8.1 (micrographs are shown in section 4.2.2). The PES10 material has a particulate microstructure, i.e. thermoplastic-rich particles are dispersed in the epoxy-rich matrix. The PES20 material has a co-continuous microstructure, and the PES25 material has a phase inverted microstructure, i.e. epoxy-rich particles are dispersed in the thermoplastic-rich matrix.

Table 8.1 Microstructures of the PES copolymer modified epoxies

Material	PES copolymer (phr)	Microstructure	Figure
PES0	0	single phase	---
PES10	14.61	particulate	Fig.4.4(a)
PES20	32.67	co-continuous	Fig.4.4(b)
PES25	43.82	phase-inverted	Fig.4.4(c)

Note : "phr" means "per hundred resin"

8.2.1 Particulate microstructure

The fatigue crack growth rates of the PES0 (unmodified epoxy) and PES10 materials are shown in Fig.8.1. The PES10 material contains spherical thermoplastic-rich particles and continuous epoxy-rich matrix, similar to the rubber modified epoxies in the present study. Thus, according to the results from the rubber modified epoxies, it had been expected that there would be little difference in the fatigue crack growth rates between the PES0 and PES10 materials in a relatively low K_{max} region, but that the PES10 material would have a better fatigue resistance than the PES0 material in higher K_{max} region. However, it is observed that there is a very little difference in the fatigue curves between the two materials over the complete K_{max} region, not only in the threshold region. These fatigue results also reflect the fact that there is a very little difference in the values of the fracture toughness between the PES0 and PES10 materials, as discussed in section 4.5.2. The values are 0.50MPam$^{1/2}$ for the PES0 material and 0.61MPam$^{1/2}$ for the PES10 material.

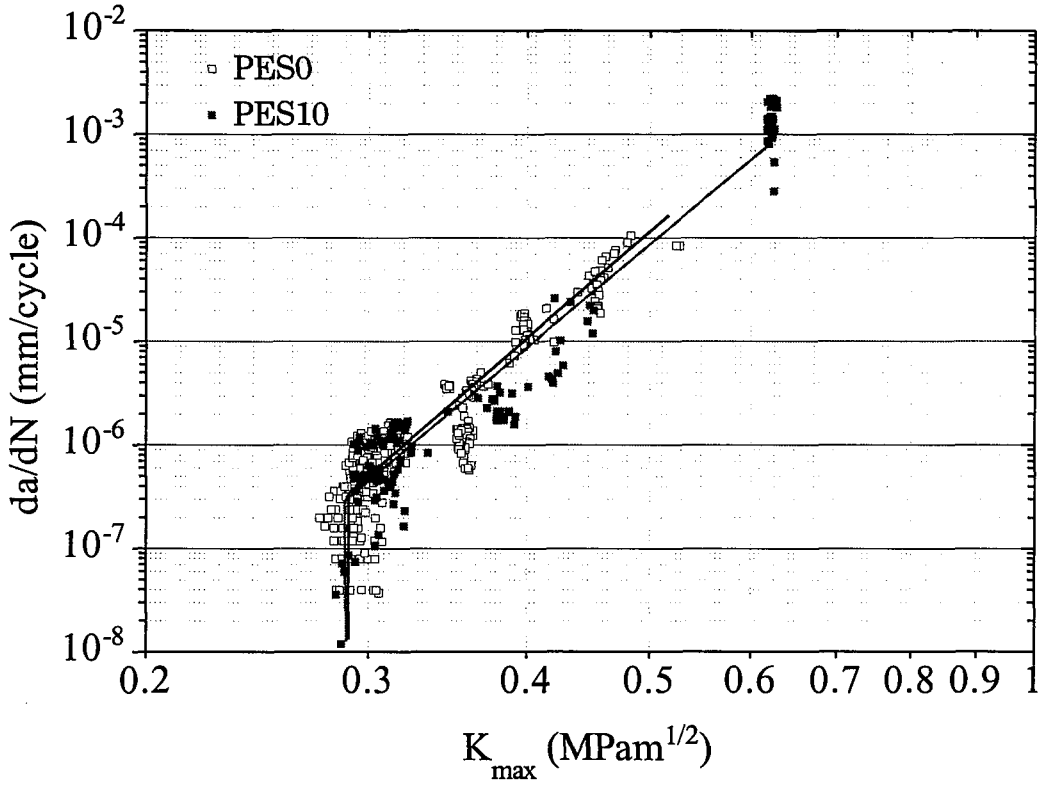


Fig.8.1 Fatigue crack growth rates for the PES0 and PES10 materials

Fig.8.2 shows the SEM micrographs of the fatigue surfaces of the PES10 material. Although the presence of the thermoplastic-rich particles can be seen, there is no signs of cavitation or debonding of the thermoplastic-rich particles. There are also no sign of plastic yielding of the epoxy-rich matrix surrounding the thermoplastic-rich particles. Kinloch et al. [96] also reported similar results on the static fracture of the PES copolymer modified epoxies, which had a thermoplastic particulate microstructure. It also can be seen in Fig.8.2 that there is faint evidence of ductile tearing in the thermoplastic-rich particles. Hence, from the work of Bucknall and Gilbert [116] and Hedrick et al. [117], the fatigue crack propagation process should be as follows. The first stage of crack propagation is brittle failure of the epoxy-rich matrix, leaving the more ductile thermoplastic-rich particles bridging behind the advancing crack front. Then, the thermoplastic-rich particles are torn apart. This bridging of the thermoplastic-rich particles would dissipate only a little energy, since rubber bridging in the rubber modified epoxies also dissipates only a small amount of energy during fatigue crack propagation, as discussed in Chapter Seven.

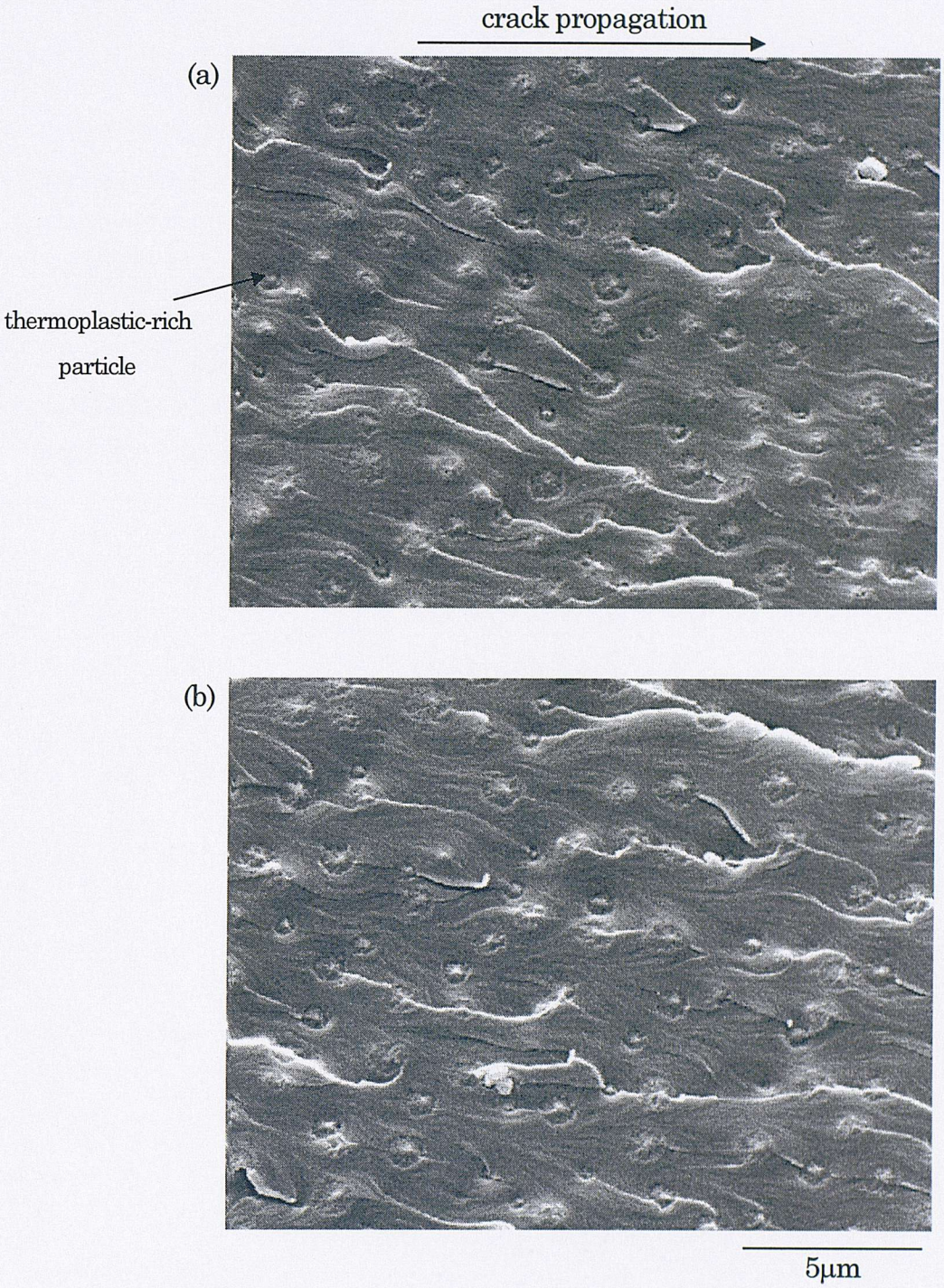


Fig.8.2 SEM micrographs for the PES10 material in fatigue fracture: (a) K_{max}=0.3MPam$^{1/2}$,(b) K_{max}=0.6MPam$^{1/2}$

8.2.2 Co-continuous microstructure

The fatigue crack growth rates of the PES0 (unmodified epoxy), PES10 (particulate microstructure) and PES20 (co-continuous microstructure) materials are shown in Fig.8.3. The fatigue resistance of the PES20 material, which has the co-continuous microstructure, is significantly improved compared with the PES0 and PES10 materials, whereas there is little difference in the fatigue resistance between the PES0 and PES10 materials. It may also be observed that the threshold value is increased from 0.29MPam$^{1/2}$, for PES0 and PES10, to 0.42MPam$^{1/2}$, for PES20. This suggests that the co-continuous microstructure is beneficial to the improvement of the fatigue resistance in the present system.

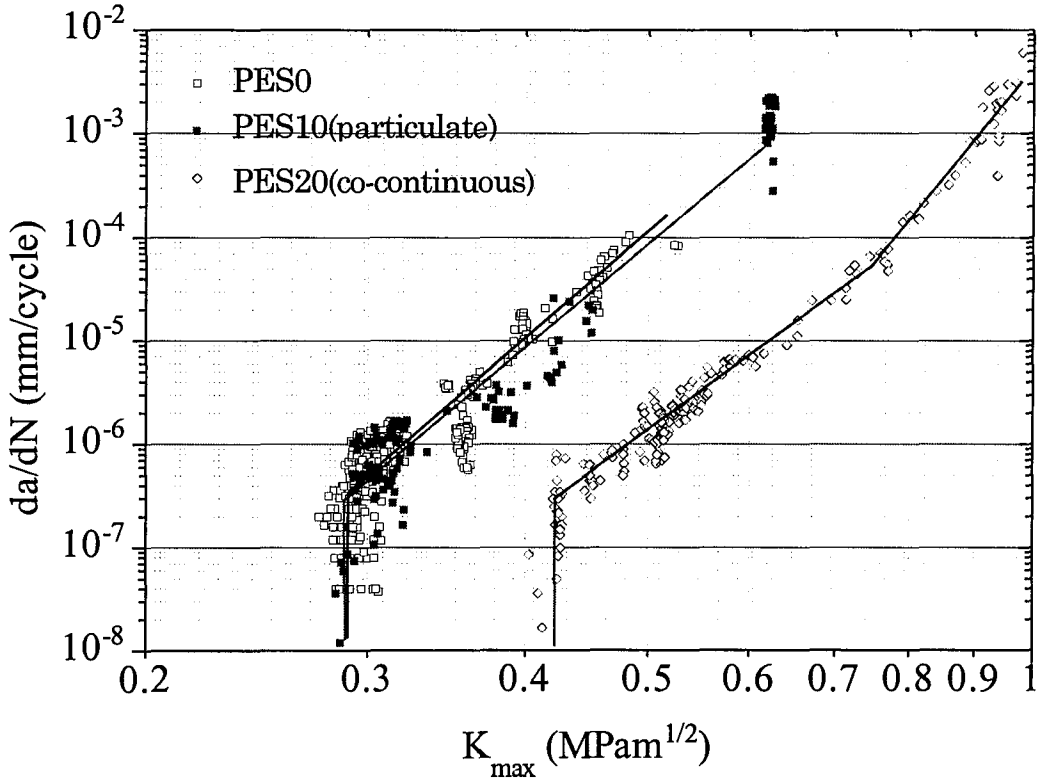


Fig.8.3 Fatigue crack growth rates for the PES0, PES10 and PES20 materials

In the material with the co-continuous microstructure, the crack must advance by the fracture of the thermoplastic-rich phase. It is considered that the thermoplastic-rich phase is more ductile than the epoxy-rich phase, and this is supported from the evidence of the ductile tearing of the thermoplastic-rich particles which was observed via the SEM studies, as discussed in section 8.2.1.

Further, the thermoplastic-rich phase of the PES20 material contains a certain amount of the dissolved epoxy, because the glass transition temperature, T_g, of the thermoplastic-rich phase (187.6°C) is higher than that of the pure PES copolymer. (The T_g value of the pure PES copolymer should lower than the T_g value (185.4°C) of the thermoplastic-rich phase in the PES10 material. The T_g values of the thermoplastic-rich phases are shown in Table 4.3 in section 4.3.2.) The molecular weight of the thermoplastic PES copolymer could be increased by chain extension through its reactive end-groups with the epoxy, and such chain extension reactions are known to be possible and to lead to an increase in the toughness of the thermoplastic [96]. Therefore, the thermoplastic-rich phase should be tougher than the epoxy-rich phase. Hence, as a result of the co-continuous microstructure, the crack is forced to advance through the tougher thermoplastic-rich phase, and this must lead to an increase in the fatigue resistance.

SEM micrographs of the fatigue surfaces of the PES20 material are shown in Fig.8.4. This figure clearly shows that the fatigue crack propagation has occurred through both the epoxy-rich and thermoplastic-rich domains. In the epoxy-rich domain, the fracture surface is relatively smooth and the thermoplastic-rich sub-particles can be observed, as for the PES10 material. On the other hand, in the thermoplastic-rich domain, the fracture surface is rather rough and appears to be relatively ductile in nature. It is also observed in the thermoplastic-rich domain that the sub-particles, with a radius of approximately 1μm (which should be epoxy-rich sub-particles) are embedded in the thermoplastic-rich matrix, and that the fatigue crack has propagated only through the thermoplastic-rich matrix (i.e. not through the epoxy-rich sub-particles).

Comparing the thermoplastic-rich domain at K_{max}=0.45MPam$^{1/2}$ and that at K_{max}=1.0MPam$^{1/2}$, the latter seems to have a rougher surface than the former. This implies that more fracture surface is created at K_{max}=1.0MPam$^{1/2}$ than at K_{max}=0.45MPam$^{1/2}$, during the fatigue crack propagation. This reflects the fact that more energy is dissipated during crack propagation in the higher K_{max} region.

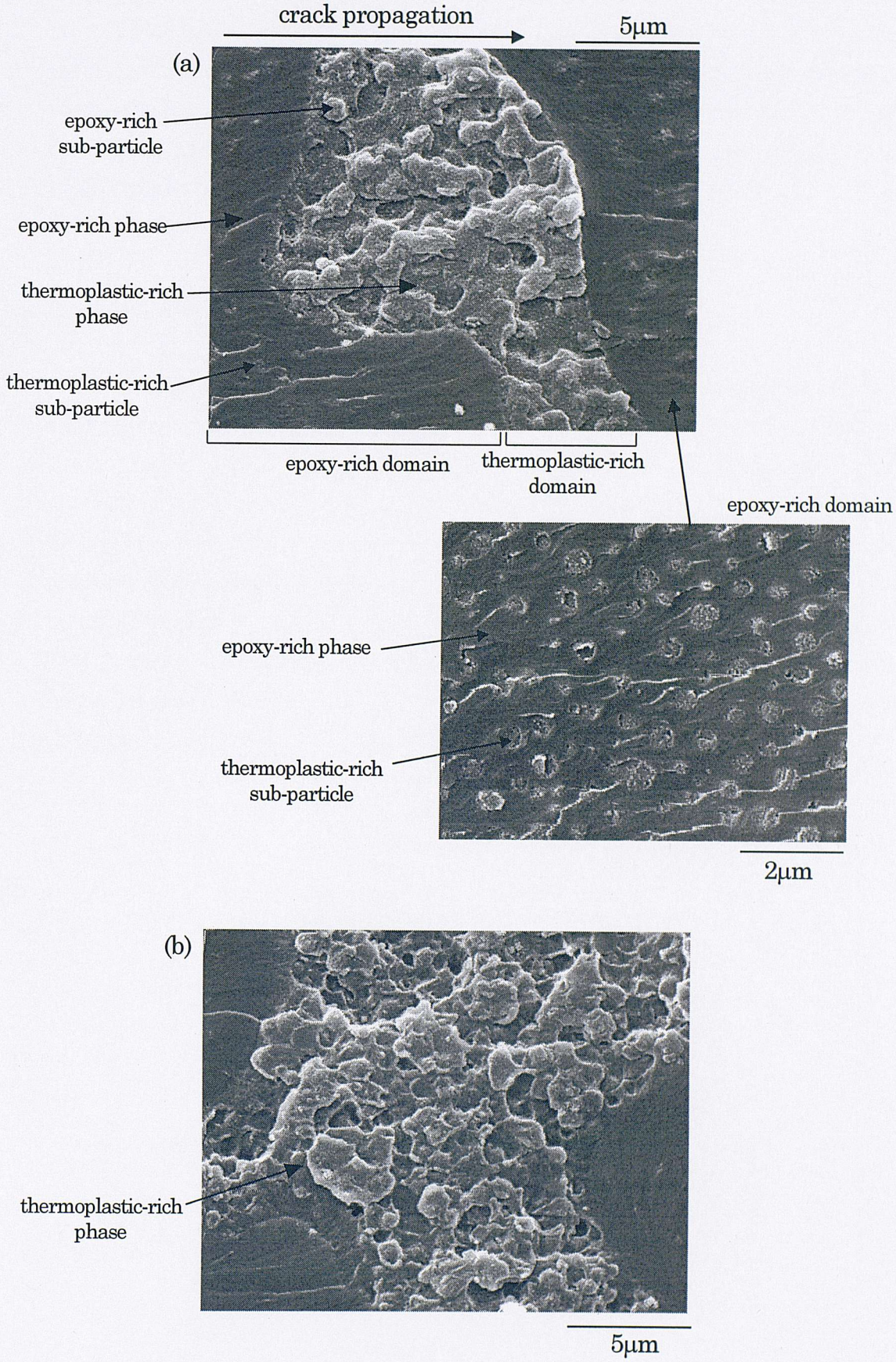


Fig.8.4 SEM micrographs for the PES20 material in fatigue fracture: (a) K_{max}=0.45MPam$^{1/2}$,(b) K_{max}=1.0MPam$^{1/2}$

The above SEM results clearly suggest that the crack has advanced through the tougher thermoplastic-rich phase. Since the crack propagation in the thermoplastic-rich phase dissipates more energy than in the epoxy-rich phase, during the fatigue crack propagation, the SEM micrographs also suggest that the PES20 material should indeed have a better fatigue resistance than the PES0 and PES10 materials.

8.2.3 Phase-inverted microstructure

The PES25 material possesses a phase-inverted microstructure, i.e. the epoxy-rich particles are dispersed in the thermoplastic-rich matrix. The fatigue crack growth rates of the PES0 (unmodified epoxy), PES20 (co-continuous microstructure) and PES25 (phase-inverted microstructure) materials are shown in Fig.8.5. The fatigue resistance of the PES25 material, which has a phase-inverted microstructure, is further improved compared with that of the PES20 material, which has a co-continuous microstructure. The threshold value of the PES25 material is also increased to 0.49MPam$^{1/2}$. This implies that the phase-inverted microstructure is more effective for the improvement of the fatigue resistance than the co-continuous microstructure.

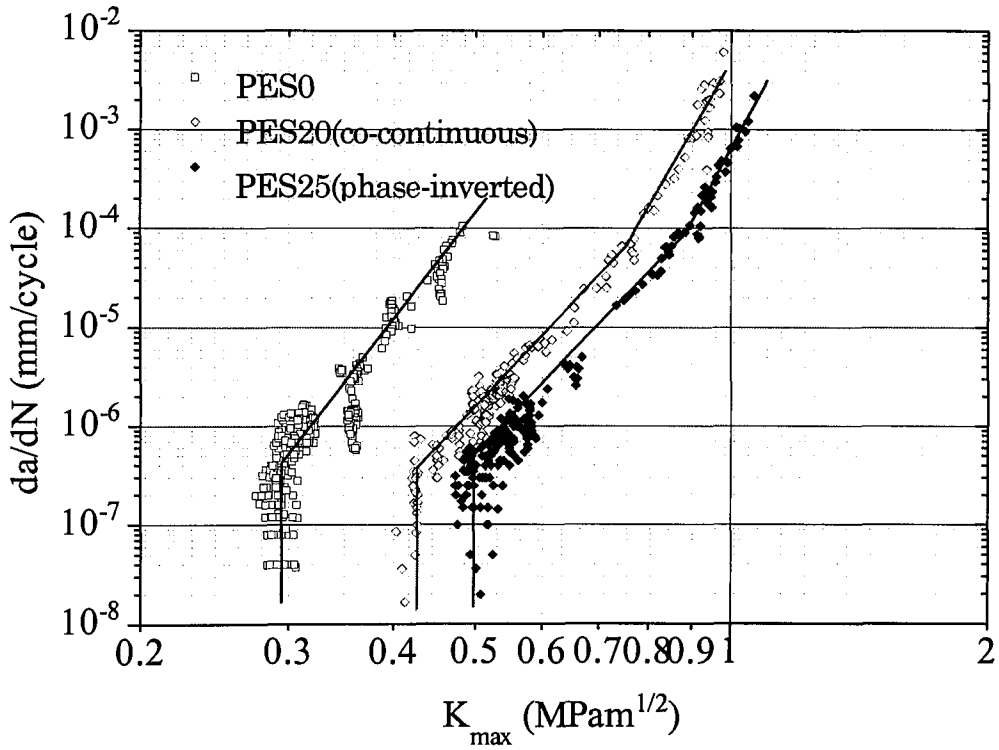


Fig.8.5 Fatigue crack growth rates for the PES0, PES20 and PES25 materials

This further improvement may be caused due to the disappearance of the brittle epoxy-rich domain. For the phase-inverted microstructure, the crack propagation has to, at least for the majority of the time, always occur within the thermoplastic-rich phase. On the other hand, for the co-continuous microstructure, the fatigue crack propagation does not always occur in the thermoplastic-rich phase, but the fatigue crack propagation sometimes occurs in the epoxy-rich phase, since epoxy-rich domains (where the epoxy-rich phase is the matrix) exist. The epoxy-rich phase is likely to be less tough than the thermoplastic-rich phase. Hence, the fatigue resistance for the co-continuous microstructure should be somewhat poorer than that for the phase-inverted microstructure. This may be why the material possessing a phase-inverted microstructure has the better fatigue resistance than the material possessing a co-continuous microstructure.

As shown in Table 4.3 in section 4.3.2, the glass transition temperature, T_g, of the thermoplastic-rich phase in the PES25 material is 191.6°C, which is higher than the T_g value (187.6°C) of the PES20 material. This implies that the amount of the epoxy dissolved into the thermoplastic phase in the PES25 material is greater than that in the PES20 material. As discussed in section 8.2.2, the dissolution of the epoxy resin into the thermoplastic could lead to an increase in the toughness of the thermoplastic due to chain extension reactions [96]. Thus, the thermoplastic-rich phase in the PES25 material itself could be somewhat tougher than that in the PES20 material, and this may also cause an increase in the fatigue resistance.

Hence, from the above discussions, the difference in the fatigue resistance between the PES20 and PES25 materials could be considered to arise partly from the difference in the microstructure and partly from the difference in the toughness of the thermoplastic-rich phase itself.

SEM micrographs of the fatigue surfaces of the PES25 material are shown in Fig.8.6. It is observed that the particles, with a radius of approximately 1μm (which should be epoxy-rich particles) are embedded in the thermoplastic-rich matrix. It is also observed that the fatigue crack has propagated through the thermoplastic-rich matrix, as for the thermoplastic-rich domain in the PES20 material.

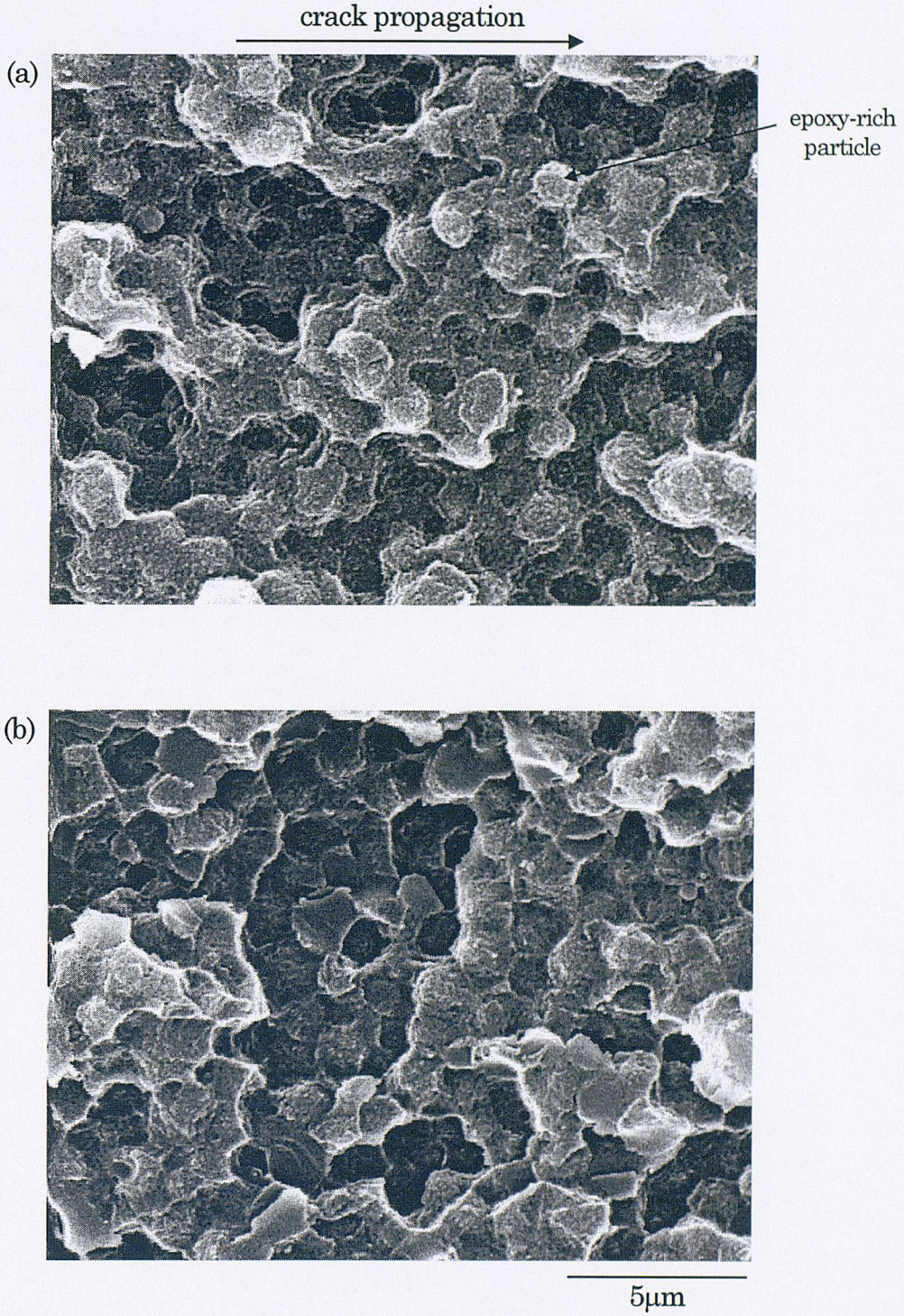


Fig.8.6 SEM micrographs for the PES25 material in fatigue fracture: (a) K_{max}=0.5MPam$^{1/2}$, (b) K_{max}=1.1MPam$^{1/2}$

Generally, for the material which has hard particles dispersed in a soft

matrix, a crack propagates only through the soft matrix due to the stress concentrations at the polar regions of the hard particles. In other words, the crack deflects and avoids the hard particles, as schematically shown in Fig.8.7. For the PES25 material, the dispersed particles are epoxy-rich and the matrix is thermoplastic-rich. This means that the hard particles are dispersed in the softer matrix. Therefore, the crack propagation process is likely to occur for the PES25 material, as shown schematically in Fig.8.7. This may explain why the fatigue crack has propagated only through the thermoplastic-rich matrix.

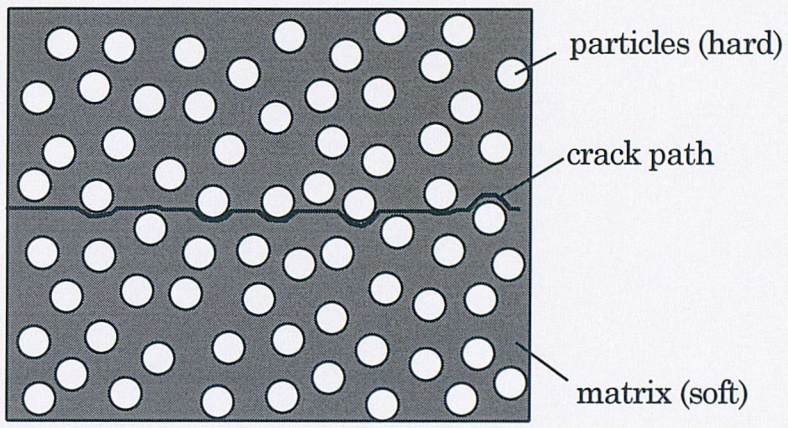


Fig.8.7 Crack deflection for the material possessing hard particles dispersed in a soft matrix

Comparing the fatigue surface at K_{max}=0.5MPam$^{1/2}$ and that at K_{max}=1.1MPam$^{1/2}$, the latter seems to be rougher than the former. This implies that more surface is created at K_{max}=1.1MPam$^{1/2}$ than at K_{max}=0.5MPam$^{1/2}$, during the fatigue crack propagation. Hence, as expected, more energy is dissipated during crack propagation at K_{max}=1.1MPam$^{1/2}$, than at K_{max}=0.5MPam$^{1/2}$.

8.2.4 Summary of the effect of microstructure

The fatigue crack growth rates of the PES copolymer modified epoxies in this study are schematically summarised in Fig.8.8. When the particulate microstructure is achieved, i.e. the thermoplastic-rich particles are dispersed in the epoxy-rich matrix, the improvement of the fatigue resistance due to the presence of

the thermoplastic-rich phase is minimal. This observation is suggested to arise because the thermoplastic-rich particles work only as bridging particles, and because (i) no cavitation (or debonding) of the thermoplastic particles, and (ii) no plastic yielding of the epoxy-rich matrix occurs.

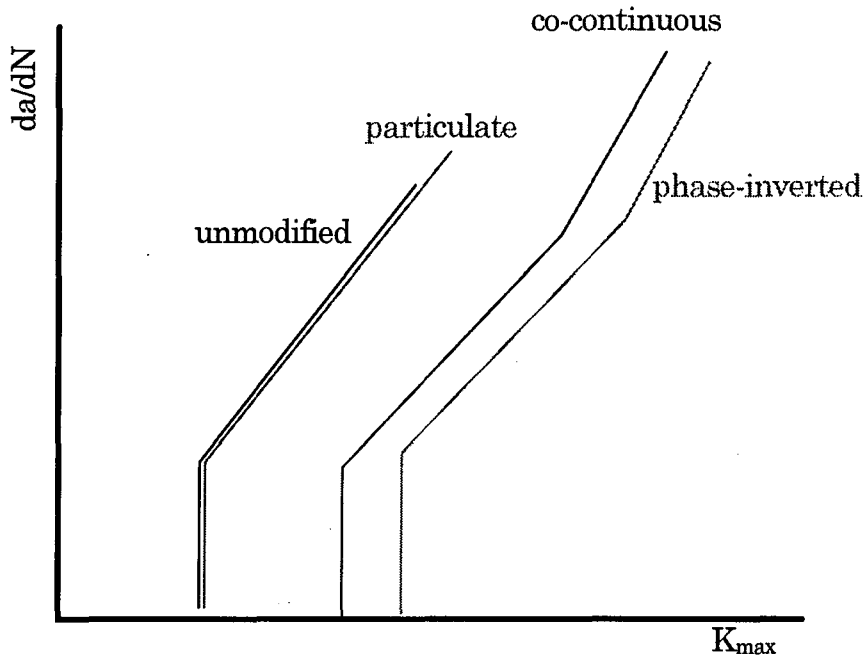


Fig.8.8 Schematic graph of the fatigue crack growth rates for the PES copolymer modified epoxies

When the microstructure is co-continuous or phase-inverted, the fatigue resistance is significantly improved, including the threshold values. In these microstructures, the tougher material now constitutes the continuous phase, since the thermoplastic-rich phase is most likely to be tougher than the epoxy-rich phase, as discussed before in section 8.2.2. Hence, the crack must advance through the tougher thermoplastic-rich phase, and this leads to an increase in the fatigue resistance.

The difference between the co-continuous and phase-inverted microstructures is in the proportion of the thermoplastic-rich domain to the whole specimen. The crack propagation always occurs inside the thermoplastic-rich matrix phase for the phase-inverted microstructure, whereas a certain amount of

the fatigue crack propagation occurs inside the epoxy-rich phase for the co-continuous microstructure; since there exist epoxy-rich domains as shown schematically in Fig.8.9. Hence, the fatigue resistance for the material with the co-continuous microstructure is poorer than that for the material with the phase-inverted microstructure.

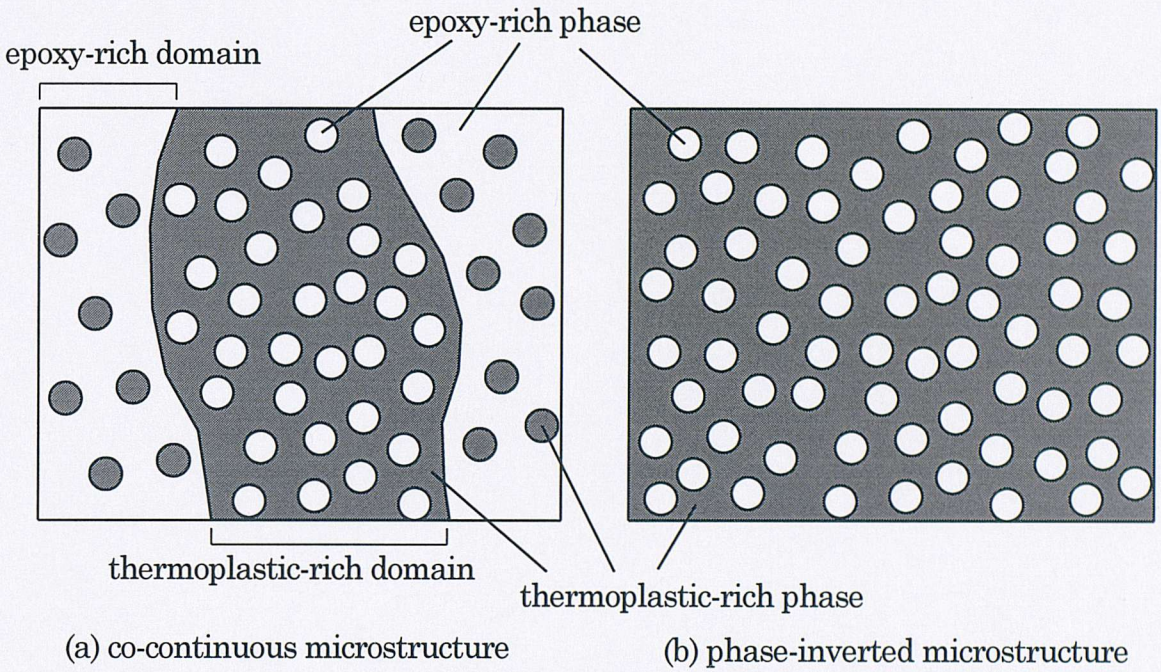


Fig.8.9 Schematic drawing of (a) co-continuous microstructure, (b) phase-inverted microstructure

From the above discussions, it may be concluded that for the material with the co-continuous microstructure, the lower the extent of the epoxy-rich domains, the better the fatigue resistance, as shown in Fig.8.10. However, the fatigue resistance should still be somewhat poorer than that for the phase-inverted microstructure, since epoxy-rich domains (i.e. continuous epoxy-rich phase) exist in the co-continuous microstructure. Hence, it is considered that a phase-inverted microstructure is necessary to achieve the best fatigue resistance for the PES copolymer modified epoxy materials examined in the present study.

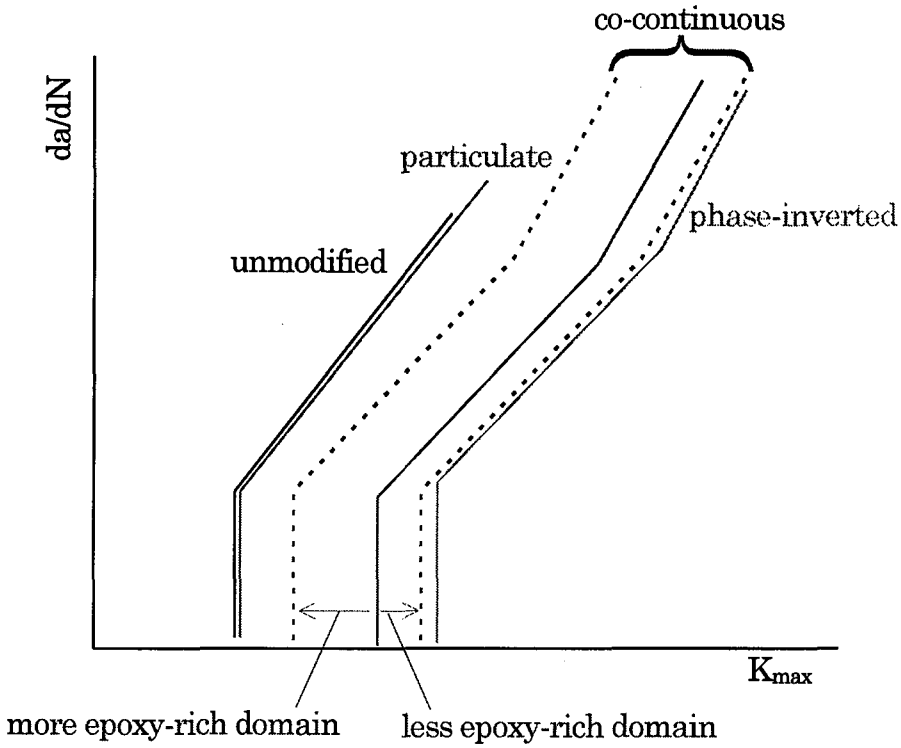


Fig.8.10 Influence of the epoxy-rich domain in the fatigue resistance of the material with the co-continuous microstructure

8.3 Thermoplastic modified epoxies and rubber modified epoxies

Fig.8.11 shows the fatigue crack growth rates of the PES25 material (i.e. the thermoplastic modified epoxy with the best fatigue performance) and the 15phrRME160 and 15phrRME120 materials (i.e. both rubber modified epoxies) plotted against the K_{max} values. The fatigue resistance of the PES25 material is better than that of the 15phrRME160 and 15phrRME120 materials when the applied K_{max} value is relatively low. On the other hand, in the higher K_{max} region, the 15phrRME160 and 15phrRME120 materials have a better fatigue resistance than the PES25 material.

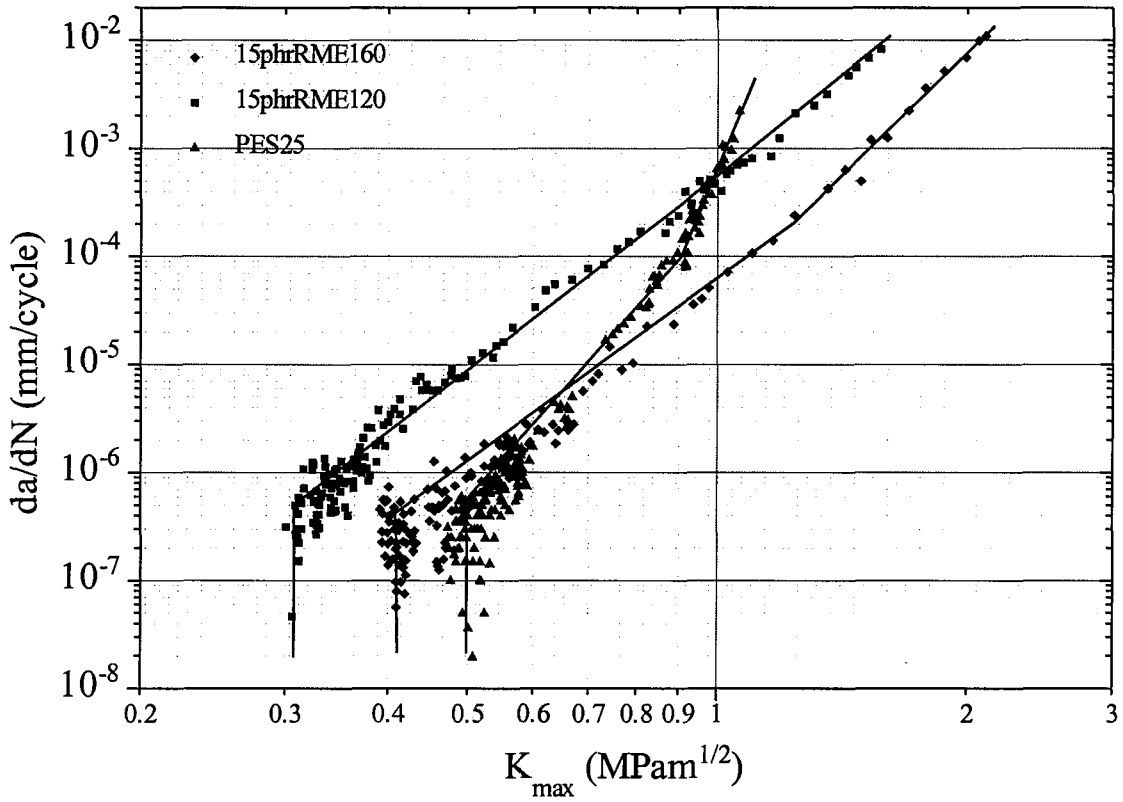


Fig.8.11 Fatigue crack growth rate for 15phrRME160, 15phrRME120 and PES25 plotted against K_{max}

Since the basic epoxy polymer is different between the thermoplastic modified epoxies and the rubber modified epoxies, it is rather difficult to assess precisely the influence of the microstructural parameters on the fatigue behaviour. However, the experimental results may be interpreted as discussed below.

For the 15phrRME160 and 15phrRME120 materials, the toughening mechanisms which involve plastic deformation are not sufficiently active when the applied K_{max} value is relatively low, as discussed in section 5.4. Therefore, the fatigue behaviour in this region is determined by the intrinsic fatigue resistance of the matrix epoxies. However, for the PES25 material, due to the phase-inverted microstructure, the fatigue crack propagates always through the thermoplastic-rich phase, which is the matrix phase, as discussed in section 8.2.3. Therefore, the fatigue behaviour is determined by the fatigue resistance of the thermoplastic-rich phase.

As discussed in section 4.5.1 and 4.5.2, the fracture toughness, K_{Ic}, is 0.81MPam$^{1/2}$ for UME120, 1.20MPam$^{1/2}$ for UME160 and 1.16MPam$^{1/2}$ for PES25. Therefore, it is suggested that the thermoplastic-rich matrix phase in the PES25 material is tougher than the epoxy matrix in the 15phrRME120 material. Although the basic toughness of the thermoplastic-rich phase in the PES25 material may be similar to that of the epoxy matrix in the 15phrRME160 material, due to the crack deflection (see section 8.2.3), the PES25 material is likely to be inherently tougher than the 15phrRME160 material. This may be why the PES25 material possesses the better fatigue resistance than the 15phrRME160 and 15phrRME120 materials, when the applied K_{max} value is relatively low.

When the applied K_{max} value is relatively high, the toughening mechanisms which involve plastic deformation of the matrix epoxy become active and substantial energy is dissipated during fatigue crack propagation in the 15phrRME160 and 15phrRME120 materials. However, for the PES25 material, no toughening mechanisms such as plastic void growth become active, since the epoxy-rich phase (i.e. dispersed particle) is not rubbery in nature and does not readily undergo cavitation. Hence, the 15phrRME160 and 15phrRME120 materials possess a better fatigue resistance then the PES25 material in the relatively high K_{max} region.

Summarising the above discussion, from the present study, the thermoplastic modified epoxies possess a better fatigue resistance in the relatively low K_{max} region, and the rubber modified epoxies possess a better fatigue resistance in the relatively high K_{max} region. If the fatigue resistance in a low K_{max} region is important, then the thermoplastic modified epoxies are recommended. However, the rubber modified epoxies would be preferred if the fatigue resistance in a high K_{max} region is important.

The fatigue crack growth rates plotted against the normalised K_{max} value, K_{max}/K_{Ic}, for the 15phrRME160, 15phrRME120 and PES25 materials are shown Fig.8.12. Similar plots for the UME160, UME120 and PES0 materials (i.e. unmodified epoxies) are shown in Fig.8.13. Comparing both figures, the fatigue curves of the 15phrRME160 and 15phrRME120 materials are shifted to the low K_{max}/K_{Ic} region compared with those of the UME160 and UME120 materials. On the other hand, for the PES25 material, the fatigue curve is still located in a

relatively high K_{max}/K_{Ic} region, as is also seen for the PES0 material.

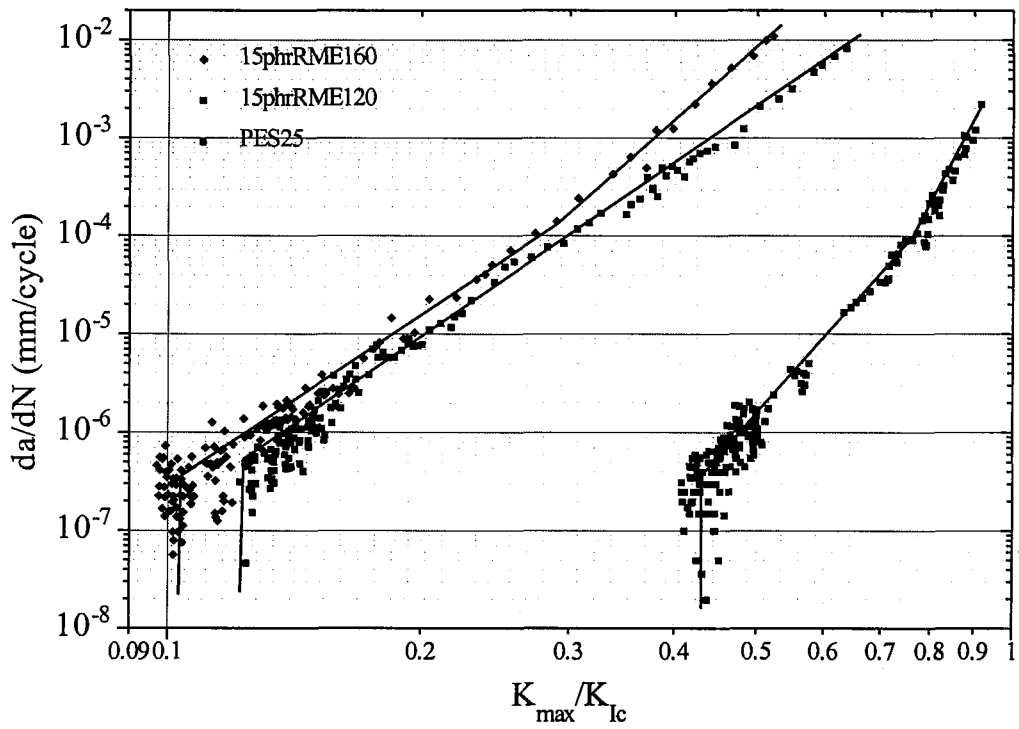


Fig.8.12 Fatigue crack growth rate for 15phrRME160, 15phrRME120 and PES25 plotted against K_{max}/K_{Ic}

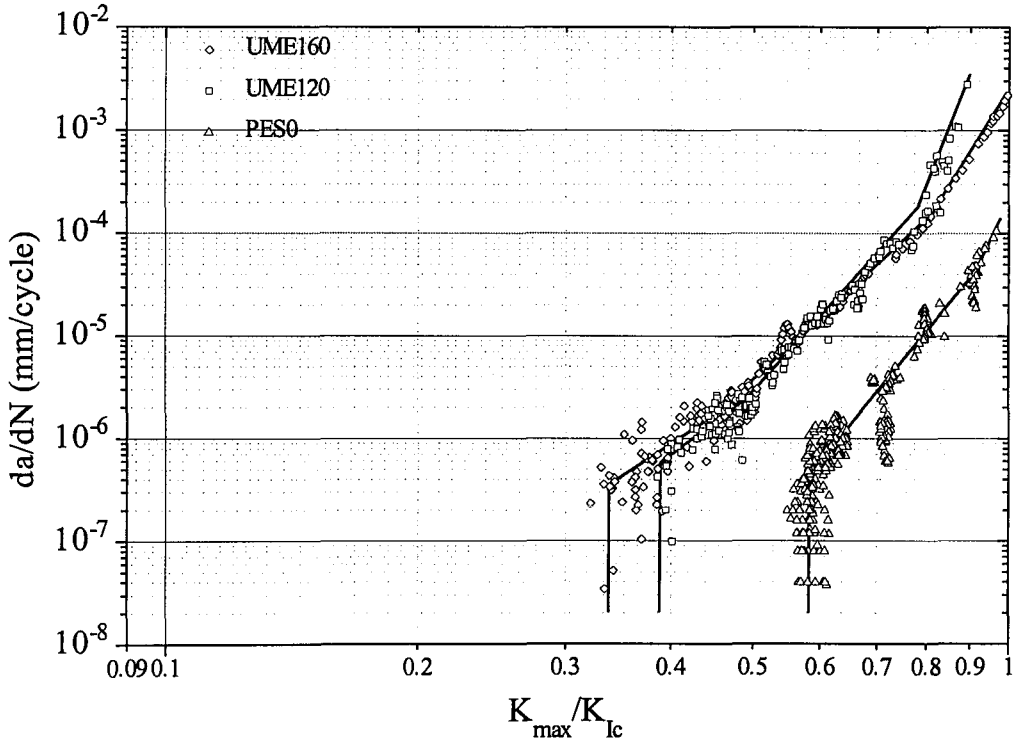


Fig.8.13 Fatigue crack growth rate for UME160, UME120 and PES0 plotted against K_{max}/K_{Ic}

The toughening mechanisms arising from the presence of the rubber particles clearly improve the K_{Ic} value, but not the threshold value, K_{th}. This causes the shift of the fatigue curve to the low K_{max}/K_{Ic} region, as discussed in detail in section 5.3.4 for the 15phrRME160 and 15phrRME120 materials. However, for the PES25 material, both the K_{th} and K_{Ic} values are increased compared with the values of the PES0 material. Hence, only a small shift of the fatigue curve for the PES25 material is observed, since the K_{th}/K_{Ic} value of the PES25 material is not significantly different compared with that of the PES0 material. (The K_{th}/K_{Ic} value is 0.43 for PES25 and 0.56 for PES0.) This is why the fatigue curve of the PES25 material is still located in a relatively high K_{max}/K_{Ic} region, as is also seen for the PES0 material.

8.4 Concluding remarks

The fatigue behaviour of the PES copolymer modified epoxies has been investigated and the effect of the microstructure on the fatigue resistance has been discussed in this Chapter. The results suggest that the particulate microstructure is not significantly effective in improving the fatigue resistance in the present thermoplastic modified epoxy system, and that only the co-continuous and phase-inverted microstructures improve the fatigue resistance significantly, including the threshold values. These observations arise because the thermoplastic-rich phase is likely to be tougher than the epoxy-rich phase, and hence a continuous thermoplastic-rich phase leads to an increase in the fatigue resistance.

However, our understanding of the influence of the microstructure and the toughening mechanisms in the case of the thermoplastic modified epoxies is relatively qualitative. Further investigations will be needed for a more quantitative and detailed discussion.

Chapter Nine

Conclusions

The static fracture and fatigue behaviour of several types of rubber modified and thermoplastic (PES copolymer) modified epoxies have been studied in the present research. The toughening mechanisms in both static and fatigue conditions were also investigated using TOM, SEM and TEM. Furthermore, a theoretical model of the toughening mechanisms active in the rubber modified epoxies during fatigue fracture was developed, and the energy dissipated by each toughening mechanism was calculated using the theoretical model. Based on the results obtained from this study, the following conclusions can be drawn.

(1) The fatigue behaviour of the rubber modified epoxies was studied from a relatively low K region, i.e. near the threshold region, to a relatively high K region, near the K_{Ic} value. The effects of the crosslink density of the matrix epoxy on the fatigue resistance were investigated using the rubber modified epoxies cured at various temperatures. The experimental results suggest that the material having a relatively low crosslink density for the epoxy matrix possesses the better fatigue resistance than the epoxy having a higher crosslink density, at any applied K value, i.e. from the threshold region to the near K_{Ic} value. The ΔK^* values (i.e. the ΔK values at which the material possesses a fatigue crack growth rate of 7.5×10^{-4} mm/cycle) show an approximately linear relationship to the square root values of M_c, the average molecular weight between crosslinks. The superior fatigue resistance for the material with a lower crosslink density may be considered to arise from the greater ductility, i.e. greater ability for plastic deformation, of the epoxy resin possessing the lower crosslink density. The crack propagation which involves more plastic deformation dissipates greater energy than that with less plastic deformation. Hence, the fatigue crack growth rates in the material having a lower crosslink density are smaller than those for the material having a higher crosslink density.

(2) The effect of the volume fraction of rubber on the fatigue resistance was also investigated. with an increase in the volume fraction of rubber, the fatigue resistance of the rubber modified epoxy has been found to be improved, when the applied K value is relatively large. However, there is virtually no difference in fatigue resistance between the rubber modified epoxy and the unmodified epoxy, when the applied K value is relatively small, including the threshold region. In other words, the rubber modified epoxy has a better fatigue resistance than the unmodified epoxy only above a certain applied K value.

(3) A concept of K-transition can be introduced from the results on the effect of the volume fraction of rubber. The K-transition value can be experimentally defined as a critical K value at which the difference in the fatigue resistance between the rubber modified epoxy and the unmodified epoxy starts to appear. It may be considered theoretically that the K-transition value corresponds to the K value at which the plastic zone size equals to the rubber particle size. When the applied K value is smaller than the K-transition value, the plastic zone is smaller than the rubber particles. Plastic deformation is now restricted to a very limited region near the crack tip, and consequently the mechanisms induced by the rubber particles which involve plastic deformation are not yet active. Hence there is virtually no difference in fatigue resistance between the rubber modified epoxy and the unmodified epoxy. On the other hand, when the applied K value is greater than the K-transition value, the plastic zone is sufficiently large to engulf the rubber particles. This enables the matrix epoxy to further deform plastically, because the yield criterion of the epoxy matrix is achieved inside the plastic zone. Thus, the toughening mechanisms which involve plastic deformation become active, and more energy is dissipated during crack propagation in the rubber modified epoxy than in the unmodified epoxy. Hence, the rubber modified epoxy has a better fatigue resistance than the unmodified epoxy.

(4) The effect of the rubber particle size on the fatigue resistance was also investigated. It is observed that the rubber modified epoxy with the smaller rubber particles possesses a better fatigue resistance than the rubber modified epoxy with the larger rubber particles. The particle size affects the fatigue resistance via changing the K-transition value. The K-transition value decreases with a decrease in the particle size. Hence, the toughening mechanisms start to be active at a lower applied K value, for the rubber modified epoxy with smaller rubber particles. This

leads to a decrease in the fatigue crack growth rate at a given applied K value, and hence leads to a better fatigue resistance. The threshold values are not affected by the change in the rubber particle size. This is because the threshold value is governed by the material properties of the matrix epoxy, and is not affected by the presence of the rubber particles.

(5) From the above results, it may be concluded that the material having the lowest crosslink density of the matrix epoxy, the highest volume fraction of rubber and the smallest rubber particle size should possesses the best fatigue resistance.

(6) The toughening mechanisms of the rubber modified epoxies were studied using fractographic techniques. The fracture surfaces were investigated using SEM, TOM and TEM. For both static and fatigue fracture, internal cavitation of the rubber particles was observed. Shear yielding and plastic void growth were also observed. The extent of these toughening mechanisms was found to be affected by the crosslink density of the matrix epoxy. Under fatigue loading, when the applied K value is below the K-transition value, there is little evidence of the toughening mechanisms which involve plastic deformation, i.e. shear yielding and plastic void growth. When the applied K value is above the K-transition value, plastic deformation surrounding the cavitated particles due to shear yielding and void growth mechanisms is observed and the extent of these mechanisms increases with an increase in the applied K value.

(7) A theoretical model has been developed to quantify the energy dissipation arising from the toughening mechanisms, i.e. shear yielding, void growth and rubber bridging, under fatigue loading. The modelling of the energy dissipation for the 15phrRME160 and 15phrRME120 materials was undertaken. According to the results, the shear yielding mechanism is the dominant toughening mechanism for both materials. Although the plastic void growth mechanism dissipates less energy than the shear yielding mechanism, the importance of the void growth mechanism steadily increases as the applied K value increases. The contribution of shear yielding and void growth mechanisms to the total energy dissipation is not significant when the applied K value is relatively small, since the toughening mechanisms which involve plastic deformation are not sufficiently active under these low loads due to a relatively small plastic zone being formed at the crack tip. In any range of the applied K_{max} value, the contribution of the rubber bridging

mechanism to the total energy dissipation is approximately 10% for the 15phrRME160 material, whereas it is approximately 30% for the 15phrRME120 material. Thus, the rubber bridging mechanism plays a relatively important role in toughening the 15phrRME120 material.

(8) The PES copolymer modified epoxies have a wide variety of microstructures, from particulate to co-continuous and phase-inverted microstructures, as the amount of PES added to the formulation is increased. For the thermoplastic modified epoxies used in the present study, a particulate microstructure, i.e. thermoplastic-rich particles dispersed in the epoxy-rich matrix, is not sufficient to improve the fatigue resistance. This is because the epoxy resin is not ductile enough to undergo extensive plastic deformation, and the thermoplastic-rich particles act only as bridging particles. However, the co-continuous and phase-inverted microstructures give a significant increase in the fatigue resistance, including an improvement of the threshold values. Since the thermoplastic-rich phase may be considered to be tougher than the epoxy-rich phase, the fatigue crack must advance through the tougher thermoplastic-rich phase for both the co-continuous and phase-inverted microstructures. Hence, a significant improvement of the fatigue resistance can be achieved for these microstructures. On this basis, a phase-inverted microstructure should lead to the best fatigue resistance, and this was indeed found to be the case.

Chapter Ten

Recommendations for Future Work

A great deal of valuable information on the fatigue behaviour and the toughening mechanisms of the rubber modified epoxies and the thermoplastic modified epoxies was identified during the course of the present study. However, some unanswered questions still remain. It is therefore recommended to undertake further research, especially on the following points.

Seven formulations of rubber modified epoxies were used to investigate the effects of crosslink density, rubber content and particle size in this study. Further studies using more formulations would be useful to gain a more comprehensive understanding on the effects of these material properties on the fatigue behaviour.

Small differences still exist between the modelling results using the theoretical model and the experimental results. Thus, it may be necessary to modify the theoretical model further. For instance, in the present model, it is assumed that the plastic shear strain in the shear bands is dependent only on the distance from the crack tip. However, it may be more natural to consider that the plastic shear strain in the shear bands is also dependent on the relative position within the shear bands; it should be greater at the centre of the shear bands than near their boundary.

The strain rate in fatigue tests is considered to be significantly greater than that in general static tests. For the toughening model, we estimated the values of the strain rate in fatigue tests, and material properties, such as the yield stress and fracture strain in the fatigue tests, were estimated by extrapolating the static data to the fatigue conditions. It would be useful to measure these material properties under equivalent conditions to the fatigue tests, if possible. This would be a considerable help to improve the accuracy of the modelling work.

Some parameters such as K_{vm}, etc. used in the theoretical model were obtained from the FE analysis by Huang et al. [7,47,48]. Although they employed a

two dimensional model for the stress analysis, a three dimensional analysis could be conducted. Such a new analysis would offer more exact values for these parameters, and would also improve the accuracy of the theoretical model. Thus, it would be useful to perform further FE analyses in future studies.

In the present study, liquid CTBN rubber, which was initially dissolved in the epoxy resin, was used as a secondary phase material. As a result of using liquid CTBN rubber, it was virtually impossible to alter only one microstructural parameter, such as particle size, without introducing changes in the other parameters. This leads to some difficulties in assessing precisely the effect of each parameter on the fatigue behaviour. Utilising solid rubber particles, such as core-shell rubber particles, would be helpful for a more precise investigation.

Understanding the effects of the microstructure on the fatigue behaviour, linking the results of the rubber modified epoxies and the thermoplastic modified epoxies, is not yet comprehensive. The base epoxy resin was different between these modified epoxy polymers, and consequently the detailed toughening mechanisms are also different between them. It would be useful for a better understanding of the influence of the microstructure on the fatigue behaviour to undertake further research with the rubber modified epoxies and thermoplastic modified epoxies when both contain the same base epoxy resin.

Appendix A

Effect of the Addition of Bisphenol-A

For all formulations of RME series and RME with BPA added series, the amount of curing agent, piperidine, is 5 per hundred resin (weight). In order to simplify the calculation, we will think about UME120 and UME120+BPA, and the amount of epoxy resin is chosen as 100g.

For UME120 material, DGEBA epoxy (epoxy equivalent weight 190g/mol) 100g and piperidine (85g/mol) 5g are used. This corresponds to epoxy 0.526mol and piperidine 0.0588mol approximately. The ratio of epoxy and piperidine is as follows:

$$\text{epoxy matrix: piperidine} = 0.526 : 0.0588 = 8.95 : 1 \qquad \text{(A.1)}$$

For UME120+BPA material, epoxy 100g, piperidine 5g and BPA (228g/mol) 24g are used. This corresponds to epoxy 0.526mol, piperidine 0.0588mol and BPA 0.105mol. If whole BPA molecules become a part of epoxy matrix, the ratio of epoxy and piperidine is as follows:

$$\text{epoxy matrix: piperidine} = 0.526+0.105 : 0.0588 = 10.73 : 1 \qquad \text{(A.2)}$$

The ratio of epoxy matrix and piperidine for UME120+BPA is larger than that of UME120. This means that the amount of curing agent, piperidine, per unit epoxy molecule for UME120+BPA is less than that for UME120. Therefore, when the other curing conditions are same, the crosslink density of UME120+BPA should be smaller than that of UME120. The number of epoxy molecules between crosslinks should be related by the following equation:

$$N_{c,UME120+BPA} / N_{c,UME120} = 10.73 / 8.95 = 1.20 \qquad \text{(A.3)}$$

where $N_{c,UME120+BPA}$ is the number of epoxy molecules between crosslinks of UME120+BPA, and $N_{c,UME120}$ is that of UME120. Meanwhile, the epoxy equivalent

weight of the mixture of DGEBA 100g and BPA 24g is:

$$(100g+24g) / (0.526mol+0.105mol) = 196.5g/mol \quad (A.4)$$

Therefore, the ratio of M_c, average molecular weight between crosslinks, is expected as follows:

$$M_{c,\,UME120+BPA} / M_{c,\,UME120} = 1.20 \times 196.5 / 190 = 1.24 \quad (A.5)$$

where $M_{c,\,UME120+BPA}$ is M_c of UME120+BPA, and $M_{c,\,UME120+BPA}$ is M_c of UME120. This calculation implies that the addition of 24phr BPA causes an increase of M_c by around 24%.

Appendix B

Energy Density and Dissipated Energy

Supposing that a crack is propagating in an infinite plate, as shown in Fig.B.1, the energy dissipated in the whole plastic zone, W, is calculated by the following equation:

$$W = \iint U(x,y)\, B\, dx\, dy \qquad (B.1)$$

where U(x,y) is dissipated energy density and B is the thickness.

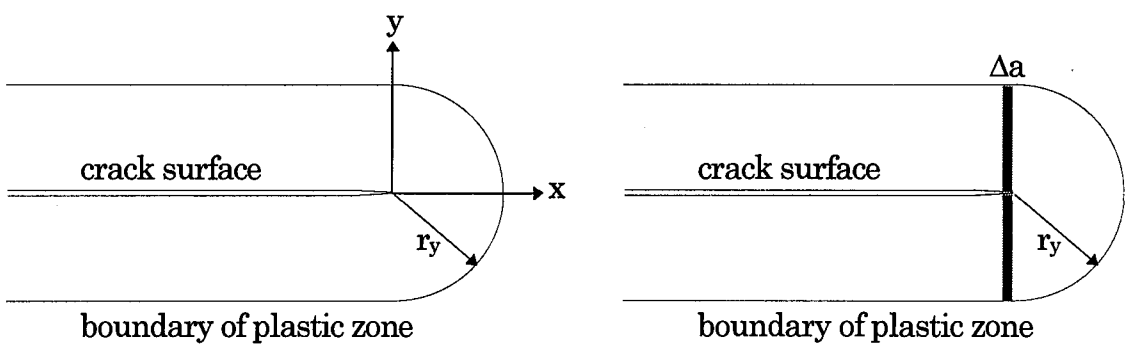


Fig. B.1 Schematic drawing of the plastic zone in the vicinity of the crack tip

If crack propagates a small distance, Δa, the energy change, ΔW, becomes:

$$\Delta W = 2 \int_0^{\Delta a} \int_0^{r_y} U(x,y)\, B\, dx\, dy \qquad (B.2)$$

where U(x,y) is the dissipated energy density and B is the thickness. As the energy density is a function of the distance from the crack tip, r, the function U(x,y) can be expressed as U(r). In the area of the integration, r is virtually equal to y. Therefore, equation B.2 can be modified as follows:

$$\Delta W = 2 \int_0^{\Delta a} \int_0^{r_y} U(y)\, B\, dx\, dy = 2\, B\Delta a \int_0^{r_y} U(y)\, dy \qquad (B.3)$$

The fracture energy, G, is defined as the energy change when a unit new surface is created. Thus,

$$G = \Delta W / B\Delta a = 2 \int_0^{r_y} U(y)\, dy = 2 \int_0^{r_y} U(r)\, dr \qquad (B.4)$$

References

[1] A.J.Kinloch and R.J.Young, "Fracture Behaviour of Polymers", Applied Science Publishers Ltd., 1983

[2] J.G.Williams, "Fracture Mechanics of Polymers", Ellis Horwood Ltd., 1984

[3] H.Liang, W.Jiang, J.Zhang and B.Jiang, J. Appl. Polymer Sci., **59**(1996), 505

[4] H.J.Sue and A.F.Yee, J. Mater. Sci., **28**(1993), 2975

[5] E.H.Andrews and A.J.Kinloch, Proc. Roy. Soc., **A332**(1973), 385

[6] A.N.Gent and J.Schulz, J. Adhesion, **3**(1972), 281

[7] Y.Huang, PhD thesis, Imperial College(1991)

[8] A.J.Kinloch, S.J.Shaw, D.A.Tod and D.L.Hunston, Polymer, **24**(1983), 1341

[9] A.J.Kinloch, S.J.Shaw and D.L.Hunston, Polymer, **24**(1983), 1355

[10] A.F.Yee and R.A.Pearson, J. Mater. Sci., **21**(1986), 2462

[11] R.A.Pearson and A.F.Yee, J. Mater. Sci., **21**(1986), 2475

[12] L.R.F.Rose, Mech. Mater., **8**(1987), 11

[13] B.Budiansky, J.C.Amazigo and A.G.Evans, J. Mech. Phys. Solids, **36**(1988), 167

[14] R.O.Ritchie, Mater. Sci. Eng., **A103**(1988), 15

[15] A.J.Kinloch and D.L.Hunston, J. Mater. Sci. Lett., **5**(1986), 909

[16] A.C.Garg and Y.W.Mai, Compos. Sci. Technol., **31**(1988), 179

[17] A.A.Griffith, Phil. Trans. Roy. Soc., **A221**(1920), 163

[18] E.Orowan, Fracture and Strength of Solids, Reports on Progress in Physics. **XII**(1948), 185

[19] G.R.Irwin, "Fracture Dynamics", Fracturing of Metals, American Society for Metals, Cleveland (1948)

[20] D.S.Dugdale, J.Mech.Phys.Solids, 8(1960), 100

[21] A.N.Gent and P.B.Lindley, Proc. Roy. Soc., **A249**(1958), 195

[22] A.N.Gent and D.A.Tompkins, J. Appl. Phys., **40**(1969), 2520

[23] R.L. Dencouer and A.N.Gent, J. Polymer Sci., A2, **6**(1968), 1853

[24] A.N.Gent and D.A.Tompkins, J. Polymer Sci., A2, **7**(1969), 1483

[25] C.B.Bucknall, A.Karpodinis and X.C.Zhang, J. Mater. Sci., **29**(1994), 3377

[26] C.B.Bucknall, V.L.P.Soares, H.H.Yang and X.C.Zhang, Macromol. Symp., **101**(1996), 265

[27] H.Eyring, J. Chem. Phys., **4**(1936), 283

[28] C.Bauwens-Crowet, J.C.Bauwens and G.Homes, J. Polymer Sci., A2, **7**(1969), 735

[29] R.A.Ducket, S.Rabinowitz and I.M.Ward, J. Mater. Sci., **5**(1970), 909

[30] I.M.Ward, J. Mater. Sci., **6**(1971), 1397

[31] I.M.Ward, "The mechanical properties of solid polymers", Wiley, London (1971)

[32] P.B.Bowden, in "The physics of glassy polymers", Ed. by R.N.Haward, Applied Science Publishers Ltd., London (1973)

[33] P.B.Bowden, Phil. Mag., **22**(1970), 455

[34] P.B.Bowden and J.A.Jukes, J. Mater. Sci., **7**(1972), 52

[35] A.F.Lu, PhD thesis, Swiss Federal Intsitute of Technology, Lausanne(1995)

[36] J.B.C.Wu and J.C.M.Li, J. Mater. Sci., **11**(1976), 434

[37] J.C.M.Li and J.B.C.Wu, J. Mater. Sci., **11**(1976), 445

[38] A.J.Kinloch and J.G.Williams, J. Mater. Sci., **15**(1980), 987

[39] J.G.Williams, "Stress analysis of polymers", 2nd Edn., Ellis Horwood, 1980

[40] A.J.Kinloch, "Structural Adhesives: Developments in Resins and Primers", Elsevier Applied Science Publishers, London and New York, 1983

[41] L.A.Pottick, Proceeding of the ACS Division of Polymeric Materials: Science and Engineering, **63**, Fall Meeting 1990, Washington D.C.

[42] H.S.Kim and P.Ma, J. Appl. Polymer Sci., **61**(1996), 659

[43] J.F.Hwang, J.A.Manson, R.W.Hertzberg, G.A.Miller and L.H.Sperling, Polymer Eng. Sci., **29**(1989), 1477

[44] S.Sankaran and M.Chanda, J. Appl. Polymer Sci., **39**(1990),

[45] C.B.Bucknall, "Toughened Plastics", Applied Science Publishers Ltd., London, 1979

[46] R.J.Morgan, E.T.Mones and W.J.Steele, Polymer, **23**(1982), 295

[47] Y.Huang and A.J.Kinloch, J. Mater. Sci., **27**(1992), 2753

[48] *Ibid.*, 2763

[49] M.Tohdoh, S.K.Chaturvedi and R.L. Sierakowski, Int. J. Fracture, **75**(1996), 285

[50] A.F.Yee, D.Li and X.Li, J. Mater. Sci., **28**(1993), 6392

[51] H.R.Azimi, PhD thesis, Lehigh University(1994)

[52] D.Li, A.F.Yee, I.W.Chen, S.C.Chang and K.Takahashi, J. Mater. Sci., **29**(1994), 2205

[53] S.Kunz-Douglass, P.W.R.Beaumont and M.F.Ashby, J. Mater. Sci., **15**(1980), 1109

[54] J.Karger-Kocsis and K.Friedrich, Composites Sci. Tech., **48**(1993), 263

[55] R.A.Pearson and A.F.Yee, J. Mater. Sci., **24**(1989), 2571

[56] A.J.Kinloch, C.A.Finch and S.Hashemi, Polymer Communications, **28**(1987), 322

[57] C.B.Bucknall and T.Yoshii, Brit. Polymer J., **10**(1978), 53

[58] A.J.Kinloch and D.L.Hunston, J. Mater. Sci. Lett., **6**(1987), 137

[59] R.A.Pearson and A.F.Yee, J. Mater. Sci., **26**(1991), 3828

[60] D.S.Kim, K.Cho, J.K.Kim and C.E.Park, Polymer Eng. Sci., **36**(1996), 755

[61] A.Lazzeri and C.B.Bucknall, J. Mater. Sci., **28**(1993), 6799

[62] S.Wu, Polymer, **26**(1985), 1855

[63] S.Wu, J. Appl. Polymer Sci., **35**(1988), 549

[64] R.Bagheri and R.A.Pearson, Polymer, **36**(1995), 4883

[65] R.Bagheri and R.A.Pearson, Polymer, **37**(1996), 4529

[66] J.Kiefer, H.H.Kausch and J.G.Hilborn, Polymer Bulletin, **38**(1997), 477

[67] Y.Huang and A.J.Kinloch, Polymer, **33**(1992), 1331

[68] L.E.Nielsen, J. Macromol. Sci. - Macromol. Chem., **C-3**(1969), 69

[69] L.C.Chan, J.K.Gillham, A.J.Kinloch and S.J.Shaw, "Rubber-Modified Thermoset Resin", Edited by C.K.Riew and J.K.Gillham, Advances in Chemistry Series 208, 1984

[70] Y.Huang, A.J.Kinloch, R.J.Bertsch and A.R.Siebert, "Toughened Plastics I", Edited by C.K.Riew and A.J.Kinloch, Advances in Chemistry Series 233, 1993, p.189

[71] R.W.Hertzberg and J.A.Manson, "Fatigue of Engineering Plastics", Academic Press, 1980

[72] P.C.Paris, Proc. Sagamore Army Mater. Res. Conf., 10th(1964), 107

[73] P.C.Paris, PhD thesis, Lehigh University(1962)

[74] H.R.Azimi, R.A.Pearson and R.W.Hertzberg, J. Appl. Polymer Sci., **58**(1995), 449

[75] J.K.Jethwa and A.J.Kinloch, J. Adhesion, **61**(1997), 71

[76] M.D.Skibo, PhD thesis, Lehigh University(1977)

[77] R.W.Hertzberg, J.A.Manson and M.D.Skibo, Polymer Eng. Sci., **15**(1975), 75

[78] R.Attermo and G.Ostberg, Int. J. Fracture Mech., **15**(1971), 122

[79] R.W.Hertzberg, M.D.Skibo, J.A.Manson and J.K.Donald, J. Mater. Sci., **14**(1979), 1754

[80] J.A.Manson, R.W.Hertzberg, S.L.Kim and M.D.Skibo, Polymer, **16**(1975), 850

[81] R.W.Hertzberg, J.A.Manson and M.D.Skibo, Polymer, **19**(1978), 358

[82] E.J.Moskala, J. Appl. Polymer Sci., **49**(1993), 53

[83] M.L.Williams, R.F.Landel and J.D.Ferry, J. Am. Chem. Soc., **77**(1955), 3701

[84] Y.W.Mai and J.G.Williams, J. Mater. Sci., **14**(1979), 1933

[85] A.J.Kinloch, D.G.Gilbert and S.J.Shaw, J. Mater. Sci., **21**(1986), 1051

[86] S.Arad, J.C.Radon and L.E.Culver, J. Mech. Eng. Sci., **13**(1971), 75

[87] N.J.Mills and N.Walker, Polymer, **17**(1976), 335

[88] S.T.Sutton, Eng. Fracture Mechanics, **6**(1974), 587

[89] R.W.Hertzberg, J.A.Manson and W.C.Wu, ASTM STP **536**(1973), 391

[90] S.L.Kim, M.D.Skibo, J.A.Manson, R.W.Hertzberg and J.Janiszewski, Polymer Eng. Sci., **18**(1978), 1093

[91] H.Kishi, Y.B.Shi, J.Huang and A.F.Yee, J. Mater. Sci., **32**(1997), 761

[92] J.Karger-Kocsis and K.Friedrich, Colloid and Polymer Sci., **270**(1992), 549

[93] H.R.Azimi, R.A.Pearson and R.W.Hertzberg, J. Mater. Sci., **31**(1996), 3777

[94] ASTM Standards, E647-86

[95] A.S.Holik, R.P.Kambour, S.Y.Hobbs and D.G.Fink, Microstruct. Sci., **7**(1979), 35

[96] A.J.Kinloch, M.L.Yuen and S.D.Jemkins, J. Mater. Sci., **29**(1994), 3781

[97] E.E.Underwood, "Quantitative Stereology", Addison-Wesley Publishing Co., Reading, Massachusetts, 1970

[98] D.H.Kim and S.C.Kim, Polymer Eng. Sci., **31**(1991), 289

[99] H.S.Y.Hsich, J. Mater. Sci., **26**(1991), 3209

[100] G.M.Maistros, H.Block, C.B.Bucknall and I.K.Partridge, Polymer, **33**(1992), 4470

[101] J.P.Chen and Y.D.Lee, Polymer, **36**(1995), 55

[102] M.Taha, V.Perrut, A.A.Roche and J.P.Pascault, J. Appl. Polymer Sci., **65**(1997), 2447

[103] G.F.Tudgey, private communication

[104] F.Bueche, "Physical Properties of Polymers", Interscience Publishers, 1962

[105] O.Ishai and L.J.Cohen, Int. J. Mech. Sci., **9**(1967), 539

[106] T.Murayama and J.P.Bell, J. Polymer Sci., **A2**, **8**(1970), 437

[107] H.R.Azimi, R.A:Pearson and R.W.Hertzberg, Polymer Eng. Sci., **36**(1996), 2352

[108] A.C.Roulin-Moloney, "Fractography and Failure Mechanisms of Polymers and Composites", Ed. by A.C.Roulin-Moloney, Elsevier Applied Science, London, 1989

[109] D.Li, A.F.Yee, I.W.Chen, S.C.Chang and K.Takahashi, J. Mater. Sci., **29**(1994), 2205

[110] Y.Huang and A.J.Kinloch, J.Mater. Sci. Lett., **11**(1992), 484

[111] H.J.Sue, J. Mater. Sci., **27**(1992), 3098

[112] H.Liang, W.Jiang, J.Zhang and B.Jiang, J. Appl. Polymer Sci., **59**(1996), 505

[113] A.J.Kinloch in Rubber-Toughened Plastics, Ed. C.K.Riew, Advances in Chemistry Series 222, American Chmical Spciety, Washington D.C., 1989

[114] J.W.Smith, "Deformation induced failure mechanisms in particulate filled epoxy resins", PhD thesis, Ecole Polytechnique Federale de Laisanne (1989)

[115] S.C.Kunz and P.W.R.Beaumont, J. Mater. Sci., **16**(1981), 3141

[116] C.B.Bucknall and A.H.Gilbert, Polymer, **30**(1989), 213

[117] J.L.Hedrick, I.Yilgor, M.Jurek, J.C.Hedrick, G.L.Wilkes and J.E.McGrath, Polymer, **32**(1991), 2020